ELUCIDATION OF DENDRITIC CELL RESPONSE-MATERIAL PROPERTY RELATIONSHIPS USING HIGH THROUGHPUT METHODOLOGIES

A Dissertation
Presented to
The Academic Faculty

by

Peng Meng Kou

In Partial Fulfillment
of the Requirements for the Degree
Doctor of Philosophy in Bioengineering
in the
Department of Biomedical Engineering

Georgia Institute of Technology
August 2011

ELUCIDATION OF DENDRITIC CELL RESPONSE-MATERIAL PROPERTY RELATIONSHIPS USING HIGH THROUGHPUT METHODOLOGIES

Approved by:

Dr. Julia Babensee, Advisor
Department of Biomedical Engineering
Georgia Institute of Technology

Dr. Barbara Boyan
Department of Biomedical Engineering
Georgia Institute of Technology

Dr. Andrés García
School of Mechanical Engineering
Georgia Institute of Technology

Dr. Melissa Kemp
Department of Biomedical Engineering
Georgia Institute of Technology

Dr. Philip Santangelo
Department of Biomedical Engineering
Georgia Institute of Technology

Date Approved: June 23, 2011

ACKNOWLEDGEMENTS

TABLE OF CONTENTS

LIST OF TABLES

LIST OF FIGURES

LIST OF ABBREVIATIONS

aaDC: alternatively activated DCs

Ab: antibody

APC: Antigen presenting cell

BAMP: biomaterial-associated molecular patterns

CFA: complete Freund's adjuvant

CLR: C-type lectin receptor

CpG-ODN: CpG-rich oligodeoxynucleotide

CR: complement receptor

CTLA-4: cytotoxic T lymphocyte-associated antigen 4

DAI: DNA-dependent activator of interferon-regulatory factor

DAMP: danger-associated molecular patterns

DAP12: DNAX activating protein

DC: dendritic cells

DC-SIGN: dendritic cell-specific intercellular adhesion molecule grabbing nonintegrin

DC-STAMP: dendritic cell-specific transmembrane protein

ECM: extracellular matrix

FcR: Fc receptor

FN: fibronectin

Foxp3: forkhead box P3

IC: immune complex

iDC: immature dendritic cell

IFA: incomplete Freund's adjuvant

iNOS: inducible nitric oxide synthase

GM-CSF: granulocyte-macrophage colony-stimulating factor

HMGB-1: high mobility group box 1

IL: interleukin

ICAM: intercellular adhesion molecule

LPS: lipopolysaccharide

MΦ: macrophage

MCP-1: monocyte chemotactic protein-1

MDA5: melanoma-differentiation-associated gene 5

mDC: mature dendritic cell

MHC: major histocompatibility complex

MLR: mixed lymphocyte reaction

MMP: matrix metalloproteinases

MP: microparticle

MPL: monophosphoryl lipid A

MR: mannose receptor

NK cell: natural killer cell

NP: nanoparticle

NOD: nucleotide-binding oligmerization domain

OVA: ovalbumin

PAMP: Pathogen-associated molecular patterns

PCA: principal component analysis

PD-1: programmed cell death 1

PDGF: platelet-derived growth factor

PEO: polyethylene oxide

PGE2: prostaglandin E2

pHEMA: polyhydroxyethylmethacrylate

pIBTMA: poly(isobutyl-*co*-benzyl-*co*-terahydrofurfuryl)methacrylate

PLG: polylactide-*co*-glycolide

PLGA: poly(lactic-*co*-glycolic acid)

PLSR: partial linear squares regression

pMA: polymethacrylate

PRR: Pattern recognition receptor

PS: phosphatidylserine

PVDF: polyvinylidene fluoride

RIG-I: retinoic acid-inducible gene I

SAM: self-assembled monolayer

SC: scaffold

siRNA: Silencing RNA

SIRP-α: signal-regulatory protein-α

T_{reg}: Regulatory T cells

RIG-I: retinoic-acid-inducible gene I

TCR: T-cell receptor

TGF-β: transforming growth factor-β

T_h: T helper

TLR: Toll-like receptor

TRP2: tyrosinase-related protein 2

VEGF: vascular endothelial growth factor

VN: vitronectin

SUMMARY

Ongoing advances in tissue engineering with the goal to address the clinical shortage of donor organs have encouraged the design and development of biomaterials to be used in tissue-engineered scaffolds. Furthermore, biomaterials have been used as delivery vehicles for vaccines that aim to enhance the protective immunity against pathogenic agents. These tissue-engineered constructs or vaccines are usually combination products that combine biomaterial and biological (e.g. cells, proteins, and/or DNA) components. Upon introduction into the body, the host response towards these products will be a combination of both a non-specific inflammatory response towards the biomaterial and an antigen-specific immune response towards the biological component(s) [1]. Recently, the biomaterial component was shown to influence the immune response towards a co-delivered antigen. Specifically, poly(lactic-co-glycolic acid) (PLGA), but not agarose, scaffolds or microparticles (MPs) enhanced the humoral response to a model antigen, ovalbumin [2-4]. This *in vivo* result echoed with the *in* vitro study that PLGA, but not agarose, supported a mature phenotype of dendritic cells (DCs), the most potent antigen-presenting cells. Therefore, it is hypothesized that the effect of biomaterials on DC phenotype may influence the adaptive immunity against a co-delivered antigen. Understanding how biomaterials affect DC response will facilitate the selection and design of biomaterials that direct a desired immune response for tissue engineering or vaccine delivery applications.

The objectives of this research were to elucidate the correlations between material properties and DC phenotype, develop predictive models for DC response based on material properties, and uncover the molecular basis for DC response to biomaterials. Well-defined biomaterial systems, including clinical titanium (Ti) substrates and two polymer libraries, were chosen to study induced DC phenotype.

Due to the time-consuming nature of conventional methods for assessing DC phenotype, a high-throughput (HTP) method was first developed to screen for DC maturation based on surface marker expression (CHAPTER 4). A 96-well filter plate-based HTP methodology was developed and validated for the assessment of DC response to biomaterials. A "maturation factor", defined as CD86/DC-SIGN and measured by immunostaining, was found to be a cell number-independent metric for DC maturation and could be adapted to screen for DC maturation in a microplate format. This methodology was shown to reproducibly yield similar results of DC maturation in response to biomaterial treatment as compared to the conventional flow cytometric method upon DC treatment in 6-well plates. In addition, the supernatants from each treatment could easily be collected for cytotoxicity assessment using glucose-6-phosphate dehydrogenase (G6PD)-based assay and cytokine profiling using multiplex technology. In other words, the 96-well filter plate-based methodology can generate three outcomes from one single cell culture: 1) maturation marker expression, 2) cytotoxicity, and 3) cytokine profile.

To examine which material properties were critical in determining DC phenotype, a set of three clinical titanium (Ti) substrates with well-defined surfaces was used to treat DCs (CHAPTER 5). These Ti substrates included pretreatment (PT), sand-blasted and acid-etched (SLA), and modified SLA (modSLA), with different roughness and surface energy. DCs responded differently to these substrates. Specifically, PT and SLA induced a mature DC (mDC) phenotype, while modSLA-treated DCs remained immature based on surface marker expression, cytokine production profiles and cell morphology. Both PT and SLA induced higher CD86 expression as compared to iDC control, while modSLA maintained CD86 expression at a level similar to iDC. PT- or SLA-treated DCs exhibited dendritic processes associated with a mDC phenotype, while modSLA-treated DCs were rounded, a morphology associated with an iDC phenotype. Furthermore, PT induced increased secretion of MCP-1 by DCs compared to iDCs, indicating that PT

promoted a pro-inflammatory environment. SLA induced higher IL-16 production, which is a pleiotropic cytokine, by DCs, most likely as a pro-inflammatory response due to the enhanced maturation of DCs induced by SLA. In contrast, modSLA did not induced enhanced production of any cytokines examined. Principal component analysis (PCA) were used to reduce the multi-dimensional data space and confirmed these experimental results, and it also indicated that the non-stimulating property of modSLA co-varied with certain surface properties, such as high surface hydrophilicity, % oxygen and % titanium of the substrates. In contrast, high surface % carbon and % nitrogen were more associated with a mDC phenotype. Furthermore, PCA also suggested that surface line roughness (R_a) did not contribute to the expression of CD86, an important maturation marker, suggesting that roughness had little impact on DC response (CHAPTER 5).

DC response-material property relationships were also derived using more complex materials from a combinatorial library of polymethacrylates (pMAs) (CHAPTER 6). Twelve pMAs were selected and were found to induce differential DC response using the HTP method described in CHAPTER 4. These pMAs resulted in a trend of increasing DC maturation represented by the metric CD86/DC-SIGN, which was consistent with the trends of the production of pro-inflammatory cytokine, TNF-α, and chemokine, IL-8. Interestingly, this set of pMAs induced an opposite trend of IL-16 production, which is most likely released as an anti-inflammatory cytokine in this situation. These polymers were characterized extensively for a number of material properties, including surface chemical composition, glass transition temperature (T_g), air-water contact angle, line roughness (R_a), surface roughness (S_a), and surface area. Similar to the results from the Ti study, PCA determined that surface carbon correlated with enhanced DC maturation, while surface oxygen was associated with an iDC phenotype. In addition, T_g, R_a, and surface area were unimportant in determining DC response. Partial square linear regression (PLSR), a multivariate modeling approach, was implemented using the pMAs as the training set and a separate polymer library, which

contained methacrylate- and acrylate-based terpolymers, as the prediction set. This model successfully predicted DC phenotype in terms of surface marker expression with $R^2_{prediction}$ = 0.76. Furthermore, prediction of DC phenotype was effective based on only theoretical chemical composition of the bulk polymers with $R^2_{prediction}$ = 0.80 (CHAPTER 6). Nonetheless, one should note that a predictive model can be only as good as what it is trained on and cannot be used to predict the DC response induced by a type of materials different from the training set. Also, this model might not contain all the important material properties such as polymer swelling and cannot predict specific types of immune responses. However, these results demonstrated that a generalized immune cell response can be predicted from biomaterial properties, and computational models will expedite future biomaterial design and selection (CHAPTER 6).

From the pMA library, pMAs that induced the two extremes of DC phenotype (mature or immature) were identified for elucidating the mechanistic basis of biomaterial-induced DC responses (CHAPTER 7). Two pMAs, polyhydroxyethylmethacrylate (pHEMA) and poly(isobutyl-*co*-benzyl-*co*-terahydrofurfuryl)methacrylate (pIBTMA), were selected because they induced the least and the most mature DC phenotype, respectively. These pMAs were used to elucidate the activation profiles of transcription factors in DCs after biomaterial treatment and were compared to the iDC and mDC controls. In addition, a combined treatment of pHEMA and LPS was also included to determine if pHEMA could maintain an iDC phenotype in the presence of LPS. Interestingly, pIBTMA induced DC maturation primarily through the activation of NF-κB, while pHEMA mediated suppression of DC maturation through multiple TFs, including the activation of ISRE, E2F-1, GR-PR, NFAT, and HSF. GR-PR and E2F-1 have been shown to be associated with the suppression of DC maturation; ISRE, E2F-1, and NFAT are linked to apoptosis induction; HSF regulates the production of heat shock proteins (HSPs) that induce DC maturation and inhibit apoptosis. The activation of HSF by pHEMA was most likely a natural defensive mechanism against the other apoptotic

signals. Therefore, pHEMA suppressed DC maturation through the induction of apoptosis. Surprisingly, in the presence of pHEMA, the effect of LPS was completely eliminated, suggesting that biomaterials can override the effect of soluble factors. The morphology and surface marker expression of DCs treated with these different biomaterials or controls were consistent with TF activation profiles (CHAPTER 7).

Overall, this research illustrates that biomaterial properties, within the chosen biomaterial space, can be correlated to DC phenotype and more importantly, can be used as predictors for relative levels of DC phenotype. Furthermore, the differential responses induced by different biomaterials were mediated through the distinct activation profiles of transcription factors. Together, these findings are expected to facilitate the design and selection of biomaterials that direct desired immune responses.

CHAPTER 1:   INTRODUCTION

Biomaterials are widely used as scaffolds for tissue-engineered constructs and as delivery vehicles for vaccines, both of which often combine biological and biomaterial components. The success of such engineered products relies on their ability to minimize or maximize host immune response, respectively. In addition to the non-specific inflammatory response against the biomaterial component, the biologics can induce antigen-specific immune response from the host. However, the potential of biomaterials to modulate the specific immune response towards the antigens associated with the biological component, through an adjuvant effect, has only been recently explored [3,4].

Biomaterials commonly used in combination products were previously shown to differentially affect DC phenotype *in vitro*. Specifically, PLGA and chitosan films promote DC maturation, agarose films maintain an iDC phenotype, and hyaluronic acid films promoted an even more immature phenotype [5,6]. In addition, PLGA, but not agarose, enhanced the humoral immune response towards a co-delivered antigen *in vivo* in a murine model through a biomaterial adjuvant effect [3,4]. These studies suggested that biomaterials can be employed to modulate DC phenotype, thereby controlling the associated *in vivo* host immune response towards the biologic components in combination products. However, the biomaterial systems used previously were not sufficient in determining which material properties directed the distinct DC response. Therefore, well-characterized material systems and combinatorial libraries of polymers are expected to allow for the elucidation of correlations between DC phenotype and material properties, which will provide guidelines for immuno-modulatory biomaterial design for both tissue engineering and vaccine delivery applications.

However, the assessment of DC maturation by flow cytometry is a time-consuming process that is suitable to evaluate only a limited number of biomaterials. As a result, a high-throughput (HTP) methodology to study DC phenotype is desired to facilitate the derivation of biomaterial property-DC phenotype relationships as well as the development of computational models for predicting DC response from material properties. Furthermore, although toll-like receptors (TLRs) and integrins have been recently shown to play a role in mediating DC response, the exact mechanisms by which DCs recognize and respond to biomaterials remain to be elucidated.

The objectives of this thesis research were to derive DC phenotype-biomaterial property relationships and to correlate DC response to biomaterials with activation profiles of transcription factors. The *central hypothesis* was that using well-defined biomaterial systems with controlled variations in material properties, correlations can be drawn between material properties and DC response. More specifically, DCs respond to the biomaterials differentially due to the different material properties, which result in differential presentation of proteins on the surfaces as shown previously [7]. It was hypothesized that different biomaterials trigger differential DCs respond through signaling pathways leading to distinct activation profiles of transcription factors.

The overall objectives were accomplished by testing our central hypothesis in the following specific aims:

Specific Aim 1: Validate a 96-well filter-plate-based, high-throughput screening methodology to assess the effects of biomaterials on dendritic cells. The *working hypothesis* was that DC treated with biomaterials in a 96-well format would respond similarly as the DCs treated in the conventional 6-well format with the results obtained by the fluorescent plate reader for CD86 expression (DC maturation) being equivalent to the flow cytometry analysis, in this way validating the HTP analysis.

Different cell fixation schemes were examined to choose the best fixation method for DCs in the filter plate method. Cell normalization methods by DC-specific markers, including CD1c and DC-SIGN, were investigated. The assessment of DC maturation by the filter-plate methodology was compared to the conventional flow cytometric analysis. Finally, biomaterials with known effects on DC maturation were used to validate the HTP methodology by comparing the results to conventional flow cytometric analysis.

Specific Aim 2: Correlate DC phenotype upon treatment with biomaterial surfaces of controlled changes in material properties using the high-throughput screening methodology. The *working hypothesis* was that correlations between DC maturation and material properties could be derived using controlled biomaterial systems.

Through collaboration with Drs. Barbara Boyan and Zvi Schwartz at Georgia Institute of Technology, titanium (Ti) disks of distinct surface roughnesses, hydrophilicity, and chemistry were used to study DC phenotype. DC response was assessed by maturation marker expression using flow cytometry, cell morphology using scanning electron microscopy, and cytokine profiles by multiplex bead-based cytokine assay based on the Luminex xMAP technology. Principal component analysis was used to confirm the differential responses induced by the different Ti surface and derive material property-DC response relationships.

Through collaboration with Dr. Joachim Kohn at Rutgers University, two combinatorial libraries of polymers, namely, a pMA library and a methacrylate- and acrylate-based terpolymer (simplified as "terpolymer") array were used to further study the correlations between DC phenotype and biomaterial properties. Twelve polymers from each of the libraries were selected. Material properties characterized included a) surface roughness (R_a and/or S_a), b) contact angle, c) T_g, and d) surface chemical composition for both libraries. For the terpolymer library, additional characterization was carried out, including water modulus and time of flight secondary ion mass

spectroscopy (ToF-SIMS). DC phenotype was characterized using the HTP method developed in Specific Aim 1, which provided surface maturation marker information as well as cytokine profile data. PCA was then performed on the DC phenotype data derived from the pMA library to discover covariations between material properties and DC phenotype. Furthermore, several partial linear squares regression (PLSR) models were developed using the pMA library as the training set and the terpolymer library as the prediction set. PLSR models aimed to optimize the correlations between X and Y data matrices, where X included the material property information and Y contained DC phenotype data.

Specific Aim 3: Correlate biomaterial-induced DC response with activation profiles of transcription factors. The *working hypothesis* was that using the pMA library and the HTP method, pMAs that induced the two extremes of DC phenotype (mature or immature) could be identified, and the differences in DC behavior to material properties could be mediated by distinct activation profiles of transcription factors. Two pMAs, polyhydroxyethylmethacrylate (pHEMA) and poly(isobutyl-*co*-benzyl-*co*-terahydrofurfuryl)methacrylate (pIBTMA), were chosen from Specific Aim 2 because they induced the least and most mature DC phenotype, respectively. The activation profiles of eight transcription factors, including NF-κB, ISRE, AP-1, E2F-1, CREB, GR/PR, NFAT, and HSF, induced by these two pMAs were analyzed and compared to the TCPS-treated immature DC (iDC) or LPS-treated mature DC (mDC) control. Specifically, nuclear extracts were prepared from differentially treated DCs and were quantified for the binding of target transcription factors to specific DNA probes. The morphology and surface marker expression of differentially treated DCs were also assessed to further confirm the effects of the two pMAs on DCs.

CHAPTER 2:   RESEARCH SIGNIFICANCE

As of 2005, in the United States, there were nearly 90,000 patients registered to receive 95,000 organ transplants. However, the total number of available organs for transplantation was approximately 27,000 (Transplant Statistics: The Organ Procurement and Transplantation Network / The Scientific Registry of Transplant Recipients). Furthermore, the current national healthcare costs are in excess of $1.5 trillion annually, or 13% of Gross Domestic Product (GDP). With the ageing population, it is estimated that 25% of the U.S. GDP would be contributed to health care by 2040 (U.S. Department of Health and Human Services).   As a result, health care economics are now driving industry to produce cures and vaccines rather than simply therapies, and tissue engineering and preventative medicine have emerged to be prospective alternatives to organ transplantation and a means to prevent diseases, respectively[1,8,9].

Biomaterials are widely used as the carriers of biologics in combination products for tissue regeneration [10,11] or vaccine delivery [12]. In order for tissue engineered devices to reach their full therapeutic potential, they must be accepted by the host to integrate in a fully functional manner.   In contrast, vaccine delivery seeks to enhance or maximize a protective immunity.   These devices may evoke both an adaptive immune response against the biologics and a non-specific inflammatory response against the biomaterial component. The success of such products relies on their ability to minimize or maximize host immune response, respectively.

Biomaterials commonly used in tissue engineering or vaccine delivery were previously shown to differentially influence DC phenotype *in vitro* [5,6], which were translated into corresponding *in vivo* humoral response against a co-delivered antigen [3,4]. Understanding how biomaterials elicit such distinct DC responses will facilitate the design and selection of future biomaterials for tissue engineering or vaccine delivery,

where distinct and optimal immune responses are desired. However, the material systems used in previous studies were not sufficiently controlled to determine which material properties contributed to such differential effects.

The objectives of this research were two-fold. First, it aimed to derive correlations between material properties and DC phenotype as well as to develop computational model for predicting DC phenotype based on material properties. Second, this research sought to correlate DC's response to biomaterials with the profiles of transcription factor activation. With the understanding of DC phenotype-material property relationships, the computational models developed could predict DC response based on the chemical composition of the polymers, which is expected to expedite future biomaterial design for immunomodulatory effects on DCs. Such predictive models will reduce research costs overall because they allow for rational selection of biomaterial formulations before any synthesis, characterization, and biological experiments are performed. Furthermore, the understanding of the transcription factor activation profiles upon biomaterial treatment will facilitate the design of biomaterials that can trigger the activation of certain TFs. Specifically, for tissue-engineered devices or modulation of transplant rejection, biomaterials that trigger the activation of immunosuppressive TFs should be selected. In contrast, for vaccine delivery or cancer therapy, biomaterials that can trigger strong activation of immunostimulatory TFs should be selected for maximal and effective immunity.

CHAPTER 3:   LITERATURE REVIEW[*]

3.1. Innate and adaptive immunity

Vertebrates are protected by two systems of immunity: innate and adaptive. Innate immunity serves as the first line of defense against foreign entities that is achieved by conserved effector functions such as complement activation to mark foreign entities with activation fragments [13] that can be recognized by phagocytes [14,15] for clearance and destruction of the invader. It is a rapid and non-specific response by the host to clear the foreign pathogens or materials, to repair tissue damage and to remove apoptotic cells [16-18]. The complement system is composed of a set of plasma proteins that can bind to the pathogen surfaces leading to proteolytic cleavage, whose fragments mediate an inflammatory response, pathogen recognition by phagocytes and ultimately resulting in cell lysis through the membrane attack complex [19,20]. The recognition of pathogens by these phagocytes results in the release of cytokines and chemokines that attract monocytes and neutrophils to infiltrate into the infected tissues from circulation and initiate the inflammatory response [21].

Host organisms can also detect the presence of pathogens by recognizing a limited number of conserved structures, called pathogen-associated molecular patterns (PAMPs), associated only with micro-organisms [22,23]. Professional APCs including DCs and MΦs bind to PAMPs via pattern recognition receptors (PRRs) [24]. The ligation of PRRs often results in activation of the APCs for their enhanced abilities to stimulate T cells, which then causes the direct lysis of the infected cells by cytotoxic T cells, or activation of B cells to differentiate into plasma cells and synthesize antigen-specific antibodies [25,26]. An important family of PRRs is the toll-like receptors (TLRs) family, which, for

---

[*] Adapted and Modified from Kou PM and Babensee JE. Macrophage and dendritic cell phenotypic diversity in the context of biomaterials. *Journal of Biomedical Materials Research Part A*, 96:239-260 (2011).

mammals, has 13 members in different cellular locations (both intra- and extracellularly) and has specificity to a broad array of microbial epitopes [25,27-31]. Other PRRs on DCs include C-type lectin receptors (CLRs), which bind to carbohydrates [32,33] and scavenger receptors, which has broad specificity to a variety of polyanionic ligands [27]. In addition to these receptors, DCs can also recognize intracellular pathogens or pathogenic components with nucleotide-binding oligmerization domain (NOD) proteins[34], retinoic acid-inducible gene I (RIG-I)-like receptors such as melanoma-differentiation-associated gene 5 (MDA5, also known as Ifih1 or helicard) [35] and RIG-I and DNA-dependent activator of interferon-regulatory factors (DAI) [36].

3.2. Dendritic cells

Since the initial discovery of DCs by Steinman and Cohn [37], DCs have been demonstrated to play a pivotal role in the host responses to a variety of foreign entities [38]. Dendritic cells are sparsely but widely distributed APCs of hematopoietic origin that are specialized in the uptake, transport, processing and presentation of antigens to T cells [39-41]. Among APCs, which also include MΦs and B cells, only DCs are believed to be capable of stimulating naïve T cells [42]. Approximately 10 years ago, monocytes, initially thought to be the precursors of MΦs *in vivo*, were also found to migrate to injured sites and differentiate into DCs [43] in response to granulocyte-MΦ colony-stimulating factor (GM-CSF) and IL-4 [44,45]. Interestingly, in the presence of fibroblasts, which generate IL-6, monocytes differentiated into MΦs despite the presence of GM-CSF and IL-4 [46]. Thus, IL-6 may play a role in regulating the development of monocytic DCs and MΦs. Analogous to MΦ's M1 and M2 phenotypes, DCs can be induced into an inflammatory or a tolerogenic phenotype [47] (Figure 3-1).
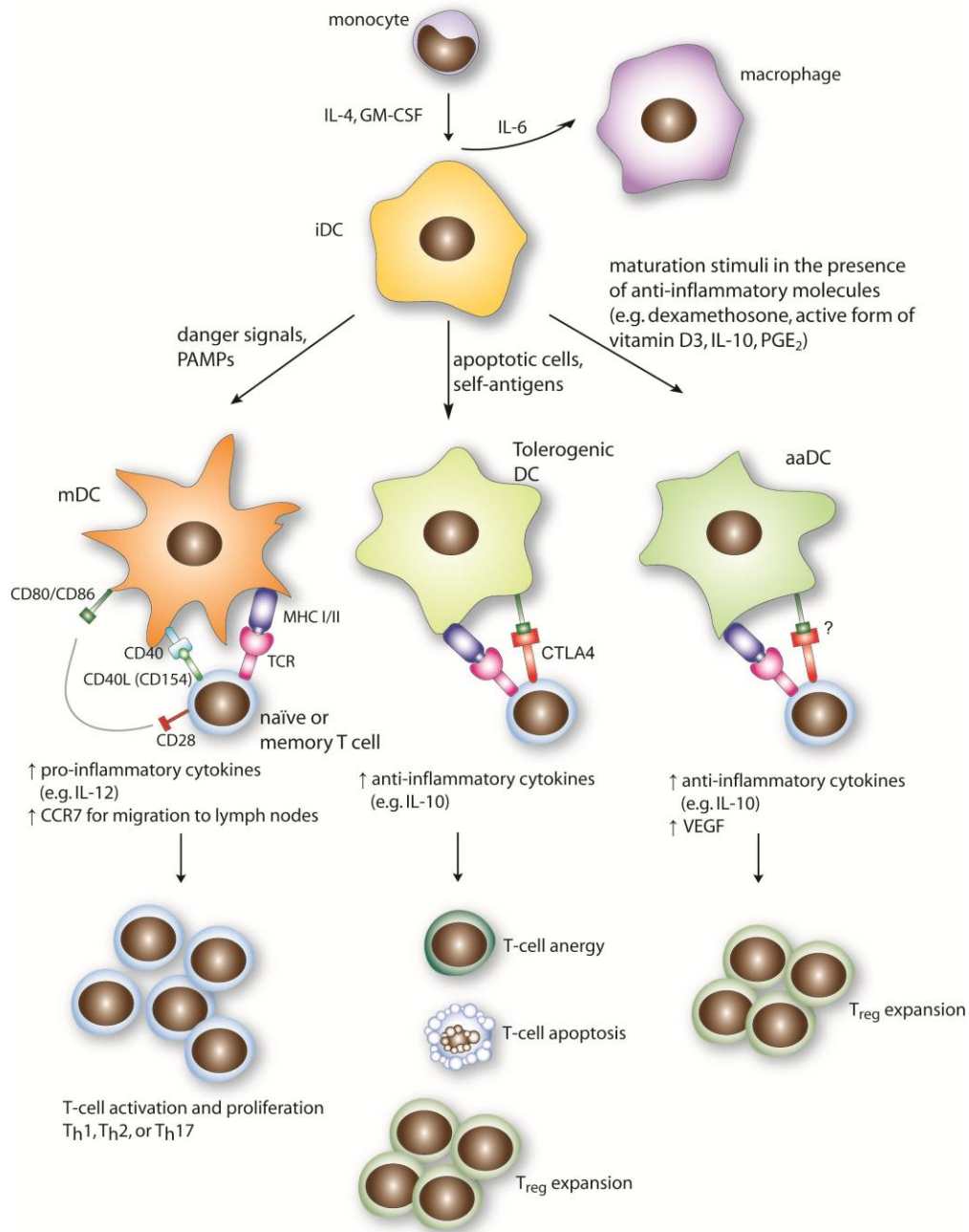
Figure 3-1: Different subsets of monocyte-derived DCs, their inducers, phenotype, and functions. Immature DCs (iDCs) can be derived from monocytes in the presence of IL-4 and GM-CSF. IL-6 may maintain the differentiation of monocytes into MΦ despite the presence of IL-4 and GM-CSF. DCs can acquire different phenotypes in response to stimuli. Danger signals and PAMPs can activate iDCs into classical mDCs that express higher levels of costimulatory molecules (CD80/86 and CD40), MHC class II molecules, release pro-inflammatory cytokines, migrate to the lymph nodes and stimulate naïve or memory T cells. During the steady state, tolerogenic DCs are naturally actively induced in response to apoptotic cells and self-antigens. These tolerogenic DCs release anti-inflammatory cytokines such as IL-10 and induce T-cell anergy, T-cell apoptosis and/or T_{reg} expansion. DCs can also be alternatively activated by anti-inflammatory molecules such as dexamethosone and IL-10. These aaDCs have been shown to release anti-inflammatory cytokines, induce T_{reg} expansion and promote angiogenesis.

3.2.1. Inflammatory DCs (of myeloid origin)

In the immature state, DCs act as sentinels in peripheral tissues, constantly sampling their microenvironment for potentially dangerous or foreign antigens and self/non-self proteins [41,48]. Immature DCs take up antigens through actin-dependent process of phagocytosis for particulate antigens and macropinocytosis or receptor-mediated endocytsis for soluble antigens [48,49]. The receptors involved in endocytosis of pathogens include Fc receptors for antigen-antibody complexes, CLRs for glycans and complement receptors for complement fragment-coated pathogens. Interestingly, CLRs and TLRs undergo cross-talk; that is, the binding of a ligand to one receptor can modulate or fine-tune the immunological outcome that arises from the binding of another ligand to the other [50]. Fc and complement receptors (CRs) are expressed on DCs and their expression alters upon DC activation. For instance, during DC maturation, the percentage of CR3 positive cells decreased. CR3 (CD11b/CD18) and CR4 (CD11c/CD18) recognizes iC3b, the ligation of which facilitates antigen uptake. In addition, DCs express FcγRs, FcαRs and FcεRs. Binding of these FcRs to immobilized immunoglobulins leads to different DC responses [51]. For example, the ligation of CD32a (FcγRIIa), but not CD32b (FcγRIIb), with immobilized IgG induces DC maturation [52]. Furthermore, immature and mature DCs themselves can produce complement components C1q, C7, C8 and C4b binding protein [53,54]. The presence of complement component, C3, is also important in supporting functional DC differentiation and maturation in response to LPS *in vitro* [55]. Understanding the functions and interplay of these receptors and complement components during innate immune responses will provide insights into how DCs regulate immunity and tolerance.

In addition to mediating the endocytosis of antigens, the recognition of pathogens by PRRs initiates signaling cascades (e.g., activation of NFκB, AP-1, MAPK and others) that leads to the maturation of DCs, which results in the change of morphology, the up-regulation of co-stimulatory molecules (notably CD80 [B7.1] and CD86 [B7.2] in the B7

family) and MHC class I and II molecules and the release of pro-inflammatory cytokines [49,56]. Activated DCs transiently enhance antigen uptake but down-regulate their endocytic capacity after several hours [57,58] through the inactivation of a required rhoGTPase called Cdc42 [59]. Furthermore, DCs express different chemokine receptors at different stages of maturation. Immature DCs express "inflammatory" chemokine receptors such as CCR2, CCR5, CCR6, CXCR1 and CXCR2 that allow them to respond to the chemokines released at the sites of inflammation. Upon encountering maturation stimuli, DCs down-regulate the "inflammatory" chemokine receptors, up-regulate CCR7 and migrate towards draining lymph nodes where they prime naïve T helper (T_h) cells. CCR7, which regulates chemotaxis and migratory speed, binds to the chemokine, CCL21, expressed on the endothelial cells lining the lymphatic vessels and to CCL19 expressed on the T cell area of the lymph node [60,61]. Matrix metalloproteinase-9 (MMP-9) was demonstrated to be involved in DC migration through epithelial tight junction [62].

Besides PRR ligands, extracellular matrix (ECM) proteins have also been found to affect DC phenotype. For example, type I collagen, but not fibronectin or laminin, induced a fully matured DC phenotype, including the up-regulation of co-stimulatory molecules and enhanced allostimulatory capacity [63,64]. Furthermore, DCs possess many adhesion molecules such as the β_1-integrin (CD29/CD49) [65] and β_2-integrin family (CD11/CD18) [65,66]. These integrins mediate interactions between DCs and the ECM and may modulate DC phenotype. Recently, the β_2-integrin, CD18, was suggested to play a role in regulating DC behavior [67]. The maturation of DCs is a continuous process initiated in the periphery upon the encounter of antigens and the balance of pro- and anti-inflammatory cytokines and completed during the DC-T cell interaction in the secondary lymphoid organs [49,68].

In the secondary lymphoid organs, mature DCs provide three signals to T cells to trigger their clonal expansion: "Signal 1" is the binding of antigen-loaded MHC molecule

with the T-cell receptor (TCR); "Signal 2" derives from the costimulatory molecules from mature DCs; "Signal 3" generates from cytokines that the cells secrete [58]. These signals also function to instruct the polarization of T cells and tune the immune response by modulating the amplitude or the type of the response depending on the type of pathogen [69]. In a 3D collagen matrix model, DC/T cell interactions were shown to be dynamic and short lived, and these repetitive short-term contacts trigger signaling for effective antigen presentation [70]. Furthermore, priming of T cells was inhibited in mindin deficient mice, suggesting that efficient T cell priming depends on the ECM protein mindin [71].

The selection of effector immune functions is controlled by antigen-specific T_h cells, which include T_h1-, T_h2-, T_{reg}- and the recently discovered T_h17-type cells at different ratios [58,72-74]. The most potent T_h1 response inducer is thought to be IL-12, whose source seems to be restricted to the populations of APCs. IL-12 directs the development of T_h1 cells that express the T-box transcription factor T-bet and produce high amounts of IFN-γ. In contrast, IL-4 directs T_h2 response, causing the T_h2 cells to express the zinc-finger transcription factor GATA3 and secret IL-4 [75]. More recently, pro-inflammatory cytokine IL-23 was shown to take a prominent role in the expansion of IL-17 secreting T cells and hence the name T_h17 response [74]. These T_h cells are differentially regulated and have distinct functions in immunity. The antigen-specific T_h2 cells that are activated by DCs can secret a copious amount of IL-4, which supports B-cell production of antibodies [58]. In contrast, the T_h1 cells can be activated by DCs to generate cytotoxic T cells [76]. T_h17 cells are important in fighting bacterial and fungal infections [74]. T_{reg} cells keep immune response in check and prevent autoimmunity [77]. Hence, DCs not only play a crucial role in bridging innate and adaptive immunity, but they also possess the capability to direct a particular pathway of immune response. The balance of these T_h responses is critical in maintaining effective immunity and homeostasis.

3.2.2. Tolerogenic dendritic cells

When DCs capture immunogenic antigens, it is likely that they also process and present self-derived and harmless environmental antigens to T-cells. If the presentation of such self or environmental antigens induces adaptive immune response, autoimmunity or chronic inflammation against harmless agents may be developed. As a result, intrinsic or extrinsic mechanisms have evolved to induce different types of peripheral tolerance. Dendritic cells induce deletion or anergy of T-cells in the thymus in the intrinsic mechanism, or regulatory T cells (T_{reg}) in the extrinsic mechanism, respectively [77,78]. DCs pulsed with low doses of blood-borne circulating C5 protein were able to delete C5 reactive transgenic thymocytes in culture, and they were also evidenced to induce deletional tolerance *in vivo*, which delineates the role of DCs in central tolerance [79,80]. In peripheral tolerance, T_{reg}s express high affinity IL-2 receptor (CD25) and transcription factor, forkhead box P3 (Foxp3), secrete copious amount of IL-10 and have a suppressive role in host responses [73,81,82]. DCs that express low levels of CD80/CD86 are able to induce Foxp3$^+$ T_{reg} from Foxp3$^-$ precursors and induce abundant IL-2 from the T-cells in the presence of TGF-β, whereas other APCs failed to stimulate IL-2 secretion and T_{reg} expansion [83,84]. Low doses of soluble antigens targeted to DCs at steady state can induce peripheral tolerance through the deletion of naïve peripheral T cells [77]. Apoptotic cells, rather than necrotic cells, can also trigger the apoptosis of cytotoxic cells as well as the induction of T_{reg} and T_h2 cells, resulting in tolerance [85]. It has been shown in an *in vivo* model that the induction of peripheral CD8$^+$ T cell tolerance depends on PD-1 and CTLA-4 [86]. Therefore, DCs are specialized APCs that can actively induce the formation of T_{reg}s in the periphery and play a central role in immunological self-tolerance. These DCs that develop naturally to prevent autoimmunity are tolerogenic DCs. In order to generate DCs with tolerogenic phenotype for therapeutic applications, various strategies have been developed to induce regulatory DCs, or often called alternatively activated DCs.

3.2.3. Alternatively activated DCs (aaDCs)

In contrast to the DC maturation-inducing PAMPs, many agents were found to suppress DC maturation, inducing a tolerogenic phenotype, in both human and mice. These "alternatively activated" DCs, or "regulatory DCs", are generally characterized by low allogeneic T cell stimulation and low expression of maturation markers and co-stimulatory molecules [77]. For instance, glucocorticoids such as dexamethasone, methylprednisolone and prednisone severely impeded the differentiation and antigen-presentation capability of DCs [87]. Another well-known example is IL-10, which induced immature DCs into tolerogenic APCs *in vitro* and inhibited ovalbumin-specific T cell proliferation in an *in-vivo* mouse model [88]. Murine bone marrow-derived DCs treated with IL-10 and TGF-β secreted IL-10, induced Foxp3$^+$ T$_{reg}$ expansion, induced alloantigen-specific hypo-responsive T cell proliferation and prolonged the survival when delivered in a donor-strain heart graft by co-stimulatory blockade with CTLA4-Ig [89]. Interestingly, human DCs that matured in the presence of calcitriol, PGE$_2$, or IL-10 produced higher level of the pro-angiogenic cytokine VEGF as compared conventionally activated DCs that were only treated with LPS [90], suggesting that aaDCs may participate in wound healing by promoting angiogenesis − an interesting link between immunity and regeneration.

In addition, a new subset of regulatory DCs, termed diffDCs, was discovered by co-culturing mature DCs with splenic stroma. The diffDCs were found to maintain immune homeostasis by activating NK cells, which in turn kill surrounding diffDCs [91,92]. Human monocyte-derived DCs treated with anti-inflammatory molecules such as dexamethasone, 1α,25-dihydroxyvitamin D3 (the active form of vitamin D3), in the presence of LPS acquired a semi-mature phenotype and anti-inflammatory cytokine profile. These DCs primed both naïve and memory T cells to inhibit primary CD4$^+$ and CD8$^+$ T cell responses; however, these aaDCs were not able to induce Foxp3$^+$ T$_{reg}$ expansion [93]. A semi-mature state of DCs may also be induced by the ligation of

signal-regulatory protein-α (SIRP-α) to CD47 on DCs. After the treatment, DCs first appeared to become mature and migratory, but at later time points, DCs reverted back to their immature-like state. Such a semi-mature stage may represent a checkpoint for the regulation of DC maturation [94]. The identification and development of non-pharmacological biomaterial-based means of obtaining DCs with distinct functional phenotypes is a powerful strategy to control immune and wound healing responses.

3.2.4. Modulation of dendritic cell phenotype by innate immune cell types

The cells from innate immunity have been demonstrated to modulate DC maturation. Co-culture of activated platelets with DCs induced the up-regulation of CD80, CD86 and ICAM-1 by DCs to a level similar to LPS-stimulated maturation. Activated platelets also enhanced the production of IL-12 and IL-6 by DCs [95]. Such activated platelet-induced DC maturation might have been mediated through CD154 and may suggest a link of blood coagulation to adaptive immunity by the maturation of DC. Interestingly, platelets had a neutralizing effect by binding Gp96, a heat shock protein released from cells after tissue damage, thereby modulating Gp96-induced DC maturation. This may represent a control mechanism by which HSP-induced DC activation is limited locally during wound healing processes [96]. In addition, activated neutrophils were shown to induce DC maturation and enabled these DCs to trigger strong T cell proliferation and T_h1 polarization by the interaction of the C-type lectin, DC-SIGN on DCs and Mac-1 (CD11b/CD18) on neutrophils [97]. Furthermore, antigens from live and from apoptotic neutrophils could be acquired by DCs, which then elicited antigen-specific T cell responses [98]. These insights suggest that cross-talk between innate immune cells with DCs can lead to modulation of adaptive immunity.

3.3. Dendritic cell response to biomaterials

Unlike macrophage (MΦ) response to biomaterials, which has been investigated for decades, DC response to biomaterials has only recently been studied, beginning in the context of adjuvant effects of biomaterials in combination products on associated immune responses. An increasing number of combination products that incorporate both biomaterial and biological components have been designed for tissue-engineering and vaccine delivery applications [1,99-102]. While the biomaterial component elicits a non-specific inflammatory response that is mediated through a number of components such as platelets, polymorphonuclear cells and MΦs, the immunogenic biological component may induce an antigen-specific immune response [1]. Because DCs are the most potent antigen-presenting cells (APCs) that can activate naïve T-cells, and because the primary mechanism by which adjuvants enhance an adaptive immune response is the maturation of APCs, primarily DCs, the effect of biomaterials on DCs has been investigated. Conversely, because DCs are central in inducing T_{reg}s, their ability to induce tolerance is emerging as a significant area for research for tissue engineering/transplantation applications in which biomaterials are used.

3.3.1. Biomaterials in combination products

Since the advent of "tissue engineering" in 1987, it has demonstrated a potential of revolutionizing treatment and therapies for patients [103]. Tissue-engineered devices are typically composed of biomaterial and biologic components [1,99]. Polymers are increasingly favored to be the biomaterial component because of their high processibility and controllable degradability [104]. For example, polymeric biomaterials have been used as a scaffold to bridge peripheral nerve gaps [105], to encourage vascularized tissue growth[106], and to repair bone defects [107]. In addition to tissue-engineered constructs, polymers have also been widely used as carriers for biologic drugs, nucleic acids, and vaccines [100-102]. However, the process of implantation and delivery of the

biomaterial results in an injury to host tissues, which perturbs the homeostatic mechanisms and leads to wound healing, a classical outcome of an innate immune response [108]. The biologics, such as cells and proteins, if immunogenic, may be a source of antigens from the biomaterial carriers and initiate a specific adaptive immune response [1]. Elucidating how the presence of biomaterials alters the host immune response to co-delivered biologics will provide insight into improved modulation of host response against combination products.

3.3.2. Biomaterial adjuvant effect on DCs

Biomaterials were previously shown to have an adjuvant effect that enhances the immunogenicity of a model antigen, ovalbumin (OVA). OVA adsorbed on non-biodegradable polystyrene microparticles (MPs), or OVA co-delivered in biodegradable 75:25 Poly(lactic-*co*-glycolic acid) (PLGA) MPs or scaffolds (SCs) were found to support a moderate humoral immune response that was maintained for the 18-week duration of the experiment, and the response was primarily T_h2 response as indicated by the predominant IgG1 isotype [2]. The OVA co-delivered PLGA SCs induced a higher and longer lasting humoral response, while the MP counterpart induced a more transient response [3]. Such enhanced immune response is presumably due to the implantation-associated tissue injury that released "danger signals", which act as endogenous adjuvants [3]. Upon tissue injury, HMGB1, a potent danger signal, is released by necrotic cells [109] and is found at higher concentration in exudates from subcutaneously implanted PLGA SCs in comparison to naïve control [110]. This result suggested the possible role of danger signal biomaterial-induced adjuvant effect.

3.3.3. Biomaterials affect DC phenotype

Treatment of human monocyte-derived DCs with PLGA MPs or films induced enhanced expression levels of costimulatory molecules (CD40, CD80, and CD86), MHC

17

class II molecules (HLA-DQ and HLA-DR) and DC maturation marker (CD83) as compared to the untreated immature DC (iDC) control, but to a lesser extent as compared to the LPS-treated positive mature DC (mDC) control [111]. PLGA-treated DCs possess dendritic processes resembling those on mDCs and enhanced allostimulatory capability to stimulate T-cell proliferation in a mixed lymphocyte reaction (MLR) [111]. A study investigating the different effects of PLGA and agarose on mouse bone-marrow derived DCs showed similar DC maturation in response to PLGA, but DC maturation of agarose-treated DCs was not significantly different from iDCs [112]. In addition, cytokine analysis showed that DCs treated with PLGA secreted higher amounts of TNF-α, IL-8, IL-6 and IL-10 than those secreted by agarose-treated DCs. Interestingly, DCs treated with PLGA MPs released increasing amount of these cytokines in a MP-dose dependent manner, but they produced low amounts of IL-1β and IL12-p70. Such biomaterial-induced DC maturation was found to require cell-biomaterial contact in a transwell assay [111].

Furthermore, a differential effect of DC maturation was induced by different biomaterials. More specifically, PLGA or chitosan films induced DC maturation while alginate and agarose did not and hyaluronic acid film exhibited suppressed DC maturation [113]. Mixed lymphocyte reaction showed that DCs treated with PLGA and chitosan films supported higher levels of T-cell proliferation as compared to iDCs, DC treated with hyaluronic acid films induced lower levels of T-cell proliferation, and DCs treated with agarose and alginate films did not differ from iDCs in allostimulatory capacity [114]. Surprisingly, both PLGA and agarose induced higher NFκB activation than iDCs, and the activation level is much higher in the DCs treated with agarose [6,112].

Importantly, biomaterial-specific *in vitro* induced DC phenotype could be translated into *in vivo* host responses by the studies that demonstrated that PLGA, but not agarose, enhanced the humoral immunity against a co-delivered model antigen *in vivo*

[3,4]. Clearly, biomaterials can affect DC phenotype and can be manipulated to modulate immune responses. However, the biomaterials used in these studies have very different properties and it is impossible to deduce which material properties are the most important in affecting DC phenotype.

In order to understand the correlation between biomaterial properties and DC maturation, materials with better defined surface chemistries were used to study the biomaterial effects on DCs. DCs were treated with self assembled monolayer (SAM) surfaces of alkanethiols with defined and distinct terminal groups (-CH$_3$, -OH, -COOH and -NH$_2$). Based on cell morphology, allostimulatory capacity or expression of maturation markers, all four SAMs elicited modest DC maturation in comparison with iDCs, while -CH$_3$ SAMs were found to be the least activating. However, these DCs secreted the highest levels of pro-inflammatory cytokines TNF-α and IL-6, which contradicts the least mature phenotype. The investigation into DC viability revealed that CH$_3$ SAMs supported fewer live human monocyte-derived DCs. The number of early apoptotic, late apoptotic and necrotic and nonviable cells was significantly higher on CH$_3$ SAMs than any other surface or controls. Surprisingly, CH$_3$ treated DCs induced higher expression of CTLA-4 on T-cells, which is a negative signal for T cell proliferation [115]. These results are opposite to those previously observed using MΦs wherein the CH$_3$ functional group induced more leukocyte adhesion and more fibrosis [116].

In addition to the treatment of DCs with biomaterial films, studies have also been carried out to investigate the interactions of DCs with porous scaffolds. The phenotype of DCs upon seeding the cells on PLGA or agarose scaffolds was examined. It was found that, similar to treatment of DCs with the film versions of these polymers, DCs treated with PLGA scaffolds displayed moderately mature phenotype with dendritic processes, elevated expression of maturation markers and increased secretion of pro-inflammatory cytokines to the level similar to cells treated with PLGA films, while agarose scaffold did not induce DC maturation [117]. It was also found that biomaterial

scaffolds engineered with proper lymphoid microenvironment allow DC migration and interaction with T-cells, which represents a promising strategy to create ectopic lymphoid tissue [118].

3.3.4. Mechanisms by which DCs respond to biomaterials

The exact mechanisms by which DCs recognize biomaterials remains to be elucidated. It is possible that complement, plasma proteins (with associated carbohydrate modifications) and other "danger signals" adsorb to the biomaterials, which are then recognized by the PRRs, primarily CRs, CLRs and TLRs, on DCs (Figure 3-2) [119]. Recent research using MyD88 and TLR knocked out mice demonstrated that DCs use TLR2, TLR4 and TLR6 for the responses to a group of chemically and physically diverse biomaterials [120]. Mice lacking any of these TLRs or MyD88 had impaired expression of activation markers and reduced production of pro-inflammatory cytokines relative to the wild type controls [120]. Recently, β integrins were shown to play a role in mediating DC adhesion and response to biomaterials [121]. The other receptors such as FcR and CR as well as their cross-talk with PRRs may also play a role in biomaterial-induced DC phenotype (Figure 3-2). ECM proteins adsorbed on tissue-culture polystyrene plates have been shown to affect DC morphology, cytokine production and allostimulatory capacity. For example, DCs cultured on collagen or vitronectin substrates released higher levels of IL-12p40, while DCs treated on albumin or serum-coated substrates generated higher amounts of IL-10 compared to other substrates. Higher levels of IL-12p40 release correlated with enhanced CD4$^+$ T cell priming and T_h1 response [122]. Therefore, intelligently engineered biomaterials may guide the presentation, orientation or conformation, of adsorbed proteins in such a way that these "biomaterial-associated molecular patterns (BAMPs)" either induce DC activation or tolerance against co-delivered antigens. Biomaterials represent an exciting non-pharmacological tool, by

which DC phenotype may be modulated to achieve a desired host immune response to combination products.
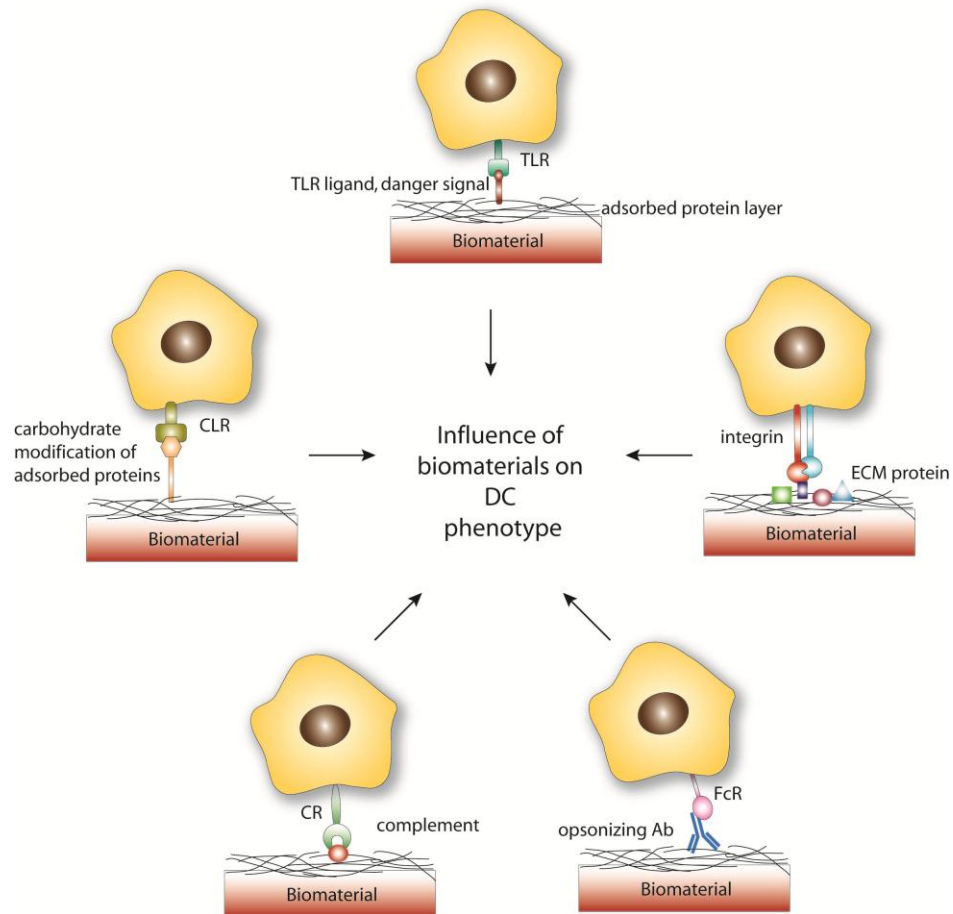
Figure 3-2: Possible mechanisms by which biomaterials influence DC responses. Complement and plasma proteins differentially adsorbed to the biomaterials are likely to be recognized by the PRRs, primarily TLRs and CLRs, on DCs. Other receptors such as FcR, CR, and integrins and their cross-talk with TLRs and CLRs may also play a role in biomaterial-induced DC phenotype.

3.4. Vaccines and adjuvants

Biomaterials have also been used to enhance immunogenicity of vaccines as alternatives to the only FDA-approved aluminum-based adjuvants. In addition to enhancing immunogenicity, adjuvants may also skew the response toward a particular type, such as humoral or cell-mediated immunity. This is of paramount importance because the immunity to different pathogens may require distinct types of immune

21

protection [69]. Many adjuvants have been developed to enhance the efficacy of vaccines, but their mechanisms have not been fully understood. Mineral salts (e.g. alum), liposomes and biodegradable polymer microspheres are believed to enhance immunogenicity by causing a depot effect at the site of injection [12,123], while others such as complete Freund's adjuvant (CFA) and incomplete Freund's adjuvant (IFA) act as immunostimulators [12,124,125]. Although CFA is a potent adjuvant, it is too toxic for human use [124]. To date, only alum, MF59 (oil-based emulsion) and monophosphoryl lipid A (MPL) are licensed for human applications [123]. Better and more effective adjuvants that can direct controlled T_h1 or T_h2 responses are desired and of great research interest.

3.4.1. DCs and biomaterial adjuvants

Because of DCs, as nature's responders to adjuvants, possess potent capability of activating naïve T-cells and initiating adaptive immunity, they have become the major target of vaccine design and development. Certain polymers, especially in particulate forms, have shown to act as adjuvants due to their ability to induce DC maturation [6,101,111,113]. Furthermore, block copolymers with both hydrophilic and hydrophobic domains were found to have increased adjuvant activity with higher percentage of hydrophobic monomers. It is possible that hydrophobic polymers activate DCs in a way that mimics the hydrophobic domains of PAMPs [119]. As proposed by Seong and Matzinger in the "hyppo hypothesis", although TLR ligands are different in structure, all of them have hydrophobic domains, which may function as "damage-associated molecular pattern" (DAMP) that trigger PRR activation [16].

Biomaterial MPs and nanoparticles (NPs) have been widely used in vaccine delivery. Particulate adjuvants cause pro-inflammatory cytokine IL-1β secretion from DCs when associated with LPS. Interestingly, processing of pro-IL-1β requires inflammasomes, complex intracellular proteins consisting of NALP3, ASC, CARD and

22

Casp1 and the uptake of particulate adjuvants by DCs activates NALP3 inflammasomes [126]. Furthermore, biomaterials may also be manipulated to modulate trafficking of the co-delivered immunogen, thereby controlling the efficiency of cross-presentation by DCs. Cross-presentation of immunogens is important in mediating cytotoxic CD8^{+} T cell response against intracellular pathogens. PLGA MPs encapsulated with OVA were able to induce CD8 response towards an exogenous antigen at antigen concentration of 1000-fold lower than soluble antigen and 10-fold lower than antigen-coated latex beads [127]. MPs, instead of NPs, were able to induce higher cross-presentation *in vitro*, possibly due to the fact that larger particles take longer to be degraded in the endosomal pathway and hence protect the antigen, to allow it to be available intracellularly for loading to MHC class I molecules [128]. However, in an *in vivo* study, NPs were shown to be more efficient in accessing DC population in the lymph nodes due to their readily being taken up into lymphatics after interstitial injection [129]. Therefore, a balance between uptake and cross presentation efficiency needs to be optimized for cytotoxic T cell response. In addition, pH-sensitive "smart" polymer has also been developed to protect the antigen from being degraded intracellularly [100]. Another strategy to shift the immune response to CD8 T cell response is to deliver silencing RNA (siRNA) against IL-10 to DCs. Co-delivery of siRNA and DNA antigens to DCs by MPs was shown to induce strong DC activation and T cell proliferation, switching the response to cytotoxic CD8 response [130]. Subsequently, a model DNA vaccine delivery system was developed using *in-situ* crosslinking hydrogels that only gel *in vivo* for the delivery of chemokines and MPs encapsulating siRNA against IL-10 and DNA antigen. Such system was shown to enhance DC recruitment to the MPs and effective IL-10 silencing [131].

A high-throughput MP microarray platform was recently developed to facilitate the optimization of particle-based vaccines for DCs. PLGA microparticles were printed on adhesive islands on a glass coverslip, and DCs cultured atop were found to co-localize

with the MPs. This platform may allow the assessment of the effects of a large array of MP formulations on DC function [132].

3.4.2. DC anti-tumor activity and DNA vaccines

Furthermore, DCs have been found to play a critical role in anti-tumor immunity. PLGA NPs co-delivering the poorly immunogenic melanoma antigen, tyrosinase-related protein 2 (TRP2) and TLR 4 ligand, 7-acyl lipid A, into mice with melanoma B16 tumors led to induction of TRP2-specific CD8 T cell response. Cytokine analysis revealed that these CD8 T cells were able to secret IFN-γ in lymph nodes and spleens. The tumor size in the immunized mice with co-delivered TRP2 and 7-acyl lipid A was also the smallest [133]. MΦ and DC uptake of biodegradable, pH-sensitive poly-β amino ester MPs was shown to be more efficient than PLGA MPs, suggesting that this polymer can cause higher transfection efficiency of the APCs and be a more effective non-viral genetic vaccine delivery vehicle. Mice bearing tumor vaccinated with DNA vaccine delivered by poly-β amino ester MPs had significantly smaller tumor size than control or PLGA DNA vaccine [134]. Self-gelling alginate matrix encapsulating activated DCs, CCL21, or SIY peptide was designed for its potential application in immunotherapy. Alginate gels containing activated DCs attracted both host DCs and T cells to matrix *in vivo*. In an adoptive transfer model, gels containing SIY peptide loaded DCs primed T cell response and recruited activated antigen-specific specific T cells to the matrix. In addition, these alginate gels facilitated cellular infiltration and possibly provided a milieu for efficient DC-T cell interactions. Such strategy may be an effective way to engineer "vaccination nodes" at tumor site to direct strong immune response [135,136].

The most recent research endeavor also started to consider the balance among different DC subsets for anti-tumor vaccine development. Macroporous polylactide-*co*-glycolide (PLG) matrices were fabricated and loaded with GM-CSF, CpG-rich oligodeoxynucleotide (CpG-ODN) and tumor lysate. These matrices were implanted into

subcutaneous pockets on the back of mice and were found to recruit higher ratios of $CD8^+$ cDCs and pDCs, which are DC subsets that collaborate to enhance cross presentation of tumor antigens in $CD8^+$ DCs to T_h1 cells and CTLs. The enhanced populations of $CD8^+$ cDCs and pDCs are correlated with increased IL-12 and IFN production, attenuation of $FoxP3^+$ T_{reg}s and immunosuppressive cytokines TGF-β and IL-10 and, most importantly, the decreased tumor growth and improved survival in mice bearing melanoma tumors [137]. This work shows that the balance of DC subsets is critical in the proper activation of effective immunity, and that biomaterials can be used as delivery vehicles for biologics that induce the preferential recruitment of target cell populations. However, it is still unclear if biomaterials themselves can be manipulated to recruit different DC subsets. Elucidating the effects of biomaterials on the recruitment of desirable DC populations will allow the use of the intrinsic properties of the materials alone without the incorporation of danger signals such as CpG-ODN.

Biomaterials have also been manipulated to induce mucosal immune responses using DNA vaccines. By control release of DNA using poly(ethylene-co-vinyl acetate), local mucus IgA production was induced for a prolonged period of time (8 weeks) in murine vaginal tract [138]. Other recent advances in the applications of biomaterials in vaccine design have been summarized in an excellent review [139].

Taken together, biomaterials represent a great tool for vaccine development because of their flexibility and multifunctionality. Biomaterials can be designed to be loaded with biomolecules, such as TLR agonists, chemokines, siRNAs and/or antigens, during preparation for controlled release of biomolecules; the biodegradability can be adjusted to reduce long-term fibrosis around implants; the porosity of a biomaterial scaffold can be manipulated to facilitate cell migration into the scaffold for antigen uptake or response to co-delivered biomolecules; and biomaterials that have intrinsic adjuvant effects (e.g. PLGA or chitosan) on DCs can be used to control DC phenotype and its associated immunological outcome. The biomaterial properties and their adjuvant

effects may be correlated to provide rational design of vaccines to induce a desired strength and type of effective immunity.

3.5. Biomaterial systems used to study cell response

The traditional mode of biomaterials design begins with the synthesis of a new material, followed by its characterization, and completed by the culturing of certain cells on it. However, this process for the discovery of a suitable biomaterial is slow; hence, the adoption of combinatorial and computational approaches to biomaterials design is desirable [140,141]. First, Anderson et al. developed an impressive nanoliter-scale synthesis of biomaterial combinatorial array of different compositions and observed distinct differentiation of human embryonic stem cells on those materials [142,143]. Second, microcontact printing and chemisorption chemistry were used to fabricate structures with controlled topography and hydrophobilicity/hydrophilicity to study cell behavior [144]. Although these are discrete biomaterial array systems, no defined wells were created to separate cells. As a result, the major drawback of these systems is their applicability to only strongly adherent cells. By contrast, continual biomaterial libraries have also been developed. For example, Meredith et al. created a system with continual changes of topography on glass slide with graded changes in chemical composition using blends of poly(D,L-lactide) (PDLA) and poly(ε-caprolactone) (PCL) by exploiting their lower critical solution temperature phase behavior, which generated a linear, homogeneous crystallinity (nanoscale roughness) gradient. They identified preferred microstructural feature sizes for UMR-106 (rat osteoblastic cell line) and MC3T3-E1 (mouse osteoblastic cell line) cells [145,146]. Similar systems were developed with poly(L-lactic acid) (PLLA) [147] or PLLA and PDLA [148]. In addition to these continual biomaterial systems, others have produced surfaces with well-defined biocompatible polymer brush nanostructures by using varying graft density of poly(2-hydroxyethyl methacrylate) (PHEMA) [149,150]. However, the continual nature of

material property variations on a single surface renders these systems unsuitable for loosely adherent cells such as dendritic cells.

Discrete combinatorial libraries in micro-liter plate formats have also been developed using sebacic acid and 1,6-bis(*p*-carboxyphenoxy)hexane (CPH) [151], tyrosine-containing polyarylates [152], polymethacrylates [153-155], or tyrosine-derived polycarbonates [156], the later three systems developed by Dr. Joachim Kohn at Rutgers University. Such systems utilize micro-liter plate to create isolation between biomaterials, and therefore are suitable for the study of non-adherent or loosely adherent cells such as DCs that cannot be studied using standard cell-based ELISA techniques. The libraries of tyrosine-containing polyarylates, polymethacrylates, and polycarbonates are of particular interest because of the extensive characterization performed on those polymer surfaces and the graded variations in material properties with little changes in chemistry [152-158]. More recently, Topochip, fabricated with polyethylene oxide/polybutyl terephthalate (PEO/PBT) or polylactic acid (PLLA) and each composed of 10,000 distinct topographies, has been developed [159]. This TopoChip system allows for the screening of cell response to nanotopographies in a high-throughput manner. Ti substrates represent another valuable biomaterial system for studying induced DC phenotype due to their well-defined microtopography and surface energy and have been shown to induce distinct responses of human osteoblast-like MG63 cells as well as normal human and rat osteoblasts [160-162].

CHAPTER 4: A HIGH-THROUGHPUT METHODOLOGY

FOR DC PHENOTYPE ASSESSMENT[†]

4.1. Introduction

Biomaterials are widely used as the carriers of biologics, such as cells, nucleic acids, and/or proteins, in combination products for tissue regeneration or vaccine delivery. These products may evoke both a non-specific inflammatory response against the biomaterial component and an adaptive immune response against the immunogenic biologics. Furthermore, the biomaterials also play a role in modulating the host responses due to their adjuvant or immunosuppressive effect. Obviously, the goal of tissue engineering is to minimize the host response to allow the proper functioning of the device and its integration to the host tissue. In contrast, vaccine delivery aims to enhance or maximize a protective immune response to the delivered antigen.

DCs have been hypothesized to be important in mediating the host response towards immunogenic antigens co-delivered with biomaterials. DCs are the most APCs that are specialized in the uptake, transport, processing, and presentation of antigens to T cells [41,163,164]. Using PRRs expressed on DCs, the ligation of pathogens or "danger signals" leads to the maturation of DCs [165,166]. Activated DCs transiently enhance antigen uptake but down-regulate their endocytic capacity after several hours [57,58], accompanied by a decreased expression of C-type lectin, DC-SIGN (DC-specific intercellular adhesion molecule-grabbing nonintegrin), which is primarily expressed in certain subsets of DCs, including monocyte-derived DCs [167].

The primary mechanism by which adjuvants enhance an adaptive immune response is the maturation of DCs, which results in their efficient antigen presentation

and T cell stimulation that generate an adaptive immune response to associated antigens. Although previous studies indicate that biomaterials commonly used in tissue engineering and vaccine delivery can modulate DC phenotype [6,113] via biomaterial adjuvant effect, it was unclear which biomaterial properties caused such differential effects. In order to translate a differential biomaterial effect on DC phenotype into design rules for biomaterials with distinct immunomodulatory effects, it is necessary to draw correlations between biomaterial physiochemical properties and effects on resultant DC phenotype using biomaterials with controlled graded variations in their properties in a combinatorial array. Such correlations will serve as criteria for the biomaterial design of combination products to modulate the host responses.

The assessment of DC maturation in response to biomaterials typically involves the treatment of immature DCs (iDCs) with biomaterials pre-placed in wells of a 6-well plate to allow for a sufficient number of cells for the assessment of DC phenotype using immunological assays such as flow cytometry for the expression of DC-specific or maturation surface markers or allostimulatory ability in a mixed lymphocyte reaction. Using extensive immunological assessment assays, the effect of different biomaterials on various aspects of DC phenotype and function have been assessed [6,111]. However, our conventional method would be time-consuming and require large quantities of reagents for the assessment of DC responses to large libraries of polymers. Hence, the goal of this research was to develop and validate a HTP methodology to assess DC phenotype upon the contact with combinatorial libraries of biomaterials with graded material properties.

The culture characteristics of DCs presented a unique challenge in that the DCs are loosely-adherent or non-adherent in culture; hence, a traditional cell-based Enzyme-Linked ImmunoSorbent Assays (ELISAs) could not be used due to expected cell loss during wash steps. To enhance the efficiency in sample processing and subsequent measurement, many cell-based assays have been processed in filter plates [168,169]. Such plates are 96- or 384-well standard-sized plates with an individual filter membrane

29

welded in each well. Because the fast and simple removal of supernatants is assisted by the application of a vacuum manifold, we expected that the filter plates would provide a suitable platform for the development of a HTP screening methodology for the simultaneous quantification of maturation markers of many DC samples. By far, black 96-well filter plates have offered the most promising means to rapidly wash the cell samples without any cell loss and offered fluorescence detection *in situ*. Therefore, here, we present the validation of a 96-well filter plate-based HTP screening methodology for DC phenotype upon biomaterial contact. Briefly, after treatment with biomaterials in a 96-well plate, the DCs are transferred to a black 96-well filter plate and stained with anti-CD86-PE and DC-specific anti-DC-SIGN-FITC monoclonal antibodies. The ratio of CD86-PE/DC-SIGN-FITC, or "maturation factor", is a DC number-independent parameter to represent DC maturation. The supernatants can be easily collected into a 96-well plate using a centrifuge, assayed for cytotoxicity, and stored for cytokine profiling. Figure 4-1 illustrates the experimental scheme of the conventional assessment of DC maturation as well as the filter plate-based HTP screening methodology.
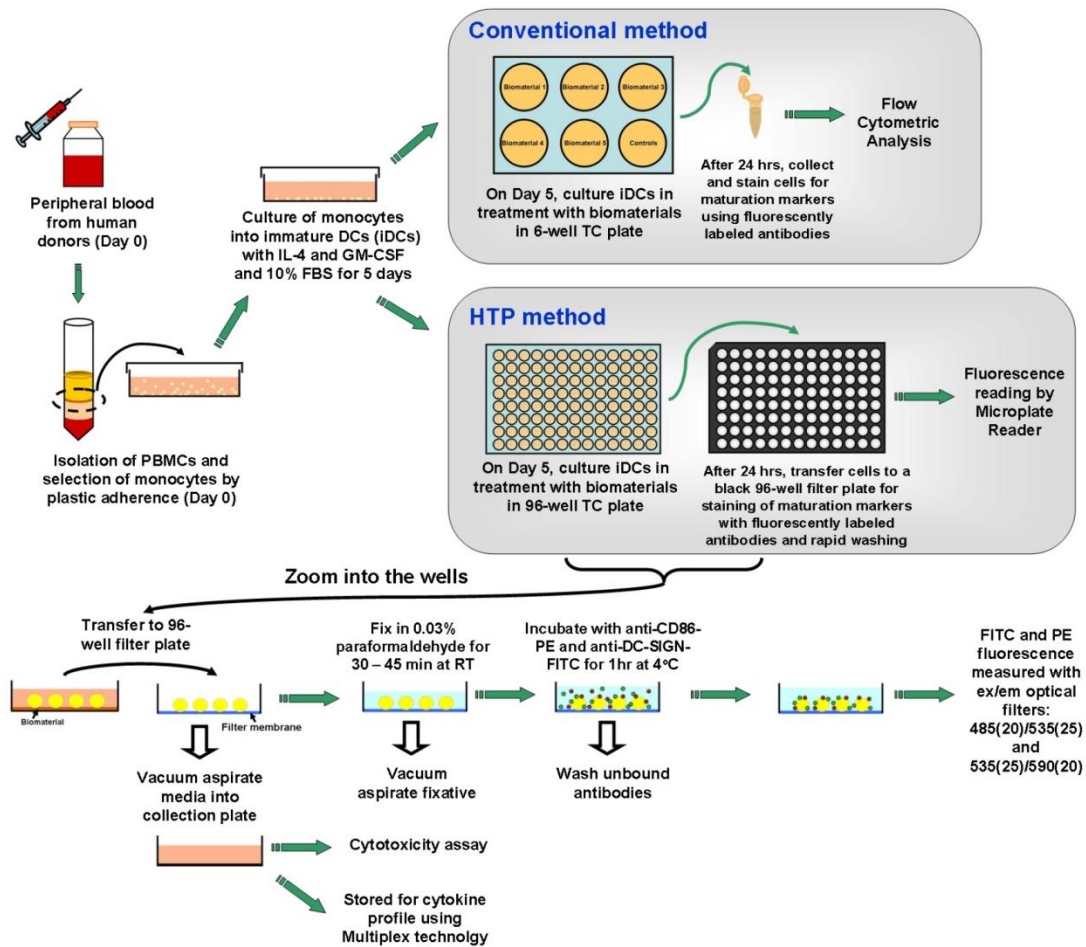
Figure 4-1: A schematic of the conventional method and the HTP method for analyzing DC response to biomaterials. For both of the analysis methods, DCs were derived from human peripheral blood mononuclear cells (PBMCs) using the same procedures until day 5. On day 5, for the conventional method, DCs were treated with biomaterials in a 6-well plate for 24 hours. The cells after treatment are then collected and stained, and flow cytometry is performed to analyze the cell surface marker expression. In contrast, for the HTP method, DCs are treated with biomaterials in a 96-well plate for 24 hours. On day 6, DCs are transferred to a 96-well filtration plate, fixed and then stained with anti-CD86-PE and anti-DC-SIGN-FITC antibodies for 1 hour and washed. The relative fluorescence intensity is subsequently measured by a Tecan Infinite F500 microplate reader. Simultaneously, the cell culture supernatants from each well can be aspirated into a collection plate and tested for cytotoxicity and stored for cytokine profiling using Multiplex technology.

4.2. Materials and methods

4.2.1. Derivation of immature DCs (iDCs)

Human blood was collected from donors with informed consent and heparinized (333 U/ml blood) (Abraxis Pharmaceutical Products, Schaumburg, IL) at the Student Health Center Phlebotomy Laboratory, in accordance with the protocol (No. H05012) of

the Institutional Review Board of Georgia Institute of Technology. Dendritic cells were derived from human peripheral blood mononuclear cells (PBMCs) using a previously described method [170] with some modifications. Briefly, the collected blood was diluted with a 1:1 ratio in Mg^{2+}- and Ca^{2+}-free phosphate buffer saline (D-PBS; Invitrogen, Carlsbad, CA), and peripheral blood mononuclear cells (PBMCs) were isolated by differential centrifugation using lymphocyte separation medium (Cellgro MediaTech, Herndon, VA). After the lysis of erythrocytes with RBC lysing buffer (155 mM NH_4Cl, 10 mM $KHCO_3$, 0.1 mM EDTA) and washing steps, PBMCs were resuspended at a concentration of 5×10^6 cells/ml in DC media, which was prepared by filter-sterilizing RPMI-1640 containing 25 mM HEPES and L-glutamine (Invitrogen), supplemented with a final concentration of 10% heat inactivated fetal bovine serum (h.i. FBS; Cellgro MediaTech, Herndon, VA) and 100 U/ml of Penicillin/Streptomycin (Cellgro MediaTech). The cells were plated in a volume of 10 ml/plate in a Primaria 100 $\times 20$ mm^2 tissue-culture dish (Becton Dickinson, Franklin Lakes, NJ) and incubated for 2 hours at 95% relative humidity and 5% CO_2 at 37^oC to select for adherent monocytes. After this incubation, the dishes were washed three times with warm DC media to remove non-adherent cells. The remaining adherent cells were supplied with 10 ml/plate new warm DC media, supplemented with 1000 U/ml GM-CSF and 800 U/ml IL-4 (PeproTech, Rocky Hill, NJ), and incubated for 5 days without changing the media to induce the differentiation of monocytes into iDCs. Immature DCs were treated with biomaterial films in the wells of 6-well or 96-well plates (the HTP methodology) with assessment of resultant DC phenotype using flow cytometry or fluorescent plate reader, as described in sections 4.2.3 or 4.2.4, respectively. As a part of culture characterization, DCs were purified using magnetic sorting based on manufacturer's protocol (Miltenyi Biotec, Auburn, CA). Briefly, the cell population harvested on day 5 of DC culture first underwent CD19^{+} B cell depletion (negative selection), followed by CD1c^{+} DC isolation (positive selection). The purity of DC population was approximately 95% or above.

4.2.2. Preparation of PLGA and agarose film

Poly(DL-lactic-*co*-glycolic acid) (PLGA, molar ratio: 75:25, inherent viscosity: 0.70 dL/g in trichloromethane, MW = 100,000 Da; Birmingham Polymers, Birmingham, AL) films were prepared by solvent casting without a porogen as previously reported [113]. Briefly, PLGA was dissolved 20% w/v in dichloromethane (DCM) overnight at room temperature and poured into a 50-mm Teflon dish (Cole-Parmer, Vernon Hills, IL) in a chemical fume hood. After evaporation of the solvent and drying to form films (48-72 hours), the PLGA films were punched to fit into the wells of a 6-well plate or a 96-well plate, followed by three washing steps using endotoxin-free water (Cambrex, East Rutherford, NJ) and UV sterilization for 30 min on each side in the tissue culture hood before iDCs were plated on them. Agarose (type V, high gelling, gel strength of $\geq$ 800g/cm^2 at 1.0%, MW unknown; Sigma, St. Louis, MO) was prepared to form 3% w/v aqueous solution by boiling of agarose in ddH$_2$O in a microwave until the agarose was completely dissolved. The films were prepared by dispensing 1 ml of agarose solution into a well of a 6-well tissue culture plate (Corning, Corning, NY), or 50 μl in a well of a 96-well tissue culture plate (Corning). The films were allowed to solidify at 4°C for at least 30 min and brought back to room temperature for another 30 min in a tissue culture hood without any further sterilization step prior to culturing iDCs on them. The endotoxin content of PLGA and agarose films was measured using a chromogenic substrate (QCL-1000 LAL assay; Cambrex) and determined less than 0.1 EU/mL, which is well below the FDA limit of 0.5 EU/ml [6,113]. Previous study showed that a minimum *Escherichia coli* endotoxin concentration of 100 EU/ml or 10 ng/ml was required for DC maturation [171].

4.2.3 Treatment of DCs with biomaterials in 6-well plates with assessment of DC phenotype using Flow Cytometry

After 5 days of cell culture, the PLGA films were placed into the wells of a 6-well plate with sterilized gaskets (Cole-Parmer, Vernon Hills, IL) to secure the films. Agarose films were prepared as described in Section 4.2.2 directly in the wells. Non-adherent and loosely-adherent cells were collected, resuspended in new pre-warmed DC media at a concentration of 5×10^5 cells/ml, and plated at the volume of 3 ml (1.5×10^6 cells/well) in each well. The cells were then supplemented with cytokines (1000 U/ml GM-CSF, 800 U/ml IL-4). Dendritic cells were treated for 24 hours with biomaterials with known effects on DCs (i.e., PLGA or agarose), treated with 1 μg/ml of lipopolysaccharide (LPS) (*E. coli* 055:B5; Sigma) to become mature DCs (mDCs; positive control), or left untreated to remain iDCs (negative control). The levels of surface marker expression were monitored after 24 hours of biomaterial treatment by flow cytometry per the methods described previously [111] and compared to the controls. The cells were collected by centrifugation at 1100 rpm for 10 min, resuspended in 0.1 % BSA and 2 mM EDTA in PBS, pH = 7.2 (cell-staining buffer), and stained with fluorescently-labeled antibodies CD40 (clone B-B20; mouse IgG$_1$κ), CD86 (clone BU63; mouse IgG$_1$κ) (Ancell Corporation, Bayport, MN), CD83 (clone HB15a; mouse IgG$_{2a}$κ) (Immunotech, Marseille, France), CD80 (clone BB1; IgMκ), HLA-DQ (clone TU169; mouse IgG$_{2a}$κ), HLA-DR (clone TU36; mouse IgG$_{2a}$κ) (BD Biosciences), CD1c (clone AD5-8E7; mouse IgG$_{2a}$) (Miltenyi Biotec, Auburn, CA), or DC-SIGN (clone 120507; mouse IgG$_{2b}$) (R&D Systems). The cells were stained for 1 hour at 4°C, and analyzed using a BDLSR flow cytometer (Beckton Dickinson, San Jose, CA). Data analysis was performed using FlowJo (Tree Star, Ashland, OR) based on the differential shift of histograms compared to the controls unless otherwise indicated. The "maturation factor" values were determined by dividing the gMFIs of CD86-PE by that of DC-SIGN-FITC. The antibody binding capacity of CD86 expressed on DCs or B cells were determined by staining the

cells with anti-CD86-PE, gating the distinct DC and B cell populations on the scatter plot, measuring the gMFIs of the populations, and comparing the gMFIs to a standard curve created by beads with known number of CD86 antibody binding sites (Quantum Simply Cellular® kit; Bangs Laboratory, Fishers, IN). To quantify the percentage of DCs and B cells or B cells and T cells in the culture system, the cells were double-stained with anti-CD19-APC (clone HIB19; mouse $IgG_1\kappa$) (BD Biosciences) and anti-DC-SIGN-FITC or anti-CD19-APC and anti-CD3-PE (clone UCHT1; BD Biosciences). The percentage of B cells ($CD19^+$), T cells ($CD3^+$) and DCs ($DC-SIGN^+$) were analyzed using FlowJo based on the differential shift of cell populations in the dot plots.

4.2.4 Treatment of DCs with biomaterials in the 6 or 96-well plate HTP format with assessment of DC phenotype using Fluorescent Microplate Reader

On day 5 of DC culture, the PLGA or agarose films were prepared as described in Section 4.2.2, and iDCs (3 ml, 5×10^5 cells/ml) were plated onto each well in the 6-well plate. In the 96-well format, the PLGA films were slightly wetted on one side with endotoxin-free water and adhered to the wells of the 96-well tissue-culture plate in triplicate, while agarose films were formed by dispensing 50 µl of agarose solution directly into the wells and solidified. One hundred microliters of iDCs (5×10^5 cells/ml) was plated onto each well in the 96-well plate, and secure adherence of the PLGA film was checked by visual inspection. The wells for the negative control of iDCs remained untreated and those for the positive control of mDCs were treated with LPS. The DCs cultured in a 96-well plate were pre-incubated at room temperature for 30 min to reduce the edge effect by minimizing thermal gradients in the edge wells [172]. Subsequently, the DCs were cultured in an incubator at 95% relative humidity and 5% CO_2 at 37°C for 24 hours. On day 6, the DCs treated in the 6-well plate were harvested, and 100 µl of the cell suspension was transferred to wells of a 96-well black filter plate, while the DCs treated in the 96-well plate were transferred directly to other wells in the same filter plate.

The supernatants were then removed by a vacuum manifold (Millipore, Bedford, MA) with vacuum pressure pre-adjusted to 2–4 inHg. To each well, 100 μl of cold working fixation solution (0.03 % paraformaldehyde) was added, and the plate was incubated for at least 30 min at room temperature on a microplate shaker at 600 rpm (VWR, West Chester, PA), followed by the removal of the fixative by the vacuum manifold. Subsequently, 100 μl of staining solution containing 1.5 μg/ml anti-CD86-PE and 1.5 μg/ml anti-DC-SIGN-FITC (monoclonal antibodies as used for flow cytometry) was added into each well containing sample to be stained. IgG_1-PE (clone MOPC31C) (Ancell) and IgG_{2B}-FITC (clone 133303) (R&D Systems) isotype-stained DCs were used for background fluorescence subtraction in separate treatment or control wells. The plates were washed three times with 200, 250, and 300 μl/well of cell staining buffer. Again, the vacuum manifold was used for each supernatant removal. The relative fluorescence units (RFUs) were measured with a Tecan Infinite F500 microplate reader (Tecan US, Durham, NC) using excitation filters of 535/25 and 485/20, and emission filters of 590/20 and 535/25, for PE and FITC, respectively. Because no difference in the RFUs from the isotype controls among iDCs, mDCs, PLGA-treated, and agarose-treated DCs was observed, only the isotype control of iDCs was used for the subtraction from the raw data to eliminate the background fluorescence. The ratio of background-subtracted CD86-PE to background-subtracted DC-SIGN-FITC from each well was determined, and the average ratio ("maturation factor") was calculated from the triplicate.

4.2.5. Assessment of Biomaterial-induced Cytotoxicity

Cytotoxicity associated with biomaterial treatment was assessed by measuring the release of cytosolic enzyme glucose-6-phosphate dehydrogenase (G6PD) into the media from cells cultured in the presence or absence of biomaterials. G6PD is released from damaged or dead cells, and its presence was measured using the Vybrant Cytotoxicity Assay (Molecular Probes, Eugene, OR). The supernatants were easily collected from

cells cultured with or without biomaterials of PLGA or agarose films or from controls from a 96-well plate filter plate into a 96-well collection plate by stacking the filter plate on top of the collection plate and centrifuging at $250 \times g$ for 2 min. Fifty microliters of the supernatants were assayed immediately according to the manufacturer's protocol, because freeze-thawing the supernatants decreased the enzymatic activity substantially. The medium from cells lysed with 0.5% Triton X served as a positive control. The fluorescence readings were taken after 30 min incubation at $37^{o}C$ with excitation and emission filters 535/25 and 590/20, respectively. This experiment was repeated 3 times.

4.2.6. Statistical analysis

Two-sided pairwise student t-test was used to compare the sample group to the appropriate control group. To observe any significant differences between all sample groups in pairs, pairwise general linear model of the two-way ANOVA with a mixed model and repeated measure followed by Tukey post test was used. For all statistical methods, the Minitab software (Version 14, State College, PA) was used. If otherwise indicated, the p-value equal to or less than 0.05 was considered significant.

4.3. Results

4.3.1. DC-SIGN was a suitable marker for the definition of "maturation factor", which represents the degree of DC maturation

Biomaterials could not be cast onto the filter plates because the filter membranes would be clogged. For this reason, the cell samples cultured on biomaterials in a regular 96-well tissue-culture plate were required to be transferred to a 96-well black filter plate for staining and analysis. Hence, the cell numbers in the wells in the filter plate may vary significantly and a cell number normalization method was required to account for the variations in cell number. Cell number normalization by total DNA or a DC-specific surface marker was investigated. CD86, a costimulatory molecule, was used as the

maturation marker because of its high expression level and its large fold change upon DC maturation, including upon biomaterial treatment [6,111].

The conventional method was used to derive iDCs and mDCs, and the DC culture was previously determined to primarily consist of DCs and lymphocytes by day 5 and day 6 [173], and $\geq$ 90% of the lymphocytes were found to be CD19$^+$ B cells based on dual antibody staining for CD3$^+$ T cells and CD19$^+$ B cells. The same culture system was used in this study. It was determined that the DC:B-cell ratios and B cell percentages changed significantly between iDCs and mDCs, and the B cell content varied significantly among different donors (Figure 4-2). Such variations could introduce substantial noise in the analysis of the DC maturation results. To eliminate the variability in the cell population ratios in the culture system, DCs were purified by magnetic sorting on day 5 prior to the LPS treatment. However, the purified DCs were significantly less responsive to the LPS treatment than the unpurified population (Figure 4-3); hence purified DCs could not be used for treatment with biomaterials. B cells were necessary in the culture system to achieve full responsiveness of DCs, possibly due to the profile of cytokines and natural antibodies produced by B cells even in the absence of support from T cells in the culture system [174-176]. A potential issue with B cell presence in the culture system is that they can also express the maturation marker, CD86 [177]. However, it was determined that the B cells in this culture system expressed very low CD86 compared to the DCs. Although approximately 9.4% and 7.3% of B cells were CD86$^+$ in the iDC culture and mDC culture, respectively, the contribution of CD86 from B cells was less than 5% of the CD86 that is expressed on iDCs and less than 2% on mDCs (Figure 4-4). Furthermore, no DNA stain was found to be compatible with the filter plate assay, primarily due to their broad excitation and emission spectra and the strong background fluorescence generated by the possible binding of the stain to the filter membrane. Consequently, the strategy of data normalization by total DNA was not further pursued.
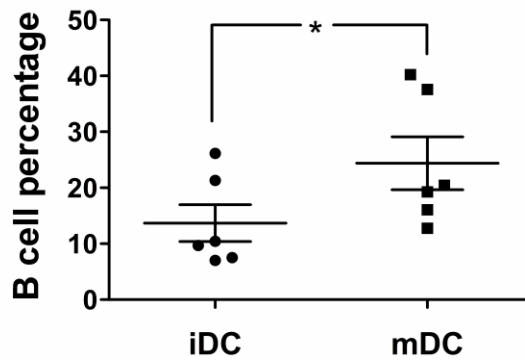
Figure 4-2: B-cell percentage in the iDC and mDC cultures by flow cytometric analysis. The B cell percentages in the DC culture are shown with mean ± SEM, n=6 different donors. *: p<0.05 and represents statistical difference between iDCs and mDCs.
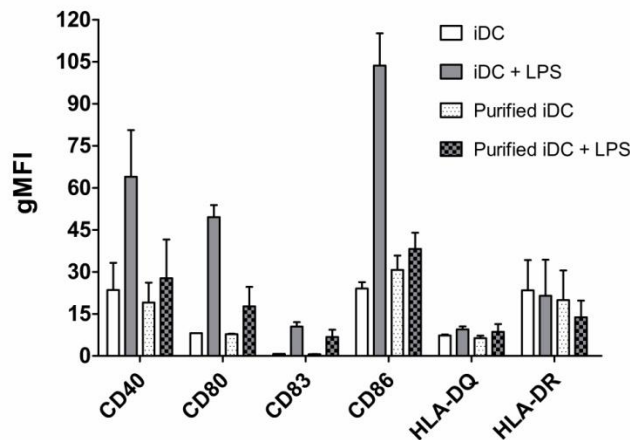
Figure 4-3: Dendritic cells purified by magnetic sorting were less responsive to LPS stimulation in comparison to unpurified counterparts. On day 5 of DC culture, DCs were magnetically isolated by removing CD19$^+$ B cells and then positively selecting CD1c$^+$ DCs, treated with LPS for mDCs or left untreated for iDCs. These purified DCs were analyzed for surface marker expression after 24 hrs and compared to the unpurified counterparts with mean ± range, n=2 donors.

CD1c was initially considered as a normalization factor because some studies reported that CD1c expression only slightly increased during DC maturation [178] and because previously we observed negligible levels of CD1c expression on B cells in the culture system making it specific for DCs (data not shown). However, here CD1c expression increased significantly upon DC maturation (Figure 4-5). This may offset the increase in CD86 expression, if used as a normalization factor, which is undesirable. That is, when CD1c increases upon maturation along with CD86, the ratio of

CD86/CD1c may show no difference compared to iDCs. As a result, CD1c was not suitable as a normalization factor.
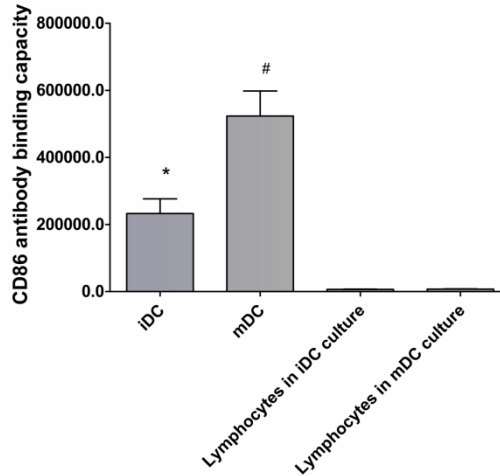
Figure 4-4: CD86 expression on DCs and lymphocytes in the culture system. The antibody binding capacity of CD86 on DCs and B cells was measured by comparing the gMFIs of CD86 expression to a stardard curve created by beads that bound unknown number of antibodies using the BD FACSDiva software with mean ± SEM, n=6 donors. *: $p < 0.05$, lower than mDCs and higher than lymphocytes; #: $p < 0.05$, higher than iDCs and lymphocytes.
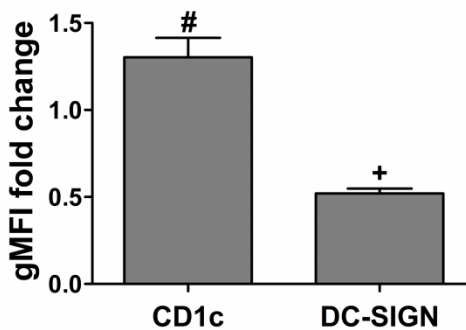
Figure 4-5: Dendritic cell expression of CD1c and DC-SIGN by flow cytometric analysis. The fold change of geometric mean fluorescence intensity (gMFI) for mDCs was compared to iDCs among donors with mean ± SEM, n=6 donors. #: $p < 0.05$, compared to iDCs and higher than iDCs; +: $p < 0.05$, compared to iDCs and lower than iDCs.

As an alternative marker for DC phenotype, C-type lectin DC-SIGN was then examined for its applicability as a normalization factor in the HTP assay. Consistent with the literature [167], DC-SIGN expression level was lowered upon DC maturation (Figure

4-5). Furthermore, DC-SIGN is only expressed by DCs in the culture system, and the ratio of CD86/DC-SIGN was DC number-independent in the assay. Therefore, DC-SIGN was used in the definition of "maturation factor", the ratio of CD86/DC-SIGN, to represent DC maturation.

4.3.2. Equivalent assessment of biomaterial effects on dendritic cells were observed validating the filter-plate method

To validate the 96-well filter plate-based method as far as DC treatment with biomaterials in the 96-well plate format and analysis of levels of CD86 and DC-SIGN expression using the fluorescent plate reader, a biomaterial study using biomaterials with known effects on DCs phenotype, namely, PLGA or agarose films, was conducted. The results in Figure 4-6A showed that the trend for the fold change of "maturation factor" of the cell samples, whether treated with biomaterials in a 96-well or a 6-well tissue-culture plate, were similar; hence, the use of a 96-well format for biomaterial treatment on DCs was appropriate. In addition, the samples from the 6-well plate were analyzed by the 96-well filter plate format using the fluorescence plate reader or by the conventional flow cytometric analysis to yield similar trends, further confirming previous results [6,111], in which PLGA films induced DC maturation, but agarose films did not. The flow cytometric analysis of other maturation markers such as CD40, CD80, CD83, CD86, HLA-DQ, and HLA-DR also confirmed differential DC maturation in response to different biomaterials treated using the 6-well format (shown for CD86 in Figure 4-6B; data for other markers were similar to previously published results [6]). Collectively, this experiment validated the filter plate approach for assessing DC phenotype upon biomaterial contact. Furthermore, in such experimental setup, the signal/background (S/B) and signal/noise (S/N) ratios for FITC ranged from 2.3 to 3.3 and from 52.3 to 71.7, respectively. The corresponding ratios for PE ranged from 3.5 to 8.8 and from 53.2

to 113.8. Because of the large S/N ratios, signals could easily be distinguished from the background.
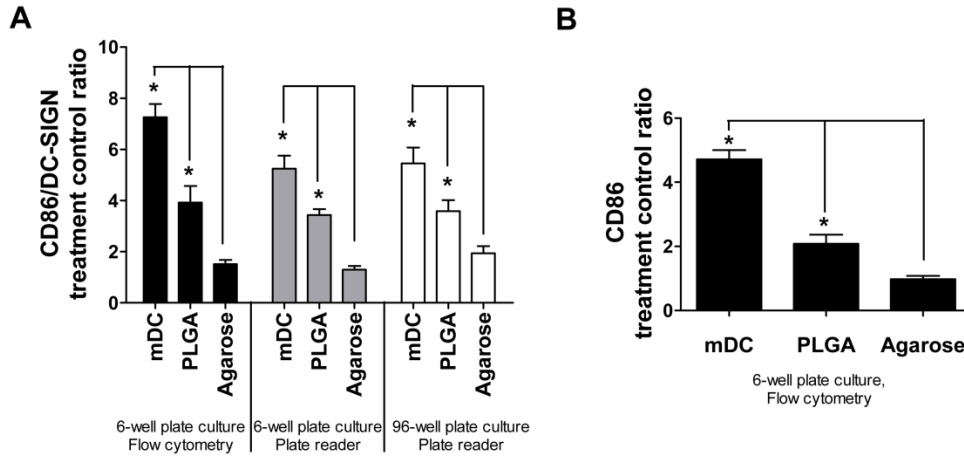
Figure 4-6: Validation of the HTP methodology for assessing DC responses to biomaterials. A) Treatment/control ratios of 'maturation factor' (defined as CD86/DC-SIGN) for DCs treated with biomaterials or controls in the 6-well format and analyzed by flow cytometry (set of black bars), in the 6-well format and analyzed by fluorescent plate reader (set of grey bars), and in the 96-well format and analyzed by fluorescent plate reader (set of white bars). B) Treatment/control ratios of CD86 expression for DCs treated and analyzed using the conventional format of 6-well plates and flow cytometry for DCs treated with biomaterials or controls. Mean±SEM; n=8 (6 donors). *: p<0.05, statistically different from iDCs and higher than iDCs.   Brackets: p<0.05, statistically different between two biomaterial treatments or between biomaterial treatment and mDCs.

The use of filter plate puts biomaterial-treated DCs in contact with the filter membrane (another material) and therefore fixation of DCs is required to prevent any DC maturation effects due to the filter membrane. Therefore, one issue was whether the level of surface molecule expression detected would be equivalent on the DCs with and without prior fixation. Another issue was whether paraformaldehyde fixation in the filter plate would cause undesired cell bonding to the filter membrane, thereby affecting subsequent surface marker staining. To address the first issue, it was demonstrated that the levels of CD86, DC-SIGN, and CD1c expression detected by flow cytometry were equivalent for DCs with and without fixation in an Eppendorf tube prior to staining with the monoclonal antibodies (Figure 4-7). Furthermore, to address the second issue,

equivalent levels of these markers were determined by flow cytometry for DCs fixed and stained in filter plate as compared to DCs stained in Eppendorf tubes without fixation (Figure 4-7).
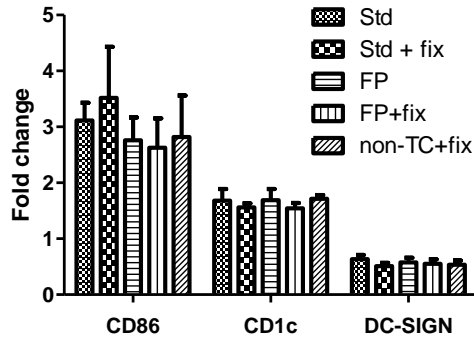
Figure 4-7: GMFIs of cells fixed and stained with 3 different schemes and compared to controls. Std: unfixed cells were stained in Eppendorf tubes, which is the conventional staining method. Std + fix: cells were fixed and then stained in Eppendorf tubes. FP: unfixed cells were stained in filter plate. FP + fix: cells were fixed and stained in filter plate. Non-TC + fix: cells were fixed in a 96-well non-tissue-culture-treated polystyrene plate and then transferred to a 96-well filter plate for staining. All the cell samples were collected and gMFIs determined by flow cytometry. Three experiments with different donors were performed. Fold changes of surface markers are shown with mean±SEM. No statistical significance was determined among fixation and staining schemes.

4.3.3. Biomaterial-induced cytotoxicity

After 24 hr of treatment with biomaterials, cell supernatants were collected and assayed for the release of G6PD into the medium. DCs treatment with PLGA films was found to induce higher levels of released G6PD into the media as compared to iDC (Figure 4-8). This result is consistent with previous result in which DCs treated with PLGA induced higher annexin V staining than iDC but not mDC or agarose films (J. Park and J E. Babensee, unpublished observation). As expected, the lysed iDC and mDC samples induced very high G6PD release, and the fluorescence signal was saturated (Figure 4-8).
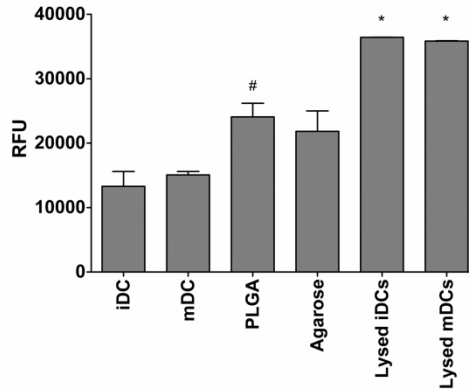
Figure 4-8: Effect of PLGA and agarose on DC glucose-6-phosphate dehydrogenase (G6PD) release. Dendritic cells were cultured with or without biomaterials PLGA or agarose films in a 96-well format for 24 h. The supernatants were collected into a 96-well plate by centrifugation at $250 \times g$ for 2 min and then measured for G6PD release using the Vybrant Cytotoxicity Assay at $37^{o}C$. The fluorescence was measured at 30 min using a Tecan Infinite 500 microplate reader. Mean±SEM; n =3. *: $p<0.05$ higher than all the treatment groups; #: $p<0.05$ higher than iDC and mDC.

4.4. Discussion

A 96-well filter plate-based HTP methodology has been optimized and validated for the assessment of DC responses to biomaterials. In this methodology, after treatment with biomaterials, DCs were transferred to a black 96-well filter plate, supernatant collected for analysis of soluble mediators/indicators of cell viability and remnant cells analyzed for expression of the "maturation factor", CD86/DC-SIGN, using a fluorescent plate reader. Using this methodology, DC responses to the biomaterials, PLGA or agarose films, were consistent with results obtained using conventional flow cytometry analysis. Specifically, DCs treated with biomaterials in a 96-well or a 6-well tissue-culture plate format yielded similar trends of maturation; therefore, a 96-well format was appropriate for DC treatment with biomaterials. In addition, the DC samples from the 6-well plate (conventional method) were analyzed in a 96-well filter plate format using the fluorescence plate reader or by the standard flow cytometric analysis and yielded similar trends, further confirming previous results, in which PLGA films induced DC maturation but agarose films did not. Analysis of biomaterial-induced DC cytotoxicity by measuring

release of G6PD into supernatants by damaged cells showed that PLGA-treated DCs showed higher annexin V staining than iDCs consistent with independent experiments (J. Park and J.E. Babensee, unpublished observations). Since unstained PLGA-treated DCs showed similar autofluorescence as iDCs, the observed PLGA-induced maturation and the resulting higher fluorescence signal were not due to the autofluorescence from apoptotic DCs or associated apoptotic bodies. DC culture media supernatants can also be stored for cytokine profiling experiments using Multiplex technology.

The HTP methodology developed herein offers several benefits for analyzing non-adherent or loosely-adherent DC responses to biomaterials as compared to other approaches. Although flow cytometry is a powerful analytical tool, both sample preparation and data analysis are time-consuming, especially when a large number of samples are analyzed. Automated sample loaders for 96-well plate or tubes for flow cytometry are available commercially (e.g. Guava Technologies) to address this issue, but these systems are usually very expensive, poorly accessible to most laboratories, and have long sampling times (approximately 1.5 to 2 hours for automated sampling a 96-well plate) for a large number of samples. The latter characteristic is prohibitive for living cells (particularly responsive leukocytes). Although high-throughput biomaterial arrays exist for cell studies such as the nanoliter-scale biomaterial combinatorial arrays developed by Anderson et al. [142,143], these arrays are only applicable for adherent cell types and the cellular response to biomaterial differences was measured by immuno-detection or ELISA-based methods which was possible because the cells were localized to a "spot". For DCs used herein, a filter plate-based method was necessary instead of a traditional cell-based ELISA due to the loosely-adherent or non-adherent nature of the cells, which would result in expected cell loss during washing steps using centrifugation and aspiration in a regular microplate during the ELISA analysis. Furthermore, supernatant collection from a regular microplate is time-consuming and inaccurate due to the aspiration of supernatant from individual well with a pipette, while supernatants from

all the samples in a filter plate can be simultaneously collected into a collection plate without any cells being collected. An efficient means of defining biomaterial "hits" in a combinatorial library of test polymers can be defined herein for this HTP methodology as a significant ($p < 0.05$) increase or decrease in the value of the "maturation factor" as compared to iDCs. Furthermore, the S/N and S/B ratios were sufficient for the analysis.

There were, however, complexities in the development of this HTP methodology for the analysis of DC responses to biomaterials which required attention. The first complexity was the non-homogeneous cellular population i.e. presence of B cells. As such, total DNA could not be used to normalize the fluorescent signal which was further justified by the vastly varied DC:B-cell ratios in the culture and the lack of a compatible DNA stain. To consider whether DC responses to biomaterials could be assessed using purified DCs (no B cells) which would clearly make analysis easier, resident B cells in the culture were removed using positive selection and subsequent negative selection of DCs by magnetic sorting. However, the purification of DCs significantly decreased their responsiveness to LPS, which may be explained by the important role of B cells in modulating DC maturation and function, possibly due to the release of cytokines or natural antibodies from B cells (even in the absence of T cells) in the culture system [175]. Although the results herein appear to be contrary to some reports that purified DCs respond well to LPS, it is important to note that the response of purified DCs may be highly dependent on the purification protocol. For example, Jefford et al. reported that DCs differentiated from purified CD14$^+$ monocytes or from CD1c$^+$ peripheral blood DCs responded very differently to maturation stimuli [179]. Therefore, the DC types and culture methods should be considered for particular clinical applications. DCs differentiated from purified CD14$^+$ monocytes or from CD1c$^+$ peripheral blood DCs, or from CD34$^+$ cells from cord blood [180], are the most commonly employed purified DC types. Herein, iDCs were purified (removal of resident B cells) on day 5 of culture after iDCs differentiation had been fully completed. Purifying iDCs at this later stage, rather

than performing the purification step at the beginning of the culture for precursor cells, may render the purified iDCs less responsive to maturation stimuli. The DC culture system in this study represents one of the most widely used and well-characterized DC culture systems [173], and without the DC purification step, less stress is exerted on the sensitive DCs.

The second complexity was that given that the presence of B cells in the DC culture can be beneficial for DC function (as presented below) their contribution to the measured CD86 level needed to be minimal to none (as compared to the DCs). B cells were found to release cytokine(s) (e.g. IL-16) and natural antibodies (e.g. CD40-reactive natural antibody) (in the absence of T cells) that aid in monocyte-derived DC migration, differentiation, and maturation [174,176], indicating that B cells can support DC function without T cell activation. Furthermore, the presence of B cells in the culture system may better represent the physiological multicellular host response to biomaterials *in vivo* and presumably provides insight into how DCs specifically respond to biomaterials. For the DC culture system used herein, MΦs were not present even though their cultures start with a common monocytic precursor [173], due to the presence of the cytokine IL-4, which induces DC differentiation but inhibits MΦ differentiation [181]. Thus, there would be no contribution from MΦs to the CD86 expression level in this study. Of note, the B cells in our culture system expressed only less than 5% of the CD86 that is expressed on iDCs and less than 2% on mDCs. Thus, the B cells in the culture negligibly contributed to the CD86 fluorescence signal. In addition, previous research indicated that DCs are much more potent in stimulating T cells compared with B cells [182]. Therefore, the presence of B cells is not expected to confound the analysis of DC maturation in this assay. Results presented here indicated that although 9.4% and 7.3% B cells were CD86$^+$ in the iDC and mDC culture, respectively, B cells expressed minimal level of CD86 as compared to DCs. In addition, the expression of CD86 on B cells in the iDC and mDC culture was not different. On the contrary, blood peripheral B cells have

47

been widely reported to express CD86 at low level (7% CD86$^+$ of total B cells) in the resting population and at high level (30.3% CD86$^+$ of total B cells) in the activated population [177]. In addition, B cells have also been reported to upregulate their CD86 expression in response to LPS stimulation [183]. Human B cells are often isolated by FACS cell sorting or magnetic isolation, and then cultured in complete medium as used for DCs in the study herein but without the cytokines IL-4 and GM-CSF [174]. As such, although IL-4 induces CD86 expression on tonsillar B cells [184], presumably the presence of GM-CSF results in the low CD86 expression on B lymphocytes and their unresponsiveness to LPS in the DC culture system herein. However, side-by-side comparison of CD86 expression by DCs and B cells has not been reported in the literature.

Given that total DNA was not a suitable normalization factor for CD86 expression the third complexity was identifying a suitable normalization marker. Of the possible choices, CD1c functions to initiate adaptive immune responses against self or microbial lipid antigens [185-187] and is a characteristic of human DC populations [188]. In addition to DC populations, CD1c has been reported to be expressed on subsets of B cells [188]. Nonetheless, results here showed only a negligible level of expression of CD1c on B cells as compared to DCs (data not shown). Furthermore, some studies reported that CD1c expression only slightly increased during DC maturation [178] and therefore was initially considered as a normalization factor. However, our results showed that CD1c expression increased significantly upon DC maturation (Figure 4-5), which may offset the increase in CD86 expression. Therefore, CD1c was not suitable as a normalization factor.

Another possible normalization factor considered was the DC-specific cell surface molecule, C-type lectin DC-SIGN. DC-SIGN is a DC-specific adhesion and endocytic receptor [189] that is highly expressed on immature human monocyte-derived DCs [50,167]. Ideally, an invariant DC marker that is DC-specific and does not change upon

DC maturation would be preferred as a normalization factor. However, since no such marker was found, we defined the parameter "maturation factor." Our rationale of using DC-SIGN were the following: 1) DC-SIGN is expressed on only the monocyte-derived DCs used in our system; therefore, the fluorescent signal measured is specific to the DCs in our culture; 2) The nature that DC-SIGN down-regulates upon DC maturation [167] causes the ratio of CD86/DC-SIGN to further increase, which may in fact give rise to a more sensitive assay for the assessment of DC maturation; 3) If a biomaterial changes DC-SIGN expression significantly while keeping CD86 expression unaltered, such material also becomes a "hit" (a false positive in the context of CD86 expression) and may be further studied due to the importance of DC-SIGN in immunity. Thus, DC-SIGN serves as an additional marker for DC response to stimuli and was selected for defining the DC number-independent parameter – "maturation factor," CD86/DC-SIGN.

To our knowledge, this is the first report describing a microliter plate-based HTP analysis of DC maturation which takes into account the non-adherent nature of these cells, the inherent heterogeneity of this culture, and the sensitivity of these cells. Table 4-1 compares the HTP filter plate and the flow cytometric methods. The HTP 96-well plate format is superior to the 6-well format because it offers a number of advantages: 1) it provides much higher throughput in the assessment of DC response to biomaterials within the same experimental time frame; 2) this format allows for the simple collection of cell culture supernatants from the DC samples and their storage for multiple cytokine profiling using Multiplex technology; 3) the HTP assay significantly reduces the quantity of biomaterial samples and the time for sample preparation and measurement; 4) data acquisition requires a microplate reader, which is much less expensive and easier to maintain than a flow cytometer. However, the HTP assay also has a few obvious disadvantages: 1) it only provides an average maturation signal from the well but not a distribution or histogram of the cells (more precisely, the events) provided by flow cytometry, so it is impossible to deduce the population or percentage of DCs that are

actually affected by the presence of the biomaterials; 2) the HTP assay requires highly expressed and movable markers, while flow cytometer can measure markers of much lower expression level. Despite these disadvantages, the value of the HTP assay lies in its ability to allow for the screening of a large number of biomaterials in a combinatorial biomaterial array. The biomaterial "hits" can be selected and their effects on DCs can then be further probed using conventional assays such as flow cytometry, mixed lymphocyte reactions, endocytosis assay, cytokine profiling, which have been used and continue to be used to analyze DC responses to biomaterials [6,190].

Table 4-1: The comparison between the conventional flow cytometric method and the filter plate-based HTP method.

	Flow Cytometry	Filter Plate
Plate format	6-well plate	96-well plate
Fixation step	No generally	Yes
Equipment	Flow cytometer	Microplate reader
Experimental time	3 hours (1 hr incubation)	2.5 – 3 hours (1.5 hr incubation) for 3 plates
# of materials	5	Up to 279 (or 135 if duplicate) in 3 plates
Size of biomaterial in well	9.5 cm^2	0.32 cm^2
Data acquisition time	30 – 60 min	30 – 60 second per plate, 2 fluorophores
Data	Expression of 6 surface markers with histograms and dot plots	A ratio from the average expression of a limited set of surface markers
Marker expression level	Very low to high (for markers with any expression level)	Relatively high and movable (appropriate for markers with high expression level and huge fold change upon response)

The discovery of compounds for new drugs has been dramatically changed with the advent of combinatory chemistry [191]. Similarly, combinatorial arrays of well-controlled and characterized biomaterials are expected to enable the discovery of biomaterials that alter cell behavior. A number of studies have used combinatorial libraries to study cellular response to biomaterial properties. For example, Anderson et al. developed an impressive nanoliter-scale synthesis of biomaterial combinatorial array of different compositions and observed distinct differentiation of human embryonic stem cells (hESCs) on those materials [142,143]. Meredith et al. created a system with

continual changes of topography on glass slide using blends of poly(D,L-lactide) (PDLA) and poly(ε-caprolactone) (PCL) and identified preferred microstructural feature sizes for the attachment, spreading, and proliferation of UMR-106 (rat osteoblastic cell line) and MC3T3-E1 (mouse osteoblastic cell line) cells [145,146]. Mei et al. created surfaces with well-defined biocompatible polymer brush nanostructures by using varying graft density of poly(2-hydroxyethyl methacrylate) (PHEMA) and showed decreased fibroblast spreading and attachment with increased grafting density [149]. Brocchini et al. developed a polyarylate-based combinatorial array and showed that fibroblast proliferation was more sensitive to chemical structure than contact angle [157]. However, most of these studies investigated basic cell functions such as adhesion or proliferation to well-defined combinatorial polymer libraries with the exception that Anderson's system investigated biomaterial effects on the differentiation of hESCs. Furthermore, none of these HTP systems allow for the screening of loosely- or non-adherent cells. In contrast, the HTP assay developed and validated herein will be used to study the maturation of a highly sensitive and loosely- and non-adherent cell type, DCs. More importantly, correlations between DC phenotype and material properties can be drawn from the HTP assays using well-characterized combinatorial arrays. Such correlations are highly advantageous due to their potential as a guide for immunomodulatory biomaterial design for both tissue engineering and vaccine delivery applications. Clearly, thorough characterization of the members in the combinatorial array is important in the derivation of such correlations. However, very few good HTP methodologies exist for polymer characterization [140]. As a result, the number of polymers in a well-characterized combinatorial array may be tens to a few hundred, which is well within the capability of the 96-well plate-based methodology developed and validated in this study. Importantly, the success in such a HTP assay relies heavily on the sensitivity of the microplate reader. As a final note, the sensitivity of this methodology may potentially be further improved by using time-resolved fluorescence or

51

miniaturized to a 384-well format with properly optimized conditions and fluorescent dyes to accommodate a larger combinatorial biomaterial library.

CHAPTER 5:   DENDRITIC CELL RESPONSES TO

SURFACE PROPERTIES OF CLINICAL TITANIUM

SURFACES[‡]

5.1. Introduction

As the most potent APCs, DCs are central in bridging the innate and adaptive immunity. They are not only critical in mediating T cell polarization for effective immune response [58,192,193] but also pivotal in immunological self-tolerance by actively inducing the formation of T_{reg}-cells [77]. In addition, DCs are also key players in osteoimmunology. In particular, DCs have been identified in the synovial tissue and synovial fluid of joints in rheumatoid arthritis (RA) patients [194,195] and have been implicated in inflammation-induced osteoclastogenesis and bone loss [196]. Human or mouse activated $CD4^+$ T cells induced by environmental stimuli were shown to up-regulate surface-bound and soluble receptor activator of NF-κB ligand (RANKL), which is a prime regulator of osteoclast differentiation and activation [197]. The ligation of RANKL to its receptor, RANK, on osteoclast precursors resulted in inflammation-induced bone loss in diseases such as RA and periodontitis [198-201]. Therefore, upon inflammation, DCs can become mature and initiate T cell activation, which in turn promotes the differentiation and survival of osteoclasts.

Biomaterials commonly used in combination products were previously shown to differentially affect DC phenotype *in vitro* [5,6], and their effects could be translated to *in vivo* situations [3,202]. These studies demonstrated that biomaterials can be used to control the DC phenotype, thereby potentially modulating associated *in vivo* immune responses. This potential of biomaterials to affect host response can be manipulated to

---

either suppress immune responses induced by a tissue-engineered construct, or enhance the protective immunity induced by a biomaterial-based vaccine. Elucidation of the biomaterial properties that control DC phenotype are expected to inform immuno-modulatory biomaterial design. However, due to the limitations of the biomaterials used in the previous studies, it was unclear which biomaterial properties determined distinct responses. In order to delineate material property–DC phenotype relationships, a well-defined biomaterial system with detailed material characterization is needed.

In this study, clinical titanium (Ti) surfaces commercially available, including PT, SLA and modSLA, for dental implants were used to 1) analyze DC response to material properties and 2) determine the possible immunological outcomes induced by the different Ti substrates, using DC phenotype as an indicator of inflammatory response. These surfaces have been prepared to possess distinct microtopography and surface energy. PT substrates were chemically polished to have a smooth finish; SLA surfaces were prepared by sand-blasting and acid-etching of the PT surfaces for increased roughness; modSLA surfaces had the same roughness as SLA, but were protected from contamination by hydrocarbons and carbonates naturally occurring in the atmosphere to maintain its high surface energy. The surface material properties of these Ti substrates have been extensively characterized and were shown to induce distinct responses of human osteoblast-like MG63 cells, as well as normal human and rat osteoblasts [160,161,203]. The osteoblastic differentiation of MG63 cells was enhanced on rougher Ti surfaces such as SLA, and such differentiation was sensitive to both micron and submicron surface structures [204,205]. Furthermore, superior to PT or SLA, modSLA substrates promoted enhanced differentiation of osteoblasts and production of local osteogenic factors such as prostaglandin E_2 (PGE_2), transforming growth factor beta-1 (TGF-β1) and osteocalcin, indicating that high surface energy and surface roughness synergistically support an osteogenic microenvironment [160]. In addition, modSLA implants significantly increased bone-to-implant contact in miniature pigs as compared to

SLA surfaces [206] and more rapid peri-implant bone formation in humans [207,208], consistent with the *in vitro* enhancement of osteoblast differentiation on modSLA surfaces.

PT, SLA and modSLA surfaces were used to treat DCs and resulted in differential phenotype, which was then covaried to the surface properties of the Ti substrates, using principal component analysis (PCA). Furthermore, the overall results indicated that modSLA may promote a more immature phenotype of DCs, which is anti-inflammatory, thereby potentially supporting osteoblast differentiation by suppressing local inflammation.

5.2. Materials and Methods

5.2.1. Ti substrates

Ti disks were prepared from 1-mm thick sheets of grade 2 unalloyed Ti (ASTM F67; "Unalloyed titanium for Ti for surgical implant applications") and kindly supplied by Institut Straumann AG (Basel, Switzerland). The Ti disks were punched to be 15 mm in diameter for snug fit in the wells of 24-well tissue culture polystyrene (TCPS) plates (Costar) (Corning, Corning, NY). The methods used to produce the PT, SLA and modSLA Ti substrates were previously described [160,209]. The surface properties of the Ti substrates were previously extensively characterized and are summarized in Table 1 for air-water contact angle, mean-peak-to-valley roughness (R_a) and surface chemical composition [161,210].

5.2.2. Human dendritic cell culture

Human DC culture was performed in the same manner as in Section 4.2.1. in accordance with an updated protocol H10011 of the Institutional Review Board of Georgia Institute of Technology.

5.2.3. Exposure of DCs to Ti substrates

On day 5 of culture, loosely adherent and non-adherent cells containing iDCs were harvested and resuspended in DC media with 1000 U/ml GM-CSF and 800 U/ml IL-4 at 5×10^5 DCs/ml. One milliliter of cell suspension (5×10^5 DCs) was plated on Ti disks in the wells of a 24-well plate, treated with 1 µg/ml LPS for the positive control of mDCs, or left untreated in TCPS plates for the negative control of iDCs. Differentially-treated DCs were collected after 24 h for analysis. The loosely- or non-adherent fraction was collected by gentle pipetting of the cell suspension from the tissue culture plates. The cell culture supernatants were collected after centrifugation of the cell suspension at 1100 rpm for 10 min and stored at -20°C until cytokine analysis. To remove the adherent fraction, 0.5 ml warm cell dissociation buffer (Sigma) was added into each well and incubated at 37°C for 20 min. The plate was gently tapped against the bench-top for 30 times every 5 min to dislodge adherent cells. The cell number of both fractions was quantified using a Multisizer^{TM} 3 Coulter Counter (Beckman Coulter, Brea, CA).

5.2.4. Flow cytometry for surface marker expression

After 24 h exposure to Ti substrates, DCs were harvested and analyzed for surface expression of DC maturation-associated markers, including CD83, CD86, and HLA-DQ, whose levels are up-regulated upon DC maturation. CD83 is a DC maturation marker; CD86 is a co-stimulatory molecule; HLA-DQ is a major histocompatibility (MHC) class II molecule. Twelve independent experiments were performed using DCs each derived from a different donor. The levels of surface marker expression were monitored by flow cytometry using previously described methods [211]. The cells were collected by centrifugation at 1100 rpm for 10 min, resuspended in cell-staining buffer (0.1% BSA and 2 mM EDTA in D-PBS, pH 7.2), and stained with fluorescently-labeled antibodies, including CD83 (clone HB15a; mouse IgG$_{2b}$) (Immunotech, Marseille, France), CD86 (clone BU63; mouse IgG$_1\kappa$) (Ancell Corporation, Bayport, MN), and HLA-DQ (clone

TU169; mouse IgG$_{2a}$κ) (BD Biosciences, San Jose, CA). The cells were stained for 30 min at 4°C, and analyzed using a BD LSR II flow cytometer (Beckton Dickinson, San Jose, CA). Data analysis was performed using FlowJo (Tree Star, Ashland, OR).

5.2.5. Scanning electron microscopy (SEM) of adherent DCs

DCs were cultured on the Ti disks in a 12-well TCPS plate to ensure easy removal of the disks during SEM sample preparation. After 24 h of culture, the disks were washed three times with warm D-PBS to remove the non- or loosely-adherent cells. The cells/Ti samples were fixed with 1 ml 3.5% EM grade glutaraldehyde (Sigma) with 2% (w/v) tannic acid (Sigma) in 0.1 M Sorenson's phosphate buffer (P-buffer) overnight. The cells were washed three times with P-buffer and were post-fixed with 0.5 ml 1% osmium tetroxide (OsO$_4$, Sigma) in P-buffer for 1 h to impart partial conductivity [212]. After three washes, the cells were treated with 1 ml 2% (w/v) aqueous tannic acid for 1 h (to preserve the fine structures of cells and aid in the subsequent OsO$_4$ reduction at its binding sites). After three washes, the cells were post-fixed again with 0.5 ml 1% OsO$_4$ in P-buffer for 1 h. The cells were then dehydrated in a sequential series of increasing concentrations of acetone: 15%, 30%, 45%, 75%, 90%, and 100% acetone for 30 min at each concentration. Subsequently, the samples were dried in an E3000 Critical Point Dryer (Quorum Technologies, Guelph, Ontario, Canada) and sputter coated with a thin layer (~5 nm) of gold (Polaron Sputter Coater SC7640; Quorum Technologies). The micrographs were collected using Hitachi S-800 scanning electron microscope.

5.2.6. Multiplex cytokine profiling

The supernatants collected from the cell culture medium in the presence of Ti substrates or controls were stored at -20°C and were thawed only once for multiplex cytokine analysis. The levels of cytokines and chemokines in the cell culture supernatants were measured using Bio-Plex suspension array systems (Bio-Rad,

Hercules, CA) as per the manufacturer's protocol. Briefly, beads conjugated with capture antibodies for the target analytes were mixed and transferred to a 96-well filter plate (Millipore, Billerica, MA). Supernatant samples were added to the wells for 30 min incubation. After the beads were washed three times in the filter plate using a vacuum manifold (Pall Life Science, Ann Arbor, MI), the beads were incubated with biotinylated detection antibodies for 30 min. After another three washes, the beads were incubated with streptavidin-PE for 10 min. After three final washes, the beads were analyzed using a Bio-Plex 200 instrument with Bio-Plex Manager 4.0 software. Through 12 independent experiments each with a different donor, 4-plex cytokine analysis was performed for TNF-α (pro-inflammatory), IL-1ra, IL-10 (anti-inflammatory), and MIP-1α (chemokine). The production of these cytokines was normalized by the cell number in the well. Because normalization did not affect the results in the 4-plex analysis, a wider panel of cytokines and chemokines [pro-inflammatory cytokines (IL-1β, IL-12p70, IL-15, IL-18 and TNF-α), anti-inflammatory cytokines (IL-1ra and IL-10), a pleiotropic cytokine (IL-16), and chemokines (IL-8, MCP-1, and MIP-1α)] were analyzed in a separate experiment with three different donors but were not normalized by the cell number.

5.2.7. Statistical analysis

To observe any significant differences between all sample groups in pairs, a pair-wise general linear model of the two-way ANOVA with a mixed model followed by Tukey post test was used. For all statistical methods, the Minitab software (Version 14, State College, PA) was used, and the p-value equal to or less than 0.05 was considered significant.

5.2.8. Principal component analysis (PCA)

PCA was performed to analyze the phenotype and Ti substrate property data and to draw correlations between DC response and material properties. PCA allows for the

simultaneous analysis of the original large set of variables by reducing the number of dimensions to a few principal components (PCs). This is achieved by finding new axes to represent dimensions with maximal variability and highlight the global covariance patterns of the variables. Typically, only two to three axes (PCs) are sufficient to capture most information from the data [213]. The phenotype variables included levels of surface markers, CD83, CD86 and HLA-DQ, and cytokine production of TNF-α, IL-1ra, IL-10 and MIP-1α; the material properties variables included air-water contact angle, surface roughness and surface chemical composition, % C, O, N and Ti. The measurements from the experiments with twelve donors were organized into a data matrix, to which the PCA algorithm was applied to extract the latent correlations among the variables. All data were pre-processed by log transformation, mean centering and unit-variance scaling [214]. Log transformation ensured Gaussian distributions of data, while mean centering and unit-variance scaling allowed the variances of different variables to have equal chances of being projected onto the PCs [215]. Despite the large variances, all data points were included, and the variances were accepted as natural variations of human primary immune cell responses.

Two PCAs were performed using different sets of variables for extracting different information from the multi-dimensional data. The first analysis aimed to determine the overall effects of PT, SLA and modSLA on DC phenotype relative to the controls. Average values of the phenotype variables and all of the five treatments, including PT, SLA, modSLA, TCPS and TCPS + LPS, were organized into a data matrix. The phenotype variables were organized in the columns of the matrix and the treatments in the rows of the matrix (Figure 5-7A). The objective of the second analysis was to draw correlations between material properties of Ti substrates and DC phenotype. For this analysis, individual values of the phenotype variables from the three biomaterial treatments (PT, SLA and modSLA) were used. The material properties were also included in this data matrix. The phenotype variables and the material properties were

organized in the columns and the treatments from each donor in the rows of the matrix (Figure 5-8A). PCA was performed using the software SIMCA P+ (Umetrics, Malmö, Sweden).

5.3. Results

5.3.1. The expression of DC maturation-associated markers was substrate-dependent

As shown in Figure 5-1, PT- and SLA-treated DCs both expressed higher CD86 levels as compared to the TCPS-treated iDC control; however, no difference was found between PT and SLA treatments for CD86 expression in DCs. In contrast, modSLA-treated DCs expressed CD86 at a level similar to the iDC control. However, DCs treated with modSLA substrates were still able to fully mature in response to LPS (Figure 5-2). LPS-treated DCs expressed higher CD86 levels compared to DCs treated with any of the substrates. The expression levels of CD83 or HLA-DQ were not significantly affected upon treatments with the different Ti substrates. Furthermore, SEM micrographs showed that DCs treated with PT or SLA substrates exhibited more dendritic processes associated with mDCs, while modSLA treated DCs were rounded, which is a morphology associated with iDCs (Figure 5-3A-C).
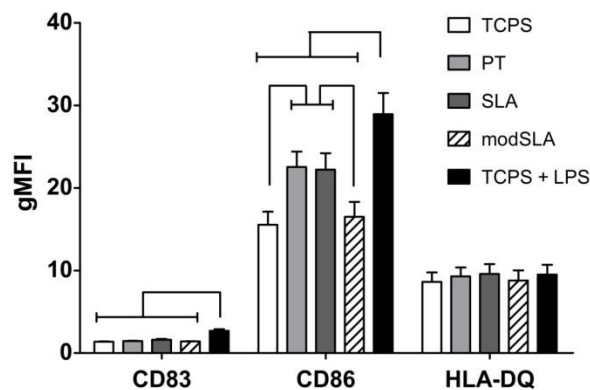
Figure 5-1:Surface marker expression of DCs in response to treatment with different Ti surfaces (PT, SLA or modSLA) as compared to the iDC (TCPS) and mDC (TCPS+LPS) controls. Geometric mean fluorescent intensities are shown for n = 12 donors (mean±SEM). Brackets represent statistical significance among treatments with $p \leq 0.05$.

After a 24 h exposure to the Ti substrates, the percent DC recovery (recovered DCs / plated DCs) was similar for both the loosely- or non-adherent and adherent fractions of cells (Figure 5-4). Percent DC recovery from the LPS-treated culture was higher than from DCs cultured on TCPS or treated with modSLA. Furthermore, the percent adherent DCs (adherent DCs / recovered DCs) was not different among the different Ti substrates, but percent adherent DCs on TCPS was lower than on any of the substrates (Figure 5-4). Low magnification (150x) SEM images of cells remaining on the substrates after non-adherent cells were washed away, indicating that the number of adherent DCs on these Ti substrates was similar (Figure 5-3D-F).
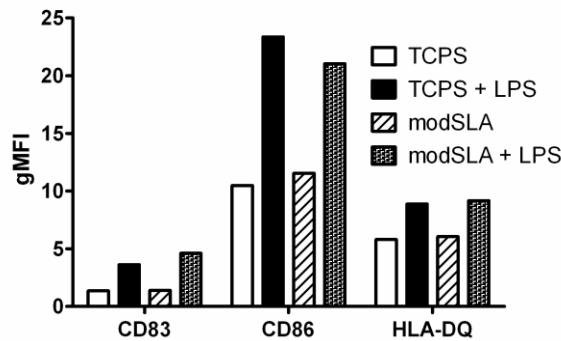
Figure 5-2: DCs treated with modSLA substrates were still able to fully mature in response to LPS.
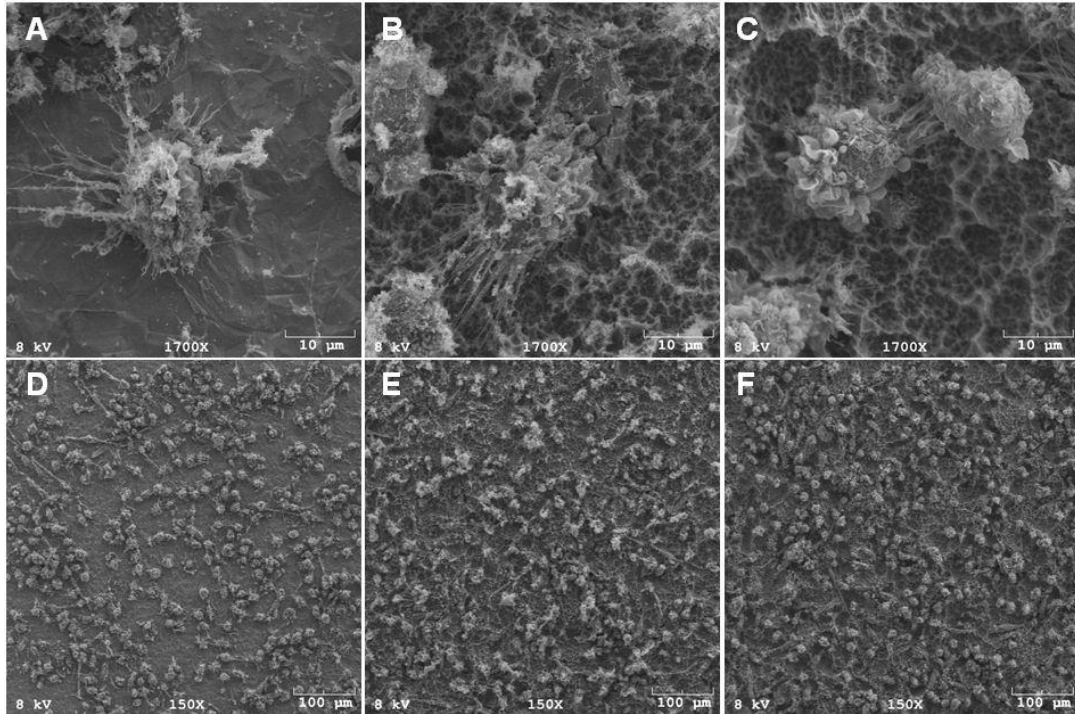
Figure 5-3: SEM of DCs on Ti surfaces. High magnification micrographs (1700x) show that DCs on PT (A, D) or SLA (B, E) exhibited highly dendritic morphology, which is associated with mDCs; DCs on modSLA (C, F) exhibited rounded morphology, which is associated with iDCs. Low magnification scans (150x) (D, E and F) show that the different Ti surfaces adhere similar numbers of DCs. Data are from one of two separate experiments, both with comparable results.
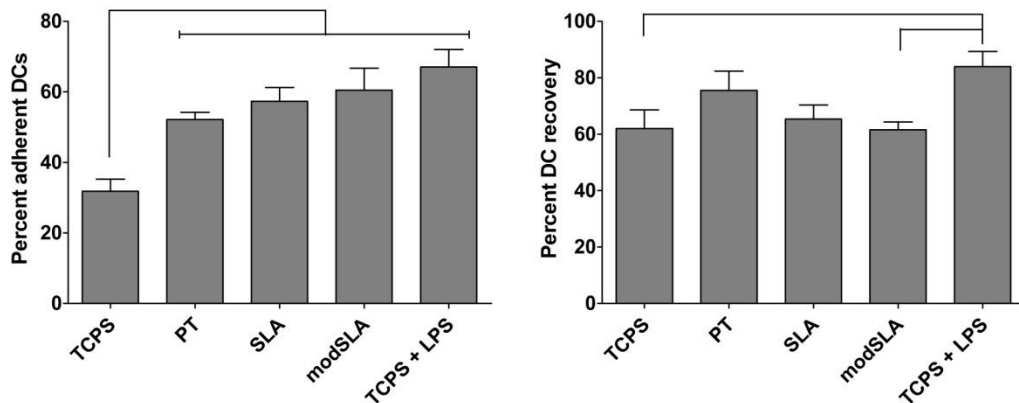
Figure 5-4: Percent adherent cells on and percent DC recovery from the Ti substrates and controls. Left: Percent of cells (adherent DCs/recovered DCs) adherent to the different Ti surfaces (PT, SLA or modSLA) was not significantly different from each other. Right: Percent DC recovery from modSLA was lower compared to mDC control (TCPS+LPS). n=6 donors (mean±SEM). Brackets represent statistical significance among treatments with p≤0.05.

5.3.3. Ti substrates induced differential cytokine production by DCs

Multiplex cytokine analysis showed that production of factors was substrate-dependent. PT surfaces induced higher levels of IL-1ra production by DCs compared to the negative control or modSLA substrates. As expected, LPS-treated DCs released higher amounts of IL-1ra compared to the iDC control (Figure 5-5). Although some trends in the production of TNF-α, IL-10 and MIP-1α were observed among the Ti substrates, the differences were not statistically significant. LPS-treated DCs produced higher TNF-α, IL-10 and MIP-1α relative to any other treatments.
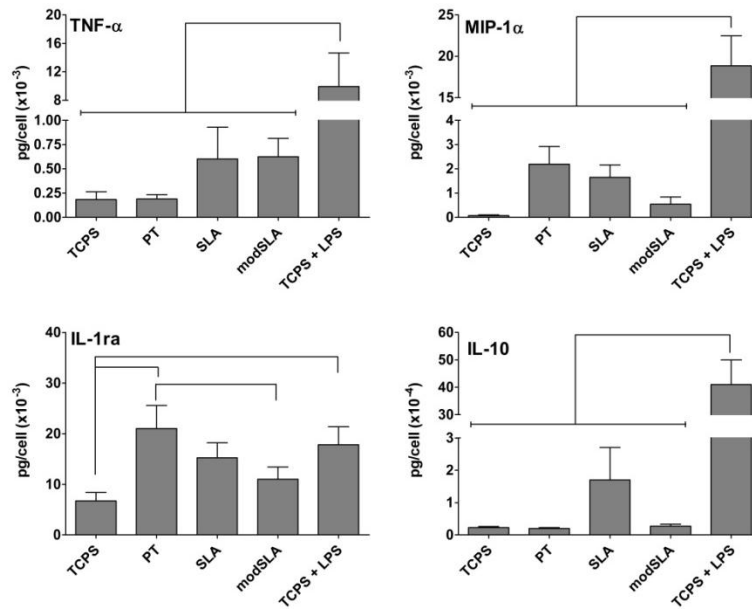
Figure 5-5: Cytokine and chemokine release for DCs treated with Ti surfaces (PT, SLA or modSLA) as compared to the iDC (TCPS) and mDC (TCPS+LPS) controls. The cytokine amount was normalized to the total cell number in the well. n=12 donors (mean±SEM). Brackets represent statistical significance among treatments with p≤0.05.

The analysis of a wider array of cytokines and chemokines (Figure 5-6) indicated that SLA surfaces induced higher levels of IL-16 production by DCs compared to modSLA or TCPS, while PT-treated DCs released higher amounts of MCP-1 relative to the TCPS control and to a level not different from LPS-treated DCs. LPS induced increased production of MCP-1 compared to TCPS, SLA or modSLA. Furthermore, all

of these three Ti substrates induced minute productions of pro-inflammatory cytokines (IL-1β, IL-12p70 and IL-18) compared to LPS treatment of DCs. Although the substrate-induced production of IL-8 by DCs followed the trend of SLA > PT > modSLA, the differences were not significant. In addition, LPS-treated DCs released higher IL-8 compared to TCPS or any substrate treatment. All Ti substrates induced IL-15 production by DCs at levels below detection limit (data not shown). Trends of TNF-α, IL-1ra, IL-10 and MIP-1α production were similar to Figure 5-5.
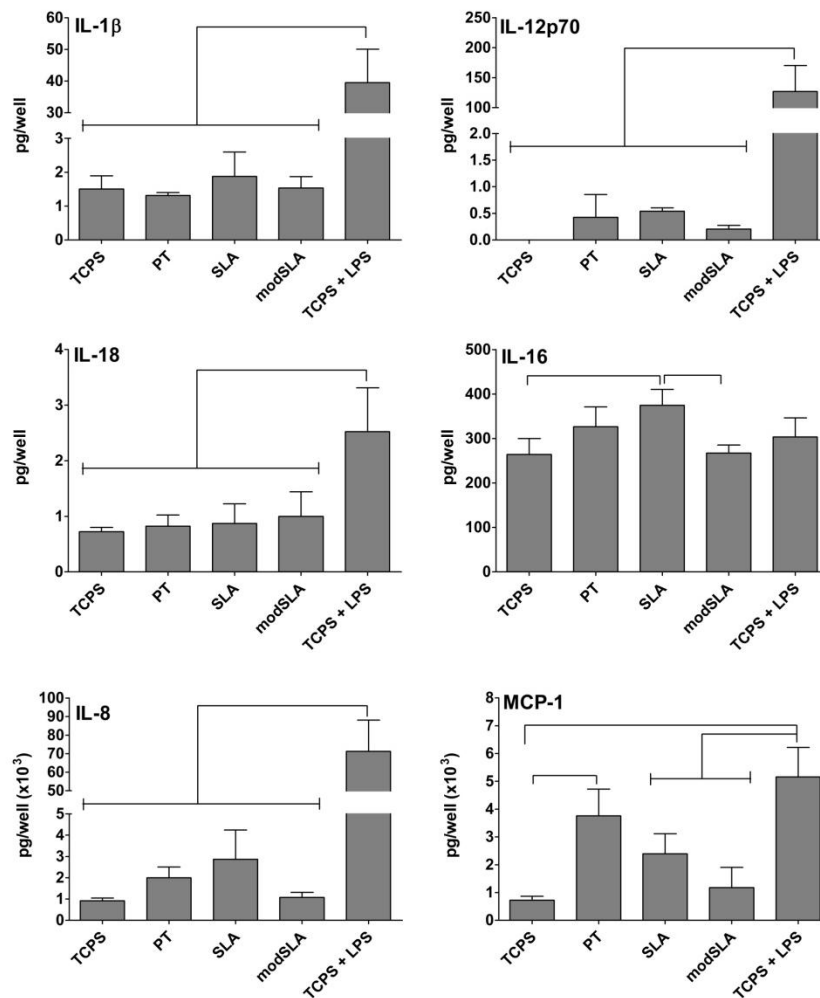
Figure 5-6: Cytokine and chemokine release for DCs treated with Ti surfaces (PT, SLA or modSLA) as compared to the iDC (TCPS) and mDC (TCPS+LPS) controls. The cytokine amount produced by the cells in the well is shown. n=3 donors (mean±SEM). Brackets represent statistical significance among treatments with p≤0.05. The trends of production of TNF-α, IL-1ra, IL-10 and MIP-1α were similar to those in Figure 4 and hence not shown.

5.3.4. PCA indicated differential levels of DC maturation were induced by Ti substrates

The first PCA analysis confirmed experimental data that extents of DC maturation were substrate-dependent (Figure 5-7). The data set could be modeled using two PCs, which were able to represent 95.9% of the data. The PCA biplot indicated that modSLA clustered with TCPS for its effects on DC responses, while SLA and PT formed another cluster that was closer to the LPS treatment. As expected, LPS induced drastic phenotypic changes in DCs and was strongly associated with the phenotype variables along the far end of the first PC (PC1) (thick black ellipse in Figure 5-7). Consistent with the experimental result, PT treatment was more strongly associated with IL-1ra production than the other two Ti treatments as shown along the second PC (PC2) (thin black ellipse in Figure 5-7). Overall, SLA induced higher DC maturation as compared to PT because it was situated closer to the phenotype variables along PC1, while modSLA-treated DCs were negatively associated with the phenotype variables (Figure 5-7).
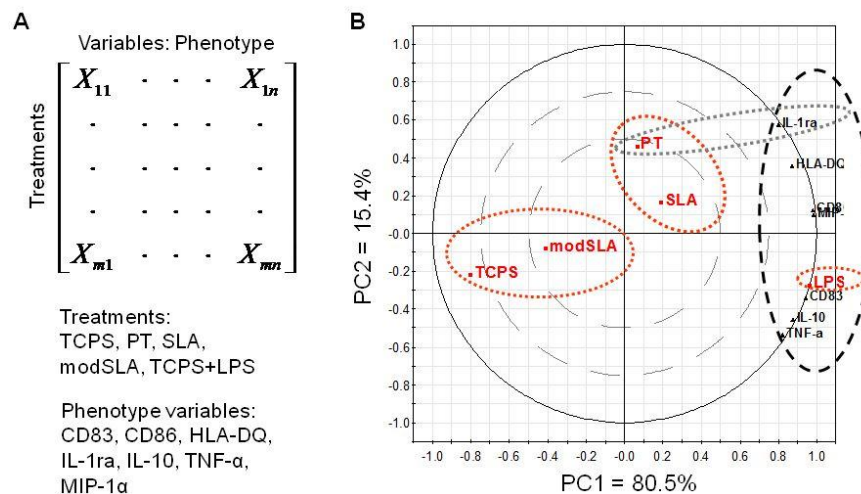
Figure 5-7: Confirmation of the relative effects of Ti substrates (PT, SLA or modSLA) on DC phenotype relative to the iDC (TCPS) and mDC (TCPS+LPS) controls using PCA. (A) The organization of data into a matrix for PCA. (B) PCA biplot of the DC phenotype variables, including surface marker expression of CD83, CD86 and HLA-DQ and production of TNF-α, IL-1ra, IL-10 and MIP-1α, for PT, SLA, modSLA, TCPS and LPS treatments of DCs. PC1 represents 80.5% of data variance, and PC2 explains 15.4% of data variance, which together capture 95.9% of data variance with little loss of information. The red ellipses represent clustering of similar treatment groups (e.g. TCPS and modSLA form one cluster, while PT and SLA form another cluster). The thick black ellipse indicates the location of phenotype variables, which is strongly associated with LPS-treated DCs along the far end of PC1. The gray ellipse represents the association of PT treatment and IL-1ra release along PC2.
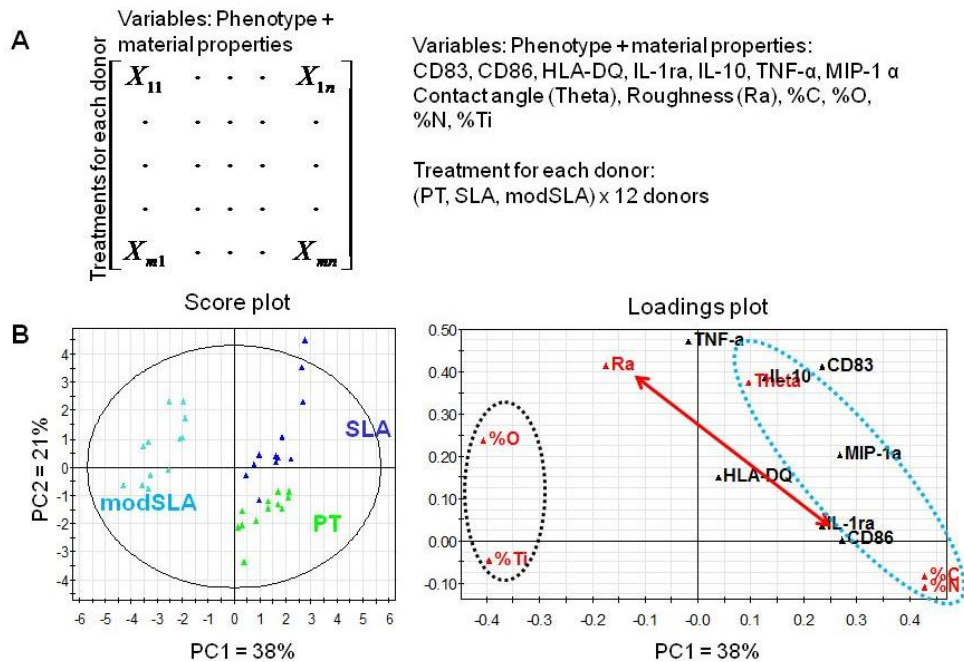
Figure 5-8: Assessment of material property–DC phenotype relationships using PCA. (A) The organization of the data into a matrix for PCA. (B) PCA score plot and loadings plot for the first two PCs. PC1 represents 38% of data variance, and PC2 explains 21% of data variance, which together capture 59% of data variance. The red double-headed vector indicates that CD86 and Ra primarily influence PC1 and PC2, respectively, suggesting that roughness has little effect on CD86 expression. The blue dotted ellipse indicates that material properties of air-water contact angle (Theta), surface %C and %N are more associated with the phenotype variables. Conversely, the black dotted ellipse shows that properties such as %O and %Ti are situated on the opposite side of the phenotype variables, suggesting that these material properties are more associated with an iDC phenotype. The data set can be best modeled by 3 PCs that capture a total of 74.4% information. However, because score plot and loading plots of PC1 and PC3 yield similar conclusions as those of PC1 and PC2, and because plots of PC2 and PC3 do not yield meaningful information, only the plots of PC1 and PC2 are shown for simplicity.

5.3.5. PCA suggested DC phenotype-material property relationships

The second PCA analysis suggested DC phenotype–material property relationships (Figure 5-8). The data set could be modeled by three PCs capturing a total of 74.4% of information. The first 2 PCs (PC1 and PC2) were able to represent 59% of data variance. Instead of a biplot, the score plot and loadings plot are shown for clarity. The relative locations of PT, SLA and modSLA in the score plot were consistent with the PCA biplot shown in Figure 5-8B. In addition, in the loadings plot, CD86 expression and surface roughness (R_a) primarily contributed to PC1 and PC2, respectively, suggesting

that roughness had little effect on CD86 expression, which was consistent with the experimental result. Furthermore, air-water contact angle (Theta), surface %C and %O were more associated with a mDC phenotype due to their clustering with phenotype variables that were up-regulated upon DC maturation (blue dotted ellipse in Figure 5-8B). Higher values of these surface characteristics were associated with PT and SLA substrates, which were shown to promote DC maturation. In contrast, surface %O and %Ti, which were higher on modSLA substrates, were on the opposite side of the phenotype variables (black dotted ellipse in Figure 5-8B), indicating that these surface properties were associated with an iDC phenotype. Interestingly, air-water contact angle was strongly associated with IL-10 production, and %C and %N were similar in their effects on DC phenotype. Information from plots of PC1 and PC3 provided similar conclusions as PC1 and PC2, while plots formed by PC2 and PC3 resulted in meaningless covariations (data not shown).

5.4. Discussion

The phenotype of DCs was differentially modulated by PT, SLA and modSLA surfaces. Specifically, although the expression levels of DC maturation marker, CD83 and MHC class II molecule, HLA-DQ, were not altered significantly, PT and SLA treatment of DCs induced higher co-stimulatory molecule, CD86, expression relative to DCs cultured on TCPS (iDC control). DC treatment with modSLA did not affect CD86 expression as compared to iDCs, presumably maintaining a non-inflammatory environment. Our previous experience indicates that CD86 is the most sensitive marker for DC response to biomaterial treatments and is a valid variable for determining DC maturation levels [5]. Furthermore, both PT- and SLA- treated DCs exhibited much more extensive dendritic processes, a morphology associated with mDCs. Consistent with the CD86 expression results, DCs treated with modSLA possessed a rounded morphology that is associated with iDCs. Therefore, PT or SLA promotes an mDC

phenotype, whereas modSLA-treated DCs possess an iDC phenotype. Despite the non-stimulating nature of modSLA substrates, DCs treated on modSLA were able to fully mature upon LPS challenge, indicating that modSLA does not suppress DC's capability to respond to bacterial stimuli, an important aspect for clearance of any device-associated infection.

PT and SLA surfaces have very similar surface chemical composition, but differ in average peak-to-valley roughness (R_a) and surface air-water contact angle [161]. Both of these surfaces are hydrophobic; hence, the most important difference lies in the surface roughness between PT and SLA substrates. The comparable levels of CD86 expression for DCs treated with PT or SLA surfaces suggested that surface roughness is not crucial in modulating DC phenotype. Conversely, modSLA surfaces have the same surface roughness as SLA substrates, but were prepared to retain their high surface energy (approximately 0° air-water contact angle) by preventing surface contamination with atmospheric hydrocarbons and carbonates. The results presented herein that modSLA-treated DCs were non-stimulating indicated the importance of surface hydrophilicity as a material property that modulates DC phenotype.

Surprisingly, despite the vast differences in surface energy and cellular responses, as many DCs adhered to modSLA substrates as to PT or SLA surfaces, indicating that cell adhesion alone is not sufficient in inducing DC maturation. Previous study demonstrated that distinct adsorbed ECM proteins on TCPS affected DC morphology, cytokine production, and allostimulatory capacity [122]. In addition, chemically-defined self-assembled monolayers were shown to present differential glycan profiles as well as induce distinct DC responses [7,115]. Therefore, the distinct DC responses induced by the Ti substrates were likely due to the differential protein adsorption profiles from the cell culture medium onto the Ti surfaces. Although the adsorbed proteins allowed similar extents of DC adhesion to the different Ti substrates, the difference in the presentation or

conformation of these proteins presumably provided DCs with differential molecular patterns, resulting in distinct responses. This hypothesis will be tested in the future to understand which adsorbed protein profiles on the Ti substrates govern DC response. Specifically, it is necessary to understand the receptors and adsorbed matrix proteins critical for the modulation of DC responses to biomaterials.

In addition, DCs treated with Ti surfaces produced differential cytokine profiles. Contrary to the high expression level of CD86 and dendritic morphology, PT-treated DCs released higher amounts of anti-inflammatory cytokine, IL-1ra, compared to iDCs or modSLA-treated DCs. Although some trends in the release of TNF-α, IL-10 and MIP-1α were observed, the differences were not statistically significant, primarily due to the large variances in the cytokine production by individual donors. A wider array of cytokines and chemokines were subsequently analyzed in order to better delineate the cytokine responses upon DC treatment with Ti surfaces. Treatment of DCs with PT surfaces promoted enhanced production of the chemokine MCP-1, compared to iDCs, and to a level similar to LPS-treated mDCs. In addition, treatment of DCs with SLA surfaces induced higher levels of IL-16 production relative to iDCs or modSLA-treated DCs. The production of pro-inflammatory cytokines such as IL-1β, IL-12p70 and IL-18 induced by DC treatment with Ti substrates were low and not different among each other.

MCP-1 is a potent chemokine for monocytes and a variety of other immune cells such as activated CD4$^+$ and CD8$^+$ memory T cells [216]. Furthermore, MCP-1 was released at high levels by osteoblasts in the bone with associated inflammation [217]. The elevated levels of MCP-1 production by DCs treated with PT surfaces are consistent with the enhanced expression of CD86 and mDC morphology observed for DCs treated with PT, indicating a pro-inflammatory DC phenotype. Counter-intuitively, IL-1ra production was also enhanced by PT surfaces. However, it is well-known that upon maturation, DCs naturally up-regulate the production of anti-inflammatory cytokines as a

negative feedback [218]. Therefore, the up-regulated IL-1ra production by DC treated with PT surfaces was presumably initiated by the activated DCs to alleviate the pro-inflammatory response. In addition, DC treatment with SLA substrates increased the production of IL-16, which is a pleiotropic cytokine that can have both pro- and anti-inflammatory properties. IL-16 has been shown to be a chemoattractant for CD4 expressing peripheral immune cells, including $CD4^+$ T cells, monocytes, eosinophils and DCs [219], and the elevated production of IL-16 was directly associated with airway inflammation [220]. In contrast, IL-16 was also demonstrated to inhibit mixed lymphocyte reaction by inhibiting TCR signaling [221], and that the administration of IL-16 reduced the RA symptoms in a murine model [222]. Therefore, the functions of IL-16 are likely dependent on the presence of surrounding cell types and cytokines in the microenvironment. Because of the mature phenotype suggested by the enhanced CD86 expression and dendritic morphology, SLA-treated DCs likely produce IL-16 as part of a pro-inflammatory response. Collectively, the results indicate that treatment with PT or SLA surfaces promote a more mature phenotype of DCs, while treatment with modSLA surfaces does not affect DC phenotype.

PCA was performed in order to draw correlations between DC phenotype and material properties of Ti surfaces from the multi-dimensional dataset. PCA was applied to the data in a blinded fashion to reduce the number of dimensions of the data, thereby facilitating the analysis of latent relationships. Consistent with the experimental data, PCA results suggest that PT and SLA surfaces were pro-inflammatory for DCs, while modSLA appeared to promote a non-inflammatory environment (Figure 5-7B). Furthermore, along with air-water contact angle, surface % C and N were associated with a mDC phenotype, and higher values of these surface characteristics were associated with PT and SLA substrates. In contrast, surface % O and % Ti contents were associated with a non-inflammatory DC phenotype and were detected at higher levels on modSLA

surfaces. In addition, air-water contact angle was heavily associated with IL-10 production as compared to other surface material properties. The proximity of %C and N on the loadings plot indicated that their effects on DC phenotype were similar and presumably redundant. Taken together, PCA not only suggested possible material property–DC response relationships, but it also further supported the experimental results that PT and SLA surfaces are pro-inflammatory, while modSLA surfaces are non-inflammatory, for DCs.

Previous research demonstrated that the high surface energy and microtopography of modSLA surfaces synergistically enhanced the differentiation of osteoblasts and production of local osteogenic factors such as PGE_2, TGF-β1 and osteocalcin [160]. In contrast to PT or SLA surfaces, the study herein showed that modSLA surfaces did not induce a pro-inflammatory environment due to its non-stimulatory effect on DC phenotype, thereby potentially minimizing the innate immune response. Numerous studies have indicated the central role of DCs in osteo-immunology. Elevated numbers of DCs have been found in joints of RA patients [194,195] and have been attributed to the bone loss induced by inflammation [196]. Furthermore, human or mouse activated CD4$^+$ T cells induced by environmental stimuli were shown to up-regulate RANKL, which supports osteoclast differentiation and activation. The over-activity of osteoclasts results in inflammation-induced bone loss [197,198]. Among APCs, DCs are the most potent in bridging innate to adaptive immunity by initiating and regulating T and B cell responses. Activation or maturation of DCs by environmental stimuli, including biomaterial treatments, was shown to induce T cell proliferation [111]. Hence, upon inflammation, DCs can become mature and initiate T cell activation, which can in turn promote the differentiation and survival of osteoclasts. Furthermore, PT-treated DCs were shown in this study to release elevated levels of MCP-1. MCP-1 was previously demonstrated to induce the formation of multinucleated osteoclast-like cells from human

71

primary mononuclear precursors *in vitro* [223]. In another study, MCP-1 and RANKL synergistically promoted the differentiation of and fusion of mouse bone marrow cells into osteoclasts as well as enhanced the mineral dissolution in mouse bone marrow MΦ cultures on calcium phosphate disks [224]. In contrast, modSLA-treated DCs remained immature, evaluated by surface marker expression, morphology and cytokine profile. The ability of surface roughness and energy to induce osteogenesis and improve osseointegration is not only because of its effect on osteoblast and mesenchymal cells [205,206,210,225], but may also be due to its effect on the inflammation process. As a consequence, a non-inflammatory implant material such as modSLA is expected to promote osteoblast differentiation by minimizing local inflammation and associated osteoclast differentiation and to promote peri-implant formation clinically [207].

CHAPTER 6: PREDICTING DC PHENOTYPE FROM POLYMER MATERIAL PROPERTIES THROUGH MULTIVARIATE ANALYSIS[§]

6.1. Introduction

DCs, the most potent APCs, are pivotal in both effective immunity and immune tolerance. Upon challenge with pathogens or pro-inflammatory cytokines, DCs mediate T cell polarization for optimal immune response [58,192,193]. Simultaneously, DCs also actively maintain immunological tolerance towards self or non-harmful antigens by actively inducing the formation of T_{reg}-cells [77]. Furthermore, the phenotype of DCs can be modulated by the biomaterials used to treat the DCs via a biomaterial adjuvant effect [6,113]. In CHAPTER 4, the biomaterial property-DC phenotype relationships began to be investigated using well-characterized biomaterial system implementing multivariate analysis such as PCA. In order to derive more detailed correlations, particularly for polymeric systems, more complex systems with a larger number of biomaterials are expected to be necessary.

Combinatorial and computational approaches in biomaterial design can potentially accelerate the discovery of new biomaterials and increase the diversity of promising polymeric structures for biomedical uses [140,226]. Quantitative structure-property relationship (QSPR) modeling has long been used in drug discovery [227]. This approach was translated into predicting biological response to polymeric biomaterials. For instance, computation models, including artificial neural network (ANN), surrogate modeling, and partial linear squares regression (PLSR), were developed to successfully predict fibrinogen adsorption, rat lung fibroblast growth, and/or metabolic activity after

---

culture on a combinatorial library of 112 polyarylates from a number of material descriptor, including hydrophobicity, glass transition temperature (T_g), and chemical structure [228-231]. Furthermore, computational modeling has been used successfully to create a large virtual library of 40,000 pMAs by the Kohn laboratory with predictable fibrinogen adsorption, fibroblast attachment, and fibroblast growth based on a selection of material descriptors [154]. These models allow for rational design of biomaterials before any polymers are synthesized or any biological experiments are performed and are expected to unprecedentedly expedite the discovery of biomaterials and advance the field of biomaterials.

Previously, a differential equation-based model has been developed to describe primary MΦ fusion in response to different common biomaterials [232]. However, this model did not directly predict host response based on material properties as the predictors. Thus far, no computational models have been developed to describe or predict the response of human primary immune cells to biomaterial properties, which is of outstanding clinical relevance. In this report, the biomaterial-mediated DC phenotype was assessed for a selection of the pMAs developed in Kohn laboratory. This selected set of pMAs was previously shown to induce a wide range of biological response in terms of fibrinogen adsorption, fibroblast adhesion and growth [154]. The material properties of these pMAs were characterized and were shown to co-vary to different extents with phenotypic variables by PCA. PLSR models were then built to predict DC response from different sets of material property predictors. DC maturation based on surface marker expression could be predicted from the material properties with $R^2_{prediction} = 0.76$. Interestingly, the prediction performance was maintained with $R^2_{prediction}=0.80$ when only theoretical chemical composition values were used as the predictor variables. Taken together, the study herein demonstrates for the first time that immune cell response to biomaterials can be predicted from material properties and will expedite *in silico* rational design of future immuno-modulatory biomaterials.

6.2. Materials and Methods

6.2.1. Synthesis pMA combinatorial library

pMAs (Table 6-1) were prepared using chain-growth polymerization via free radical solution (FRS) and reversible addition-fragmentation transfer (RAFT) [233]. All chemicals were high purity, reagent-grade, or HPLC-grade and used as received except as noted: (i) AIBN was recrystallized from MeOH, (ii) Monomers (Figure 6-1) were purified through a column of alumina to remove inhibitors, and (iii) Solvents, solutions, and monomers were degassed with nitrogen or argon before use in free radical or RAFT polymerizations.

The polymerization was carried out using an automated parallel synthesizer. Briefly the synthesizer was inertized by five cycles of evacuation under vacuum at $120^{o}C$ and degassed monomers (single or multiple monomers in desired mole ratios for desired target ratios), stock solutions of either AIBN (for FRS) or a co-solution of AIBN and 2-cyanoprop-2-yl dithiobezoate (for RAFT) and solvents were charged to the reactors that were vortexed at 600 rpm at $70^{o}C$ for 6 hours (FRS) or 20 hrs (RAFT) under Argon. More than 90 reactions were carried out in a single run. The reactors were cooled to room temperature and the polymers were precipitated manually and dried under vacuum for more than 24 hours at $60^{o}C$. The pMAs used in this study were selected from more than 150 members of the pMA library that were synthesized using this method and consisted of homo-, co- and ter-polymers. Proton NMR was used to determine the composition and gel permeation chromatography for molecular weight determination [233]. Table 6-1 lists the pMAs and the corresponding abbreviations used in PCA and PLSR plots.
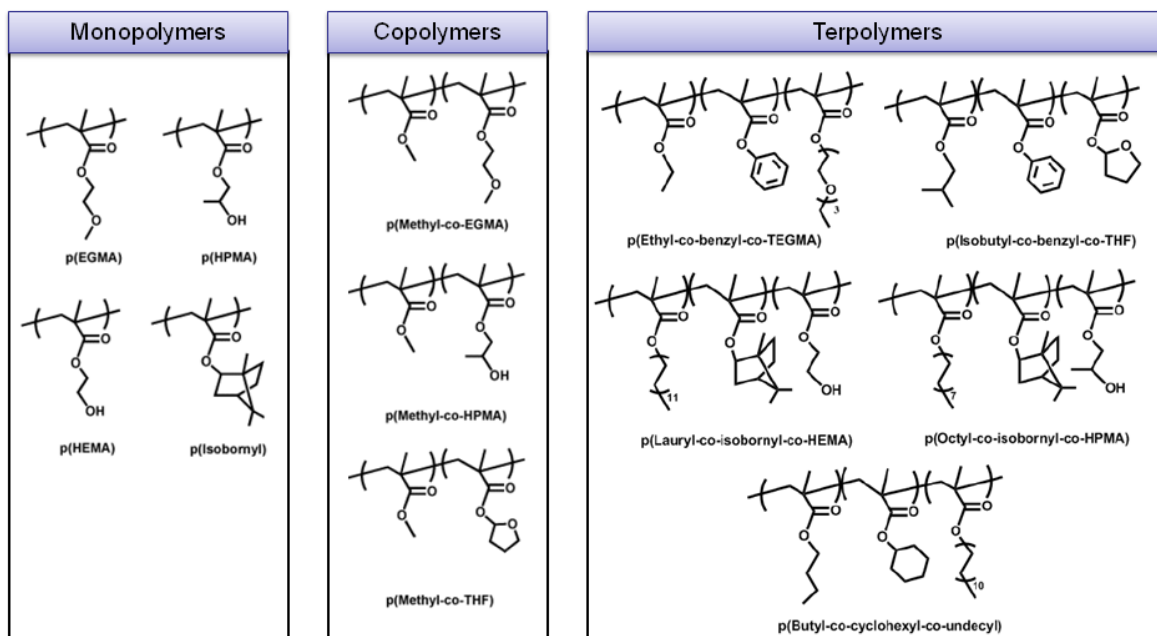
Figure 6-1: Chemical structure of the pMA monomers

Table 6-1: List of pMAs that were used for the training set.

pMA#	Name	Abbreviation
1	Ethylene Glycol Methyl Ether MA	EGMA
2	Hydroxypropyl MA	HP
3	Isobornyl MA	Isobornyl
4	Methyl-EGMA	Me-EGMA
5	Methyl-hydroxypropyl MA	Me-HP
6	Methyl-tetrahydrofurfuryl MA	Me-THFF
7	Ethyl-Benzyl-TEGMA	E-B-TEGMA
8	Isobutyl-Benzyl-THFF MA	I-B-THFF
9	Lauryl-Isobornyl-Hydroxyethyl MA	L-I-HE
10	nButyl-Cyclohexyl-Undecyl MA	nB-C-Undecyl
11	Octyl-Isobornyl-Hydroxypropyl MA	O-I-HP
12	HEMA	HEMA

6.2.2. Coating of pMA in 96-well plate

Each of the pMAs were dissolved 0.5% (w/v) in tetrahydrafuran (THF; Sigma), and the solutions were used to fill the wells of a 96-well polypropylene (PP) plate (Corning, Corning, NY) to ensure that the walls of the wells were coated. The filled plate

was then transferred into an Isotemp vacuum oven (Fisher Scientific). The temperature of the oven was increased 10°C/h from 40°C to 80°C. Vacuum was generated at 80°C, and the solutions were dried under vacuum for 5 days until uniform coatings were formed. Uniform coating of the wells, including the walls, was inspected by mixing the pMA solution with fluorescein to check for homogeneous fluorescence.

6.2.3. Synthesis and coating of terpolymer combinatorial library

The synthesis of terpolymers (Table 6-2) has been described previously [155]. The monomers (Figure 6-2) hydroxyethyl methacrylate (ophthalmic grade) (HEMA or H), 2-ethylhexyl acrylate (EHA or A), triethyleneglycol monomethylether monomethacrylate (TEGMA or T), N-ispropylacryamide (NIPAAM or N), glycidylmethacrylate (GMA or G), and azobisisobutyronitrile (AIBN) were purchased from either Sigma-Aldrich or Polysciences and used as received. The polymers were synthesized by AIBN-initiated radical polymerization of the three monomers in DMF at 70°C. A typical reaction such as the synthesis of 40%HEMA-co-35%TEGMA-co-25%GMA was carried out as follows: HEMA (0.78 mL, 0.006 mols), TEGMA (1.29 mL, 0.005 mols), GMA (0.53 mL, 0.004 mols), and AIBN (2.5mg, 0.015 mmol) were taken place in a round bottomed flask. Dimethylformamide (DMF) (12 mL) was added and the reaction was purged by a stream of nitrogen. The reaction was heated at 70°C for 6 h with rapid stirring. The polymer was precipitated in diethyl ether. The obtained polymer was re-dissolved and precipitated 2x, after which the polymer was dried for 2 days under vacuum. Terpolymer coating procedure was carried out the same way as pMAs. The terpolymers were used as the prediction set.

6.2.4. Surface roughness and surface area measurements

All surface roughness was measured in pMA-coated 96-well wells after cutting off the walls of the wells. Line roughness (R_a) of the pMA coatings were measured by

Wyko optical profilometer (Veeco, Plainview, NY) with a 5x objective. Surface area, surface roughness (S_a), and other surface roughness variables (Table A1-2) were measured by LEXT OLS4000 3D material confocal microscope (Olympus, Center Valley, PA) using a 20x objective in an organic cleanroom in the Marcus Nanotechnology Building at Georgia Tech. Two measurements were performed on each of three coatings for each pMA. The value for each pMA was the average of the six measurements. Representative surface images are shown in Appendix 9.
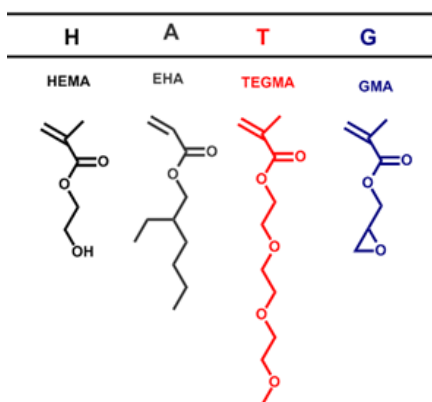
Figure 6-2: Chemical structure of the monomers that made up the terpolymer prediction set.

Table 6-2: List of terpolymers that were used for the prediction set

terpolymer #	Abbreviation	Composition
1	2A	A55T20G25 – 55%A-co-20%T-co-25%GMA
2	2B	A40T35G25 – 40%A-co-35%T-co-25%GMA
3	2D	A10T65G25 – 10%A-co-65%T-co-25%GMA
4	5B	H40T35G25 – 40%H-co-35%T-co-25%GMA
5	5C	H25T50G25 – 25%H-co-50%T-co-25%GMA
6	5D	H10T65G25 – 10%H-co-65%T-co-25%GMA
7	6A	A55H20G25 – 55%A-co-20%H-co-25%GMA
8	6B	A40H35G25 – 40%A-co-35%H-co-25%GMA
9	6C	A25H50G25 – 25%A-co-50%H-co-25%GMA
10	HEMA	100% H

6.2.5. Water-air contact angle and glass transition temperature (T_g) measurements

Polymers were coated on coverslips by solvent casting for contact angle measurements at Rutgers University. Contact angles were determined on a Ramé-Hart goniometer equipped with a camera and DropImage software. A drop of deionized water was placed on the polymer film and the contact angle measured within $1 - 3$ s. T_g was measured by differential scanning calorimetry (2910 Modulated DSC, TA Instruments)

6.2.6. Surface chemical composition measurements by X-ray photoelectron spectroscopy (XPS)

XPS was performed on pMA-coated 96-well wells after cutting off the walls of the wells at the University of Toronto. The samples were analyzed on the Thermo Scientific K-Alpha XPS spectrometer (ThermoFisher, E. Grinstead, UK) located at the University of Toronto. Measurements were obtained at a take-off angle (relative to the surface) of 90°. A monochromatic Al K_α X-ray source was used with a spot area of 400 μm. Charge compensation was necessary and was provided using the flood gun supplied with the instrument. Survey spectra were obtained at low energy resolution (pass energy = 150 eV) in a scanned mode. Quantification was obtained from low resolution spectra acquired in a snapshot mode. The C 1s spectrum was also recorded at high resolution (PE = 25 eV) in a scanned mode. All data processing was performed using the software package supplied with the instrument (Avantage). The high resolution peak fitting was independently performed at Georgia Tech, which included the basic C-C, O-C=O, and C-O bonds (denoted as GT), and in University of Toronto, which included beta carbons and slight C=O contamination in addition to the three basic bonds (denoted as UT). Theoretical values were calculated based on polymer structures and molar ratios determined by NMR. Representative high resolution C1s scans are shown in Appendix 7.

6.2.7. Human dendritic cell culture

Human DC culture was performed in the same manner as in Section 4.2.1. in accordance with an updated protocol H10011 of the Institutional Review Board of Georgia Institute of Technology.

6.2.8. Exposure of DCs to coated pMAs or terpolymers in 96-well plate

On day 5 of culture, loosely adherent and non-adherent cells containing iDCs were harvested and resuspended in DC media with 1000 U/ml GM-CSF and 800 U/ml IL-4 at 5×10^5 DCs/ml. 150 µl of cell suspension (7.5×10^4 DCs) was plated on pMA coatings in quadruplicate in the wells of a 96-well PP plate. The extent of DC maturation was compared to the reference controls cultured on TCPS 96-well plate in parallel: untreated iDCs for the negative reference control and LPS (1 µg/ml)-treated mDCs for the positive reference control. Four of the donors used in the pMA library experiment were used again in the terpolymer library experiment on different days.

6.2.9. Maturation analysis with 96-well filter plate-based high throughput (HTP) method

Differentially-treated and reference control DCs were harvested after 24 h for analysis using a HTP method previously described in CHAPTER 4 [211]. Briefly, all treated DCs and reference controls were transferred to a black 96-well filter plate, and the supernatants were immediately collected into a 96-well plate through the filters by stacking the filter plate on top of the collection plate and centrifuging at $250 \times g$ for 2 min. A portion of the supernatants were used immediately for cytotoxicity assessment by measuring G6PD release from damaged cells (described in the following section), while the remaining portion was stored at -80°C for multiplex cytokine profiling. The cells retained in the wells were assessed for maturation phenotype by immunostaining using antibodies anti-CD86-PE and anti-DC-SIGN-FITC. CD86 is a costimulatory molecule that is upregulated upon DC maturation, and DC-SIGN an endocytic receptor that is

downregulated upon LPS-stimulated maturation. The fluorescent intensities were measured with a Tecan Infinite F500 microplate reader, and the ratio of CD86/DC-SIGN, a cell number independent metric named "maturation factor (MF)", was used to represent DC maturation.

6.2.10. Cytotoxicity and Endotoxin Assessment

Biomaterial-induced cytotoxicity was assessed by the release of G6PD into the media from cells cultured with or without biomaterials following the same procedures described in Section 4.2.5. Briefly, 50 µl of the supernatants were assayed immediately, and the fluorescent intensity was compared to that of the medium from lysed cells. The fluorescence signals were measured after 30 min incubation at 37°C with excitation and emission filters 535/25 and 590/20, respectively. The endotoxin contents of the pMA coatings were measured using a chromogenic substrate (QCL-1000 LAL assay, Lonza) and determined to be less than 0.1 EU/mL, which is well below the FDA limit of 0.5 EU/mL.

6.2.11. Multiplex cytokine profiling

The supernatants collected from the cell culture media in the presence of pMAs or reference controls were stored at -80°C and were thawed only once for multiplex cytokine analysis as described in Section 5.2.6. For the pMA training set, through six independent experiments each with a different donor, cytokine analysis was performed for pro-inflammatory cytokines (IL-1β, IL-12p70, IL-15, IL-18, and TNF-α), anti-inflammatory cytokines (IL-1ra and IL-10), a pleiotropic cytokine (IL-16), and chemokines (IL-8, MCP-1, and MIP-1α). For the terpolymer prediction set, cytokine analysis was performed for IL-1β, IL-ra, IL-8, IL-16, MCP-1, and TNF-α.

81

6.2.12. Statistical analysis

To observe any significant differences between all sample groups in pairs, a pair-wise two-way ANOVA followed by Tukey post test was performed using the GraphPad Prism 5 software (La Jolla, CA), and the p-value equal to or less than 0.05 was considered significant.

6.2.13. Principal component analysis (PCA)

PCA was performed on the DC phenotype and pMA material property dataset to draw correlations between DC response and material properties. PCA is a dimension reduction technique, which finds a few principal components (PCs) (new axes in the PC space) that represent dimensions with maximal variability and highlight the global covariance patterns of the variables [213]. The data matrix $X \in R^{72x29}$ consisted of both phenotypic and material variables (29 variables). Phenotypic variables included MF (CD86/DC-SIGN) obtained in the HTP assay and production levels of seven cytokines and chemokines (IL-1β, IL-1ra, IL-8, IL16, MCP-1, MIP-1α, and TNF-α). Values of IL-10, IL-12p70, and IL-18 measurements were close to the detection limit, and IL-15 could not be detected; therefore these cytokines and chemokines were not included in the PCA analysis. Material property variables included air-water contact angle (θ or Theta), T_g, line roughness, surface roughness, and surface chemical composition by XPS (Table A1-1). The 72 observations included six independent experiments with 12 different pMAs to generate the individual phenotypic variable values. PCA algorithm was applied to the data matrix to extract the latent correlations among the variables. All variables were pre-processed by mean centering and unit-variance scaling [214,215]. Based on the distribution of the variables, some were log-transformed to ensure Gaussian distributions of data. PCA was performed using the software SIMCA P+. The performance of a PCA model can be summarized by two primary quantitative measures: goodness of fit of the model to the current dataset as given by R^2 and goodness of prediction of the model for

predicting outcomes of future experiments as given by Q^2, a measure of the cumulative fraction of the total variation of the X block that can be predicted by all PCs. A high R^2 is required for a high Q^2, and a Q^2 of > 0.5 is considered good [234].

$$R^2X = 1 - \frac{RSS}{SSX_{tot.corr.}}$$

$$Q^2X = 1 - \frac{PRESS}{SSX_{tot.corr.}}$$

Where $SSX_{tot.corr.}$ is the total sum of squares of X matrix (i.e. total variation in the X block), RSS is the fitted residual sum of squares, and PRESS is the predictive residual sum of squares calculated from cross-validation and is defined as

$$PRESS = \sum_i \sum_k (x_{ik} - \hat{x}_{ik})^2$$

where x_{ik} is the experimental values of the variables, $\hat{x}_{ik}$ is the predicted values of the variables from the reduced models during cross validation, i is the row position of data matrix, and k is the column position of the data matrix. The suitable number of PCs is determined by the optimal balance between fit and predictive ability (see reference [234-236] for details).

6.2.14. Partial Least Square Regression (PLSR) Modeling

PLSR is a powerful computational method that expresses a set of dependent variables (outcomes) in terms of linear combinations (principal components) of the independent variables (predictors). PLSR is very similar to PCA with an added algorithm for maximizing the correlations between the X (independent or predictor variable) and Y (dependent or outcome variable) blocks in the PC space. The dataset used for PLSR included all the variables in PCA as well as additional roughness variables and was divided into two matrices: $X \in R^{72 \times 119}$, consisting of the material property measurements as the predictor variables, and $Y \in R^{72 \times 1}$, containing only one DC response variable, MF.

The material variables were copied six times for the six donor trials as they were the same for each donor. Table A1-2 summarizes the variables included for each observation. The performance of a PLSR model can be determined by R^2Y and Q^2Y. A Q^2Y of > 0.5 is considered good [234]. Analogous to PCA,

$$R^2Y = 1 - \frac{RSS}{SSY_{tot.corr.}}$$

$$Q^2Y = 1 - \frac{PRESS}{SSY_{tot.corr.}}$$

where $SSY_{tot.corr.}$ is the total sum of squares of Y matrix (i.e. total variation in the Y block), RSS is the fitted residual sum of squares, and PRESS is defined as:

$$PRESS = \sum_i \sum_m (Y_{im} - \hat{Y}_{im})^2$$

where Y_{im} are the experimental values of the Y variables, $\hat{Y}_{im}$ is the predicted values of the variables from the reduced models during cross validation, i is the row position of data matrix, and m is the column position of the data matrix. The PCs derived from the PLSR model result in linear combinations of the predictor variables optimized for the maximum covariance with the dependent DC phenotypic variable. From this initial model, a pruning step was performed to remove variables with low variance influence on projection (VIP < 0.7) and low reliability as determined by jack-knifing [236]. PLSR modeling was performed using SIMCA P+.

The model performance was determined by how well the predicted values matched the observed values by evaluating the regression coefficient, $R^2_{prediction}$. Because with more explanatory terms in a model, the model fit generally tends to improve with an inflated $R^2_{prediciton}$, the adjusted $R^2_{prediction}$ ($\bar{R}^2_{prediction}$) is also presented here to penalize the use of more PCs in the models. $\bar{R}^2$ is defined as:

$$\bar{R}^2 = 1 - (1 - R^2)\frac{n - 1}{n - p - 1}$$

where n is the sample size, which is 72 (6 donors × 12 treatments) in all the models, and p is the number of explanatory terms, which is equivalent to the number of principal components necessary for the model. In addition, CV-ANOVA (cross validation-ANOVA) was performed for significance testing of the models. This technique results in F-statistcs and p-values, which are useful for evaluating the significance of the model, i.e. whether the model is developed merely by chance.

6.3. Results

6.3.1. pMAs induced differential DC response

The results of material characterization of the twelve pMAs are summarized in Table 6-3. DCs responded differentially to this set of polymers. There is a trend of increasing DC maturation as shown by the metric CD86/DC-SIGN for the ordering of polymers used to treat DCs, as represented on the x-axis (Figure 6-3A). When keeping the ordering of polymers the same, the release of pro-inflammatory cytokine, TNF-α (Figure 6-3B), and chemokine, IL-8 (Figure 6-3D), by treated DCs appeared to follow the same trend with pHEMA inducing the lowest amount of TNF-α and IL-8 production in DCs. In contrast, pHEMA induced the highest amount of IL-16 secretion from DCs, which was statistically different from iDC and mDC reference controls as well as all the other pMA treatments examined (Figure 6-3C). Furthermore, this set of pMAs induced differential levels of cytokine secretion. In particular, poly(isobutyl-benzyl-THFF)MA (pIBTMA) induced the highest levels of TNF-α (Figure 6-3B) and IL-8 (Figure 6-3D) relative to all the other pMAs, while poly(isobornyl)MA induced the most IL-16 after pHEMA (Figure 6-3C). Other cytokines and chemokines assayed did not appear to follow as a clear trend (Figure 6-4), but they induced differential levels of IL-1β (Figure 6-4A), IL-1ra (Figure 6-4D), IL-10 (Figure 6-4E), IL-18 (Figure 6-4C), and MIP-1α (Figure 6-4G) production. Generally, the pMAs on the left of the plots induced low amounts of the cytokines or chemokines from treated DCs, while the pMAs on the right

induced relatively higher amounts. Again, pIBTMA induced the highest amounts of pro-inflammatory cytokines and chemokine such as IL-1β (Figure 6-4A), IL-18 (Figure 6-4C), and MIP-1α (Figure 6-4G). The pMAs did not induce significant cytotoxicity in treated DCs. Interestingly, pHEMA induced lower cell death as compared to all the other pMAs (Figure 6-5).

Table 6-3: Summary of material property measurements for the 12 pMAs (the training set). The pMAs are ordered the same way as in Figure 6-3.

	HEMA	HP	Me-EGMA	Me-HP	EGMA	Me-THFF	E-B-TEGMA	L-I-HE	O-I-HP	Isobornyl	I-B-THFF	nB-C-Undecyl
Theta	69.5	71.2	17.2	73.8	21.5	70.5	20.8	29.0	62.8	29.2	28.7	39.0
Tg	87.6	83.8	55.8	90.7	15.2	91.3	1.6	-7.7	27.3	130.2	30.9	148.9
Si2p (E)	0.1	0.3	2.0	0.1	0.5	0.2	2.2	1.0	0.5	0.4	0.3	3.0
C1s (E)	84.6	78.7	75.3	91.5	91.7	95.7	78.4	87.0	86.3	90.4	91.5	81.2
O1s (E)	15.3	21.0	22.7	8.4	7.8	4.1	19.4	12.1	13.2	9.2	8.2	15.8
C1s (T)	66.7	70.0	75.4	72.5	70.0	72.5	78.3	87.0	85.1	87.5	78.5	87.8
O1s (T)	33.3	30.0	24.6	27.5	30.0	27.5	21.7	13.0	14.9	12.5	21.5	12.2
C-C (UT)	63.9	62.3	54.9	71.7	82.2	68.5	64.7	76.8	64.5	74.5	84.0	75.8
C-O (UT)	20.8	14.7	22.8	10.7	7.7	11.8	19.3	10.0	17.3	5.9	6.6	11.4
O-C=O (UT)	5.6	8.1	11.8	4.8	2.6	5.6	7.0	4.3	9.1	2.6	3.3	3.9
Beta C	9.7	11.5	10.5	12.8	7.5	13.1	9.0	9.0	7.6	14.9	6.1	4.9
C=O	0.0	3.4	0.0	0.0	0.0	1.1	0.0	0.0	1.6	2.0	0.0	4.0
C-C (GT)	73.6	76.4	64.9	84.9	88.9	75.5	73.8	89.2	70.8	87.9	91.3	90.3
C-O (GT)	19.8	13.8	18.5	8.0	7.3	18.9	19.0	5.0	19.5	7.0	5.9	3.6
O-C=O (GT)	6.6	9.8	16.6	7.1	3.8	5.8	7.2	5.8	9.7	5.2	2.8	6.1
C-C (T)	0.50	0.57	0.51	0.58	0.43	0.62	0.58	0.85	0.83	0.86	0.73	0.86
C-O (T)	0.33	0.29	0.33	0.27	0.43	0.14	0.31	0.09	0.10	0.07	0.12	0.07
O-C=O (T)	0.17	0.14	0.17	0.16	0.14	0.24	0.11	0.06	0.08	0.07	0.16	0.07
Ra	0.23	0.84	0.44	0.25	0.59	1.05	0.13	0.45	0.24	0.13	0.81	0.44
Sq	0.85	0.70	0.94	0.37	0.55	0.51	0.31	0.33	0.23	0.72	0.30	0.30
Ssk	1.49	0.07	1.37	-0.13	0.51	5.45	-0.53	3.68	1.84	-1.02	2.29	4.89
Sku	22.17	10.96	29.49	16.1	47.70	134.5	30.64	129.5	48.1	7.91	66.83	111.96
Sp	10.89	9.06	12.35	7.26	12.67	13.46	6.16	9.10	5.71	6.46	6.98	8.98
Sv	4.13	4.92	8.39	3.13	8.96	5.47	4.31	3.94	1.74	6.87	4.06	3.56
Sz	15.02	13.98	20.74	10.4	21.63	18.93	10.46	13.04	7.45	13.33	11.04	12.54
Sa	0.66	0.53	0.63	0.27	0.34	0.31	0.20	0.20	0.17	0.54	0.21	0.18
Sk	2.05	1.45	1.52	0.73	0.82	0.87	0.51	0.54	0.53	1.40	0.64	0.54
Spk	0.90	0.57	1.51	0.35	0.52	0.68	0.22	0.35	0.25	0.39	0.32	0.39

Table 6-3 continued:

Svk	0.67	0.97	1.19	0.60	1.13	0.55	0.64	0.51	0.22	1.28	0.32	0.31
SMr1	11.17	9.62	13.62	10.1	9.92	10.44	9.47	10.21	10.1	7.85	10.16	10.62
SMr2	89.95	85.03	87.48	86.5	86.15	87.60	87.68	88.30	88.7	82.45	89.23	89.89
Sxp	1.73	1.30	1.52	0.63	0.70	0.75	0.43	0.45	0.45	1.24	0.55	0.45
Vvv	0.09	0.10	0.12	0.06	0.10	0.06	0.06	0.04	0.03	0.13	0.03	0.03
Vvc	1.01	0.71	0.90	0.35	0.40	0.43	0.24	0.26	0.25	0.65	0.31	0.26
Vmp	0.05	0.03	0.07	0.02	0.03	0.04	0.01	0.02	0.01	0.02	0.02	0.02
Vmc	0.72	0.59	0.62	0.28	0.31	0.32	0.19	0.19	0.19	0.59	0.23	0.19
Sal	146.1	5.61	82.17	70.5	8.29	59.30	4.14	25.59	70.9	3.10	51.71	72.18
Str	0.45	0.59	0.38	0.64	0.54	0.56	0.85	0.61	0.59	0.82	0.65	0.53
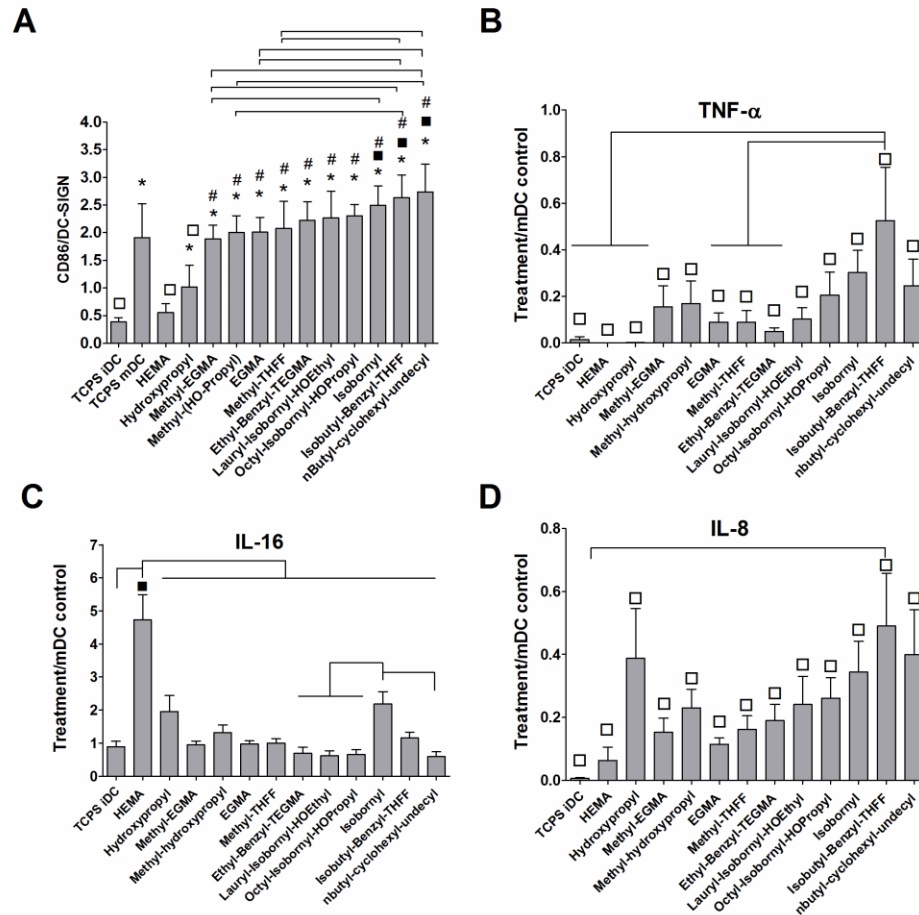
Figure 6-3: DC responded differential to the pMAs. A) Maturation factor (CD86/DC-SIGN). Release of B) pro-inflammatory cytokine TNF-α, C) anti-inflammatory cytokine IL-16, and D) chemokine IL-8 was represented by the fold change against iDC. *: p<0.05 different from iDC; #: p<0.05 different from HEMA and hydroxypropyl; ■: p<0.05 higher than mDC; □: p<0.05 lower than mDC; brackets: p<0.05 different between treatments
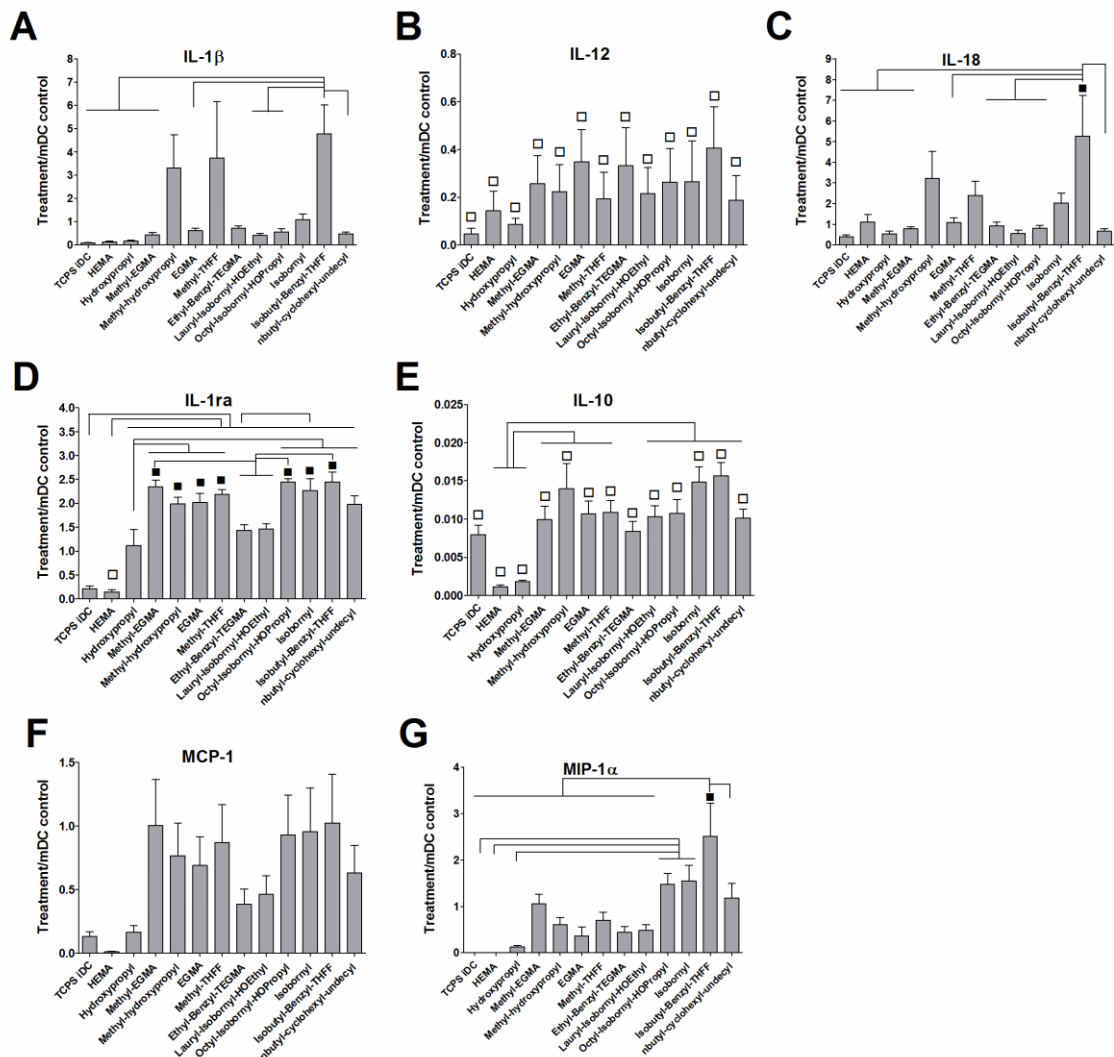
Figure 6-4: Cytokine and chemokine profiles induced by pMA treatments of DCs. This set of cytokines and chemokines analyzed did not follow as clear trend of increasing DC maturation along the same ordering of polymers listed in the x-axis. A) IL-1β, B) IL-12p70, and C) IL-18 are pro-inflammatory cytokines; D) IL-1ra and E) IL-10 are anti-inflammatory cytokines; F) and G) are chemokines. ■: p<0.05 higher than mDC; □: p<0.05 lower than mDC; brackets: p<0.05 different between treatments
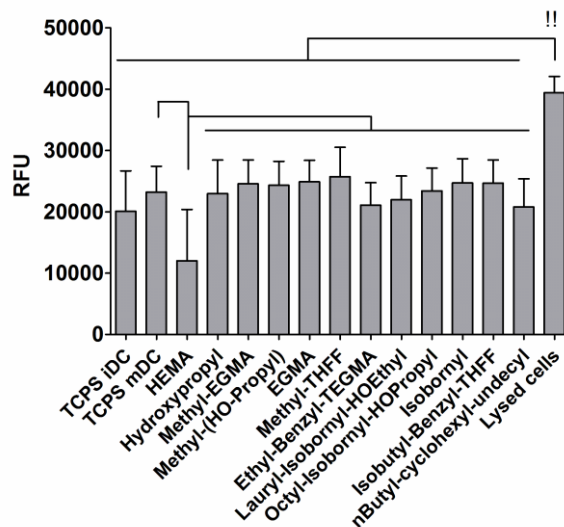
Figure 6-5: pMAs did not induce significant cytotoxicity of DCs. Brackets: p < 0.05 between treatments. !! indicates the signal was beyond upper limit for this assay.

6.3.2. PCA indicated differential DC maturation induced by the pMAs and represented correlations between DC phenotype and material properties

A five-component PCA model was determined by cross-validation to be the most optimal for representing this dataset with $R^2 = 0.78$ and $Q^2 = 0.61$, meaning that this model can capture 78% of the information in the original data space with good predictability. The five components could individually capture 33.5%, 18.2%, 10.9%, 9.6%, and 6.1% of data information, respectively. No major outliers were identified by the Hotelling's T^2 statistic, which is a multivariate generalization of the Student's T distribution. The score plots showed a wide spread nature of the projection of the observations, indicating that the pMAs induced a wide range of DC responses (Figure 6-6A). Furthermore, pMAs that induced low DC maturation in experiments, such as pHEMA and pHPMA, segregated to the left of the PC1, while pMAs that induced high DC maturation, such as pIBTMA and p(nB-C-Undecyl)MA, located to the right of PC2, suggesting that PC1 can be roughly defined as the "maturation" axis.
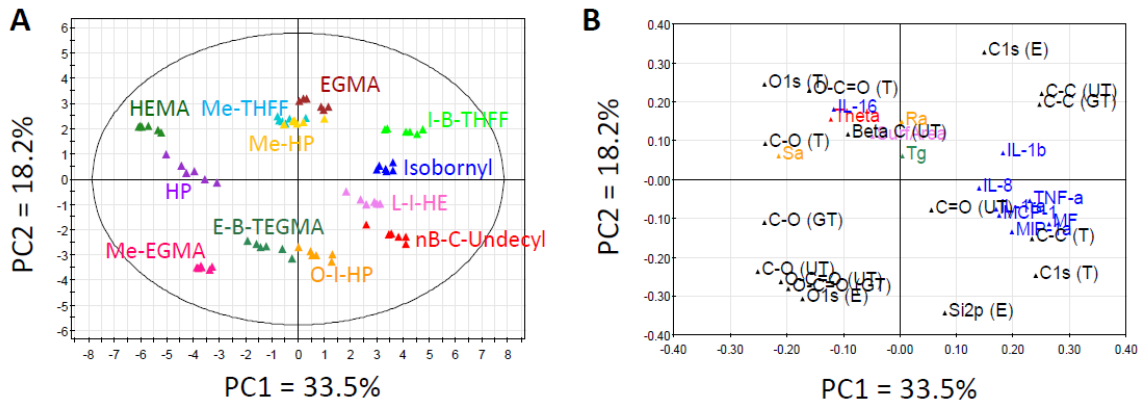
Figure 6-6: Score and loading plots showing the projection of the treatments and variables on the PC space. PC1 captures 33.5% and PC2 captures 18.2% of the data, which together represent >50% of the original data information. A) Score plot shows the projection of the pMA treatments, each with six data points obtained from six independent experiments with different donors. B) Loading plots shows the projection of the variables on the PC space. See text for detailed interpretation of the plots. The following color code is used for the loading plot: Blue: phenotypic variables; black: chemical composition; red: contact angle; orange: roughness; green: T_g; pink: surface area. The interpretation of the combination of PC1 with other PCs resulted in similar conclusion; therefore these plots are omitted for simplicity.

The loading plot represent how the material properties and DC phenotypes correlate to each other (Figure 6-6B). First, all the phenotypic variables measured strongly clustered and mostly located in a quadrant diagonally opposite from IL-16. Overall, the theoretical values of C-C, C-O, and O-C=O bond composition mostly clustered with experimental values (both fitted in U of Toronto and Georgia Tech), and they were situated away from DC maturation variables and were associated with an immature DC phenotype. Although there was difference in the projection of theoretical and experimental values of C1s onto the other PCs, these variables were always associated with the maturation phenotypic variations along PC1 (data not shown). Most importantly, the projection of O-containing bonds in the loading plots was always diagonally opposite to that of C only bonds (Figure 6-6B). In addition, contact angle and surface roughness (S_a) were located away from the maturation variables. Interestingly, line roughness (R_a), T_g, and surface area were consistently situated close to the origin of

90

the plots except that T_g had influence on PC3, and surface area had influence on PC3 and PC5, neither of which captured more than 10% of data information (data not shown). The overall results were very similar regardless of the combinations of PCs. Although the model was best fitted with five PCs, MF and most of the surface chemical compositions could be well modeled by only two PCs (Figure 6-7A). However, after five PCs were applied (Figure 6-7B), many of the cytokines and chemokines, along with T_g, R_a, and surface area, were still poorly modeled, with low R^2 or large difference between R^2 and Q^2 (an indicator of poor model performance when $R^2 - Q^2 > 0.3$).
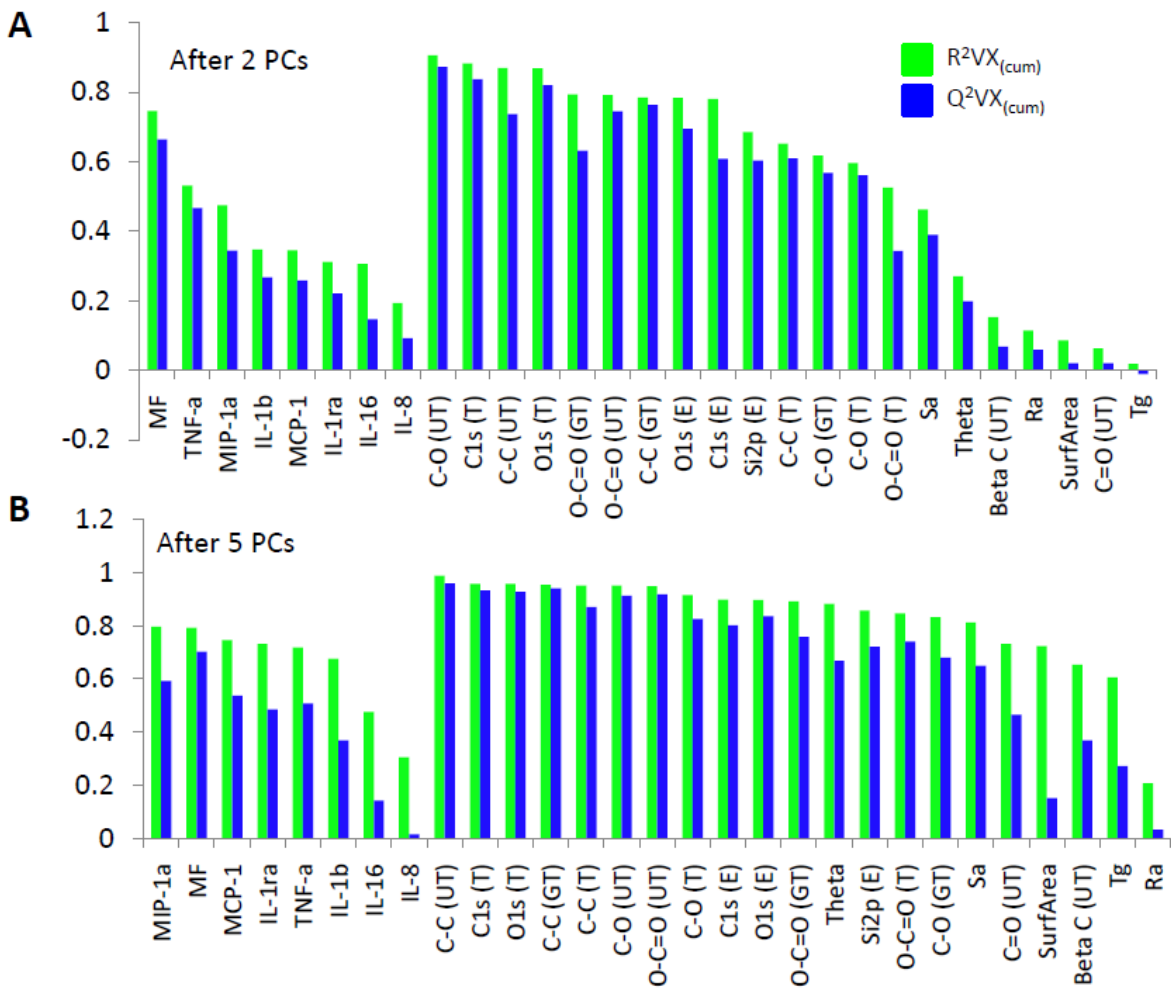
Figure 6-7: Cumulative R^2 and Q^2 after (A) 2 PCs or (B) 5 PCs for the PCA model.

6.3.3. Surface material properties could predict the relative effects of pMAs on DC's MF level

After pruning the initial PLSR model to remove variables of low importance and reliability (e.g. C=O contamination, T_g, R_a, surface area, etc.), the resulting $X \in R^{72 \times 91}$ data matrix was fitted with a two-component model with $R^2Y = 0.63$ and $Q^2 = 0.58$. CV-ANOVA determined that the model is significant with p-value = 4.41×10^{-12} (Table 6-4). Consistent with PCA, the score plot segregated pMAs that induced less DC maturation to the left of PC1, but segregated pMAs that induced high DC maturation to the right of the PC1; therefore, PC1 could also be defined as the "maturation axis" for this PLSR model (Figure 6-8A). PC1 could correlate material properties to MF with $R^2Y = 0.52$ and $Q^2 = 0.50$, while PC2 could draw additional correlation with $R^2Y = 0.12$ and $Q^2 = 0.17$.

Predictor variables that were highly correlated or anti-correlated with the outcome variable, MF, could be visualized by their relative placement in the loading plot (Figure 6-8B). Again, surface carbon, along with Si contamination, was strongly correlated to DC maturation, MF, whereas surface oxygen was strongly anti-correlated to DC maturation. The analysis of the loading weight of the variables (w*c) and the VIP underscored the importance of surface chemical composition, particularly the theoretical values, on predicting DC responses (Table A1-3–4). Specifically, among chemical composition variables, C-C (T), C1s (T), and MF had the strongest weight along positive PC1, while O1s (T), C-O (T), and OC=O (T) had the strongest weight along negative PC1 (Figure 6-8C), where "T" indicates theoretical values. As expected, the C bonds were positively weighted on PC1, while O-containing bonds were negatively weighted on PC1. Interestingly, most of the roughness structures were negatively weighted on PC1 (Figure 6-8C). In contrast, contact angle (Theta) was weighted negatively and most of the roughness variables positively on PC2 (Figure 6-8D).
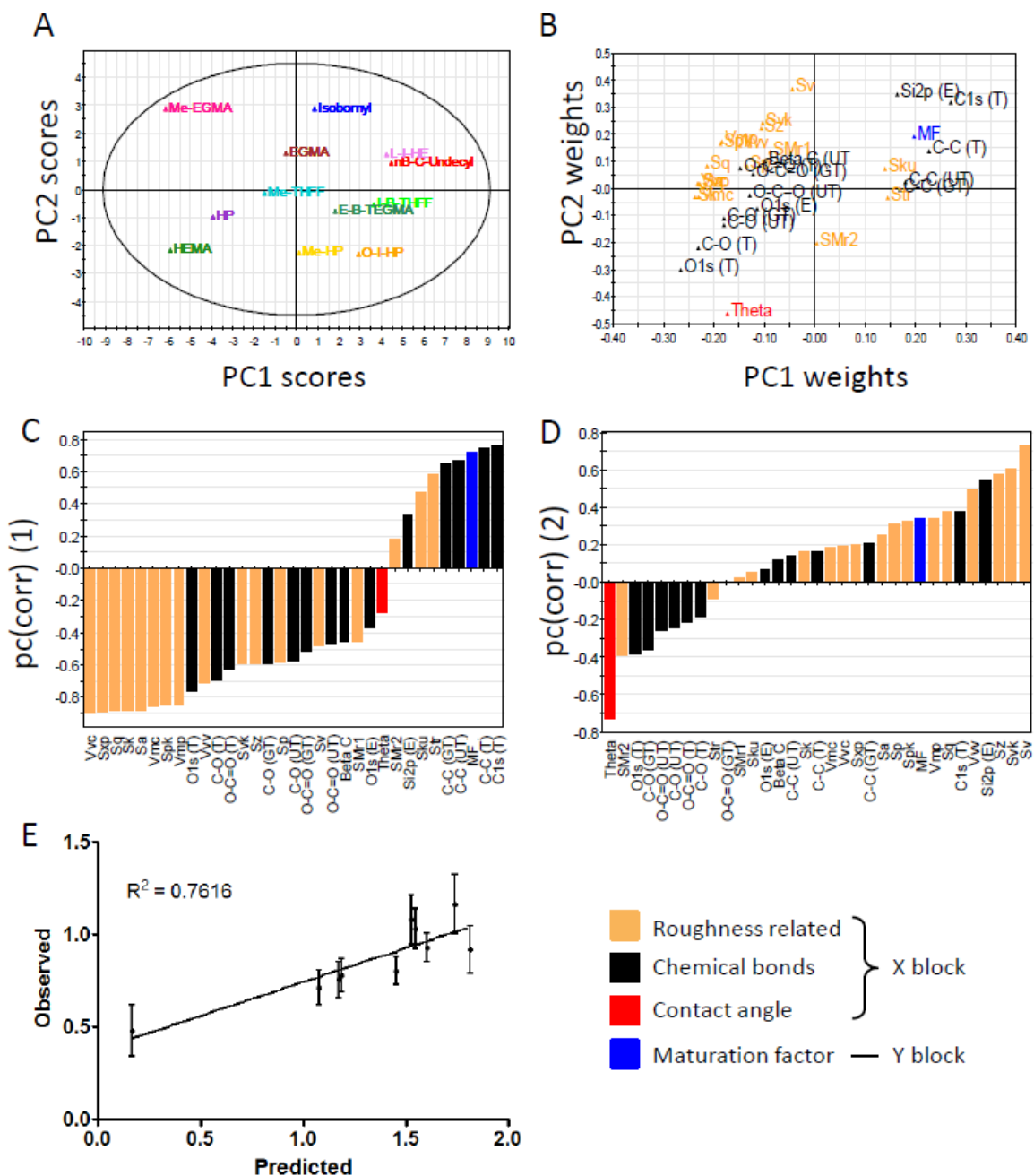
Figure 6-8: Maturation factor prediction from surface material properties using a PLSR model. A) Score plot showing the projection of the pMAs onto the PC space. B) Loading plot showing the projection of the material properties (predictor variables) onto the PC space. C-D) loading weight of the variables in PC1 (C) and PC2 (D). E) Prediction of MF induced by a different set of acrylate- and methacrylate-based polymers in six independent experiments with different donors. The error bars indicate the standard errors of the experimental values.

The robustness of this model was tested by applying it to predict the MF levels in DCs induced by the prediction set, which was derived from the experiments using a different set of acrylate- and methacrylate-based terpolymers averaged from six independent experiments with six donors. Linear regression on the prediction resulted in $R^2_{prediction} = 0.76$ (Figure 6-8E) and $\bar{R}^2_{prediction} = 0.75$ (Table 6-4), indicating that the model was able to predict future experiments well, at least with methacrylate and acrylate-based polymers. The detailed phenotypic analysis and material characterization are described in Appendix 6.

Interestingly, by removing the experimental XPS values either obtained with (in UT) or without beta carbon fitting (in GT) still resulted in strong predictive models with $R^2_{prediction} = 0.71$ and $\bar{R}^2_{prediction} = 0.70$ if beta carbon fitting is included (i.e. remove XPS values at GT) (Figure A1-1A) or with $R^2_{prediction} = 0.77$ and $\bar{R}^2_{prediction} = 0.77$ if beta carbon is not included (i.e. remove XPS values at UT) (Figure A1-1B, Table 6-4).

Analogous models were constructed to predict the cytokine levels and were found to have $R^2Y < 0.55$ and $Q^2 < 0.4$. These models were also unable to predict future experiments with low $R^2_{prediction} < 0.3$. Due to the high correlation among the maturation variables as shown by the PCA model, a full Y block containing all these variables were expected to be reduced to a few dimensions. Therefore, a PLSR model with a full Y-block: $Y \in R^{72x8}$ was also constructed with $R^2Y = 0.37$ and $Q^2 = 0.33$ (3 PCs), which was still effective in predicting MF ($R^2_{prediction} = 0.71$) but ineffective in predicting cytokine profile outcomes in future experiments with $R^2_{prediction} < 0.15$.

6.3.4. Theoretical chemical composition alone was sufficient in predicting the relative effects of pMAs on DC's MF level

A PLSR model was built using only the theoretical values of chemical compositions of the pMAs. A three-component model was fitted for this $X \in R^{72x5}$ data matrix with $R^2Y = 0.61$ and $Q^2 = 0.58$ during cross-validation (Figure 6-9) and a p-value

= 2.3×10^{-10} based on CV-ANOVA (Table 6-4). PC1 can correlate material properties to MF with $R^2Y = 0.43$ and $Q^2 = 0.41$, PC2 can draw additional correlation with $R^2Y = 0.12$ and $Q^2 = 0.18$, and PC3 can capture the remaining covariance with $R^2Y = 0.07$ and $Q^2 = 0.13$. Similar to the previous PLSR model, PC1 could be used to roughly segregate the effects of the materials that induced differential levels of DC maturation (Figure 6-9). Consistent with both PCA and previous PLSR models, surface carbon (C1s) was strongly associated with DC maturation by locating the same quadrant as MF, while surface oxygen was found to associate with an immature DC phenotype by situating oppositely to MF. In addition, surface carbon was strongly positively weighted in PC1, but surface oxygen was strongly negatively weighted in PC1 (Figure 6-9C). In contrast, C1s and O-C=O along with MF had positive influence on PC2, C-C and O1s had negative influence on PC2, and C-O had little influence on PC2 (Figure 6-9D). All five variables had strong influence on the model (Table A1-5–6). This simple model could effectively predict the MF levels in DCs induced by the prediction set (Table 6-2) with $R^2_{prediction} = 0.80$ and $\overline{R}^2_{prediction} = 0.79$, indicating strong predictive robustness (Figure 6-9E, Table 6-4).

Similar to the previous PLSR model, analogous models aimed at predicting the cytokine levels had low model performance with $R^2Y < 0.45$ and $Q^2 < 0.4$ and were unable to predict future experiments with low $R^2_{prediction} < 0.15$. In addition, a PLSR model with a full Y-block: $Y \in R^{72 \times 8}$ also resulted in a poorly performing model $R^2Y = 0.37$ and $Q^2 < 0.33$ (3 PCs), which, consistent with previous PLSR model, was still effective in predicting MF with $R^2_{prediction} = 0.79$ but ineffective in predicting cytokine profile outcomes in future experiments with $R^2_{prediction} < 0.1$.

In contrast, when experimental XPS values were used alone, the predictability of the models was much poorer. PLSR models derived from a) both experimental XPS values analyzed with (in UT) or without (in GT) beta carbon fitting, b) only experimental XPS values with carbon fitting, and c) only experimental XPS values without carbon fitting all performed poorly with $R^2Y \cong 0.2$ and $Q^2 < 0.2$. These models could predict MF

with $R^2_{prediction} \leq 0.32$ and $\bar{R}^2_{prediction} \leq 0.31$ with p-values at least five magnitudes lower than the model developed using only theoretical values (Table 6-4). These models were developed with the removal of Si contamination and C=O contamination on the surfaces because the effects of these minute contamination were amplified in PLSR modeling, where each variable is given equal weight to the problem at hand. When Si and C=O were maintained in the models, although the model fit would be improved due to the addition of two more PCs, the resulting models made even poorer prediction for MF. Alternatively, a multiplier of smaller than 1 could be manually set for variables that are not expected to contribute significantly to the modeling due to their small quantities. This approach did not result in improved models.

Table 6-4: Summary of model performance (all models have undergone pruning steps <u>except</u> for the model based on only theoretical or experimental XPS)

Predictors Used in Model	R^2Y	Q^2	$R^2_{prediction}$	$\bar{R}^2_{prediction}$	F	p-value
Full set of material properties	0.63	0.58	0.76	0.75	23.3	4.4×10^{-12}
Theoretical XPS only	0.61	0.58	0.80	0.79	14.4	2.3×10^{-10}
Experimental XPS only (both GT and UT)	0.21	0.19	0.26	0.25	8.3	5.8×10^{-4}
Experimental XPS without beta carbon fitting only (GT only)	0.19	0.17	0.24	0.23	7.2	1.5×10^{-3}
Experimental XPS with beta carbon fitting only (UT only)	0.20	0.19	0.32	0.31	7.9	8.5×10^{-4}
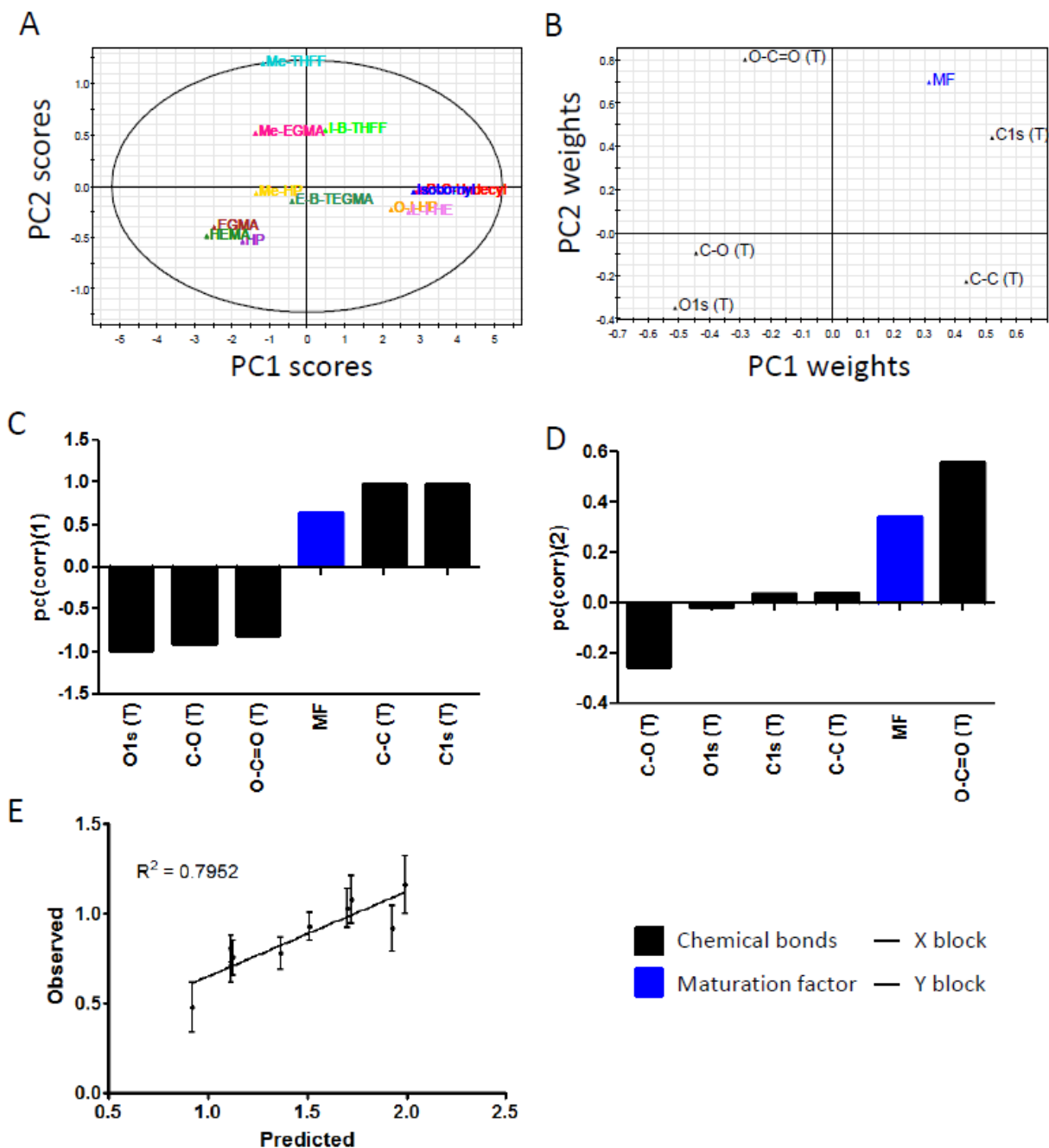
Figure 6-9: Maturation factor prediction from theoretical surface chemical composition alone using a PLSR model. A) Score plot showing the projection of the pMAs onto the PC space. B) Loading plot showing the projection of the material properties (predictor variables) onto the PC space. C-D) loading weight of the variables in PC1 (C) and PC2 (D). E) Prediction of MF induced by a different set of acrylate- and methacrylate-based polymers in six independent experiments with different donors. The error bars indicate the standard errors of the experimental values.

6.4. Discussion

The phenotype of DCs was differentially modulated by the 12 pMAs. The pMAs induced a wide range of DC response as represented by the MF metric (Figure 6-3). Interestingly, many of the pMAs induced higher level of DC maturation upon treatment represented by this metric as compared to LPS stimulation (TCPS mDC) (Figure 6-3A). When the ordering of pMAs was kept consistent throughout the other plots, the production of TNF-α and IL-8 by DCs induced by the pMAs appeared to follow roughly the same trend with pHEMA inducing the least amount of TNF-α and IL-8 release by DCs. In contrast, pHEMA induced the highest amount of IL-16 production that is significantly different from iDCs, mDCs and all other pMA treatments (Figure 6-3B, C, and D). TNF-α is a pro-inflammatory cytokine, and IL-8 is a chemokine, both of which are released upon DC maturation. IL-16 has been shown to be a pleiotropic cytokine that can have both pro- and anti-inflammatory properties. The functions of IL-16 are likely dependent on the presence of surrounding cell types and cytokines in the microenvironment [237]. Because pHEMA induced very low maturation marker expression and low secretion of cytokines and chemokines that are typically elevated in inflammation, the pHEMA-treated DCs likely produced IL-16 as a part of anti-inflammatory response.

The production of the other seven cytokines by DCs did not follow a clear trend based on the same ordering of pMAs in the x-axis (Figure 6-4), but the low amounts of cytokine release are clustered to the left while the higher amounts clustered to the right, which is consistent with the DC maturation represented by MF. Particularly, this set of pMAs induced differential levels of IL-1β (Figure 6-4A), IL-1ra (Figure 6-4D), IL-10 (Figure 6-4E), IL-18 (Figure 6-4C), and MIP-1α (Figure 6-4G) secretion. Most notably, besides TNF-α (Figure 6-3B) and IL-8 (Figure 6-3D), pIBTMA induced the highest levels of IL-1β, IL-18, and MIP-1α production by treated DCs relative to all other pMA treatments. Since pIBTMA-treated DCs also expressed high level of MF, it can be

concluded that pIBTMA potentially induced the highest level of DC maturation among these pMAs examined. Anti-inflammatory cytokines IL-1ra and IL-10 increased with enhanced DC maturation as well. Most likely, these anti-inflammatory cytokines have been naturally up-regulated as a negative feedback to modulate the inflammatory response [218]. Interestingly, pHEMA induced very low levels of all these cytokines and chemokines; in some cases, the levels were even lower than those induced by iDCs. IL-15 was only detectable in one of the six donors and the data were not shown.

PCA was applied to the dataset that contains both the DC phenotype and material property information to draw correlations among the variables. PCA reduced the dimensions of the dataset into lower dimension space to facilitate the analysis of latent relationships. Most of the cytokine variables were log-transformed due to the multi-magnitude differences induced by the pMA treatments. A five-component PCA model was the most optimal to represent the original dataset in the new principal component space with $R^2 = 0.78$ and $Q^2 = 0.61$. These values are excellent for this dataset, which contains many phenotypic and material property variables (29 variables) and large donor-to-donor variations, particularly in the cytokine profiles. pMAs were spread along PC1 in the score plot roughly based on their effects on DC maturation, so PC1 was coarsely defined as the "maturation axis" (Figure 6-6A). PCA allows the multi-dimensional data to be projected onto this reduced PC space for easy visualization of the correlations among the variables.

The loading plots represent the correlations among the variables (Figure 6-6B). Consistent with the experimental results, all the phenotypic variables associated with DC maturation formed a cluster and located diagonally opposite from IL-16 (Figure 6-6B). The strong association of the phenotypic variables suggests that high redundancy exists, and potentially only a few of these variables need to be assayed to obtain general phenotypic information about DCs. Overall, all the carbon bonds located at positive PC1 but the oxygen bonds at negative PC1 (Figure 6-6B). As expected, theoretical XPS

values mostly clustered with experimental values regardless of whether beta carbons were taken into account during peak fitting.   Material properties such as R_a, T_g, and surface area located primarily close to the origin of the loading plots, indicating that these variables are not important in predicting DC response. In contrast, high S_a is associated with lower DC maturation in this pMA library (Figure 6-6B). S_a is computed across the entire area in the field of view, while R_a only measures the roughness along some arbitrary line across a surface. For a uniform surface, R_a and S_a are expected to be very similar, but this may not be the case for a heterogeneous surface. Since the pMAs were solvent cast into the PP plates, the formation of the films was not homogeneous, and therefore S_a should be a better roughness variable for such surfaces. Generally speaking, the carbon bonds located in a quadrant was diagonally opposite from the oxygen bonds in all the loading plots (Figure 6-6B), indicating that surface carbon and oxygen anti-correlated each other in terms of inducing DC maturation. Interestingly, increase in contact angle was associated with low DC maturation for this set of pMAs. It is important to note that the range of contact angle for this set of polymers was $17.2 - 71.2°$. Therefore, the conclusion drawn in the PCA model is only valid for this range of contact angles. The higher contact angles (close to $71.2°$) are similar to that of TCPS [238], which is known to be suitable for most cell cultures and may be approximately the optimal contact angles for maintaining DC immature state. However, close inspection of Table 6-3 indicated that no strong correlation exists between DC maturation and contact angle, but pMAs with higher contact angles do group towards the left of Table 6-3 with pMAs such as pHEMA and pHPMA that caused low DC maturation.

Figure 6-7 indicated that although the model was best fitted with five PCs, the variations in MF and most of the surface chemical composition variables were well-captured by the first two PCs (Figure 6-7A). In contrast, most of the cytokines and chemokines were still poorly modeled after five PCs (Figure 6-7B), presumably due to the large high donor-to-donor variations that introduced significant noise to model.

100

Subsequently, predictive models were constructed in an attempt to predict DC phenotype using PLSR. PLSR is very similar to PCA; the major difference is that in finding the optimal PCs to describe the variations in the X-block, the algorithm also maximizes the correlations between the X- and Y-blocks, and the resulting model can be used to predict outcomes of future experiments. Because MF was determined from PC as the best DC phenotypic variable that could be modeled (Figure 6-7), a PLSR was first developed to correlate material properties and MF variations. To begin the modeling, all material variables were included into the X-block. From this initial model, pruning steps were implemented to exclude variables that have little importance or reliability to reduce the X-block, including C=O contamination, T_g, R_a, surface area, and a few others. Such procedures were successful in creating a model with $R^2Y = 0.63$ and $Q^2 = 0.58$ with model significance of p-value $= 4.4 \times 10^{-12}$, which was able to predict future experiment with a high $R^2_{prediction} = 0.76$ and $\overline{R}^2_{prediction} = 0.75$ (Figure 6-8E and Table 6-4). As expected, the score (Figure 6-8A) and loading (Figure 6-8B) plots resulted in similar conclusions as in the PCA model, with MF being the most strongly associated with surface carbon due to its proximity with carbon bonds in the loading plot (Figure 6-8B). In addition, MF were anti-correlated with surface oxygen by locating at opposite quadrants (Figure 6-8B).

Interestingly, theoretical values for XPS were weighted more heavily to the PC space (Figure 6-8C-D) with higher VIP (Table 3S-4S) as compared to the experimental values. A possible explanation is that XPS has large inherent errors ($30 - 50\%$), which affects the projection of these variables onto the PC space. Since this set of pMA films was prepared from bulk materials without further modification, the surface chemical composition should be similar to the bulk composition unless serious contamination is present. The theoretical values might actually reflect a more accurate estimation of the surface composition, while the experimental values contained extra instrumental errors that affect their projection onto the model. However, XPS was still valuable to ensure

that the material surfaces were not contaminated during regular storage. If surface modification was implemented, XPS must be performed to obtain a better estimation of surface chemical composition for model development.

After removing either set of experimental XPS values, the model was improved to have prediction regression coefficient of $R^2_{prediction} = 0.71$ and $\bar{R}^2_{prediction} = 0.70$ (if the set of experiment XPS values without beta carbon fitting [GT] was removed) and $R^2_{prediction} = 0.77$ and $\bar{R}^2_{prediction} = 0.77$ (if the set of experimental XPS values with beta carbon fitting [UT] was removed), respectively. This further supports the hypothesis that experimental XPS values could deteriorate the predictive power of this PLSR model, and that the theoretical values of surface composition may be the most informative. However, experimental XPS is expected to be necessary to determine the actual surface composition if surface modification is performed on the materials.

Analogous models for cytokine and chemokine level prediction were found to be poor in performance with $R^2Y < 0.55$ and $Q^2 < 0.4$ and were not able to predict outcomes in future experiments, likely due to the high donor-to-donor variations in cytokine profiles.

PCA indicated that a strong covariance exists among the phenotypic variables that are associated with DC maturation, suggesting their strong redundancy and that a Y-block that contains all the DC response variables would be suitable (because it can be reduced to lower dimensions). However, a PLSR model built with a full Y-block resulted in a poor model ($R^2Y = 0.37$, $Q^2 = 0.33$). Although this model has poor predictive power for the cytokines and chemokines, it was quite effective in predicting MF ($R^2_{prediction} = 0.71$). Again, this confirms that MF was the only predictable phenotypic variable among those assayed.

Since theoretical XPS values appeared to be the most important in predicting DC response for the pMA library, a simple model with only these variables as the X-block was developed (Figure 6-9). The resulting three-component model had fair performance

with $R^2Y = 0.61$ and $Q^2 = 0.58$ with model significance of p-value $= 2.3 \times 10^{-10}$. This model could predict MF levels in future experiments with $R^2_{prediction} = 0.80$ and $\overline{R}^2_{prediction} = 0.79$ (Figure 6-9E and Table 6-4). Similar to the previous PLSR model, cytokine and chemokine levels were not predictable in analogous models. In addition, a model with a full Y-block was able to predict MF ($R^2_{prediction} = 0.79$) but not cytokines and chemokines.

When experimental XPS values were used alone to construct the model, the resulting models performed prediction poorly (Table 6-4). If both sets of experimental XPS values (i.e. experimental XPS values with beta fitting [UT] and without beta fitting [GT]) were used, the model could only predict future outcomes at $R^2_{prediction} = 0.26$ and $\overline{R}^2_{prediction} = 0.25$. If the set of XPS values without beta carbon (fitted in GT) was used only, the predictability was merely $R^2_{prediction} = 0.24$ and $\overline{R}^2_{prediction} = 0.23$. If the set of XPS values with beta carbon (fitted in UT) was used only, the predictability was improved to $R^2_{prediction} = 0.32$ and $\overline{R}^2_{prediction} = 0.31$. Furthermore, the p-values for these models were at least five magnitudes lower than the previous models. Therefore, at least in this study, theoretical XPS values were the most informative for the prediction of DC response based on material characteristics.

Altogether, these results demonstrated co-variations exist between DC response and material properties as demonstrated by PCA with surface chemistry being the most influential in resultant DC response. More importantly, DC response can be predicted by basic material properties. However, not all phenotypic variables are predictable. In this study, MF was a predictable variable, while none of the cytokines and chemokines was predictive. A potential explanation for the lack of predictability of cytokines and chemokines could be that these molecules are the most downstream in the inflammatory response and are subjected to very complex post-transcriptional control [239] as well as degradation upon release into the culture medium. Large donor-to-donor variations might be caused by the individuals' unique network of mechanisms that regulate cytokine

release. These non-specific variations cannot be projected onto the PLSR models well and distort the model; therefore, they cannot be used for future predictions.

This study also demonstrated that an overall DC response represented by MF can be predicted using only theoretical chemical composition values. This has very significant implications for future biomaterial design. Researcher may potentially design a polymer based on the optimal ratios of chemical bonds to achieve a certain target DC phenotype and save many research dollars that would otherwise be spent on the testing of unnecessary polymer formulations. It is important to note that these models did not differentiate aromatic rings from single C-C bonds (as in XPS). A model with more complex chemical structure information is expected to have more predictive power.

A combined model with the Ti data from Chapter 5 did not result in a usable model, because the Ti dataset contain much fewer variables as compared to the pMA or terpolymer set, which led to a large number of non-random missing values in the data blocks. In addition, the measured outcome for the Ti set (CD86) and for the pMA or terpolymer set (MF) were different variables that cannot be combined. In the future, consistent variables should be measured for all the materials before a comprehensive model can be constructed for the desired set of experimental outcomes as based on material properties, consistent for all samples.

Several limitations of the models exist. First, the models were able to differentiate the *relative* DC response that can be induced by a set of polymers, but they do not suggest a *particular level* of DC response. Therefore, these models are the most useful for theoretically predicting the effect of a set of polymers on DCs, from which the researcher can choose materials that induce low, medium, or high DC maturation and perform further experimentation to verify the prediction. Second, the models were tested on acrylate- and methacrylate-based materials that contain only carbon and oxygen with strong predictive robustness. The models were not as effectively in predicting DC response to PP surface (data not shown) or materials from a different category. A model

can only predict what it is trained on. Therefore, predictive PLSR models are expected to be required for different classes of polymers, although a model developed with very large dataset composed of different classes of materials may be explored for its predictive power. Third, this model did not take into account other important material properties such as polymer swelling, which could be an important material property that directs DC response. It is noteworthy that pHEMA did noticeably absorb cell culture medium to a greater extent than other pMAs, which could have contributed to its non-inflammatory properties. However, polymer swelling is often measured using bulk materials and the results might not be applicable to coated thin films. More reliable evaluation methods for the swelling of polymer thin film should be employed. Finally, immune response is very complex with different polarization, including T_h1, T_h2, T_h17, and T_{reg} [72,240-242], DC response based on surface marker expression can only capture a part of the response.

Despite the limitations, these predictive models can assist future biomaterial design for the applications in tissue engineering, vaccine delivery, or cancer therapy, where effective and appropriate immune response is required. Potential immune response approximated by DC maturation factor can be predicted based on polymer formulation before any experimentation is performed, which is expected to expedite the advances in immuno-modulatory biomaterial design.

CHAPTER 7: DIFFERENTIAL POLYMETHACRYLATE-INDUCED DENDRITIC CELL PHENOTYPES ARE ASSOCIATED WITH DISTINCT TRANSCRIPTION FACTOR ACTIVATION PROFILES[**]

7.1. Introduction

DCs are critical in mediating T-cell polarization for optimal immune response by creating the proper cytokine microenvironment for T-cell priming [58,192,193]. The different cytokine profiles have been long known to be mediated through the specific ligation of different TLRs with distinct types of pathogenic molecular motifs [69]. For instance, DCs triggered through TLRs 7, 8, and 9 produced both IL-12 and interferon (IFN)-α; DCs triggered through TLR-3 produce mostly IFN-α; DCs triggered through TLR-5 produce mostly IL12p70; DCs triggered through TLR-4 produce mostly IL-12p70 and a little IFN-α. All of these TLRs induce Th1 immunity and CTL responses. In contrast, DCs stimulated through TLR-2 produce little IL-12p70 but copious IL-10, shifting the balance towards T_h2/T_{reg} profile [69]. Although TLR ligands are widely considered to promote protective immunity against pathogens, the ligation of certain ligand, such as zymosan, with TLR-2 on DCs supports the induction of T_{reg}s rather than T_h1 or T_h17 cells via TLR-2 but induces T_h1 and T_h17 autoimmune responses when signaled via dectin-1 [243].

TLR agonists polarize DCs to induce distinct T_h responses via differential modulation of signal transduction [69,244,245]. For example, TLR-4 and TLR-5 agonists, LPS and flagellin respectively, signal through p38 and c-Jun N-terminal kinase

1/2, while TLR2 agonist, Pam3cys, stabilize the transcription factor (TF) c-Fos [245]. Different stimuli, including IFN-γ, ATP, ADP, CrO, and LPS, induce differential and dynamic TF activation in XS106 murine DC line [246]. Therefore, DCs respond to the environment through the sensing of PRRs that trigger differential modulation of signaling pathways, the combination of which determined the polarization and outcome of the immunity.

Previously, the phenotype of DCs was shown to be modulated by the biomaterials used to treat the DCs via a biomaterial adjuvant effect, and more importantly, the *in vitro* observations were translated into *in vivo* responses [3,4]. These studies suggested that biomaterials can be used to modulate DC phenotype, thereby controlling associated *in vivo* immune response to the biologic components in combination products such as tissue-engineered constructs and vaccines.

Although integrins [121], TLR-2, TLR-4, and TLR-6 [247] have recently been shown to play a role in mediating DC response, the exact mechanisms by which DCs recognize and respond to biomaterials remain to be elucidated. The effects of biomaterials of DCs are directed via the presentation of proteins adsorbed on the biomaterials, which then interact with the DCs to trigger differential responses [248]. Understanding the mechanistic basis of how DCs respond to different biomaterials is expected to facilitate the selection or design of materials that direct a desired immune response. For instance, biomaterials may be tuned to trigger T_h1 or T_h17 responses for maximal protective immunity against a vaccine, or induce T_{reg} for host acceptance of donor cells in tissue-engineered constructs. In this study, two different pMAs, pHEMA and pIBTMA, with previously observed opposite effects on induced DC phenotype (CHAPTER 6, [249]) were used to treat DCs for various time points and were found to differentially affect DC maturation through distinct TF activation profiles.

7.2. Materials and Methods

7.2.1. Synthesis of pMAs

pHEMA was purchased from Sigma Aldrich and used as is. pIBTMA was synthesized in house at the Kohn laboratory at Rutgers University, using reversible addition-fragmentation transfer (RAFT) [233]. The polymerization was carried out using an automated parallel synthesizer. Briefly the synthesizer was inertized by five cycles of evacuation under vacuum at $120^{\circ}C$, and degassed monomers in desired molar ratios, stock solutions of AIBN and 2-cyanoprop-2-yl dithiobezoate and solvents were charged to the reactors that were vortexed at 600 rpm at $70^{\circ}C$ for 20 hrs under Argon. The reactors were cooled to RT and the polymers were precipitated manually and dried under vacuum for more than 24 h at $60^{\circ}C$.
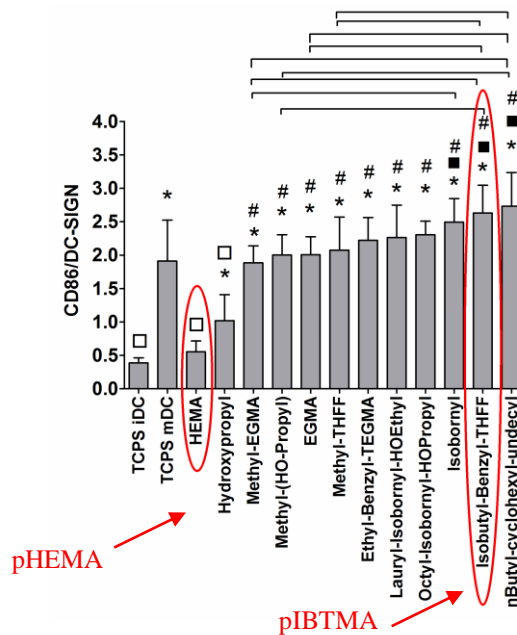
Figure 7-1: pHEMA and pIBTMA were selected from a previous study, where pHEMA was shown to induce a low level of DC maturation, whereas pIBTMA induced a high level of DC maturation as represented by the metric CD86/DC-SIGN.

These two pMAs were selected from a set of twelve pMAs, which was previously found to induce differential DC phenotype [249], because they induced the two extremes of DC maturation (CHAPTER 6). Specifically, pHEMA induced the least mature DC phenotype, whereas pIBTMA induced highly mature DCs based on surface maturation marker expression (Figure 7-1). Furthermore, cytokine profiles induced by pHEMA and pIBTMA also supported this polymer selection. pHEMA induced low levels of all the cytokines and chemokines, except IL-16, analyzed, while pIBTMA induced high levels of all the maturation-associated cytokines and chemokines but induced low levels of IL-16 (Figure 6-3 and Figure 6-4 in Chapter 6).

7.2.2. Coating of pMA in 96-well plate

The coating procedure was performed as described in Section 6.2.2.

7.2.3. Human dendritic cell culture from purified monocyte population

PBMCs were isolated in the same manner as in section 4.2.1. in accordance with an updated protocol H10011 of the Institutional Review Board of Georgia Institute of Technology. To generate a pure DC culture, monocytes were isolated from PBMCs using CD14 microbeads (Miltenyi Biotec, Auburn, CA) following the manufacturer's instructions. The purity of monocytes was routinely >95% by monoclonal CD14 antibody (clone TÜK4, mouse IgG_{2a}; Miltenyi Biotech) staining. Ten milliliters of monocytes were plated in a Primaria 100×20 mm^2 tissue-culture dish at a concentration of 1×10^6 cells/ml in DC media. After 2 h of incubation at 95% relative humidity and 5% CO_2 at 37°C, the dishes were washed $1 - 2$ times with warm DC media to remove the dead cells caused by the isolation procedure. The remaining adherent monocytes were incubated with 10 ml/plate fresh warm DC media, supplemented with 1000 U/ml GM-CSF and 800 U/ml IL-4, for 5 days to induce the differentiation of monocytes into immature DCs (iDCs). The purity of DCs (CD1a$^+$/DC-SIGN$^+$) was consistently >95% by

dual staining with monoclonal CD1a (clone HI149, mouse IgG1,κ; Biolegend, San Diego, CA)) and DC-SIGN (clone 120507, mouse IgG$_{2b}$; R&D Systems, Minneapolis, MN) antibodies and analyzing by flow cytometry (Appendix 2).

7.2.4. Exposure of DCs to coated pMAs in 96-well plate

On day 5 of culture, DCs were harvested and resuspended in DC media with 1000 U/ml GM-CSF and 800 U/ml IL-4 at 5×10^5 DCs/ml. 150 µl of cell suspension (7.5×10^4 DCs) was plated on pMA coatings in each well of a 96-well PP plate. The reference controls were cultured on TCPS 96-well plate in parallel: untreated iDCs for the negative reference control and LPS (100 ng/ml)-treated mDCs for the positive reference control. In order to collect enough cells for nuclear extraction, 12 wells for each treatment were used. Separate 96-well plates were used for different time points: 3, 6, and 11h.

7.2.5. Cell imaging

DC morphology was captured in the 96-well plates at the indicated time points immediately prior to cell harvest for nuclear extraction. Images were collected with Olympus IX71 inverted microscope (Olympus, Center Valley, PA) and Image-Pro Express software (MediaCybernetics, Bethesda, MD).

7.2.6. Nuclear extraction of DCs

All procedures were performed on ice unless specified. At each time point, DCs were collected from the 96-well plates and pooled into 15-ml conical tubes according to treatments. The wells were washed 1x with 150 µl ice-cold D-PBS and the residual cells were collected into the corresponding tubes. To remove the adherent DCs, 50 µl of ice-cold cell dissociation buffer (Sigma) was added into each well and incubated for 15 min, with gentle tapping of the plates at 5 min intervals. The cells were pelleted at 500×g at

4°C and were transferred to Eppendorf tubes. After one wash with D-PBS, nuclear extraction of the differentially treated DCs was performed using the Panomics Nuclear Extraction Kit (Affymetrix, Santa Clara, CA) following the manufacturer's protocol. Briefly, Buffer A was used to disrupt the cell membrane and release cytosolic contents and nuclei. After removing the cytosolic portions, the nuclei were incubated with Buffer B for 1 h to disrupt nuclear membranes and release nuclear contents. The nuclear extracts were stored in small aliquots at -80°C immediately. One of aliquots from each treatment was thawed for protein quantification. Although the manufacturer recommends using the Bio-Rad DC Protein Assay, the dynamic range of this assay was found to be narrow in Buffer B, and it routinely over-estimated the protein amounts. Instead, the protein contents were quantified using Bradford Reagent (Sigma), which was found to not interfere with the Buffer B in the nuclear extracts.

7.6.7. Transcription factor (TF) Plex Assay

A customized Procarta Transcription Factor Plex (Affymetrix) was used to evaluate the profile of the transcription factor activation of DCs upon treatment with different biomaterials following the manufacturer's instructions. The TFs analyzed in this study included NF-κB (nuclear factor kappa-light-chain-enhancer of activated B cells), ISRE (interferon-stimulated responsive element), AP-1 (activator protein-1), E2F-1, CREB (cAMP response element-binding), GR/PR (Glucocorticoid / progesterone response element), NFAT (nuclear factor of activated T-cells), and HSF (heat shock factor). Briefly, the nuclear extracts were incubated with 10 μl probe mix containing biotin-labeled double stranded oligonucleotides (TF binding site). TFs bound to these oligonucleotides were recovered, and the biotin-labeled probes were eluted, denatured, and then hybridized to beads conjugated with the complementary oligonucleotides. Subsequently, the beads were incubated with PE-conjugated streptavidin. The samples

were analyzed using a Bioplex 200 instrument with Bio-Plex Manager 4.0 software. The signal of each TF was normalized to TFIID, a ubiquitous TF complex.

7.6.8. Surface marker expression by flow cytometry

On Day 5, DCs were treated with pMA coated PP plates or TCPS reference control plates with eight wells used for each treatment. After 24h, the DCs were collected in the same manner as for nuclear extraction and resuspend in filter-sterilized 0.1% BSA and 2mM EDTA in PBS, pH 7.2 (cell-staining buffer). The cells were stained for 30 min with fluorescently-labeled monoclonal antibodies for CD83 (clone HB15a, mouse IgG$_{2a}$,κ; Immunotech, Marseille, France), CD86 (clone BU63, mouse IgG$_{1}$,κ; Ancell corporation, Bayport, MN), DC-SIGN (R&D Systems), CCR7 (clone TG8/CCR7, mouse IgG$_{2a}$,κ; Biolgend). CD83 is a maturation marker, CD86 is a costimulatory molecule, and CCR7 is a chemotatic receptor responsible for homing to the lymph organs. These surface markers are typically up-regulated upon DC maturation. DC-SIGN is an endocytic receptor that is down-regulated in response to LPS-stimulated maturation [250]. For Annexin V and propidium iodide staining, DCs were stained in Annexin V binding buffer following manufacturer's protocol (all from Biolegend). The samples were analyzed using a BD LSR flow cytometer (Beckton Dickinson, San Jose, CA) and FlowJo software (Tree Star, Ashland, OR).

7.6.9. Statistical analysis

To observe any significant differences between all sample groups in pairs, a pair-wise one-way ANOVA followed by Tukey post test was performed using the GraphPad Prism 5 software (La Jolla, CA), and the p-value ≤ 0.05 was considered significant.

7.3. Results

7.3.1. Contact with different pMAs induced distinct DC morphologies

As shown in Figure 2, iDCs cultured on TCPS exhibited a rounded morphology, whereas mDCs (TCPS+LPS) possessed extended cellular projections. When in contact with pIBTMA, DCs exhibited some extended processes consistent with a mature phenotype, though not to the extent as LPS-induced maturation. DCs treated with pHEMA were even more rounded than those cultured on TCPS. Interestingly, in the presence of pHEMA, the effect of LPS on DC morphology was completely abolished. DCs treated with pHEMA with LPS exhibited the same morphology as compared to those cultured on pHEMA alone. These morphologies were observed by 3 h and maintained through the time course of the study until 11 h.

7.3.2. pMAs differentially affected surface marker expression on DCs

CD86 expression on pIBTMA-treated DCs was significantly higher as compared to pHEMA-treated DCs (Figure 7-2), which is consistent with the NF-κB activation results. The expression of CD83, CCR7, and DC-SIGN by DCs was not different among the iDC reference control and the two pMAs examined for DC treatment. As expected, LPS treatment alone induced significant up-regulation of CD83, CD86, and CCR7 expression but not DC-SIGN expression. Interestingly, consistent with the results from TF profiling, the presence of pHEMA completely abolished the effect of LPS stimulation on DCs, and maintained surface marker expression of these DCs at levels similar to pHEMA treatment alone (Figure 7-2).

113
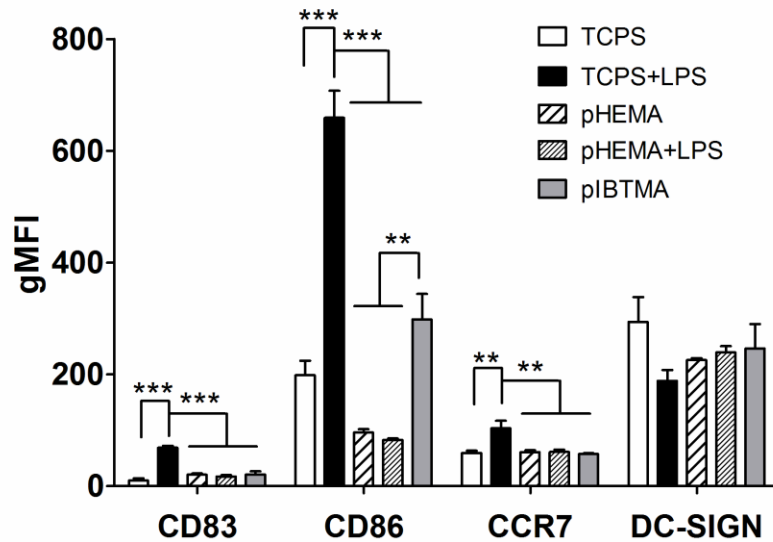
Figure 7-2: Surface expression of maturation markers by DCs treated with different pMAs as compared to the reference controls. Geometric mean fluorescent intensities (gMFI) are shown for n = 3 donors (mean ± SEM). **: p<0.01, ***: p<0.001.

7.3.3. pMAs induced different TF activation profiles in DCs

Treatment of DCs with pIBTMA induced the activation of NF-κB as compared to treatment with pHEMA by 6 h, and the statistical significance of the difference increased by 11 h (Figure 7-4A). Although NF-κB levels induced by pHEMA treatment were not statistically different from TCPS-treated iDC by 6 h or 11 h, treatment of DCs with pHEMA appeared to suppress NF-κB by 6 h. As expected, LPS strongly activated NF-κB in treated DCs by 6 h and the levels of activation increased over time (Figure 7-4A). As expected, LPS induced higher levels of AP-1 activation by 6 h as compared to TCPS and pHEMA, but the difference became insignificant by 11 h time point (Figure 7-4C). pIBTMA did not affect any other TFs examined.

pHEMA also induced the activation of a number of other TFs, including TFs that have been associated with pro-inflammatory response such as ISRE (Figure 7-4B) and HSF (Figure 7-4D), TFs that have been linked to suppression of DC maturation such as E2F-1 (Figure 7-4E) and GR/PR (Figure 7-4F), as well as cell-cycle-related TFs such as

NFAT (Figure 7-4G). Treatment of DCs with pHEMA induced higher ISRE (Figure 7-4B) activity as compared to TCPS or pIBTMA by 6 h, and induced higher HSF (Figure 7-4D) and E2F-1 (Figure 7-4E) activation as compared to TCPS, LPS, or pIBTMA. The activation of these TFs maintained high levels of activation through to the 11 h time endpoint of the experiment. In addition, pHEMA treatment of DCs induced higher levels of GR/PR activation by 6 h time point compared to LPS stimulation, and the activation was maintained by 11 h (Figure 7-4F). pHEMA treatment induced a higher levels of NFAT compared to TCPS only at 11 h time point (Figure 7-4G). The activation of CREB was not affected by any of the treatments (Figure 7-4H).

Interestingly, the effect on the TF activation on DCs from the presence of pHEMA was dominant over maturation stimulus, LPS. DCs treated with either pHEMA or a combination of pHEMA and LPS exhibited nearly identical TF profiles, which were distinct from LPS-induced TF profile in DCs (Figure 7-4). The effects of the different treatments on TF activation profiles of DC are summarized in Table 7-1.
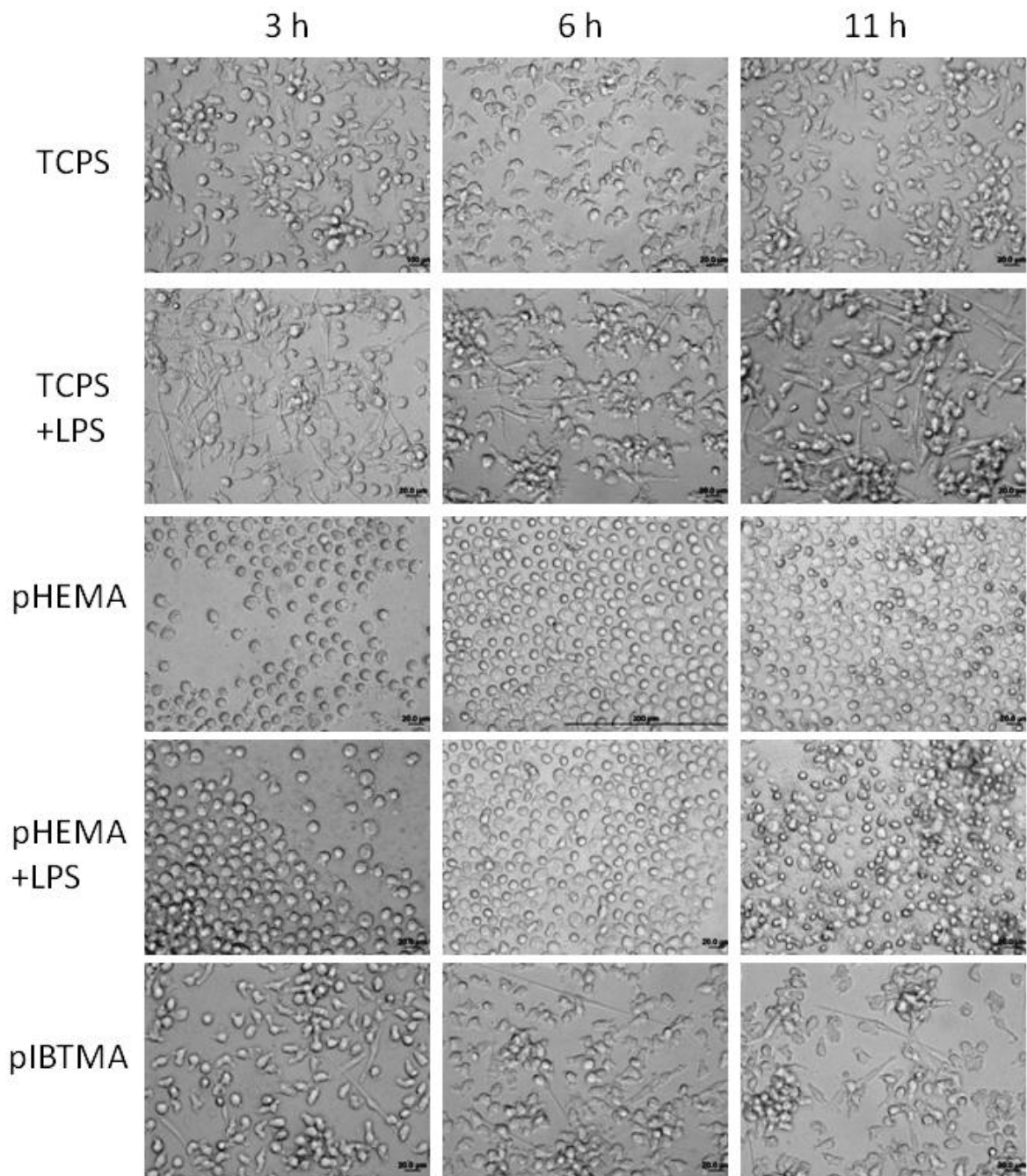
Figure 7-3: DC exhibited distinct morphologies after cultured with different treatments. TCPS treated iDCs exhibited a rounded morphology, while LPS treated mDCs have extended cellular processes. Both pHEMA and pHEMA+LPS maintained a rounded DC morphology, while pIBTMA promoted a morphology more similar to mDCs. These morphologies were maintained throughout the time course of the study.
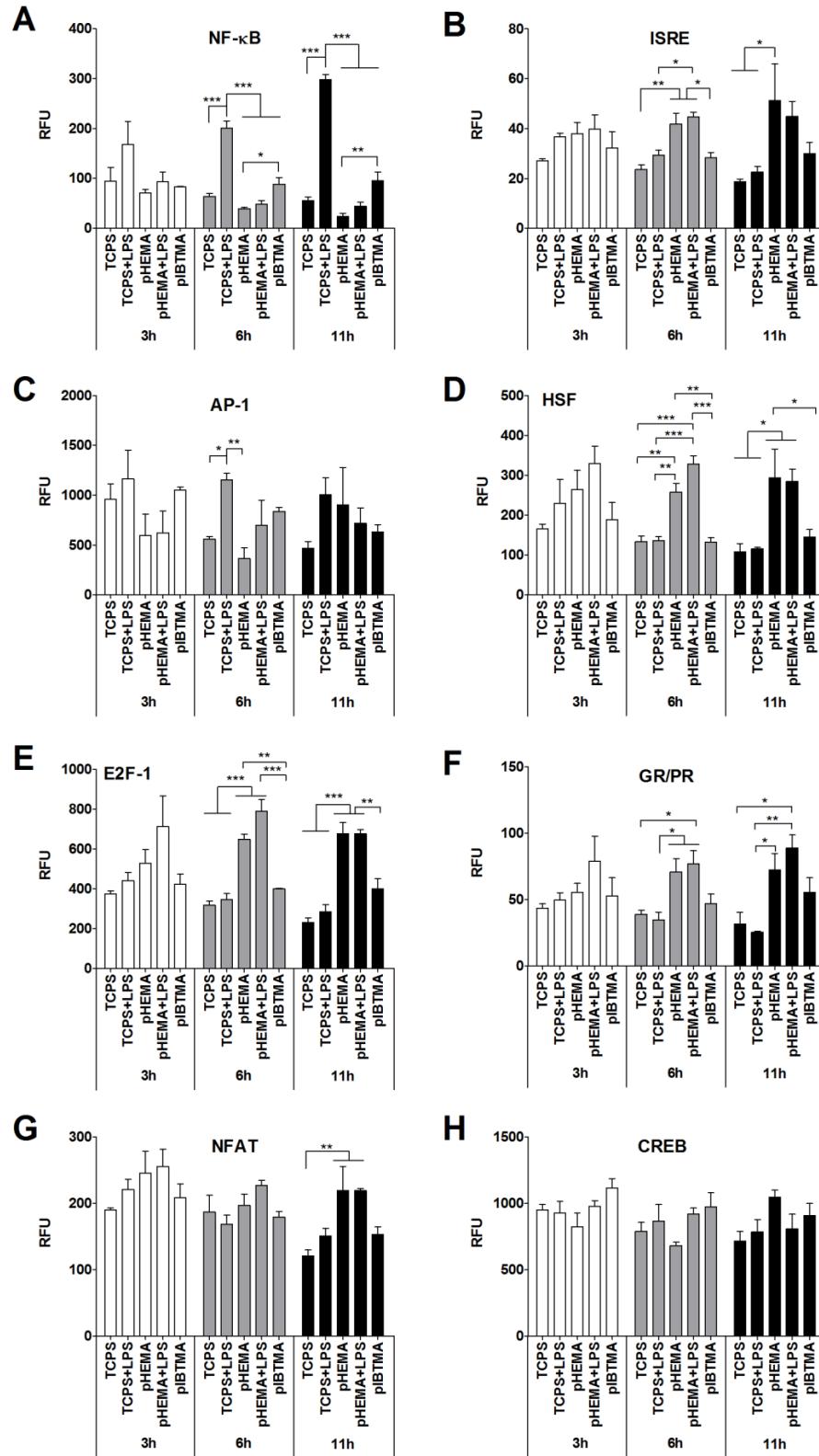
Figure 7-4: Activation of TFs of differentially treated DCs. A) NF-κB, B) ISRE, C) AP-1, and D) HSF, E) E2F-1, F) GR/PR, G) NFAT, and H) CREB. N = 3 donors (mean ± SEM). *: p<0.5, **: p<0.01, ***: p<0.001.

117

Table 7-1: Summary of the effects of different treatments on TF activation of DCs as compared the TCPS-treated iDC reference control at different time point. The three time points (3, 6, or 11 h) are each indicated by an arrow sequentially, respectively.

	TCPS + LPS	pHEMA	pHEMA + LPS	pIBTMA
NF-κB	↔↑↑	↔↓↓*	↔↔↔	↔↑↑*
ISRE	↔↔↔	↔↑↑	↔↑↑	↔↔↔
AP-1	↔↑↔	↔↔↔	↔↔↔	↔↔↔
HSF	↔↔↔	↔↑↑	↔↑↑	↔↔↔
E2F-1	↔↔↔	↔↑↑	↔↑↑	↔↔↔
GR/PR	↔↔↔	↔↑↑	↔↑↑	↔↔↔
NFAT	↔↔↔	↔↑↑	↔↑↑	↔↔↔
CREB	↔↔↔	↔↔↔	↔↔↔	↔↔↔

*: the NF-κB activation was not significant compared to iDC; however, with the decrease of NF-κB induced by pHEMA and increase of NF-κB induced by pIBTMA, statistical significance was seen between pHEMA and pIBTMA.

7.3.4. pHEMA, but not pIBTMA, induced apoptosis of DCs

After 24 h of treatment with the biomaterials, pHEMA treatment of DCs resulted in more annexin V single positive DCs, which were apoptotic DCs, as compared to iDC, mDC, or pIBTMA-treated cells (Figure 7-5A). Furthermore, the pHEMA-treated cell populations also had more annexin V/PI double positive cells, which were late-stage apoptotic or necrotic cells, as compared to iDC, mDC, or pIBTMA-treated cell populations (Figure 7-5B). Over 80% of the pHEMA-treated DCs were annexin V/PI double positive after 24 h, suggesting this time point was too long to capture early apoptotic events. However, Figure 7-5A suggested DCs treated with pHEMA underwent apoptosis. Interestingly, a combined treatment of pHEMA and LPS led to even more annexin V$^+$ or annexinV$^+$/PI$^+$ cells as compared to pHEMA treatment alone. No difference in the levels of apoptosis was observed among iDC, mDC, and pIBTMA-treated DCs, and the percentage of dead cells was low for these treatments (Figure 7-5).
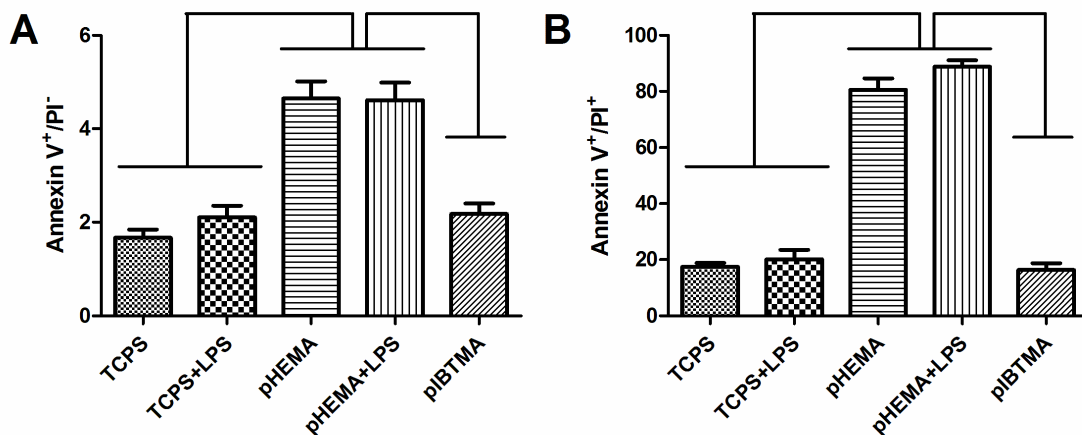
Figure 7-5: pMAs induced differential levels of cell death by 24 h. DCs were treated with the indicated treatments for 24 h and were harvested for double-staining of Annexin V-FITC and PI. A) Annexin V single positive early apoptotic DCs and B) Annexin/PI double positive late apoptotic or necrotic DCs were quantified with n = 3 different donors (mean ± SEM). Brackets indicate $p < 0.01$ between treatments.

7.4. Discussion

DC phenotype was previously shown to be differentially modulated by treatment with twelve distinct pMAs in a combinatorial library (CHAPTER 6). Two pMAs, one induced a highly mature DC phenotype and the other promoted an immature DC phenotype, were selected from the library for this study. Differentially treated DCs were imaged for their morphology, and then the nuclear extracts were prepared from the cells at various time points. As expected, throughout the time course of the study, DCs treated with pIBTMA exhibited extended cellular processes similar to the DCs treated with LPS (mDCs). In contrast, DCs treated with pHEMA coatings of a round morphology, and in fact, more rounded than TCPS-treated iDC reference control, suggesting their lack of maturation. Surprisingly, DCs treated with pHEMA and LPS exhibited morphology similar to the DCs treated with pHEMA alone. Furthermore, the expression of surface maturation markers by DCs was consistent with the differential morphologies induced by the different treatments. Specifically, CD86 expression on pIBTMA-treated DCs was significantly higher as compared to pHEMA-treated DCs (Figure 7-2). Similar to the

morphology results, the presence of pHEMA completely abolished the activating effect of LPS on DCs and maintained the levels of surface marker expression similar to pHEMA treatment alone. Therefore, consistent with previous results, pIBTMA, but not pHEMA, promoted DC maturation, and the presence of pHEMA prevented DC's response to LPS.

It is interesting to note that the effect of pIBTMA was not as strong on the DCs derived from a purified culture (Figure 7-2) as compared to the DCs derived from a heterogeneous culture that also contained B cells (Figure 7-1). This result was as expected because B cells have been found to release cytokines and natural antibodies that aid in monocyte-derived DC migration, differentiation, and maturation, suggesting that B cells can support DC function [174,176,211]. However, a purified cell culture was needed in this study for nuclear extraction to obtain DC-specific activation of TFs.

To correlate the differential effects of biomaterials to DC phenotype, TF activation profiles of DCs treated with these different pMAs were analyzed and compared to the TF profiles of the iDC and mDC reference controls (Figure 7-4). By 6 h of biomaterial treatment of DCs, though not statistically significant, pHEMA appeared to induce less, while pIBTMA induced more, NF-κB activation compared to the levels for iDCs. However, DC treatment with pIBTMA induced NF-κB activation, which was significantly higher than that induced by pHEMA treatment, and this difference became more significant by 11 h. As expected, DC treatment with LPS induced strong NF-κB activation, which increased over time during the time course of the study (Figure 7-4A). DC maturation was previously shown to be associated with the NF-κB pathway [251] and is required for STAT-4 expression, critical in IL-12 mediated T_h1 polarization, during DC maturation [252]. Furthermore, NF-κB signaling is induced by LPS stimulation and supports survival and maturation of monocyte-derived DCs [253-255]. NF-κB also plays an important role in the production of CCL19 [256], a chemokine whose production is enhanced in mDCs, regulating migration of mDCs, and is involved in naïve T cell

recruitment to the vicinity of mDCs in the T cell zones in lymph nodes [257,258]. Therefore, consistent with phenotypic outcomes, the NF-κB profiles indicated that pIBTMA treatment induced DC maturation, at least in part, through the NF-κB pathway. In contrast, treatment of DCs with pHEMA resulted in lower NF-κB activation levels, which might be partially responsible for maintaining the iDC phenotype of pHEMA-treated DCs. The lower activation levels of NF-κB may cause the imbalance of TFs that controls DC survival, which resulted in the increased apoptosis of DCs (Figure 7-5A).

AP-1 has previously been shown to be involved in the increase in MHC class II expression in DCs after LPS stimulation [259] and regulate the expression of IL-23 *p19* promoter activation in MΦs [260]. IL-23 is released by MΦs and DCs upon microbial infection and is critical for the generation of T_h17 immune response [261-263]. Thus, AP-1 is generally associated with DC maturation and is consistent with our experimental result that LPS induced higher AP-1 activation by 6 h (Figure 7-4C). Although not significant, pIBTMA-treated DCs appeared to induce increased AP-1 activation by 6 h. However, no difference was observed by 11 h among the various treatments (Figure 7-4C).

ISRE is a specific DNA motif that, in response to interferon (IFN) stimulation, binds transcription complexes formed by homo- or heterodimerized STATs (signal transducers and activators of transcription) and p48, a member of the IRF (IFN regulatory factor) family [264]. ISRE has been shown to play a role in up-regulating CCL19 transcription via IFN signaling in human DCs [256], inducing IL-12p35 gene activation through binding of IRF-3 to ISRE in RAW 264.7 cells stimulated by LPS or PolyI:C [265], and regulating IL-12 production in bone marrow-derived DCs [266]. Therefore, it seems counterintuitive that pHEMA-induced DCs enhanced ISRE activity (Figure 7-4B) because pHEMA treatment resulted in low CD86/DC-SIGN ratio (Figure 7-1) as well as rounded morphology (Figure 7-3). However, ISRE also plays a key role in mediating apoptosis [267]. ISRE is responsible for IFN-α-induced up-regulation of programmed

death-1 (PD-1) expression in MΦs [268], which leads to apoptosis. As a result, pHEMA-treated DCs possibly enhanced the activation of ISRE-binding transcription factors to induce an apoptotic response, which is consistent with the decrease in NF-κB activity.

The expression heat shock proteins (HSPs) is increased when cells are exposed to elevated temperatures or other stress (chemical or physiological) and is primarily regulated by a family of TFs, HSFs [269]. HSPs and HSFs have been mostly studied in DCs in the context of thermoregulation. Heat shock induces DC maturation by enhancing transient phagocytosis, expression of CD86 and MHC II molecules, pro-inflammatory cytokine release, localization to draining lymph nodes, and T cell stimulation [270]. However, heat shock-induced DC maturation appears to be independent of HSF-1 or extracellular HSPs [271,272]. Recently, endogenous HSP90 was shown to have a pivotal role in cross presentation at normal conditions [273]. Heat shock associated with increase in temperature during inflammation or fever has been associated with enhanced survival from infection and immunological functions [270]. HSPs are molecular chaperones that protect proteins from denaturation and misfolding, rendering them resistant to stress-induced cell damage. In addition, HSPs and their cofactors are responsible for inhibiting the apoptotic and necrotic pathways [274]. Interestingly, biomaterials have been reported to differentially influence HSP mRNA expression in HeLa S3 cells [275]. The authors found that hydrophilic surfaces (contact angles $\cong 20°C - 65°C$) induced higher expression of HSP70A, HSP70B, HSP90, and HSP70 in HeLa S3 cells as compared to hydrophobic surfaces (contact angles $\cong 70°C - 120°C$) [275]. In the current study, pHEMA and pIBTMA were measured to have contact angle of 69.5°C and 28.7°C – both are in the hydrophilic category but induced significant variation in HSF activation. It is unclear why pHEMA but not pIBTMA induced higher HSF activation (Figure 7-4D). Potentially, due to the apoptotic response the DCs experienced via the other signaling pathways, DCs produced HSF as a natural defense against cell death.

The E2F family consists of a number of activators and repressors, including E2F-1, E2F-2, E2F-3, E2F-4, and E2F-5. E2Fs play critical roles in the regulation of cell cycle progression, differentiation, development, tumor formation, and apoptosis [276]. Combined loss of E2F-1, E2F-2, and E2F-3 completely abrogates the cell cycle progression and proliferation of mouse embryonic fibroblasts [269], and E2F-3b is sufficient to support mouse embryonic and postnatal development [277]. E2Fs are also pivotal in the induction of apoptotic pathways in cells [278]. For example, mice deficient in E2F-1 have a defect in thymocyte apoptosis resulting in an excess of mature T cells [279]. E2Fs also sensitizes cells to pro-apoptotic stimuli by the disruption of NF-κB signaling via E2F-1's competition with p50 for RelA/p65 binding, thus inhibiting NF-κB DNA binding activity [280]. Recently, the role of E2F-1 in DCs was studied and was found to suppress DC maturation [281]. The expression of E2F-1 is transiently down-regulated during LPS-induced maturation of both human monocyte-derived DCs and a mouse DC cell line, DC2.4. Down-regulation of mRNA occurs between 3 – 18 h, while down-regulation of protein level occurs roughly between 9 – 18 h. Phenotypic and functional maturation was observed in DC2.4 cells with the knockdown of E2F-1 by siRNA in the absence of LPS stimulation [281]. Therefore, this finding is consistent with our results that treatment of DCs with LPS or pIBTMA did not affect E2F-1 activation and that pHEMA treatment enhanced E2F-1 binding by 6 h as compared to the level observed for iDCs (Figure 7-4E). Down-regulation of E2F-1 activation in DCs treated by LPS was not observed in our study, potentially due to the short time course of the study. pHEMA treatment significantly enhanced E2F-1 binding likely to suppress DC maturation. The increase in E2F activity may also partially explain the decrease in NF-κB (Figure 7-4A) and the induction of apoptosis of pHEMA-treated DCs (Figure 7-5A).

GR/PR binding element is designed to monitor the induction of glucocorticoid response element (GRE) through the signaling transduction pathway mediated by GR or PR. Glucocorticoid effects are mediated through GR, a TF, and result in reduction of IL-

12p70 and TNF production and impairment of T cell stimulatory function in DCs [87] via the inhibition of NF-κB and AP-1 [282]. Progesterone has been shown to have immune suppressive properties in human and rodents and inhibits mature rat DCs through PR [283]. Furthermore, progesterone hinders murine DC activation through the inhibition of STAT1 pathway [284]. Interestingly, progesterone modulates TLR-3- and TLR-4-mediated murine DC maturation differentially [285]. Specifically, progesterone reduced DC production of IL-6 entirely via GR, while IL-12p40 production via either GR or PR. Furthermore, progesterone inhibited TLR-3- but not TLR-4-induced CD40 expression [285]. Glucocorticoid also induces apoptosis of plasmacytoid DCs (pDCs) in patients and healthy donors, which decreases the levels of circulating pDCs [286]. Therefore, coherent evidence has confirmed the important role of GR/PR in mediating immune suppression. In the current study, treatment with pHEMA induced higher GR/PR activation in DCs by 6 h until 11 h (end of experimental time course) as compared to iDCs (Figure 7-4F), which is consistent with the lack of maturation of the DCs treated with pHEMA and suggests that pHEMA has immuno-suppressive property that modulates DC functions. In contrast, treatment of DCs with LPS or pIBTMA did not induce significant increase in GR/PR activation.

NFATs can be induced by several signaling pathways, including calcineurin and protein kinase C [287]. NFAT has been shown to play different roles in DC biology. For example, NFAT is activated in murine DCs and MΦs in response to yeast and zymosan stimulation via ligation of Dectin-1, which results in the up-regulation of pro-inflammatory mediators such as cyclooxygenase-2 (COX-2), IL-2, IL-10, and IL-12p70 [288]. Recently, spontaneous Ca^{2+} oscillations were found to occur in human monocyte-derived iDCs resulting in calcineurin-dependent NFAT translocation into the nucleus. Such high frequency oscillations are lost during DC maturation and therefore NFAT activation may be an endogenous characteristic to maintain DCs in the immature state [289]. Interestingly, another study shows that LPS stimulation induces the Src-family

kinase and phospholipase Cγ2 activation, influx of extracellular Ca^{2+} and calcineurin-dependent nuclear NFAT translocation exclusively via CD14 in murine DCs. NFAT activation in mDCs results in apoptosis of terminally differentiated DCs, which is critical in maintaining self-tolerance and preventing autoimmunity [290]. Our study showed that DCs treated with pHEMA had higher NFAT activation as compared to iDCs by 11 h of culture (Figure 7-4G). pHEMA treatment may trigger NFAT to maintain iDC phenotype or induce DCs to undergo apoptotic death, both of which are consistent with the phenotypic data. However, treatment of DCs with LPS, as well as with pIBTMA, did not induce NFAT activation in human monocyte-derived DCs over the time course of the study.

Several pathways are associated with CREB binding, including Jun N-terminal kinase (JNK), p38, and protein kinase A (PKA) [291]. CREB activity is associated with calcium/calmodulin kinases and CRE coactivators, the activity of which depends on Ca^{2+} and cyclic AMP levels [292]. Calcium-calmodulin-dependent kinase IV (CaMKIV) is expressed in DCs and links TLR signaling with the control of human and murine DC survival by regulating the temporal expression of Bcl-2. This CaMKIV signaling cascade controls the activation of CREB and accumulation of Bcl-2 necessary to support DCs from apoptosis. CaMKIV null mice have a decreased number of DCs in lymphoid tissues and are short-lived in response to LPS [293]. Furthermore, CREB has been shown to be involved in the up-regulation of IL-10 in human DCs in response to zymosan, even though zymosan also strongly activates NF-κB, which is a negative regulator of IL-10 [294]. Hence, CREB activity is important in modulating immune response. In the current study, the treatments on DCs did not induce significant difference in the context of CREB activation (Figure 7-4H). Our results suggest that the pMAs in question do not actively support apoptosis or modulate immune response through the activation of CREB during the time course of the study.

The roles and functions of the TFs analyzed in this study are summarized in Table 7-2. Overall, DC treatment with pIBTMA induced maturation, at least through the NF-κB pathway. Treatment of DCs with pHEMA induced the activation of TFs that have been found to possess immunosuppressive properties such as E2F-1 and GR/PR, consistent with the rounded morphology of these DCs (Figure 7-3) and immature phenotype (Figure 7-1 and Figure 7-2). Treatment of DCs with pHEMA also induced the activation of an array of TFs that have been linked to apoptosis, including ISRE, E2F-1, GR/PR, and NFAT, suggesting that pHEMA triggered strong apoptotic signals. Interestingly, HSF, which is induced as a stress response to protect cells from death, was also induced in DCs by pHEMA treatment. DCs treated with pHEMA potentially activated HSF as a natural defense against the other apoptotic signals; the balance of these signals may be critical in determining the fate of the DCs. Presumably, the apoptotic signals overrode the survival signals, rendering DCs to undergo apoptosis in response to pHEMA, but not pIBTMA, treatment (Figure 7-5). DC apoptosis is pivotal in the maintenance of immune tolerance [295]. Defective DC apoptosis leads to the accumulation of DCs, chronic lymphocyte activation, and systemic autoimmunity [296]. In addition, the uptake of apoptotic DCs induces iDCs to secret TGF-β1 and promotes the differentiation of naïve T cells into Foxp^{3+} regulatory T cells [297]. However, the evidence of apoptosis from annexin V/PI staining alone in Figure 7-5 is not sufficient to definitively prove the hypothesis that pHEMA-treated DCs are apoptotic. Therefore, additional experiments are underway to probe for the caspase 3/7 activity, which is a prominent apoptotic pathway, and DNA fragmentation by TUNEL, which is an end-stage apoptotic event [115].

Surprisingly, for DCs in the presence of pHEMA, the effects of LPS on TF activation profiles were completely abolished. Instead, DCs treated with LPS in the presence of pHEMA exhibited very similar TF profiles compared to DCs treated with pHEMA alone.

In summary, two polymers from the same class of material can exert very different effects on DC phenotype, which are mediated through distinct TF activation profiles, and very likely through distinct receptors and signaling pathways. In fact, recent research using MyD88 and TLR knock-out mice showed that DCs use TLR-2, TLR-4, and TLR-6 for the responses to a group of chemically and physically diverse biomaterials [247]. Potentially, pHEMA and pIBTMA presented differential profiles of proteins to DCs and triggered different receptors for distinct responses. For instance, DCs triggered through TLRs 7, 8, and 9 produced both IL-12 and IFN-α; DCs triggered through TLR-3 produce mostly IFN-α; DCs triggered through TLR-5 produce mostly IL12p70; DCs triggered through TLR-4 produce mostly IL-12p70 and a little IFN-α. All of these TLRs induce Th1 immunity and CTL responses. Although TLR ligands are widely considered to promote protective immunity against pathogens, the ligation of certain ligand, such as zymosan, with TLR-2 on DCs supports the induction of T_{reg}s rather than T_h1 or T_h17 cells via TLR-2 but induces T_h1 and T_h17 autoimmune responses when signaled via dectin-1 [243].

In order to effectively elucidate the molecular mechanism of DC response to biomaterials, additional experiments should be carried out to confirm the effects of the TFs. For example, blocking or siRNA knock-down experiments should be performed to decifer the effect, contribution, or time course of each TF in the DC response process. Furthermore, tracking experiments (e.g. with fluorescent marker) should be performed to validate that activated TFs indeed translocate into the nucleus to exert the observed effects.

To our knowledge, this is the first study that demonstrated that biomaterials can modulate DC response through activation of distinct TFs. In addition, biomaterials such as pHEMA were shown to be strong immunomodulators capable of overriding the effects of soluble factors and may represent a non-pharmacological strategy for inducing DC tolerance for applications in regenerative medicine and organ transplantation.

Table 7-2: Summary of specific functions of TFs in the context of DC biology based on the literature cited in the discussion section

TFs	General roles	Specific functions
NF-κB	DC maturation Cell survival	- LPS-induced maturation of monocyte-derived DCs [254] - Required for STAT-4 expression during DC maturation [252] - Supports cell survival and rescues cells from apoptosis [253-255] - Induces production of CCL19 [256]
AP-1	DC maturation Apoptosis	- Enhances MHC class II expression after LPS stimulation in DCs [259] - Regulates the expression of IL-23 *p19* promoter activation in MΦs [260]
ISRE	DC maturation Apoptosis	- Up-regulates CCL19 transcription [256] - Up-regulates IL-12p35 gene activation and IL-12 production [265,266] - Mediates apoptosis [267,268]
HSF	Heat shock response DC maturation Cell survival	- Regulates production of HSPs [269] - HSPs induce DC maturation [270] - Heat shock-induced DC maturation is independent of HSF-1 or extracellular HSPs [271,272]. - Endogenous HSP90 plays a pivotal role in cross presentation at normal conditions [273]. - HSPs inhibit apoptotic and necrotic pathways [274]
E2F-1	Suppression of DC maturation Apoptosis	- Regulates cell cycle progression, differentiation, development, tumor formation, and apoptosis [276]. - Controls the progression and proliferation of mouse embryonic fibroblasts [269] and mouse embryonic development [277]. - Induces apoptotic pathways in cells [278-280]. - Suppresses DC maturation in both human monocyte-derived DCs and a mouse DC cell line, DC2.4 [281].
GR/PR	Suppression of DC maturation Anti-inflammatory response	- Glucocorticoids reduce IL-12p70 and TNF production and impair T-cell stimulatory function in DCs [87] via the inhibition of NF-κB and AP-1 [282]. - Progesterone hinders murine DC activation through the inhibition of STAT1 pathway [284]. - Progesterone modulates TLR-3- and TLR-4-mediated murine DC maturation differentially [285]. - Induces pDC apoptosis [286].
NFAT	DC maturation Apoptosis	- Activated in murine DCs and MΦs in response to yeast and zymosan stimulation via ligation of dectin-1, resulting in the up-regulation of pro-inflammatory mediators [288]. - Activated in human iDCs as a result of spontaneous Ca^{2+} oscillations and may be linked to the maintenance of DCs in the immature state [289]. - Induces apoptosis of terminally differentiated DCs, which is critical in maintaining self-tolerance and preventing autoimmunity [290].
CREB	Cell survival Modulation of immune response	- Support human and murine DC survival by regulating Bcl-2 expression downstream of TLR signaling [293]. - Up-regulates IL-10 in human DCs in response to zymosan [294].

CHAPTER 8:   CONCLUSION AND FUTURE WORK

Understanding how biomaterials affect DC phenotype is crucial to the design and selection of biomaterials for tissue engineering or vaccine delivery applications, where appropriate and effective host immune response is necessary. In particular, elucidating the material properties that are critical in determining DC phenotype as well as the molecular mechanisms directing the distinct DC responses to biomaterials are of significant importance to material selection for tissue-engineered constructs or vaccine delivery vehicles. Therefore, the material property-DC phenotype relationships and mechanistic basis for DC response to biomaterials were investigated.

Although flow cytometry is a powerful analytical tool for assessing DC phenotype, both sample preparation and data analysis are time-consuming, especially when a large number of samples are analyzed. Due to DC's non- and loosely-adherent nature, traditional cell-based ELISA approaches were not appropriate because of the expected cell loss during washing steps. To enhance the efficiency in sample processing and subsequent measurement, a HTP 96-well filer plate-based methodology was developed to allow for the screening of DC phenotype induced by a large number of biomaterials, particularly from combinatorial libraries (Figure 4-1). In this methodology, after treatment with biomaterials, DCs were transferred to a black 96-well filter plate, where supernatants were collected conveniently and the cells remained in the wells were analyzed for the levels of DC number-independent "maturation factor" (MF), defined as CD86/DC-SIGN, using immunostaining and fluorescent microplate reading. The supernatants could be used immediately for the analysis of cytotoxicity via the release of a cytosolic enzyme, G6PD, and stored for multiplex cytokine profiling experiments.

Therefore, this methodology allowed for the measurements of three cellular outcomes from a single cell culture.

Using proof-of-concept validation experiments, DC responses to biomaterials, PLGA or agarose films, were reproducibly found to be consistent using this filter plate-based methodology as compared to the conventional flow cytometry analysis (Figure 4-6). This HTP method was also successfully down-scaled to a 384-well filter plate platform with consistent results by Nathan Hotaling in the Babensee laboratory. Besides biomaterials, this method is expected to expedite screening of DC response to various other stimuli, including soluble factors, and facilitate the discovery of treatments that promote or suppress DC maturation. Furthermore, the analysis of other loosely- and non-adherent cell populations will also find this method beneficial since no cells would be lost during the assessment of phenotype. This methodology is also amenable to quantification of other endpoints such as intracellular signaling molecules in prepared cell lysates.

Very well-defined and controlled surfaces were needed to derive the correlations between material properties and DC phenotype. Hence, a set of clinical Ti substrates, including PT, SLA, and modSLA, were one system initially chosen to study DC response as shown in CHAPTER 4. A major finding of this study was that treatment with PT or SLA promoted a more mature DC phenotype, while DC treatment with modSLA possessed an immature DC phenotype, as determined by the expression of surface maturation marker CD86 (Figure 5-1) and the production of maturation-associated cytokines and chemokines (Figure 5-5 and Figure 5-6). These results also indicated another benefit of modSLA surfaces for promoting bone formation and integration by providing a local non-inflammatory environment. Furthermore, PCA was used to reduce the multi-dimensional data space to facilitate the analysis of co-variations between material properties and DC phenotype (Figure 5-8). The primary conclusion from this

study was that surface chemistry was the most critical material property in determining DC phenotype induced by the Ti substrates. In particular, the increase in surface %C and %N were associated with enhanced DC maturation, while the increase in %O and %Ti contributed to an iDC phenotype. Furthermore, this particular material system suggested that the increase in surface hydrophilicity was also co-varied with less DC maturation. However, line roughness (R_a) was not important in determining DC response (Figure 5-8B). This finding not only offered guidelines for Ti implant design, but it also suggested that DC response could be correlated to material properties using multivariate analytical methods. Such methods are necessary because it is near impossible to vary only one material property at a time for any biomaterial systems. Whenever one property (e.g. roughness) is changed, other material properties (e.g. surface energy) also change inevitably. This challenge causes many traditional ways that attempt to isolate a single biomaterial property that dictates cell response futile as the relationships generated are typically not specific to a particular material property. Therefore, in order to confirm the relationships generated with this set of Ti substrates using PCA, separate sets of well-defined biomaterials should be used for the analysis of DC phenotype. The material property-DC response relationships generated by multivariate analysis can then be compared to those derived from the Ti substrates.

To generate polymeric material property-DC phenotype relationships, a more broad-based biomaterial system was used. This biomaterial system included twelve different pMAs, selected from a combinatorial pMA library. The material properties for these polymers were extensively characterized for surface chemical composition, air-water contact angle, T_g, surface roughness (R_a and S_a), and surface area (Table 6-3). These pMAs were shown to induce differential DC response upon treatment based on the expression of MF derived using the HTP methodology (Figure 6-3A). In addition, when the ordering of these pMAs was kept the same in the x-axis for comparison, the

131

production of pro-inflammatory cytokine, TNF-α (Figure 6-3B), and chemokine, IL-8 (Figure 6-3D), appeared to roughly follow the same trend, while pHEMA induced higher anti-inflammatory cytokine, IL-16, production compared to any other treatments (Figure 6-3C). This major result indicates that materials can be used to fine tune DC response, and carefully selected biomaterials can potentially direct desired immune responses by modulating DC phenotype.

Another major outcome from this study was that DC response could be correlated to material properties by PCA (Figure 6-6). More importantly, consistent with the results from the Ti substrate study, surface chemical composition was most useful in determining DC response. Specifically, surface oxygen and oxygen-containing bonds such as -C-O- and -O-C=O are strongly associated with an iDC phenotype, while surface carbon and carbon only -C-C- bonds are strongly associated with a mDC phenotype. In contrast, T_g, R_a, and surface area had little influence on DC phenotype (Figure 6-6B).

The most significant contribution of this study was that DC phenotype could be predicted based on the properties of the materials used to treat the DCs using PLSR, a multivariate analysis method. PLSR performs projection of the data from the original multi-dimensional data space onto a reduced principal component space in a similar way compared to PCA. In addition, it contains an added algorithm that also optimizes the correlations between the X matrix (containing predictor variables) and the Y matrix (containing outcome variables). A model was constructed based on the pMA library (as the "training set") and could predict DC response to a new set of methacrylate- and acrylate-based terpolymers (called the prediction set) in terms of the expression of MF with $R^2_{prediction}$ of 0.76 and $\overline{R}^2_{prediction} = 0.75$ (Figure 6-8E). Furthermore, theoretical values of the chemical composition of the bulk materials were sufficient in the prediction with even a higher $R^2_{prediction}$ of 0.80 and $\overline{R}^2_{prediction} = 0.79$ (Figure 6-9E). However, when using experimental XPS values alone, the model performance was very poor. It was

important to note that the models did not predict the exact level of DC maturation, but the relative levels of DC maturation induced by a set of polymers. However, this is a significant result because DC maturation is a relative term, and it is a continuum of, but not discrete, phenotype. The fact that DC response can be predicted from theoretical chemical composition will have unprecedented impact on biomaterial design because rational design and selection of immune-modulatory biomaterials can be performed prior to lengthy polymer synthesis and material characterization procedures. However, cytokine and chemokine levels were not predictable variables, presumably due to the large donor-to-donor variation in their production by DCs as well as their degradation in the cell culture medium.

From the two studies with Ti substrates and pMA library, it was consistent that biomaterial surface chemistry is the most important property that determines DC response. It is hypothesized that chemistry is the underlying property that dictates the other properties of the biomaterials, including hydrophilicity, T_g, etc., and more complex chemical information about the material surface may offer better prediction for DC response.

Although biomaterial chemistry is the most critical material property for predicting DC response *in vitro*, many previous studies have also shown that despite the differential levels of protein adsorption and short-term leukocyte infiltration induced by varied surface chemistries, similar long term inflammatory outcome of fibrous capsule formation was achieved *in vivo*. For example, polyethylene terephthalate (PET) surfaces functionalized with -OH, -NH$_2$, or -CF$_3$ induced different extents of adsorption and denaturation of fibrinogen. Although these materials also induced different numbers of total adherent phagocytes depending on the functionality (-NH$_2$> -CF$_3$> -OH) after short term implantation, the chronic fibrotic outcome was similar among these different chemistries [298]. In another study, tetrafluoroethylene-hexafluoropropylene-copolymer

(FEP) films were plasma polymerized with tetraglyme to minimize fibrinogen adsorption on the surfaces. However, *in vivo* studies showed that FEP films with or without polymerized tetraglyme provoked similar levels of fibrous encapsulation [299]. However, Thevenot et al. hypothesized that the ineffectiveness of surface chemistry on *in vivo* long-term fibrotic reactions might be due to inefficient interactions between the cells and surface functional groups [300]. By enhancing the cell-surface interaction using microspheres with different functionalities, Kamath et al. showed surfaces with -OH and -NH$_2$ groups induced stronger fibrotic reaction in comparison to -CF$_x$ and -COOH surfaces [301]. Therefore, in order to translate the *in silico* predictions into *in vivo* host response, biomaterials that cause extremes of DC phenotype should be selected based on the predictions generated by the computational model. Then, these biomaterials would first be used to validate the induced DC phenotype upon treatment *in vitro*. Subsequently, scaffolds or microspheres of these biomaterials would be created to maximize the interactions between the host and the material for optimal biomaterial effects *in vivo*. These biomaterial scaffolds or microspheres with optimal architecture for host interaction are expected to differentially modulate host response against the implanted devices according the biomaterial chemistry.

Although CHAPTER 6 demonstrated that a generalized DC phenotype represented by the expression of CD86 and DC-SIGN can be readily predicted from biomaterial properties, several major limitations exist in this model: a) only relative levels of DC maturation can be predicted, b) not containing additional important material properties such as polymer swelling, c) only as good as what material set the model is trained on for making future predictions, and d) prediction of a generalized response based on surface marker expression without consideration of immune response polarization. However, this model represents the first step into predicting immune cell response. Because a model can only predict what it is trained on, the models in

CHAPTER 6 based on pMAs with the same chemical backbones and simple elemental composition (only C and O), are not sufficient in predicting DC response induced by a different class of materials (e.g. pMAs containing nitrogen or polypropylene). Future work should aim to develop a more comprehensive model encompassing several classes of materials with more diverse chemical composition, including elements and functional groups. These polymers will be used to determine DC response in terms of the expression of MF and will be the Y matrix (outcome) in the PLSR model. More detailed theoretical chemical compositions, including aromatic rings and double bonds, should be calculated and used as the X matrix (predictors) in the model. The multivariate model with added chemical information is expected to have stronger predictive power for more diverse polymers. It is expected that in order for such models to perform satisfactorily, many members of each class of materials need to be included to account for the covariances. This kind of model would be ideal because it can offer universal guidelines for future biomaterial development. Alternatively, it is also possible that separate models need to be developed for the DC response prediction induced by different classes of materials. In this case, one may need to select a particular computational model suitable for the biomaterials of interest. Currently, these computational models can only predict induced DC response *in vitro*. Ideally, the *in vitro* responses should be translated into *in vivo* responses, and the *in vivo* health outcomes can in turn be predicted. Therefore, additional work needs to be carried out to address the potentials of computational modeling for immune response prediction.

Furthermore, although the HTP method is useful for screening a large number of treatments to identify "hit" biomaterials that promote or suppress DC maturation, it may not be as appropriate for modeling purposes. For modeling, more variables are desired to build the data matrix as a basis in order to identify the variables that can be predicted. Therefore, though slower, conventional flow cytometry is preferred over the HTP method

because it can generate additional information such as cell size (from forward scatter) and the distribution of cells being investigated for a specific marker. For example, the expression level as well as the distribution of cells (e.g. percentage of positive cells) for several surface markers that are associated with DC maturation should be measured, including CD86, DC-SIGN, and CCR7 (chemokine receptor). Simultaneously, DCs treated with different biomaterials can be analyzed for cell size distribution using the forward scatter generated by flow cytometry. Since cell shrinkage can be an indicator for apoptosis [302], material properties that potentially induce apoptosis may be identified and used to predict biomaterial formulation that can cause apoptosis.

Another major finding from this thesis research was that biomaterials induced differential DC responses via the activation of distinct TFs as described in CHAPTER 7. From the study using the pMA library, two pMAs were selected for DC treatment because they induced the two extremes of DC maturation (CHAPTER 6). These pMAs were pHEMA and pIBTMA, which caused the least and most mature DC phenotype, respectively (Figure 7-1 and CHAPTER 6). The different DC phenotype induced by the two pMAs was consistent with the surface expression CD86 (Figure 7-2) and with the morphology (Figure 7-3) of DCs treated with these pMAs. Treatment of DCs with pHEMA and pIBTMA were shown to induce activation of distinct TFs. Specifically, pIBTMA induced higher activation levels of NF-κB compared to pHEMA (Figure 7-4A). In contrast, pHEMA induced the activation of immuno-suppressive TFs such as E2F-1 (Figure 7-4E) and GR/PR (Figure 7-4F). Furthermore, pHEMA-treated DCs activated the multiple TFs of the apoptotic pathways, including ISRE (Figure 7-4B), NFAT (Figure 7-4G), and E2F-1 (Figure 7-4E), suggesting that pHEMA maintained iDC phenotype by promoting DC apoptosis, which is known to induce DC tolerance [295]. To verify this, DCs were stained for apoptotic marker, annexin V, after treatment with pHEMA or pIBTMA for 24 hrs. The number of early apoptotic cells (shown by annexin V-FITC

single positive population) induced by pIBTMA was similar to the iDC and mDC reference controls. However, DC treatment with pHEMA induced higher number of apoptotic cells (Figure 7-5). Interestingly, in the presence of pHEMA, the effects of LPS on DC morphology (Figure 7-3), surface expression of maturation markers (Figure 7-2), and the activation of certain TFs (Figure 7-4) were eliminated. This result indicates that biomaterials can override the effects of soluble factors and can be powerful tools for modulating DC response. The results shown in CHAPTER 7 demonstrated that two polymers from the same class of materials can exert very different effects on DC phenotype via the activation of distinct TF profiles, and very likely through distinct receptors and signaling pathways. This study shed light on the understanding of the molecular mechanisms that underlie DC response to biomaterials. However, additional evidence is needed to show that pHEMA-treated DCs are apoptotic; therefore, experiments to measure caspase activity and DNA fragmentation, both hallmarks of apoptosis, will be carried out.

The TF activation profile of DCs induced by the pHEMA also appeared to be consistent with the cytokine profile of pHEMA-treated DCs. pHEMA induced low production levels of all the maturation-associated cytokines and chemokines but high level of pleiotropic cytokine, IL-16 (CHAPTER 6). Consistently, pHEMA induced the activation of two potent immuno-suppressive TFs, namely E2F-1 [281] and GR/PR [282], both of which have been shown to reduce the expression of TNF-α and IL-12 as well as IL-6. Furthermore, GR could decrease MCP-1 production by altering MCP-1 mRNA stability [311]. Contradictorily, ISRE [265,266] and NFAT [288] have also been demonstrated to support the production of IL-12. Therefore, the production levels of cytokines most likely resulted from the balance of the effects of all these TFs. NF-κB is a strong activator of a number of pro-inflammatory cytokines, including TNF-α, IL-1, IL-12 [254]. Altogether, the cytokine profiles induced by pIBTMA and pHEMA (CHAPTER 6) are

consistent with the TF activation profiles induced by the respective pMAs (CHAPTER 7). Potentially, pHEMA might present ligands that trigger the destabilization of the mRNAs of TNF-α, MCP-1, and IL-1ra, leading to the even lower production of these cytokines as compared to the iDC reference control [239]. Future work should explore the ligand presentation by pHEMA and its link to mRNA destabilization, possibly through interference of HuR binding to the cytokine mRNAs [239].

Additionally, several TFs appeared to have conflicting effects on DC response (CHAPTER 7). For example, NFAT has been shown to induce DC maturation, maintain immature DC phenotype, as well as induce apoptosis; ISRE can induce apoptosis as well as DC maturation. Future work should aim to elucidate the effects of the activation of each TF on DC phenotype. In particular, blocking or siRNA known-down experiments should be performed to examine the effects of each of the TFs and verify their contribution and effects, further elucidating the mechanistic basis of DC response to biomaterials. Furthermore, tracking experiments such as with fluorescent markers are required to validate that TFs indeed are activated and translocate from the cytosolic environment into the nucleus to exert the observed effects.

Given the wide range of applications of pHEMA in clinical settings as a biocompatible biomaterial, it is of great interest to understand why and how pHEMA would induce such drastically different DC response from any other pMAs tested. Furthermore, DCs treated by pHEMA or TCPS possessed an iDC phenotype, but these two materials are very different. Understanding the similarities and differences in pHEMA and TCPS induced DC phenotype may allow for the identification of important properties that are important for biocompatibility. The Babensee lab has previously shown that DC adhesion to biomaterial is required for maturation, partially through the interaction via integrins [121]. However, adhesion is not sufficient to cause maturation as shown in CHAPTER 5, where modSLA adhered similar numbers of DCs as compared

to PT and SLA but did not affect DC phenotype. Therefore, further work should be carried out to elucidate pHEMA's ability to maintain an iDC phenotype. Potentially, such immuno-suppressive ability of pHEMA is caused by very low level of DC adhesion. Alternatively, pHEMA may present proteins in certain conformations that mimic immuno-suppressive ligands such as zymosan, whose interaction with TLR-2 has been shown to induce T_{reg} formation [243]. Furthermore, additional apoptosis assays may shed light on whether pHEMA suppressed DC maturation through induction of apoptosis of DCs, which is a strong activator of immune tolerance. Understanding how pHEMA induced suppressed DC response could guide future design of biocompatible materials for clinical applications. Specifically, one may design a biomaterial that adheres certain profiles or numbers of immune cells, directs certain presentation or conformation of serum proteins, and/or triggers apoptosis of DCs surrounding the implant material. Insights from these studies will facilitate the synthesis, discovery, or manipulation of new class of clinically-relevant biocompatible materials. Further studies are also needed to translate the *in vitro* effects induced by pHEMA into *in vivo* host responses as described next.

In addition to the *in vitro* elucidation of how DCs respond to biomaterials, understanding how pHEMA and pIBTMA, which induced extremes of DC phenotype *in vitro*, differ in modulating adaptive immune response *in vivo* would be of significant interest. These pMAs would be fabricated into scaffolds loaded with a model antigen (e.g. OVA) or allogeneic cells for implantation in wild type mice or CD11c.DTR transgenic mice. CD11c.DTR transgenic mice contain diphtheria toxin receptor (DTR) expressed under the CD11c promoter. In these mice, efficient DC depletion can be achieved over prolonged periods of time by multiple injections of diphtheria toxin (DT) [309]. The adjuvant effect of these pMAs would be assessed by quantifying the amount of antibodies in the serum. In addition, Foxp3$^+$ T_{reg}s would be quantified in the mice to

139

determine whether pHEMA could exert a tolerogenic effect *in vivo* against allogeneic cells or OVA. This study would not only translate the *in vitro* findings of these pMAs into *in vivo* outcomes, but it would also uncover the potential of pHEMA as an immunosuppressive treatment, potentially for allografts, xenografts, or tissue-engineered constructs that contain immunogenic biologics. In addition, these experiments would be performed in CD11c.DTR transgenic mice as compared to wild type mice to assess if DCs are central in the biomaterial-induced adjuvant effect or tolerance *in vivo*.

This thesis research can lead to multiple future directions, including elucidating 1) the adsorbed protein profile on the pMAs, 2) receptor/ligand pairs, and 3) signaling pathways that are central in mediating the biomaterial effects on DCs. An activating material such as PLGA was shown previously in the Babensee laboratory to induce increased DC adhesion, while a non-activating material such as agarose did not promote DC adhesion. The activating nature of PLGA was linked to its high contact angle, whereas agarose is extremely hydrophilic. It was anticipated that PLGA would induce more adsorption of serum proteins in comparison to agarose [121]. In this research, pIBTMA coating had very low contact angle (28.7°) in comparison to pHEMA coating (69.5°). However, pIBTMA was clearly an activating material, but pHEMA appeared to be a passivating material by the induction of DC apoptosis. Therefore, the effect of biomaterials on DCs is not directly linked to the hydrophobicity of the materials. The differential effects of these pMAs on DC phenotype were most likely mediated through different presentation or conformation profiles of the adsorbed protein layer. Elucidating the protein presentation is not an easy task; one of the most popular approaches is to spike 10% serum with single radiolabeled serum proteins such as fibronectin and vitronectin. After incubation of the spiked serum with the biomaterials, the surfaces would then be rinsed vigorously with PBS and the amount of radiolabeled proteins measured by a scintillation counter. This subtraction approach is expected to be

140

insensitive and variable and therefore might not yield meaningful results. Other approaches include surveying the protein conformation on biomaterials adsorbed with 10% serum proteins using atomic force microscopy (AFM). With this approach, an antibody specific to a serum protein (e.g. fibronectin) would be conjugated to the AFM scanning tip and used to measure the presence and orientation of fibronectin by rastering the tip over a defined surface. This experiment would yield insight into the conformation and presentation of different serum proteins. Furthermore, time-of-flight secondary ion mass spectroscopy (ToF-SIMS) can be used to simultaneously identify the presence of multiple proteins on an adsorbed protein layer. Previously, 16 different single protein films adsorbed on mica were used for ToF-SIMS analysis, and PCA was able to classify the proteins using only two principal components [303]. In this approach, control protein layers adsorbed from single serum protein solutions would be used for the controls. pHEMA or pIBTMA would be adsorbed with 10% serum, and the protein layers would be subjected to ToF-SIMS analysis and compared to the controls to identify the proteins that are adsorbed to the surfaces.

Systems biology approach is currently being explored in the Babensee lab to elucidate the receptors DCs employ for recognition of and response to biomaterials. The phosphorylation of signaling molecules will be measured after treatment of DCs with ligands known to be specific for certain receptors. The signaling network will then be modeled using PCA and PLSR for correlating activation of signaling molecules with receptor engagement. After quantifying the activation of signaling molecules in DCs upon treatments with certain biomaterials, such computational model will then be used to predict the receptors that are used by DCs to respond to biomaterials.

The receptors that are predicted to be involved in DC response to biomaterials can potentially be identified by silencing signaling molecules that are immediately downstream to the receptors using siRNA. For instance, MyD88 could be a target for

many toll-like receptors (TLRs), including TLR2, 4, 5, 6, and 10 on the cell membrane [304]. The target for C-type lectin, Dectin-1, would be Syk [305]. Other receptors of interest include the TNFαR1, which signals through the TNF receptor-associated death domain (TRADD) [306], and the integrin α4β1, which signals via the integrin-linked kinase (ILK) [307]. These signaling molecules can be silenced through the delivery of siRNA to primary DCs. As shown in Appendix 4, DC transfection was effective only by electroporation. Electroporation of DCs with DNA plasmids induced significant cell death by 40 h post transfection, which is not amenable to the silencing of signaling molecules because it usually takes up to 48 h for effective silencing to occur. However, transfection with siRNA using electroporation has been shown to successfully knockdown molecules in human primary DCs, potentially due to the small size of siRNA. For instance, syndecan-3 was identified as an HIV-1 attachment receptor on human primary DCs by using siRNA [308]. Therefore, conditions of electroporation will need to be optimized for delivering siRNA to human primary DCs using Amaxa Nucleofector (Lonza). Other than electroporation, a new family of biodegradable α-amino acid poly(ester amide)s (AA-PEAs) have been synthesized by Dr. C.C. Chu's laboratory at Cornell University. These AA-PEAs were found to be superior in transfecting primary cells as compared to commercial reagents (personal communication) and may potentially be used for delivering siRNA to DCs to improve DC viability post transfection. Furthermore, silencing of combination of receptor-specific signaling molecules is expected to be necessary due to their redundancy.

The detailed signaling pathways can be identified by measuring key signaling molecules, including p38, JNK, Akt, ERK1/2, and others. Multiplex phosphoprotein kits (from Millipore or Bio-rad) can be customized to measure the level of phosphorylated signaling molecules at different time points. Since signaling is expected to occur soon after the ligation of receptors and their ligands, this study should focus on early time

142

points beginning at 15 min until 2 or 3 h. This study, together with the elucidation of adsorbed protein profiles and receptors mediating the differential biomaterial effects on DCs will provide mechanistic insights into the rational design of biomaterials for modulating DC phenotype, thereby potentially directing desired immune responses *in vivo*.

The research presented in this thesis aimed to identify the material properties that are the most important in determining DC response by using multivariate analysis approach. Furthermore, DC phenotype was successfully predicted from polymer chemical composition and was shown to be mediated through distinct TF activation profiles. Altogether, these results allow for improved rational design of biomaterials that direct certain immune responses towards the biologics co-delivered in a combination product.

APPENDICES

APPENDIX 1

A.1. Supplementary data for Chapter 7: Predicting DC response using multivariate analysis.
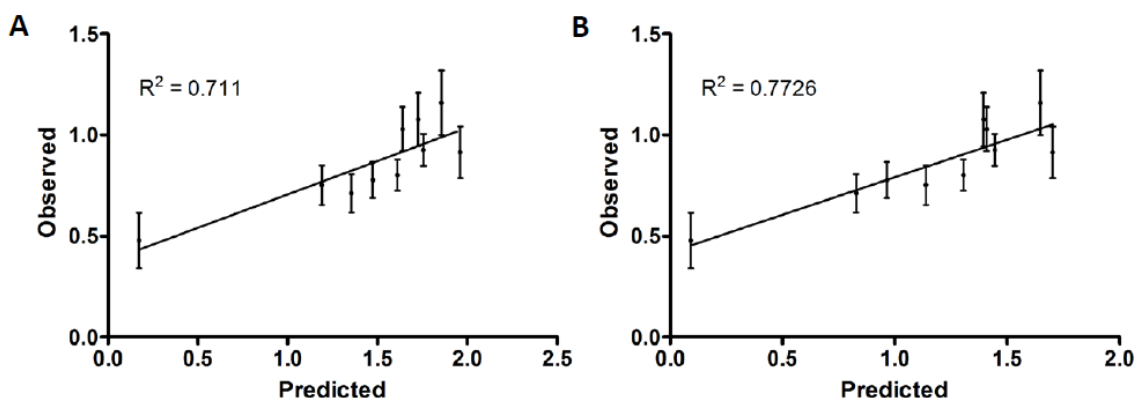
Figure A1-1: Prediction results using PLSR models similar to first PLSR model built with surface material properties but with high resolution experimental surface chemical composition fitted (A) at GT (no beta carbons and C=O) removed from the X-block, and (B) at UT (with beta carbons and C=O) removed from the X-block. After pruning steps, prediction of MF induced by the prediction set terpolymers in six independent experiments with different donors was determined. The error bars indicate the standard errors of the experimental values.

Table A1-1: List of X-variables used in the PCA model

Variable	Definition	Measured for	Number of variables
MF	Maturation factor (CD86/DC-SIGN)	Mean	1
IL-1β	Interleukin-1β	Mean	1
IL-1ra	Interleukin-1 receptor antagonist	Mean	1
IL-8	Interleukin-8	Mean	1
IL-16	Interleukin-16	Mean	1
MCP-1	Monocyte chemotactic protein-1	Mean	1
MIP-1α	MΦ inflammatory protein-1α	Mean	1
TNF-α	Tumor necrosis factor-α	Mean	1
T_g	Glass transition temperature	Mean	1
Theta	Air-water contact angle	Mean	1
Si2p (E)	Experimental Si2p	Mean	1
C1s (E)	Experimental C1s	Mean	1
O1s (E)	Experimental O1s	Mean	1

Table A1-1 continued:

C1s (T)	Theoretical C1s	Mean	1
O1s (T)	Theoretical O1s	Mean	1
C-C (UT)	Experimental C-C in U of T (fitted with beta carbon)	Mean	1
C-O (UT)	Experimental C-O in U of T (fitted with beta carbon)	Mean	1
O-C=O (UT)	Experimental O-C=O in U of T (fitted with beta carbon)	Mean	1
Beta C	Experimental Beta C in U of T(fitted with beta carbon)	Mean	1
C=O	Experimental C=O in U of T	Mean	1
C-C (GT)	Experimental C-C in GT (No beta carbon)	Mean	1
C-O (GT)	Experimental C-O in GT (No beta carbon)	Mean	1
O-C=O (GT)	Experimental O-C=O in GT (No beta carbon)	Mean	1
C-C (T)	Theoretical C-C	Mean	1
C-O (T)	Theoretical C-O	Mean	1
O-C=O (T)	Theoretical O-C=O	Mean	1
Ra	Line roughness	Mean	1
Sa	Arithmetic mean height	Mean	1
SurfArea	Surface Area	Mean	1
Total			**29**

Table A1-2: List of X-variables used in the PLSR models

Variable	Definition	Measured for	Number of variables
T_g	Glass transition temperature	Mean	1
Theta	Air-water contact angle	Mean	1
Si2p (E)	Experimental Si2p	Mean	1
C1s (E)	Experimental C1s	Mean	1
O1s (E)	Experimental O1s	Mean	1
C1s (T)	Theoretical C1s	Mean	1
O1s (T)	Theoretical O1s	Mean	1
C-C (UT)	Experimental C-C in U of T (fitted with beta carbon)	Mean	1
C-O (UT)	Experimental C-O in U of T (fitted with beta carbon)	Mean	1
O-C=O (UT)	Experimental O-C=O in U of T (fitted with beta carbon)	Mean	1
Beta C	Experimental Beta C in U of T(fitted with beta carbon)	Mean	1
C=O	Experimental C=O in U of T	Mean	1
C-C (GT)	Experimental C-C in GT (No beta carbon)	Mean	1
C-O (GT)	Experimental C-O in GT (No beta carbon)	Mean	1
O-C=O (GT)	Experimental O-C=O in GT (No beta carbon)	Mean	1
C-C (T)	Theoretical C-C	Mean	1
C-O (T)	Theoretical C-O	Mean	1
O-C=O (T)	Theoretical O-C=O	Mean	1
Ra	Line roughness	Mean	1
Sa	Arithmetic mean height	Mean	1
Sq	Root mean square	Mean	1
Ssk	Skewness	Mean	1

Table A1-2 continued:

Sku	Kurtosis	Mean	1
Sp	Maximum peak height	Mean	1
Sv	Maximum pit depth	Mean	1
Sz	Maximum height (Sp+Sv)	Mean	1
Sk	Level difference for a core part	Mean	1
Spk	Reduced peak height	Mean	1
Svk	Reduced valley height	Mean	1
SMr1	Load area ratio to separate between a reduced peak part and a core part	Mean	1
SMr2	Load area ratio to separate between a reduced valley part and a core part	Mean	1
Sxp	Load area ratio from 97.5 to 50%	Mean	1
Vvv	The void volume at valley region (load area ratio 80%)	Mean	1
Vvc	The void volume at a core part (load area ratio from 10 to 80%)	Mean	1
Vmp	The actual volume at a peak region (load area ratio 10%)	Mean	1
Vmc	The actual volume at a core part (load area ratio from 10 to 80%)	Mean	1
Sal	Auto-correlation length	Mean	1
Str	Texture aspect ratio	Mean	1
SurfArea	Surface Area	Mean	1
Total			**39**

Table A1-3: Prediction of maturation factor from surface material properties: Variable influence in projection (VIP) in the PLSR model. 95% confidence intervals were determined by jack-knifing.

Variables	Variable influence in projection	95% confidence interval
C1s (T)	1.51272	0.108265
O1s (T)	1.47516	0.118783
Theta	1.34927	0.257581
C-O (T)	1.24508	0.221662
Sk	1.21549	0.124656
Vvc	1.20151	0.099618
Sxp	1.18454	0.104798
Vmc	1.18306	0.129637
C-C (T)	1.17573	0.168358
Sa	1.17381	0.101057
Sq	1.13387	0.095736
Si2p (E)	1.12296	0.429882
Spk	1.077	0.041625
Vmp	1.07638	0.045283
C-O (UT)	0.949676	0.161907

Table A1-3 continued:

Sv	0.936893	0.135325
C-O (GT)	0.932527	0.217767
C-C (UT)	0.921093	0.113291
Vvv	0.896861	0.07768
C-C (GT)	0.870228	0.110673
Svk	0.827719	0.100776
Sz	0.807782	0.149195
O-C=O (T)	0.799988	0.084244
Str	0.758573	0.148316
Sp	0.737861	0.029967
Sku	0.721398	0.229052
O-C=O (GT)	0.657158	0.122984
O-C=O (UT)	0.656134	0.122939
O1s (E)	0.592469	0.400198
SMr1	0.588059	0.111076
Beta C	0.581602	0.099062
SMr2	0.490808	0.439456

Table A1-4: Prediction of maturation factor from surface material properties: loadings of each variable on each of the 2 PCs of the PLSR model.

Variables	w*c[1]	w*c[2]
MF	0.19797	0.190915
Theta	-0.173138	-0.461222
Si2p (E)	0.163364	0.34822
O1s (E)	-0.113471	-0.0756812
C1s (T)	0.270195	0.317214
O1s (T)	-0.265351	-0.300718
C-C (UT)	0.179885	0.0228189
C-O (UT)	-0.180422	-0.134749
O-C=O (UT)	-0.128291	-0.0270437
Beta C	-0.0979554	0.09951
C-C (GT)	0.168911	-0.00437626
C-O (GT)	-0.179336	-0.111298
O-C=O (GT)	-0.122494	0.0537237
C-C (T)	0.226236	0.138868
C-O (T)	-0.230384	-0.219871
O-C=O (T)	-0.147673	0.0749068
Sq	-0.212846	0.0819662
Sku	0.139873	0.0710063
Sp	-0.133832	0.0829999

Table A1-4 continued:

Sv	-0.0444854	0.365612
Sz	-0.105982	0.223176
Sa	-0.227223	0.0158695
Sk	-0.237384	-0.0302944
Spk	-0.186433	0.163962
Svk	-0.102861	0.24049
SMr1	-0.0886776	0.13429
SMr2	0.00385639	-0.201951
Sxp	-0.229197	0.017557
Vvv	-0.149658	0.158688
Vvc	-0.232394	0.0190704
Vmp	-0.183968	0.173644
Vmc	-0.231098	-0.0316889
Str	0.144711	-0.0353204

Table A1-5: Prediction of maturation factor from theoretical chemical composition alone: Variable influence in projection (VIP) in the PLSR model. 95% confidence intervals were determined by jack-knifing.

Variables	VIP	95% confidence interval
C1s (T)	1.07802	0.078199
O1s (T)	1.02384	0.055541
O-C=O (T)	1.0185	0.115368
C-O (T)	0.946235	0.146714
C-C (T)	0.925699	0.058274

Table A1-6: Prediction of maturation factor from theoretical chemical composition alone: loadings of each variable on each of the 3 PCs of the PLSR model.

Variables	w*c[1]	w*c[2]	w*c[3]
MF	0.315287	0.696938	0.499077
C1s (T)	0.520489	0.439407	0.725786
O1s (T)	-0.51116	-0.34823	-0.59166
C-C (T)	0.435808	-0.2265	-0.64242
C-O (T)	-0.4438	-0.09625	0.538043
O-C=O (T)	-0.28447	0.800151	0.226532

APPENDIX 2

A.2. Isolation of human monocytes for a purified DC culture used for transcription factor profiling

A heterogeneous DC culture, with B cells as the major contaminating cell type, has been conventionally used in the Babensee laboratory to assess DC response to biomaterials. The B cell percentage in this culture can range from $9 - 25\%$ depending on the donors. The presence of B cells in the culture has been shown to contribute to the full response of DCs to biomaterials [211].

In order to determine DC-specific TF activation upon biomaterial treatment, human monocytes were purified from freshly collected peripheral blood mononuclear cells (PBMCs) using $CD14^+$ magnetic bead (MACS) isolation. These beads positively selected CD14 expressing monocytes. Following isolation of monocytes using MACS, the purity was assessed via flow cytometry through the expression of CD14 (Figure A2-1), and the viability of cells was assessed by propidium iodide (PI) staining (Figure A2-2). The percentage of $CD14^+$ or PI^+ cells was determined pre- and post-isolation. Routinely, >95% of cell population post-isolation was $CD14^+$. Typically, >80% isolated monocytes were viable. After incubation of isolated monocytes for 2 h to allow for adhesion of the cells to the cell culture dish, the dish was washed gently $1 - 2$ times to remove any non-viable cells. The purified monocytes were then cultured in the presence of IL-4 and GM-CSF for 5 days for the differentiation into DCs. On Day 5, the purity of DCs were checked by double-staining the cells with monocyte-derived DC markers CD1a (Biolegend) and DC-SIGN (R&D Systems). CD1a and DC-SIGN double positive cells were determined as DCs (Figure A2-3). Routinely, >95% of the cell population on Day 5 was $CD1a^+/DC\text{-}SIGN^+$ DCs.
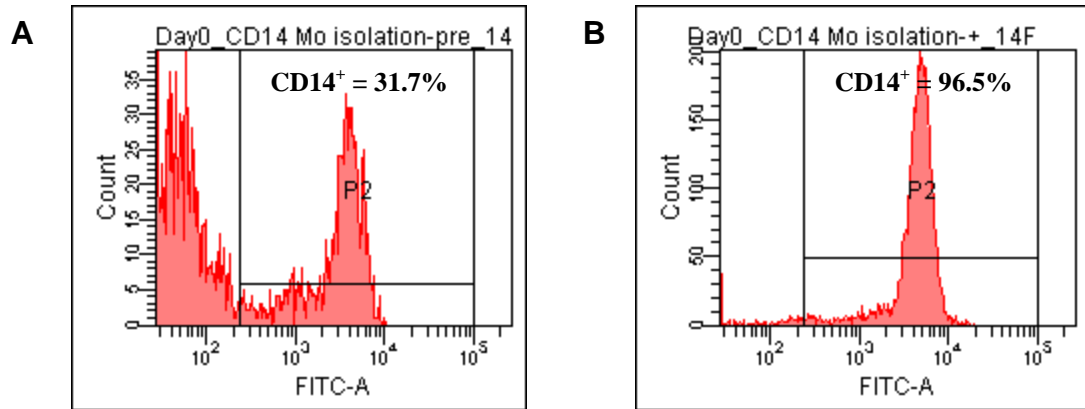
Figure A2-1: Purification of monocytes using CD14 microbead isolation. Pre-isolation (A) and post-isolation (B) levels of CD14-FITC expression are shown. Cells were stained with CD14-FITC monoclonal antibody (Miltenyi Biotec). Following isolation, cell population was generally >95% CD14$^+$ for the generation of a purified DC population.
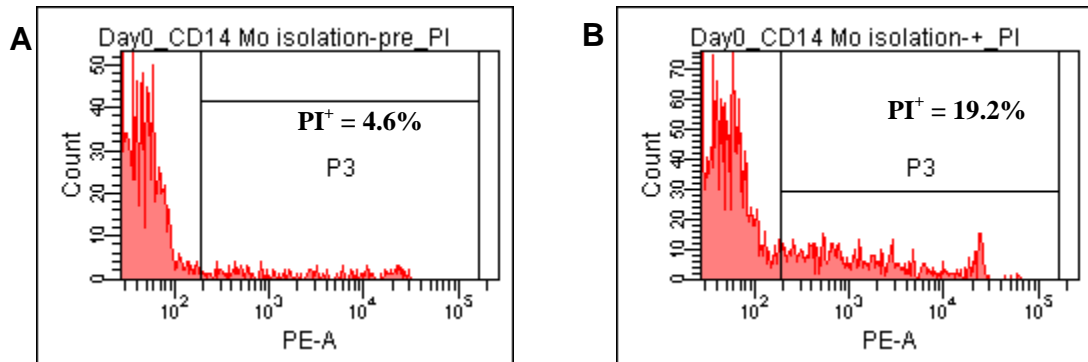
Figure A2-2: Viability of cells pre- (A) and post-isolation (B) using CD14$^+$ microbeads. Typically, >80% isolated monocytes were viable. After incubation of isolated monocytes for 2 h to allow for adhesion of the cells to the cell culture dish, the dish was washed gently 1 – 2 times to remove any non-viable cells.

Figure A2-3: Purity of DCs derived from a purified population of monocytes. Cells were double-stained with CD1a-AlexaFluor 647 (labeled as APC) and DC-SIGN-FITC monoclonal antibodies. Routinely, cell population was >95% CD1a$^+$/DC-SIGN$^+$ DCs.

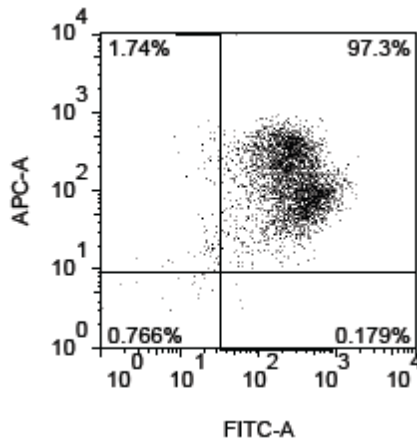DCs from this purified culture were shown to be capable of responding to biomaterials, though to a lesser extent, as compared to the heterogeneous cell culture. DCs treated with PLGA or agarose were stained for the expression of surface markers, including CD83, CD86, and DC-SIGN. It is important to note that the purified culture resulted in less variability in surface marker expression in differentially treated DCs as compared to the heterogeneous cell culture method. DCs cultured by both methods responded to LPS at similar levels (Figure A2-4).
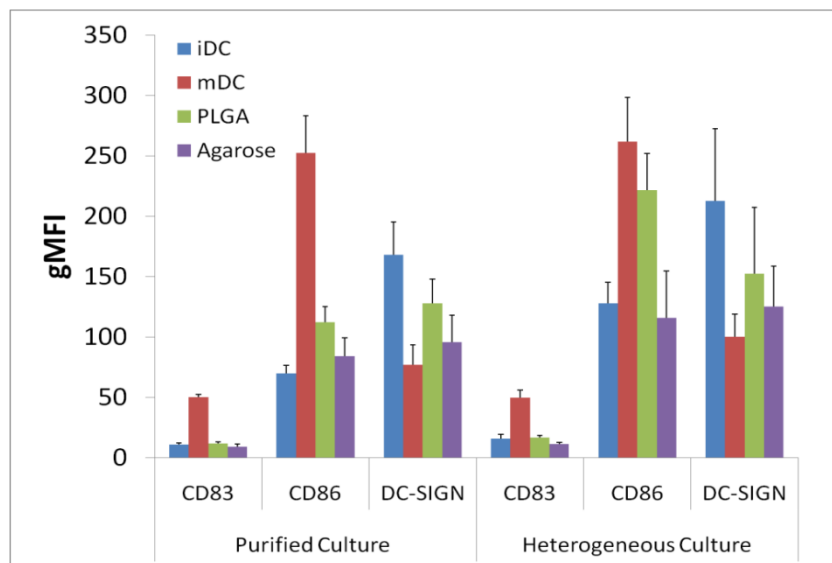

Figure A2-4: Comparison of DC response to biomaterials using DCs from purified DC culture and conventional culture method. gMFIs of the surface markers were determined by flow cytometry with n = 3 donors (mean ± SEM).

APPENDIX 3

A.3. Other approaches for developing high-throughput methodology for DC phenotype screening

In the process of developing the HTP method, a number of other approaches were attempted before the filter plate approached was validated. These methods included 1) magnetic bead approach, 2) agarose entrapment approach, and 3) transwell approach. These approaches were initially conceived to magnetically or physically "trap" DCs during washing steps due to the loosely adherent nature of DCs. Regular cell-based ELISA was unusable for the HTP method because the washing steps were expected to wash away the majority of the cells. This appendix section describes the various approaches.

A.3.1. Magnetic bead approach

Concept of magnetic bead approach

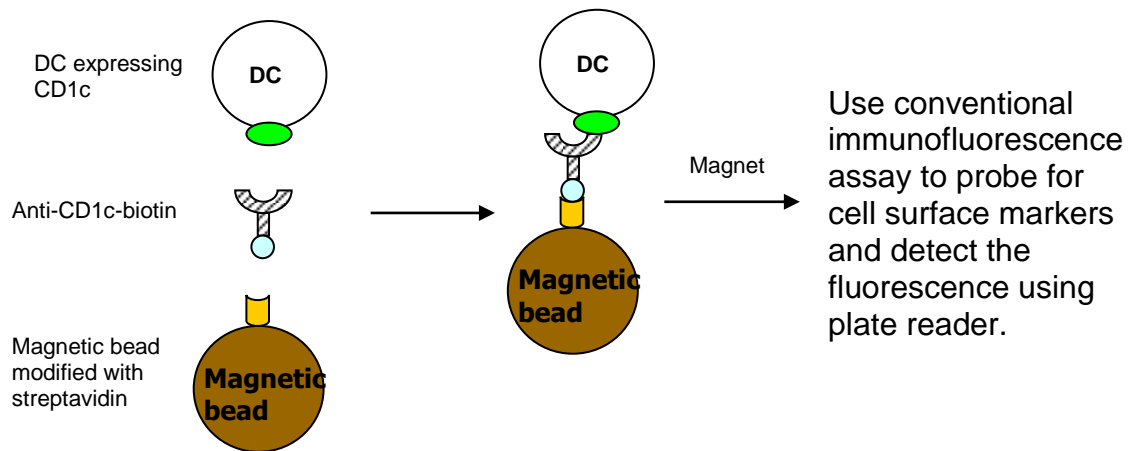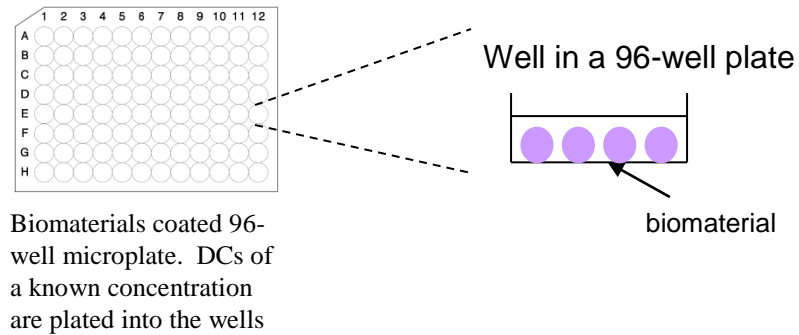**Figure A3-1: Schematic of the magnetic beads approach. DCs were linked to magnetic beads via incubation with first, an anti-CD1c-biotin antibody and second, CD1c molecule expressed on DCs. After the application of a magnet, the excess cells and fluorescently-labeled antibody can be removed, and then the fluorescent intensity in each well can be measured. Size of magnetic bead ~ 4.5 μm, and size of DC ~ 14 μm.**

Intended experimental procedure for analysis DC phenotype in 96-well plate using magnetic bead approach

A) On Day 5 of DC culture

1 2 3 4 5 6 7 8 9 10 11 12
A B C D E F G H

Biomaterials coated 96-well microplate. DCs of a known concentration are plated into the wells

Well in a 96-well plate

biomaterial

B) On Day 6 of DC culture

Detection of fluorescent intensity by a fluorescence plate reader

Hoechst 33342

Wash unbound cells

Wash unbound Antibody

1hr incubation

DC

Magnetic bead

Anti-CD86-PE

Magnet

Hoechst bound to DC DNA
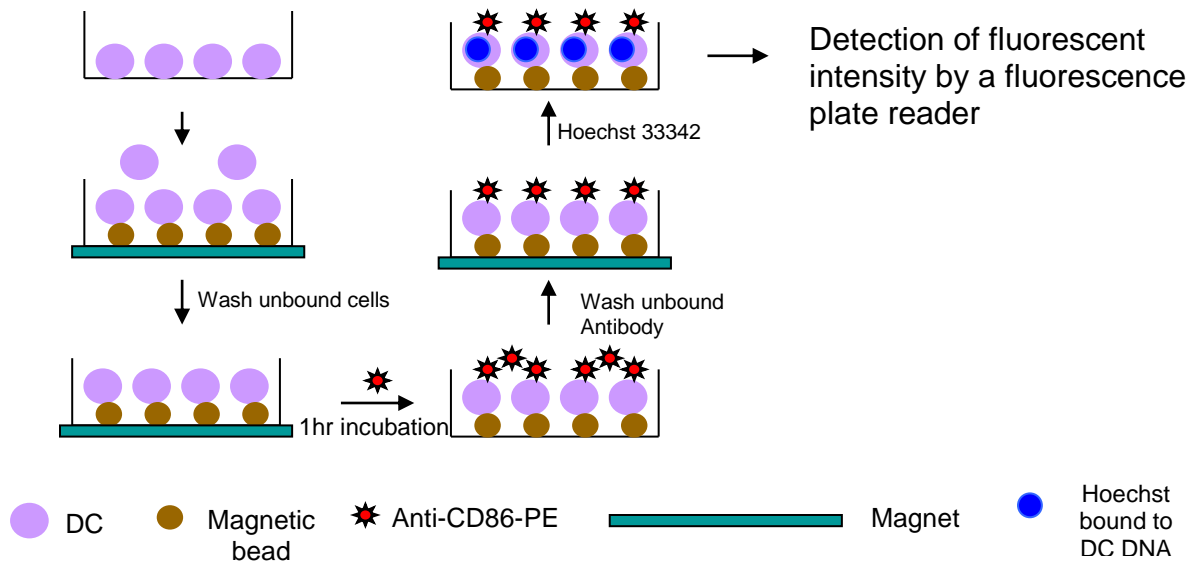
Figure A3-2: Schematic of intended experimental procedure on 96-well plate for magnetic bead approach. A) DCs are plated in 96-well plate coated with different biomaterials at a known concentration on day 5. The inset shows a single well in the microplate. B) On day 6 culture, magnetic beads coated with CD1c-biotin are incubated with the cells. A magnet is applied so that the unbound cells are washed away. The bead-bound cells are then labeled with anti-CD86-PE and Hoechst 33342 and washed with the application of a magnet. Finally the fluorescent intensity of the microplate is measured by a fluorescent plate reader. CD86 is a costimulatory molecule that upregulates with DC maturation and is a good indicator of DC response to biomaterials. Hoechst 33342 stains the nucleus for normalization of cell number across the wells.

Before performing the actual microplate experiments, the "conjugation efficiency" needed to be determined. Conjugation efficiency was defined as (# DCs bound to magnetic beads) / (total DCs). Reasonably high conjugation efficiency was required to retain enough DCs in the wells for fluorescent detection. Figure A3-3 illustrates the experimental procedure for determining conjugation efficiency.
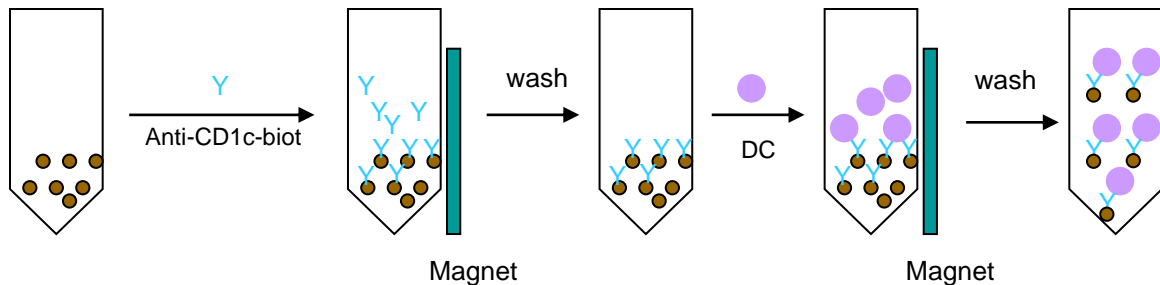

Figure A3-3: Determination of conjugation efficiency of DCs to magnetic beads. A manufacturer-recommended amount of magnetic beads were labeled with anti-CD1c-biotin antibody in an Eppendorf tube. Subsequently a known number of DCs were added to the tube for conjugation. Three washes were performed and the washes were collected for the determination of the unbound cells by Coulter counter. The difference of initial cell number and the unbound cell number was the cells that were bound to the beads.

Surprisingly, the conjugation efficiency was consistently very close to zero (i.e. less than 5%). CD1c-biotin antibody binding to the beads was analyzed by staining the CD1c-biotin antibody-coated beads with FITC-labeled antibodies against biotin or Fab fragment of the antibody. As shown in Figure A3-4, beads labeled with anti-CD1c-biotin antibodies were fluorescent after staining with either of the antibodies, and the fluorescence intensity decreased with increasing anti-CD1c-biotin density, potentially due to steric hindrance.

Subsequently, various adjustments were made to improve conjugation efficiency (Table A3-1). Unfortunately, none of these adjustments, including an indirect labeling method, improved conjugation efficiency.

Therefore, the anti-CD1c-biotin antibody was able to independently bind to the magnetic beads or DCs well. However, when the anti-CD1c-biotin antibodies were

bound to the beads first prior to the addition of DCs, the conjugation of DCs to the beads was very inefficient. This is potentially due to steric hindrance or sub-optimal orientation of the anti-CD1c-biotin antibodies presented on the magnetic beads for DCs to efficiently bind to.
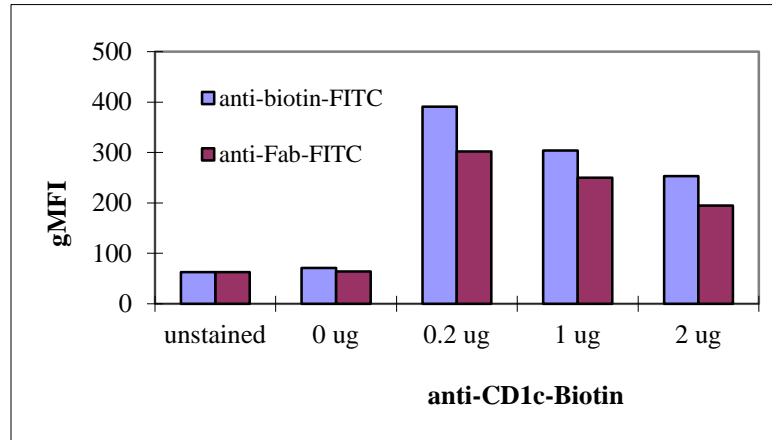

Figure A3-4: Evaluation of anti-CD1c-biotin coating. Magnetic beads coated with various concentrations of anti-CD1c-biotin antibodies were labeled with anti-biotin-FITC (blue bars) or anti-Fab-FITC (purple bars). Beads labeled with anti-CD1c-biotin antibodies were fluorescent after staining with either of the antibodies, and the fluorescence intensity decreased at higher anti-CD1c-biotin density, potentially due to steric hindrance.

Table A3-1: Changes that were made to attempt to improve conjugation efficiency.

| Adjustments	Improvement?
Increase CD1c-biotin concentration such that it will bind to the magnetic beads more efficiently	NO
Make sure the beads were properly bound by anti-CD1c-biotin	NO
Increase incubation time of DCs with the beads	NO
Change the Eppendorf tube to a flat-bottom microcentrifuge tube to ensure complete mixing during incubation	NO
Indirect method: first label cells with anti-CD1c-biot, and then incubate antibody-bound cells with magnetic beads	NO
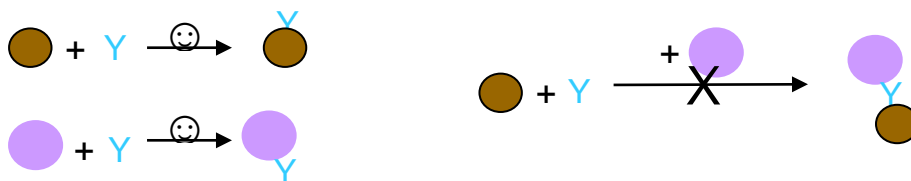
Figure A3-5: An illustration showing that the antibody can independently binds to the beads and the DCs well; however, when both beads and cells are present, the conjugation is low.

A.3.2. Agarose entrapment approach

Low melting temperature (LMT) agarose was used to trap the cells in the wells during cell washing. LMT agarose was used so that the cells would not be in contact with high temperature agarose solution. A low concentration of agarose was used so that it was easier to rinse antibodies out of the agarose gel. Figure A3-5 illustrates how agarose entrapment was used for the HTP assay.

Intended experimental procedure for analysis DC phenotype in 96-well plate using agarose entrapment approach
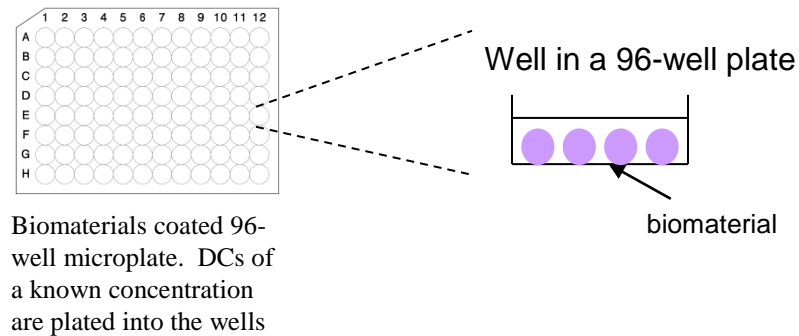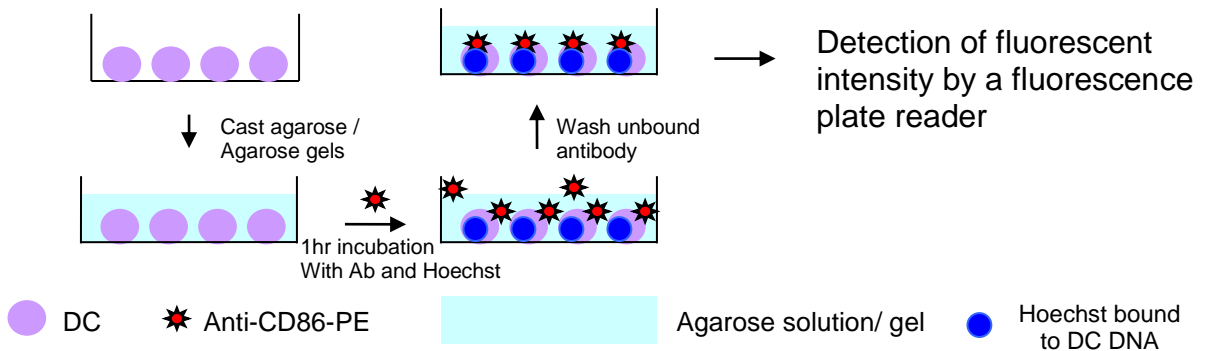
Figure A3-6: Schematic of intended experimental procedure on 96-well plate for agarose entrapment approach. A) DCs are plated in 96-well plate coated with different biomaterials at a known concentration on day 5. The inset shows a single well in the microplate. B) On day 6 culture, a low melting temperature agarose solution is cast on to the cells and gels. The entrapped cells are then labeled with anti-CD86-PE and Hoechst 33342 and washed. Finally the fluorescent intensity of the microplate is measured by a fluorescent plate reader.

To assess this method prior to the actual microplate experiments, the cells were pre-mixed with agarose (0.25%, 0.5%, or 0.75%) and then cast onto the microplate to keep volume consistent. The entrapped cells were then stained with anti-CD86-PE and Hoechst 33342.

This method requires extreme care during operation due to the delicate agarose gel. No vacuum aspiration was allowed because all three concentrations of agarose films were easily aspirated away along with the supernatants. Instead, the removal of supernatant had to be done very carefully with an Eppendorf pipette one well at a time, which resulted in a labor intensive and potentially highly erroneous procedure. At 0.25%, some agarose films were still accidentally removed by careful pipetting. In addition, it required >7 washes and >2 h to effectively remove the excess antibody from a 96-well plate (Figure A3-6), rendering this a low-throughput method due to its time-consuming nature.
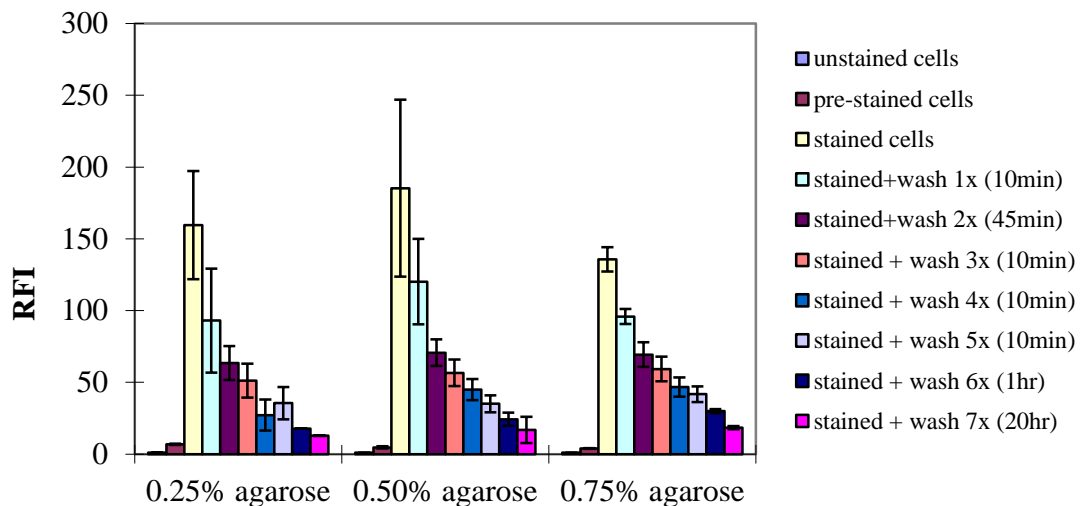
Figure A3-7: More than 7 washes were required to effectively wash away the abundant dye in the agarose film in the microplate wells. DCs were stained in the Eppendorf tubes with anti-CD86-PE and Hoechst 33342 for 1 hour. An agarose solution was added to the tubes to reach concentration of 0.25%. 0.5% or 0.75% agarose, and then plated into a 96-well plate. Buffer was then added on top of the agarose film to wash the abundant. The time indicated in the legend was the soaking time in the specified wash. Unstained cells are pre-stained cells entrapped in agarose were used as control. Pre-stained cells were stained in the eppendorf tube and washed 2x and subsequently mixed with agarose and cast into the wells. Data shown were Mean ± SD generated by triplicate. The result indicated that it required >7 washes to remove the abundant dye, which also implies that if the cells entrapped in the agarose were to be stained with dye solution added on top of the agarose film, it would probably take a long time for the antibody to diffuse into the agarose film.

A.3.3. Transswell approach

Intended experimental procedure for analysis DC phenotype in 96-well plate using transwell approach

A) On Day 5 of
DC culture

1 2 3 4 5 6 7 8 9 10 11 12
A B C D E F G H
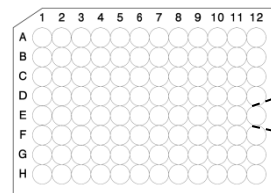
Biomaterials coated 96-well receiver plate. DCs of a known concentration are plated into the wells

Well in a 96-well receiver plate
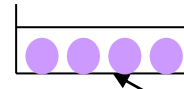
biomaterial

B) On Day 6 of
DC culture
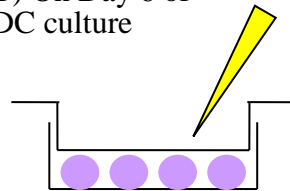
Aspirate away supernatants; remove the membrane insert

Detection of fluorescent intensity by a fluorescence plate reader
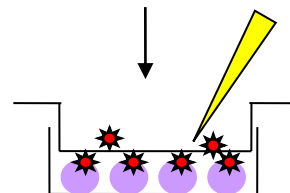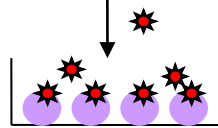
Aspirate away supernatants to remove unbound Ab
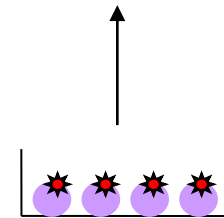
DC   ⭐ Anti-CD86-PE

Transswell membrane insert

Pipette / aspirator

Figure A3-8: Schematic of intended experimental procedure on 96-well plate for the transwell approach. A) DCs are plated in 96-well receiver plate coated with different biomaterials at a known concentration on day 5. The inset shows a single well in the microplate. B) On day 6 culture, a membrane insert is placed into the well to remove the supernatant. The cells are then labeled with anti-CD86-PE and washed. Finally the fluorescent intensity of the microplate is measured by a fluorescent plate reader

To evaluate this method before performing the actual microplate experiments, the cells were serially diluted on a black 96-well receiver plate and stained with anti-CD86-PE and CD1c-AlexaFluor 488. A membrane insert was used to trap the cells in the well during washing.

The membranes only come in two materials: polyester (PET) or polycarbonate (PC). PC membranes were very weak and therefore broke very easily during aspiration. Membranes of pore size of 0.4 μm, 1μm, and 3μm were tested but none of them resulted in a linear fluorescent intensity vs. cell number curve (Figure A3-8). Cells were lost through the cracks and therefore the method was prone to errors. On the other hand, PET membranes were much stronger but only came in very small pore size (0.4 and 1 μm) or large pore size (8μm). The small pore size membranes did not allow supernatant aspiration while large pore size caused DCs to be aspirated along with the supernatants.
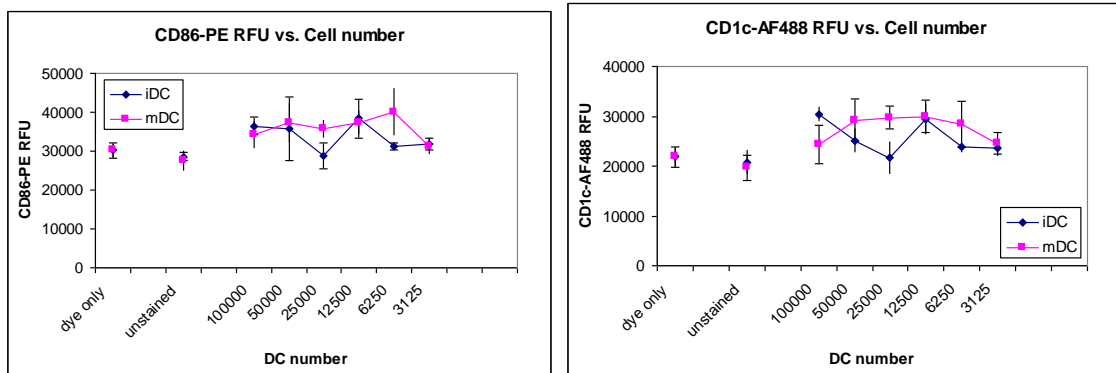
Figure A3-9: Transwell approach failed to generate linear relationship between fluorescent intensity of CD86 or CD1c surface marker and cell number. The PC membrane of the 96-well plate insert was brittle and broke very easily during aspiration.

APPENDIX 4

A.4. Transcription factor profiling using reporter gene in transfected DCs

Initially, a reporter gene approach was undertaken to understand transcription factor activation profiles of DCs treated with different biomaterials. In this approach, human primary monocyte-derived DCs were transfected with reporter plasmid whose transcription was inducible by the activation of TFs. Transfected DCs were expected to express the reporter to different levels depending on the treatment used (Figure A4-1).
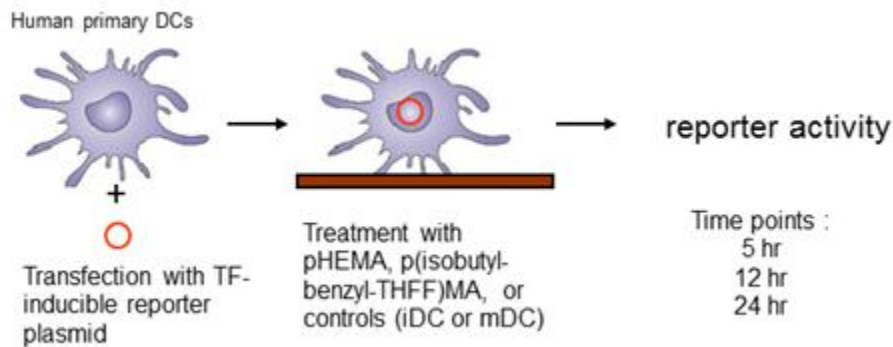
Figure A4-1: Schematic of DC TF activation profiling experiments by using TF-inducible reporter plasmid activity.

Human primary DCs are one of the most difficult cell types to transfect because they are suspension, non-proliferative, and extremely sensitive immune cell type. Two methods were primarily used for introducing external DNA into DCs, including electroporation and lentiviral transduction. The latter is cost-inhibitive, so DCs were transfected by electroporation using Nucleofector device (Lonza). Several additional steps were found to be important in optimizing transfection efficiency and cell viability post electroporation:

1. DNA plasmids used to transfect the cells needed to undergo additional PEG precipitation (in addition to endotoxin-free DNA prep) to remove any trace amount of endotoxin.

2. FBS or antibiotics must not be included in the recovery medium after DC electroporation.

3. OptiMEM was superior to RPMI in enhancing DC viability as the recovery medium after electroporation.

DC transfection protocol was optimized with GFP expressing DNA plasmids controlled by CMV promoter to a) maximize transfection efficiency, b) maximize cell viability, and c) minimize DC pre-activation during the electroporation process. Using the optimized protocol, DC transfection efficiency was 55% from the 78% viable cells by 24 h (Figure A4-2). DC viability decreased to approximately 50% by 40 h, most likely due to the electric shock and the presence of DNA plasmids inside the cells. Cell viability and transfection efficiency have been shown by others to be much higher with siRNA or mRNA. Therefore, any analysis on transfected DCs (DNA plasmid transfection) should be performed within approximately 24 – 30 h. In addition, transfected DCs were not pre-activated based on DC surface maturation marker CD83 and CD86 staining 24 h post electroporation (Figure A4-3).
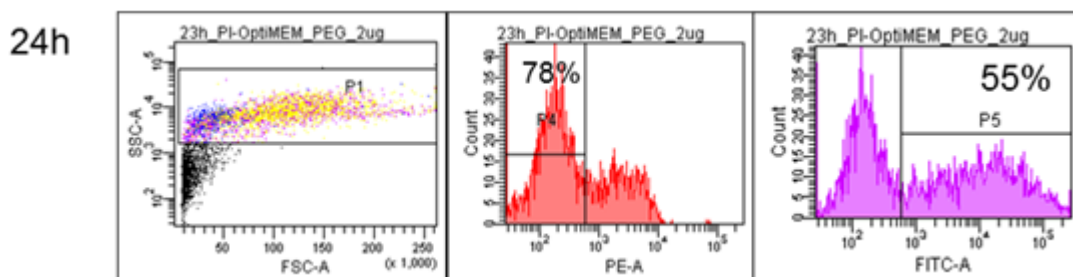
Figure A4-2: Representative transfection data from three independent trials with different donors that yielded similar results. 2×10^6 DCs were transfected with 2 μg GFP DNA plasmid. Cells were stained with propidium iodide (PI) and then analyzed by flow cytometry. 78% of DCs were PI negative (viable), while 55% of the viable cells were GFP positive (transfection efficiency). PE channel represents PI staining; FITC channel represents GFP fluorescence.
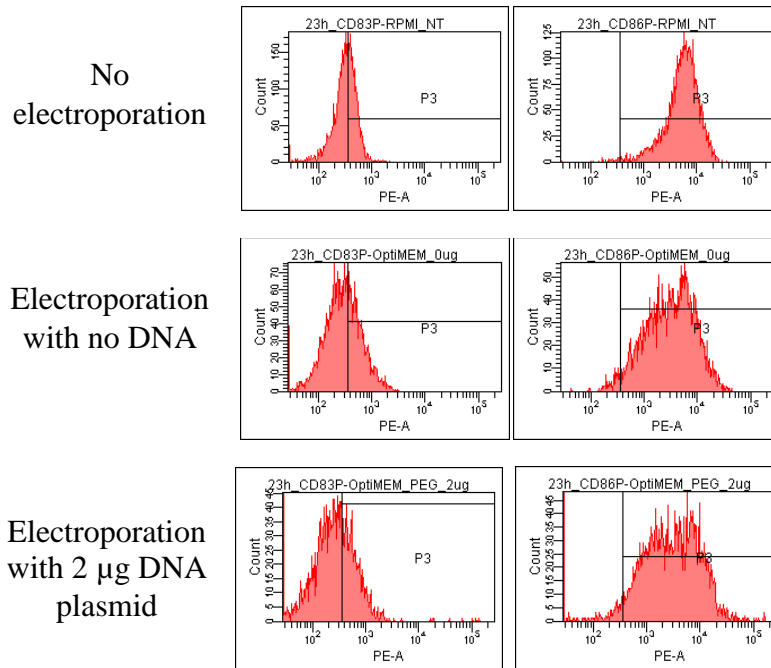
Figure A4-3: Representative transfection data from three independent trials with different donors that yielded similar results. 2×10^6 DCs were transfected with 2 µg GFP DNA plasmid. 24 h post electroporation, DCs were analyzed for surface marker expression, including CD83 and CD86, both are regulated when DCs are activated.

After DC transfection protocol was optimized, DCs were transfected with positive control plasmid with constitutive expression for the reporter SEAP (secreted alkaline phosphatase) controlled by SV40 promoter. The objective of this experiment was to determine how soon (time point) the SEAP reporter protein could be detected and if any dilution was necessary to accurately quantify the SEAP within 24 h. However, very low levels of SEAP reporter activity (close to blank) were detected (data not shown). The expression of SEAP by this positive control reporter is controlled by the promoter SV40, which is known to be much weaker than CMV (as the case in the GFP plasmid), and is often particularly weak in primary cells [310]. When DCs were transfected with CMV controlled Metluc (secretive luciferase reporter) plasmid, very high and time-dependent chemiluminescence signal was detected (Figure A4-4) in the medium. Therefore, primary DCs require strong promoter activity for the reporter protein to be expressed.
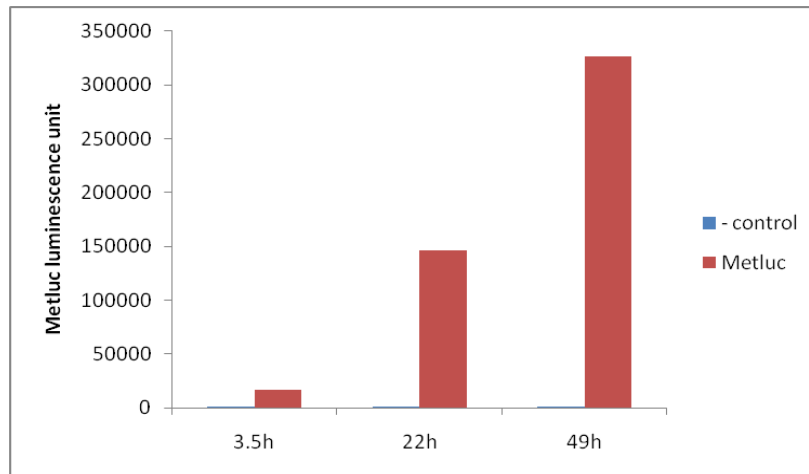
Figure A4-4: DCs strongly expressed luciferase reporter controlled by a CMV promoter at a time-dependent manner. DCs were transfected with Metluc plasmid (Clontech) and the cell culture medium was collected at the indicated time points for assaying luciferase activity as compared to empty vector transfected control. DCs strongly expressed the Metluc reporter under CMV control in a time-dependent fashion.

NFkB-inducible SEAP reporter plasmid (Clontech) was used to transfect DCs. DCs were then treated with LPS to induce NFkB activation. However, similar to the control plasmid, very low levels of reporter activity was detected – the chemiluminescence from transfected DCs with LPS treatment was only 10 fold higher than non-transfected cells (Figure A4-5), which is unacceptably low for using this plasmid for future experiments. The lack of reporter activity is most likely due to low promoter activity of the plasmid in the DCs. The enhancer element sequences as well as the accompanying minimal promoter may be altered to optimize promoter activity in DCs. Several vendors sell inducible plasmids with different designs. Unfortunately, promoter activity will need to be empirically determined.
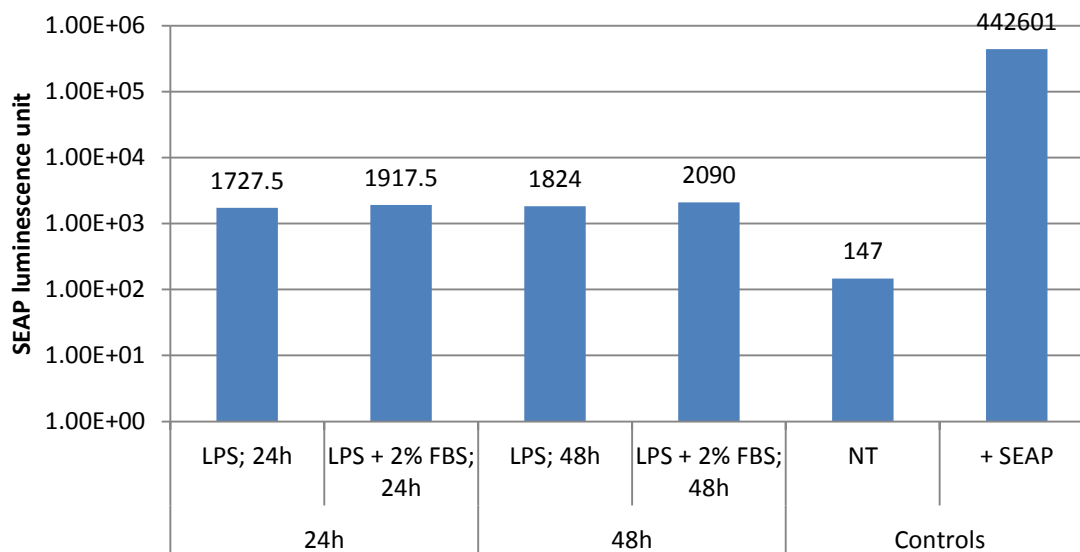
Figure A4-5: DCs transfected with NF-κB inducible plasmid and treated with LPS for 24 or 48 h in the presence or absence of 2% FBS. Transfected DCs were recovered in OptiMEM for 2 h post electroporation. At this point, either LPS alone was added or LPS + FBS were added for a final FBS concentration of 2%. NT was the non-transfected DC control, while +SEAP was the positive control with placental alkaline phosphatase. The chemiluminescence values are labeled above the bars. The LPS treated DCs only resulted in 10 fold change compared to the non-transfected control, which is unacceptable for future experiments.

Chemical or lipid reagents, including TransIT-200 (Mirus), FugeneHD (Roche), and GeneJuice (EMD), were also tested and all with close to 0% transfection efficiency with human primary DCs.

Invitrogen Neon electroporation device was also used for transfection but resulted in over 70% cell death and <20% transfection efficiency out of all 20 conditions tested.

APPENDIX 5

A.5. Dendritic Cell Response to Nanotopography

(Collaborated with Dr. Clemens van Blitterswijk at University of Twente in the Netherlands)

The TopoChip, developed by Drs. Jan de Boer and Clemens van Blitterswijk at the University of Twente in the Netherlands, was fabricated by hot embossing and was composed of 2178 unique TopoUnits in duplicate (total 4356 TopoUnits). The TopoChip provided a high-throughput system to assess DC phenotype to an important biomaterial property, nanotopography. Through the proof-of-concept experiments at University of Twente, a human DC-like cell line, KG-1 cells, was used to assess the effect of nanotopography on DC phenotype.

KG-1 cells were used due to the time limitation during the visit at the University of Twente to complete necessary experiments. Prior to using KG-1 cells with the TopoChip, the cells were characterized at Georgia Tech for their response to standard biomaterials, including PLGA and agarose, as well as PDLLA, which was the base material of TopoChip, *in vitro*. A longer culture time (48 h) was required for these cells to respond to biomaterials, as oppose to the shorter culture time (24 h) required for primary human DCs to respond (Figure A5-1).

During the three-week visit at the University of Twente, KG-1 cells were cultured on the TopoChip for 6 h without media exchange. Long-term cultures were not performed as the perfusion pump was not operable at a time. Cells were immediately fixed and stained with anti-CD86-PE monoclonal antibodies (Ancell). Each wash step was carefully performed so as not to rinse away cells. Stained cells were then mounted on a customized TopoChip loader into a BD Pathway imager for data acquisition. The image of each TopoUnit was then cropped from the original large image using a customized MATLAB script. These images were subsequently analyzed using

CellProfiler cell image analysis software (Broad Institute). KG-1 cells differentially adhered to the different TopoUnits (Figure A5-2); however, the results were not reproducible during my time at University of Twente. Due to the lack of experience with culturing loose-adherent cells on the TopoChips, more experiments need to be performed to optimize the cell culture protocol of KG-1 cells or human primary DCs onto these devices.

Transfection of KG-1 cells with a reporter plasmid was also attempted using GeneJuice or FugeneHD. However, transfection efficiency was very low (<5%) and therefore this approach was not used. Other transfection reagents might be more effective for KG-1 cells but were not tested for this project.
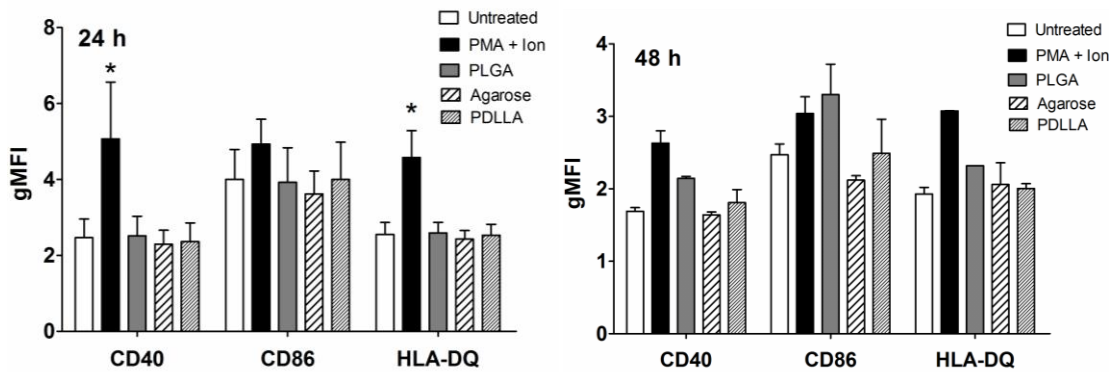
Figure A5-1: KG-1 cells required longer culture time to respond to biomaterials. KG-1 cells were cultured with the indicated treated for 24 h (A) or 48 h (B) and then the cells were collected for surface marker quantification by flow cytometry. Results were shown for N ≥ 4 (mean ± SEM) for 24 h (A) or n = 2 (mean ± range) for 48 h. It is important to note that the magnitude of surface marker expression was typically lower compared to human primary DCs.
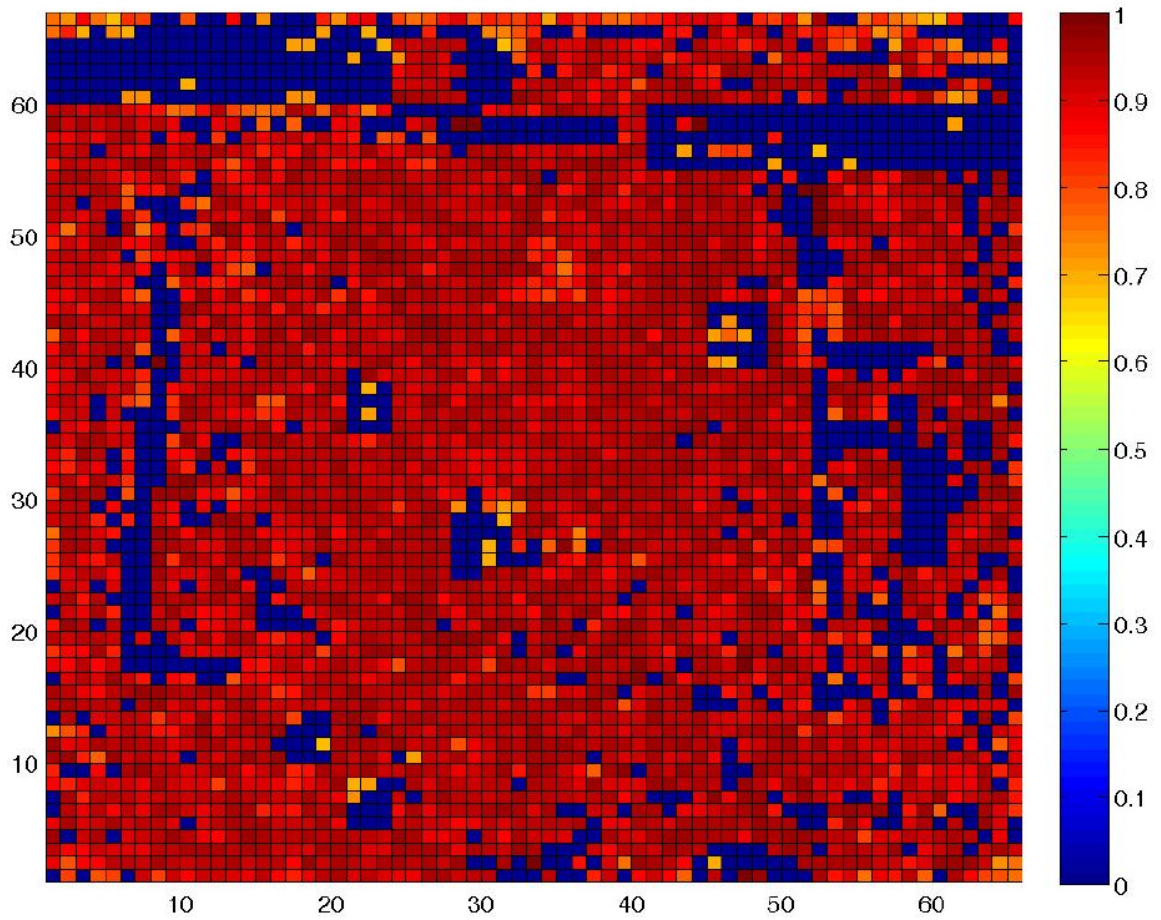
Figure A5-2: KG-1 cells differentially adhered to the TopoUnits. The color intensities indicate the number of cells remained in each of the TopoUnits (represented by each square). However, the results were not yet reproducible and required additional cell culture optimization on the TopoChips.

APPENDIX 6

A.5. Deriving DC phenotype-biomaterial property relationships using terpolymer library

As shown in CHAPTER 6, the terpolymer library was used as the prediction set to verify the robustness of the PLSR model constructed based on the pMA library training set. To make full use of the material property and DC phenotypic data DCs already generated using the terpolymer library, multivariate analysis was again performed for this set of polymers. It is important to note that the original terpolymer library also included three additional nitrogen-containing terpolymers (#10 – 12 in table A6-1) that were excluded from the prediction set in CHAPTER 6. These terpolymers were excluded because the pMAs that the PLSR model was based upon did not contain any nitrogen and therefore was not "trained" to predict DC response towards terpolymers that contain nitrogen.

Table A6-1: List of original polymers in the terpolymer library. Note that #1 – 9 and 13 were used as the prediction set in CHAPTER 6. Nitrogen-containing terpolymers #10 – 12 were excluded in the prediction set because the pMA library used for model construction did not contain any nitrogen. #13 and #14 are common biomaterials included in the study.

terpolymer #	Abbreviation	Composition
1	2A	A55T20G25 – 55%A-co-20%T-co-25%GMA
2	2B	A40T35G25 – 40%A-co-35%T-co-25%GMA
3	2D	A10T65G25 – 10%A-co-65%T-co-25%GMA
4	5B	H40T35G25 – 40%H-co-35%T-co-25%GMA
5	5C	H25T50G25 – 25%H-co-50%T-co-25%GMA
6	5D	H10T65G25 – 10%H-co-65%T-co-25%GMA
7	6A	A55H20G25 – 55%A-co-20%H-co-25%GMA
8	6B	A40H35G25 – 40%A-co-35%H-co-25%GMA
9	6C	A25H50G25 – 25%A-co-50%H-co-25%GMA
10	7B	H40N35G25 – 40%H-co-35%N-co-25%GMA
11	7C	H25N50G25 – 25%H-co-50%N-co-25%GMA
12	7D	H10N65G25 – 10%H-co-65%N-co-25%GMA
13	HEMA	100% H
14	PLLA	---

These terpolymers were initially synthesized with the goal of varying only one material property at one time (Table A6-2). However, although the certain bulk or surface properties may be maintained through careful design of polymer composition, the underlying chemistry of the polymers and potentially other material properties are inevitably altered as well. Therefore, multivariate analysis of induced DC response to these terpolymers is necessary to simultaneously analyze the effects of a combination of material properties on DCs.

Table A6-2: The wet modulus, T_g, and contact angle of terpolymers. These terpolymers were synthesized with the goal of varying one property at a time and were divided into four groups as color-coded in the table. Within each group, two of the material properties were kept similar as much as possible and the one remaining property was varied.

Abbreviation	Composition	Wet Modulus (kPa)	T_g (°C)	Contact Angle
2A	A55T20G25	32	-37	96
2B	A40T35G25	37	-37	92
2D	A10T65G25	39	-41	85
5B	H40T35G25	354	-5	75
5C	H25T50G25	157	-3	69
5D	H10T65G25	52	-28	72
6A	A55H20G25	1275	15	94
6B	A40H35G25	3380	37	82
6C	A25H50G25	2697	68	75
7B	H40N35G25	2280	138	61
7C	H25N50G25	1850	119	65
7D	H10N65G25	1150	119	64

The induced DC phenotype upon treatment with the terpolymers was measured in terms of MF, defined by CD86/DC-SIGN ratio, using the HTP method described in CHAPTER 4 (Figure A6-1). In addition, the production ofcytokines and chemokines by treated DCs was quantified using multiplex bead assay. Similarly to the pMA-induced DC response, the terpolymers also induced a trend of increasing DC maturation as shown by the expression of MF in the ordering of terpolymers in the x-axis (Figure A6-1). When keeping the ordering of polymers the same, similar trends could be observed for the release of pro-inflammatory cytokines, IL-1β (Figure A6-2A) and TNF-α (A6-2B), and chemokine, IL-8 (Figure A6-2C), by treated DCs. The production of anti-inflammatory cytokine, IL-16, also followed roughly the same trend, but with pHEMA also inducing high production of IL-16 by treated DCs (Figure A6-2D). IL-1ra (anti-inflammatory) and MCP-1 (chemokine) were also assayed but did not follow the same trend (Figure A6-3). However, it is interesting to note that pHEMA induced low levels of all the cytokines or chemokines examined. The pMAs did not induce significant cytotoxicity in treated DCs. Interestingly, pHEMA induced lower cell death as compared to all the other pMAs (Figure A6-4).
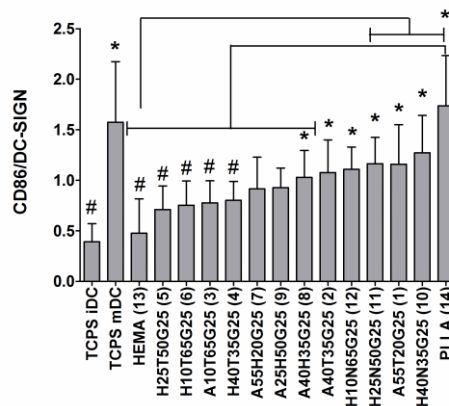
Figure A6-1: DC responded differential to the terpolymers and the common biomaterials, pHEMA and PLLA. Maturation factor (CD86/DC-SIGN) is shown with mean ± SEM (n = 6 donors). *: p<0.05 higher than iDC; #: p<0.05 lower than mDC; brackets: p<0.05 between treatments.
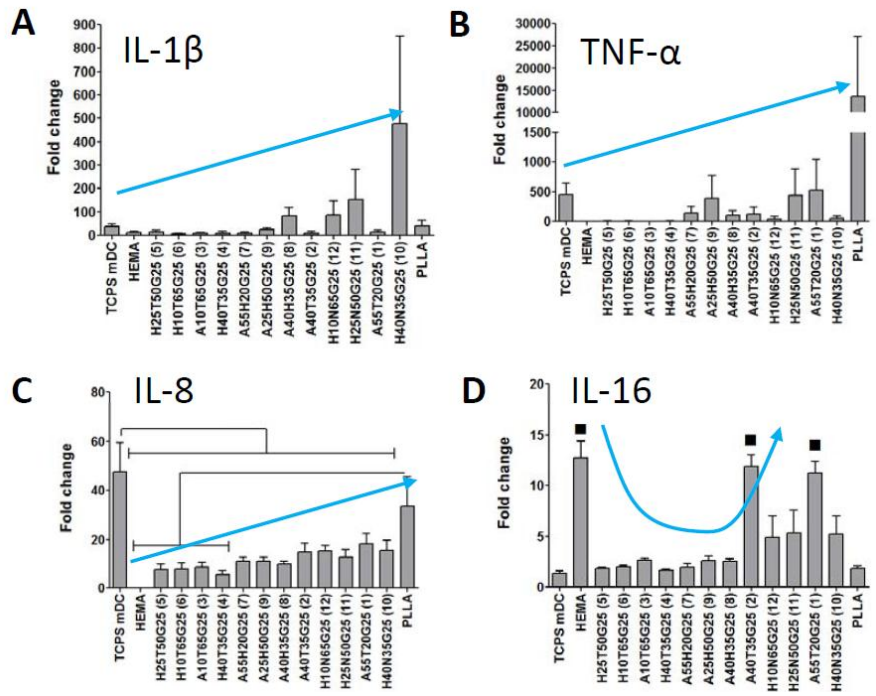
Figure A6-2: Terpolymers induced differential cytokine and chemokine production. IL-1β (A) and TNF-α (B) are pro-inflammatory cytokines. IL-8 (C) is a chemokine. IL-16 (D) is a pleiotropic cytokine. Data are shown with mean ± SEM (n = 6 donors). The numbers in parentheses correspond to Table A6-1*: $p < 0.05$ higher than iDC; #: $p < 0.05$ lower than mDC; brackets: $p < 0.05$ between treatments; ■: $p < 0.05$ different from all polymers EXCEPT HEMA, A40T35G25 (2) and A55T20G25 (1).
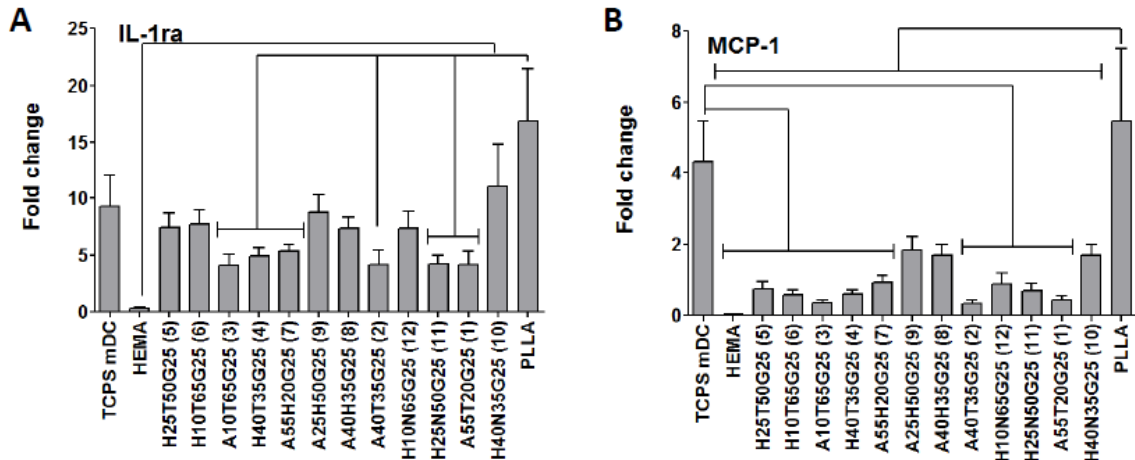
Figure A6-3: Terpolymers induced differential IL1-ra and MCP-1 production. IL-1ra (A) and MCP-1 (B) did follow the same trend of increasing DC maturation along the same ordering of polymers listed in the x-axis cytokine as compared to Figure A6-2. Data are shown with mean ± SEM (n = 6 donors). Brackets: $p < 0.05$ between treatments.
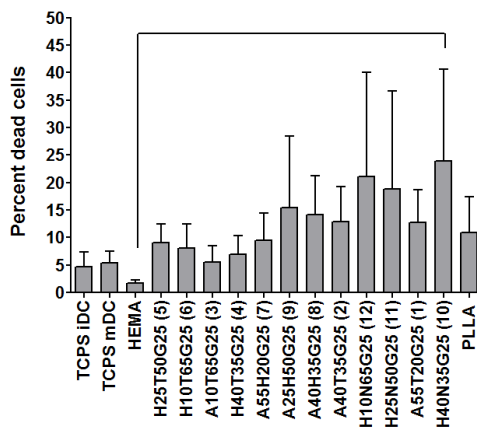
Figure A6-4: Terpolymers did not induce significant cytotoxicity as compared to iDC. It is obvious that pHEMA induced the least cytotoxicity as measured by the release of cytosolic enzyme, G6PD. The fluorescent signals from the samples were compared to a standard curve generated by lysed iDC to determine the percent dead cells. Results contained large donor-to-donor variations. Data are shown with mean ± SEM (n = 6 donors). Brackets: p<0.05 between treatments.

PCA was performed to analyze the effects of the different material properties on DC phenotype upon biomaterial treatment using the variables shown in Table A6-3. A summary of material characterization is shown in Table A6-4. Appendix 8 show the representative XPS high resolution C1s scans, and Appendix 10 show the representative surface roughness images. A six-component PCA model was determined by cross-validation to be the most optimal for representing this dataset with $R^2 = 0.88$ and $Q^2 = 0.80$, meaning that this model can capture 88% with excellent predictability. The five components could individually capture 32.6%, 22.2%, 12.8%, 10.3%, 5.6% and 4.3% of data information, respectively. No major outliers were identified by the Hotelling's T^2 statistic. Very importantly, this model was generated with the exclusion of PLLA. A model with PLLA included resulted in similar R^2 of 0.87 but a significantly poorer Q^2 of only 0.47 (results not shown). The discrepancy in model performance subjected to the inclusion of PLLA was potentially due to the dissimilarity of PLLA as compared to the rest of the members in the polymer library. We hypothesize in order to predict the effects of a more diverse group of polymers on DC phenotype, multiple members are needed for each type of chemistry so that statistically meaningful models can be derived.

Similar to the pMA study, the score plot of the terpolymers also showed a wide spread nature of the projection of the observations, indicating that the terpolymers induced a wide range of DC responses (Figure A6-5A). However, in contrast to the PCA model for pMAs, PC1 alone is not sufficient for segregating highly activating materials from nearly bio-inert polymers. Instead, both PC1 and PC2 together can roughly separate the polymers based on their ability to mature DCs, with more activating materials concentrated in the top right quadrant (Figure A6-5A). For example, pHEMA was strongly loaded on negative PC1, while 7C, which was sufficiently activating on DCs, also had negative loading on PC1 but a strong positive loading on PC2. Activating materials like 7B and 7D were projected positively to both PC1 and PC2 (Figure A6-5A).

The conclusions from the loading plots were very similar to those drawn from the pMA study, and the overall results were very similar regardless of the combinations of PCs. First, all the phenotypic variables measured strongly clustered and mostly located in the top right quadrant (associated with activating polymers in the score plot) opposite from IL-16 (Figure A6-5B). Second, the projections of the theoretical values of elemental composition and C-C, C-O, and O-C=O bond composition were very similar to the projections of the experimental values (Figure A6-5B). % carbon and % nitrogen were associated with DC maturation because they were projected positively on PC1, while % oxygen was associated with less mature DCs due to their negative projections on PC1. Since XPS cannot distinguish between C-N and C-O bonds or between N-C=O and N-C=O bonds, the experimental values of these bonds were projected as a combination of the oxygen- and the N-containing bonds. Since the amount of oxygen-containing bonds was much higher as compared to the nitrogen-containing bonds in the terpolymers, the combined effects of the two were similar to the projections of oxygen-containing bonds alone. However, the composition of these bonds could be theoretically calculated separately. When the theoretical bond information was projected, it was apparent that the oxygen-containing versions of these bonds were negatively associated with DC

maturation by being situated towards the left of the PC1, while the nitrogen-containing versions of these bonds were positively associated with DC maturation by locating in the same quadrant as the mature phenotypic variables (Figure A6-5B).
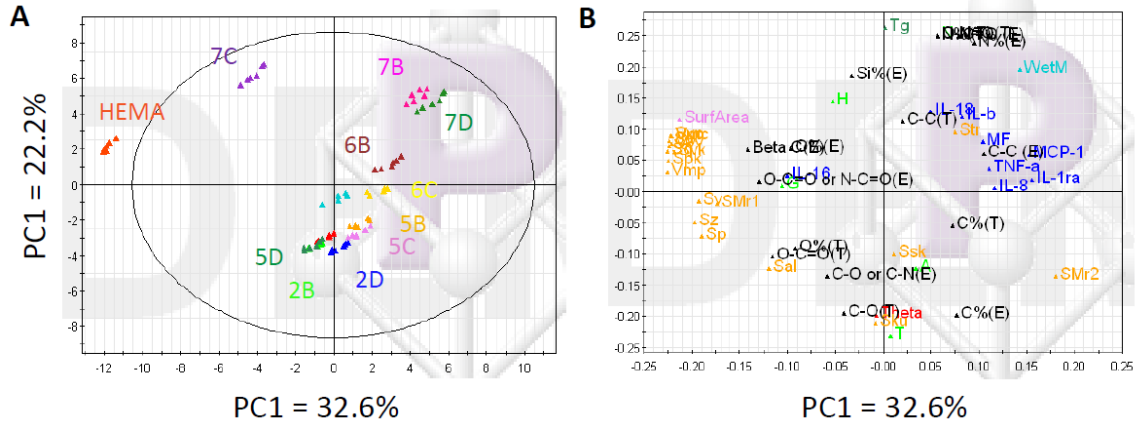
Figure A6-5: Score and loading plots showing the projection of the treatments and variables on the PC space for the terpolymer library. PC1 captures 32.6% and PC2 captures 22.2% of the data, which together represent >50% of the original data information. A) Score plot shows the projection of the pMA treatments, each with six data points obtained from six independent experiments with different donors. B) Loading plots shows the projection of the variables on the PC space. See text for detailed interpretation of the plots. The following color code is used for the loading plot: Blue: phenotypic variables; black: chemical composition; red: contact angle; orange: roughness; dark green: T_g; neon green: monomer composition; pink: surface area. The interpretation of the combination of PC1 with other PCs resulted in similar conclusion; therefore these plots are omitted for simplicity.

In addition, wet modulus (WetM) was associated with DC maturation due to its proximity with the maturation phenotypic variables (Figure A6-5B). If plotted individually against the different phenotypic variables, wet modulus could be strongly associated with TNF-α and MCP-1 with R^2 of 0.70 and 0.83, respectively. In contrast, surface roughness (S_a), as well as other roughness-related variables such as Sk, Spk, Svk, Vvv, etc., were located away from the maturation variables except for Str. Obviously, a strong redundancy was present due to the strong clustering of these variables. T_g and contact angle did not contribute to PC1, but they were projected positively and negatively on PC2, respectively (Figure A6-5B). Although this might suggest that T_g and contact angle were moderately associated with more or less DC maturation based on PC2,

respectively, these two variables had little effects on DC phenotype because their projections onto other PCs were mostly close to zero (data not shown). The projections of monomer composition of T, H, A, G, and N onto the loading plot corresponded to the positions of terpolymers in the score plot. For example, 2D, 5C, 5D were polymers that contained high percentage of T, and their positions in the score plot matched the location of T in the loading plot (Figure A6-5B).

Therefore, the PCA results herein were consistent with the conclusions from CHAPTER 6, where chemical composition was consistently the most informative data for DC phenotype. Specifically, elemental oxygen and oxygen-containing chemical bonds have been consistently shown in CHAPTER 5, 6, and this Appendix for their association with iDC phenotype, whereas elemental carbon and C-C bonds have been shown to associate with DC maturation. C=O contamination has also been consistently shown to co-vary with DC maturation. In this Appendix, elemental nitrogen and nitrogen-containing bonds were additionally shown to associate with a mDC phenotype, consistent with results shown in CHAPTER 5. Variables such as contact angle, T_g, and roughness might suggest moderate correlations with DC response depending on the systems used, but their effects have not been consistent and therefore are not expected to possess strong predictive power for DC response. Although wet modulus was shown to associate with DC maturation in this Appendix (Figure A6-5B), more studies should be conducted to confirm this finding.

Because chemical information of the polymers have been consistently demonstrated to be the most useful for modeling DC response to biomaterials, ToF-SIMS (Appendix 11) was also performed on this terpolymer library to derive more complex mass fragment information. The analysis of this is underway to determine whether PLSR model can be successfully constructed with stronger predictive power compared to the model shown in CHAPTER 6.

Table A6-3: List of X-variables used in the PCA model for the terpolymer library

Variable	Definition	Measured for	Number of variables
MF	Maturation factor (CD86/DC-SIGN)	Mean	1
IL-1β	Interleukin-1β	Mean	1
IL-1ra	Interleukin-1 receptor antagonist	Mean	1
IL-8	Interleukin-8	Mean	1
IL-16	Interleukin-16	Mean	1
IL-18	Interleukin-18	Mean	1
MCP-1	Monocyte chemotactic protein-1	Mean	1
TNF-α	Tumor necrosis factor-α	Mean	1
Si2p (E)	Experimental Si2p	Mean	1
C% (E)	Experimental C1s	Mean	1
O% (E)	Experimental O1s	Mean	1
N% (E)	Experimental N1s	Mean	1
C% (T)	Theoretical C1s	Mean	1
O% (T)	Theoretical O1s	Mean	1
N% (T)	Theoretical N1s	Mean	1
C-C (E)	Experimental C-C	Mean	1
C-O or C-N (E)	Experimental C-O or C-N	Mean	1
O-C=O or N-C=O (E)	Experimental O-C=O or N-C=O	Mean	1
Beta C (E)	Experimental Beta C	Mean	1
C=O (E)	Experimental C=O	Mean	1
C-C (T)	Theoretical C-C	Mean	1
C-O (T)	Theoretical C-O	Mean	1
C-N (T)	Theoretical C-N	Mean	1
O-C=O (T)	Theoretical O-C=O	Mean	1
N-C=O (T)	Theoretical N-C=O	Mean	1
Sa	Arithmetic mean height	Mean	1
Sq	Root mean square	Mean	1
Ssk	Skewness	Mean	1
Sku	Kurtosis	Mean	1
Sp	Maximum peak height	Mean	1
Sv	Maximum pit depth	Mean	1
Sz	Maximum height (Sp+Sv)	Mean	1
Sk	Level difference for a core part	Mean	1
Spk	Reduced peak height	Mean	1
Svk	Reduced valley height	Mean	1
SMr1	Load area ratio to separate between a reduced peak part and a core part	Mean	1
SMr2	Load area ratio to separate between a reduced valley part and a core part	Mean	1
Sxp	Load area ratio from 97.5 to 50%	Mean	1
Vvv	The void volume at valley region (load area ratio 80%)	Mean	1

Table A6-3 continued:

Vvc	The void volume at a core part (load area ratio from 10 to 80%)	Mean	1
Vmp	The actual volume at a peak region (load area ratio 10%)	Mean	1
Vmc	The actual volume at a core part (load area ratio from 10 to 80%)	Mean	1
Sal	Auto-correlation length	Mean	1
Str	Texture aspect ratio	Mean	1
SurfArea	Surface Area	Mean	1
T_g	Glass transition temperature	Mean	1
Theta	Air-water contact angle	Mean	1
WetM	Wet modulus	Mean	1
T	% T monomer as measured by NMR	Mean	1
A	% A monomer as measured by NMR	Mean	1
H	% H monomer as measured by NMR	Mean	1
N	% N monomer as measured by NMR	Mean	1
G	% G monomer as measured by NMR	Mean	1
Total			**53**

Red text indicates new variables compared to the list of variables used for the construction of PCA and PLSR models for the pMA library.

Table A6-4: Material characterization of the polymers used in the PCA model.

	2A	2B	2D	5B	5C	5D	6A	6B	6C	7B	7C	7D	HEMA
H	0	0	0	35	24	13	20	36	51	36	22	14	100
A	62	42	18	0	0	0	52	37	26	0	0	0	0
T	14	27	53	37	50	59	0	0	0	0	0	0	0
N	0	0	0	0	0	0	0	0	0	40	49	57	0
G	23	31	29	28	26	28	27	27	23	24	29	29	0
C%(E)	0.81	0.78	0.74	0.76	0.72	0.85	0.78	0.75	0.78	0.68	0.68	0.75	0.67
O%(E)	0.18	0.21	0.25	0.21	0.26	0.14	0.21	0.23	0.22	0.23	0.24	0.18	0.30
N%(E)	0.00	0.00	0.00	0.00	0.00	0.00	0.00	0.02	0.00	0.02	0.03	0.03	0.00
Si%(E)	0.01	0.01	0.02	0.02	0.02	0.01	0.00	0.01	0.00	0.06	0.06	0.04	0.03
C%(T)	0.79	0.76	0.72	0.68	0.69	0.69	0.78	0.73	0.76	0.71	0.71	0.72	0.67
O%(T)	0.21	0.24	0.28	0.32	0.31	0.31	0.22	0.27	0.24	0.25	0.23	0.21	0.33
N%(T)	0.00	0.00	0.00	0.00	0.00	0.00	0.00	0.00	0.00	0.05	0.06	0.07	0.00
C-C (E)	0.59	0.48	0.37	0.53	0.35	0.68	0.54	0.59	0.51	0.57	0.49	0.65	0.39
C-O or C-N(E)	0.25	0.34	0.46	0.31	0.46	0.21	0.23	0.21	0.26	0.23	0.27	0.20	0.31
O-C=O or N-C=O(E)	0.08	0.09	0.09	0.08	0.09	0.05	0.11	0.09	0.11	0.08	0.10	0.05	0.15
Beta C(E)	0.08	0.09	0.09	0.08	0.10	0.06	0.11	0.10	0.11	0.09	0.12	0.06	0.16
C=O (E)	0.00	0.00	0.00	0.00	0.00	0.00	0.00	0.01	0.00	0.02	0.03	0.04	0.00
C-C(T)	0.67	0.57	0.41	0.37	0.34	0.33	0.69	0.64	0.61	0.54	0.55	0.57	0.50

Table A6-4 continued:

C-O(T)	0.23	0.33	0.48	0.51	0.54	0.57	0.20	0.23	0.26	0.23	0.21	0.18	0.33
C-N(T)	0.00	0.00	0.00	0.00	0.00	0.00	0.00	0.00	0.00	0.06	0.08	0.09	0.00
O-C=O(T)	0.10	0.10	0.10	0.12	0.11	0.11	0.11	0.12	0.13	0.10	0.08	0.07	0.17
O-N=O(T)	0.00	0.00	0.00	0.00	0.00	0.00	0.00	0.00	0.00	0.06	0.08	0.09	0.00
Sq	0.52	0.40	0.28	0.24	0.22	0.55	0.41	0.27	0.25	0.21	1.43	0.21	3.09
Ssk	4.57	0.33	0.64	1.84	0.49	1.67	-1.72	-0.21	-0.27	0.04	0.18	-0.14	-0.52
Sku	106.7	66.86	13.17	46.97	9.19	35.59	33.42	5.78	13.99	7.50	6.62	4.79	7.07
Sp	12.49	8.85	4.96	6.21	3.65	7.77	6.33	3.37	4.87	3.63	8.56	2.95	13.02
Sv	4.66	8.79	3.28	3.14	2.13	4.93	8.66	1.99	4.15	2.36	7.62	2.11	13.39
Sz	17.15	17.64	8.24	9.34	5.78	12.70	14.99	5.37	9.02	5.99	16.18	5.06	26.41
Sa	0.30	0.25	0.20	0.18	0.17	0.41	0.26	0.21	0.19	0.16	1.04	0.16	2.21
Sk	0.73	0.66	0.60	0.53	0.52	1.19	0.66	0.64	0.57	0.50	1.80	0.50	4.43
Spk	0.95	0.54	0.36	0.27	0.27	0.65	0.34	0.25	0.22	0.21	2.42	0.21	5.47
Svk	0.66	0.51	0.31	0.29	0.21	0.63	0.87	0.34	0.33	0.24	1.76	0.24	4.06
SMr1	10.97	11.64	10.44	10.12	10.69	13.67	10.19	9.66	9.86	9.69	13.07	9.94	12.50
SMr2	88.15	89.18	89.34	88.73	90.68	90.38	87.85	88.41	89.14	89.08	86.40	89.14	84.45
Sxp	0.63	0.60	0.51	0.45	0.44	1.07	0.56	0.53	0.48	0.41	2.71	0.42	5.87
Vvv	0.06	0.05	0.03	0.03	0.02	0.06	0.07	0.04	0.03	0.03	0.18	0.03	0.40
Vvc	0.37	0.36	0.29	0.25	0.25	0.64	0.32	0.30	0.27	0.24	1.72	0.24	3.55
Vmp	0.05	0.03	0.02	0.01	0.01	0.03	0.02	0.01	0.01	0.01	0.08	0.01	0.21
Vmc	0.27	0.24	0.22	0.19	0.18	0.43	0.24	0.23	0.20	0.18	0.99	0.18	2.32
Sal	50.49	77.03	97.02	1.89	48.72	116.90	8.51	17.94	1.62	1.33	79.87	1.33	27.15
Str	0.53	0.46	0.49	0.69	0.36	0.40	0.70	0.68	0.66	0.62	0.54	0.56	0.50
Surface area	4.49	4.46	4.44	4.55	4.38	4.61	4.66	4.65	4.61	4.48	6.69	4.49	11.04
WetM	32.0	37.0	39.0	354	157	52.0	1275	3380	2697	2280	1850	1150	*
Tg	-37	-37	-41	-5	-3	-28	15	37	68	138	119	119	87.6
Theta	96.0	92.0	85.0	75.0	69.0	72.0	94.0	82.0	75.0	61.0	65.0	64.0	69.5

* indicates missing value

APPENDIX 7

A.7. Representative high resolution C1s XPS data for polymethacrylate library

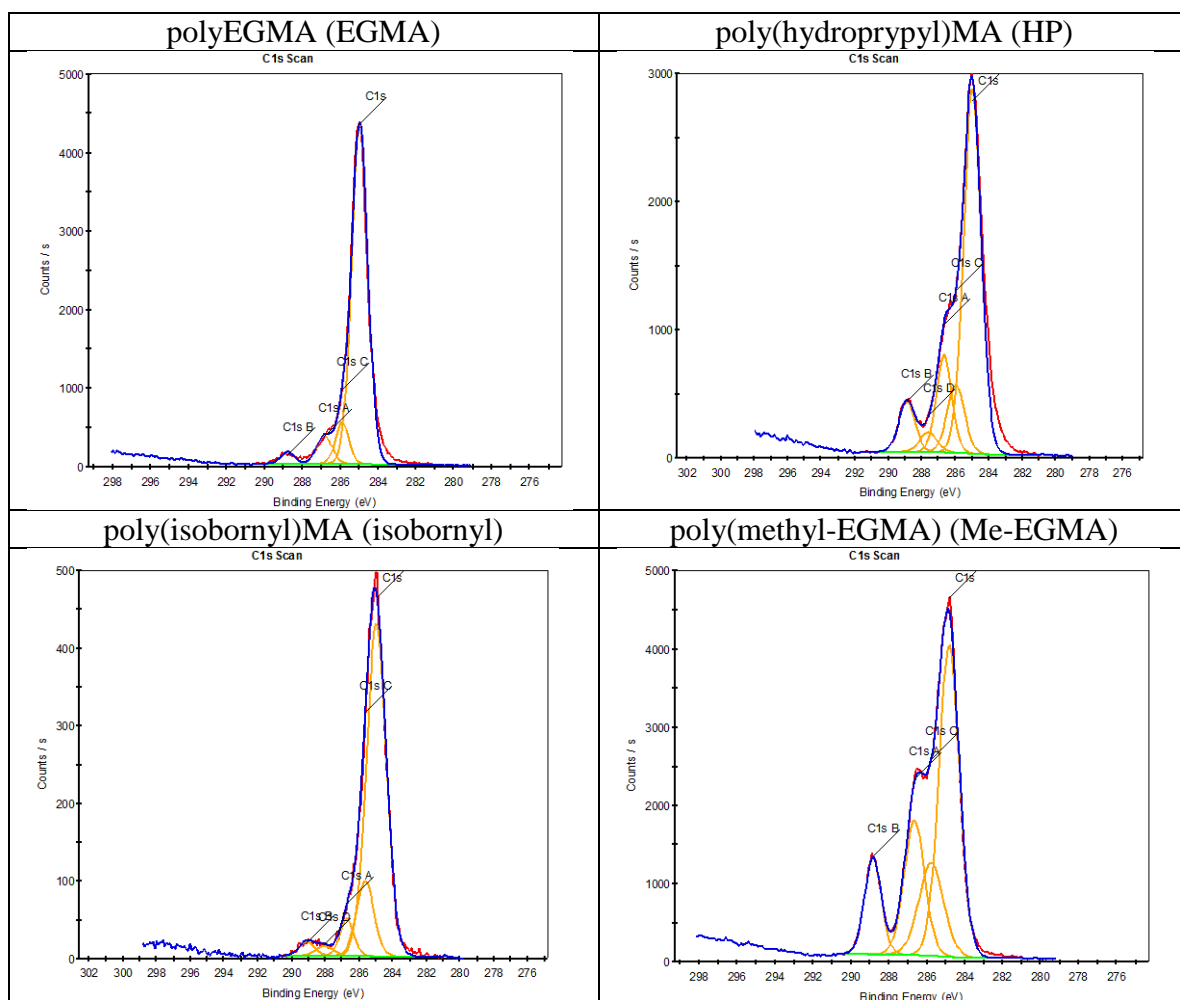These data were fitted by Dr. Rana Sodhi at University of Toronto.

C1s = C-C

C1sA = C-O

C1sB = O-C=O

C1sC = C-COO (beta carbon)

C1sD = C=O

| polyEGMA (EGMA) | poly(hydroprypyl)MA (HP) |
| poly(isobornyl)MA (isobornyl) | poly(methyl-EGMA) (Me-EGMA) |

poly(methyl-hydropropyl)MA (Me-HP)	poly(methyl-tetrahydrofurfurl)MA (Me-THFF)
poly(ethyl-benzyl-TEGMA) (E-B-TEGMA)	**poly(isobutyl-benzyl-THFF)MA (E-B-TEGMA)**
poly(lauryl-isobornyl-hydroxyethyl)MA (E-B-TEGMA)	**poly(lauryl-isobornyl-hydroxyethyl)MA (E-B-TEGMA)**
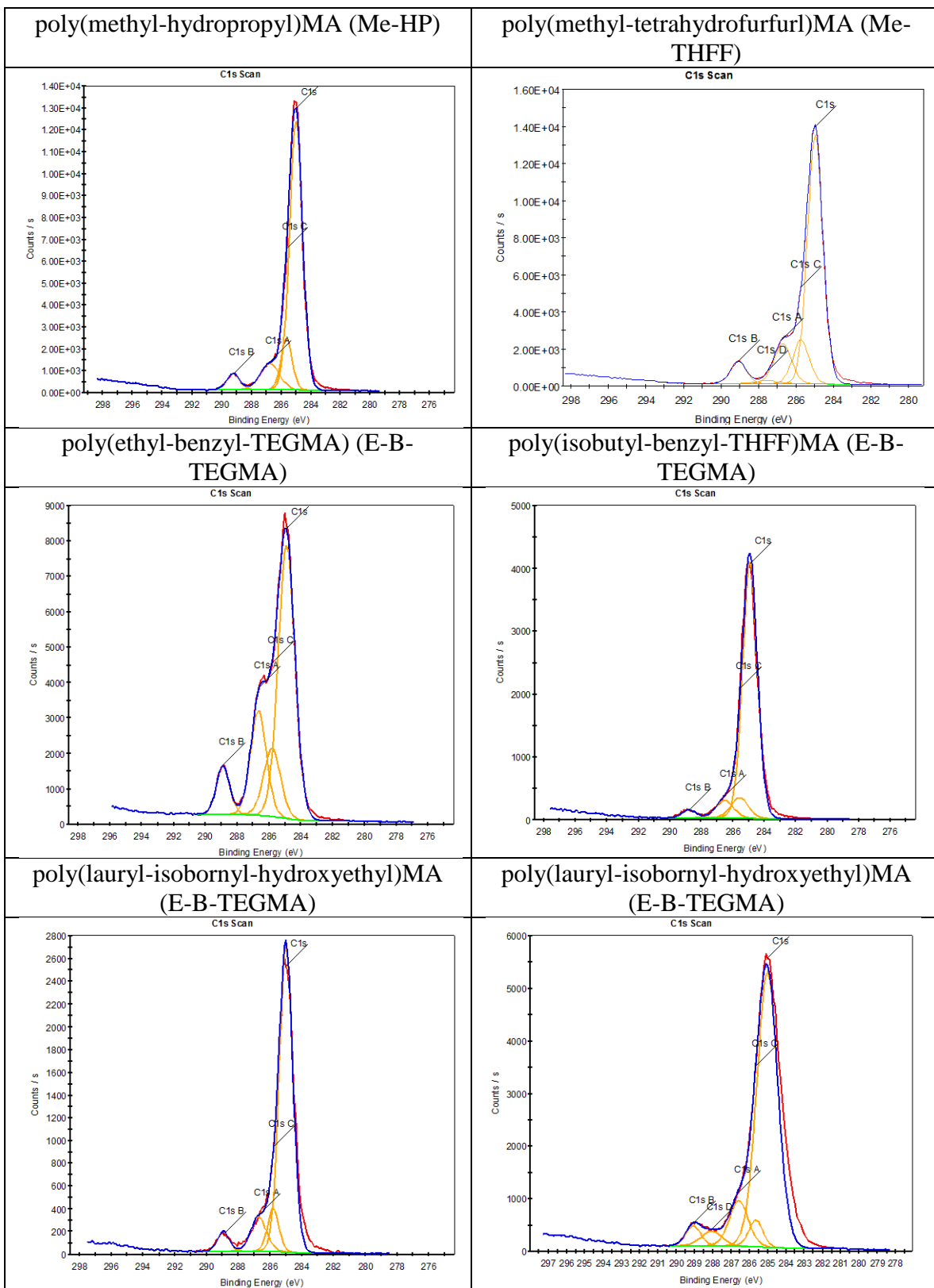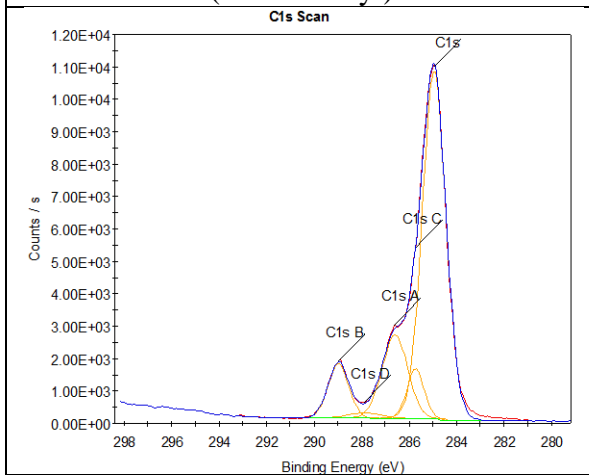
poly(octyl-isobornyl-hydroxypropyl)MA (O-I-Undecyl)	polyHEMA (HEMA)

APPENDIX 8

A.8. Representative high resolution C1s XPS data for terpolymer library

These data were fitted by myself at Georgia Institute of Technology.

C1s = C-C

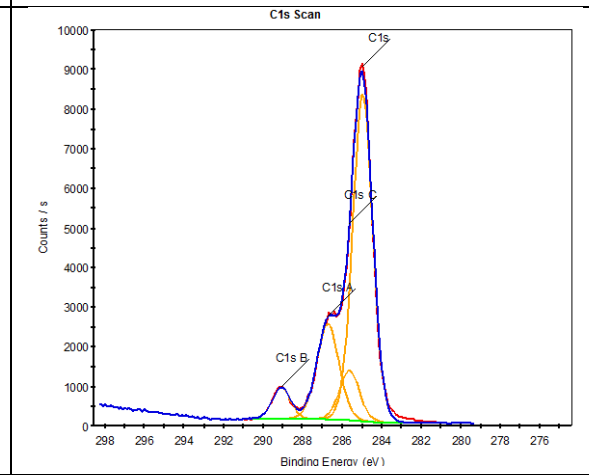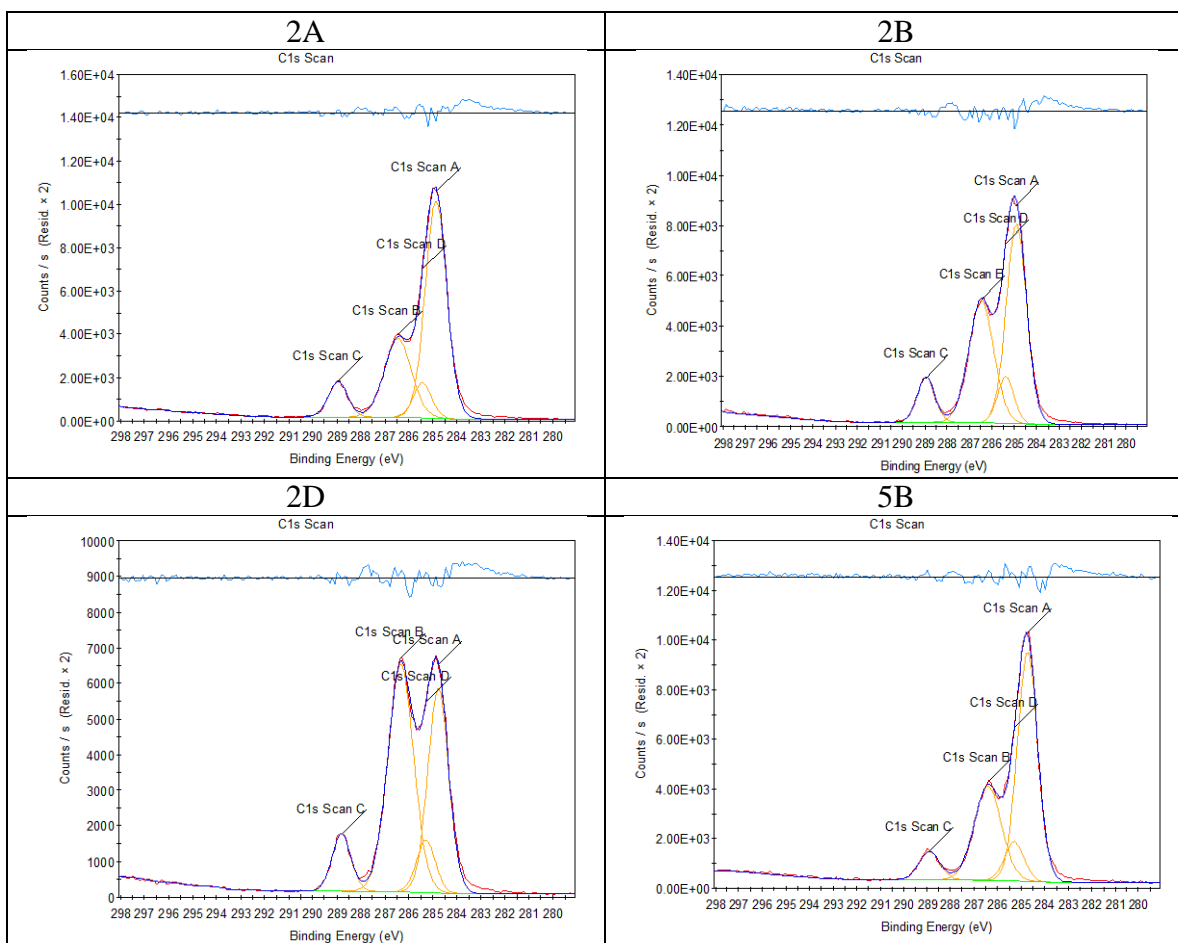C1sA = C-O

C1sB = O-C=O

C1sC = C-COO (beta carbon)

C1sD = C=O

5C	5D

6A	6B

6C	7B

7C	7D
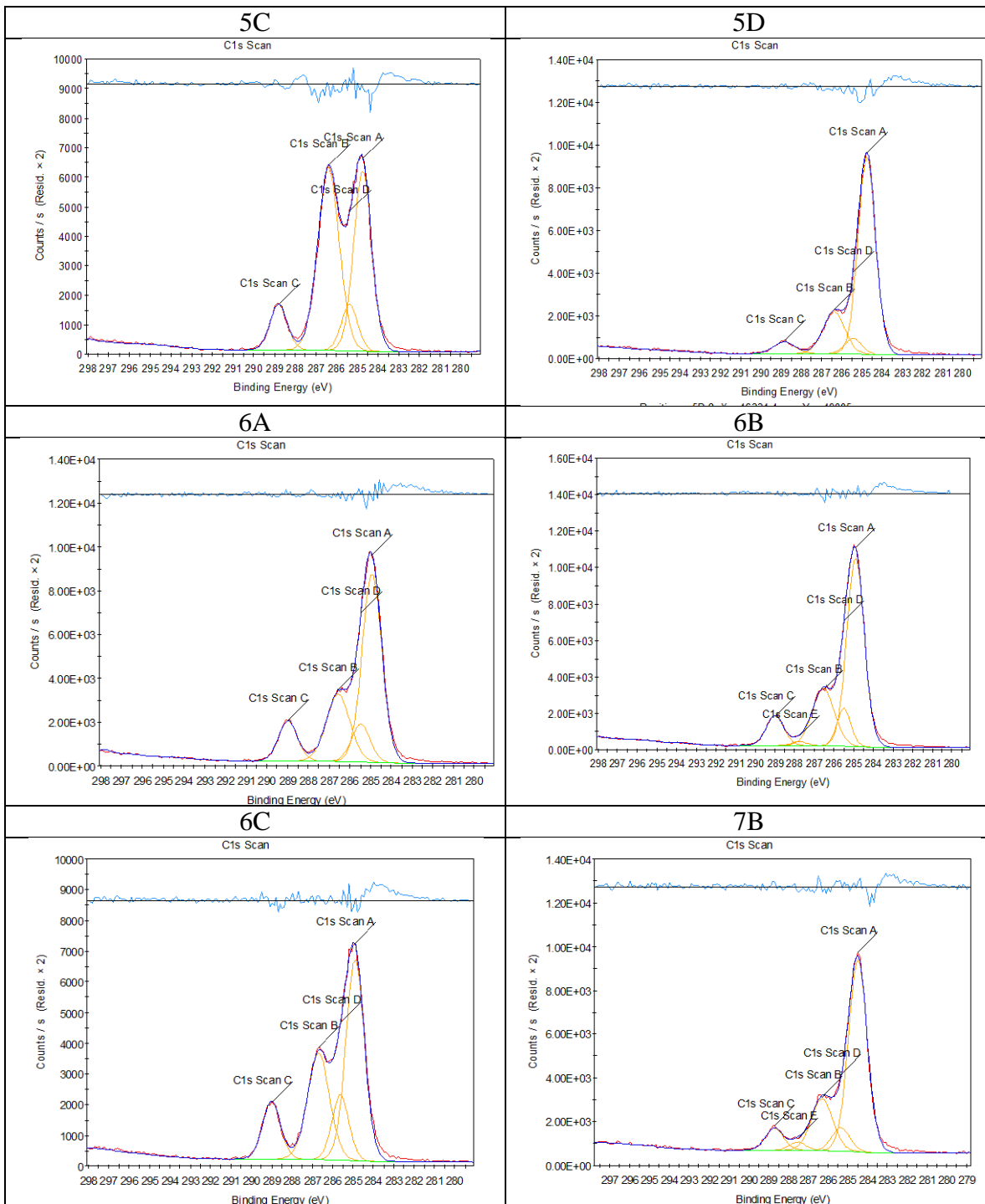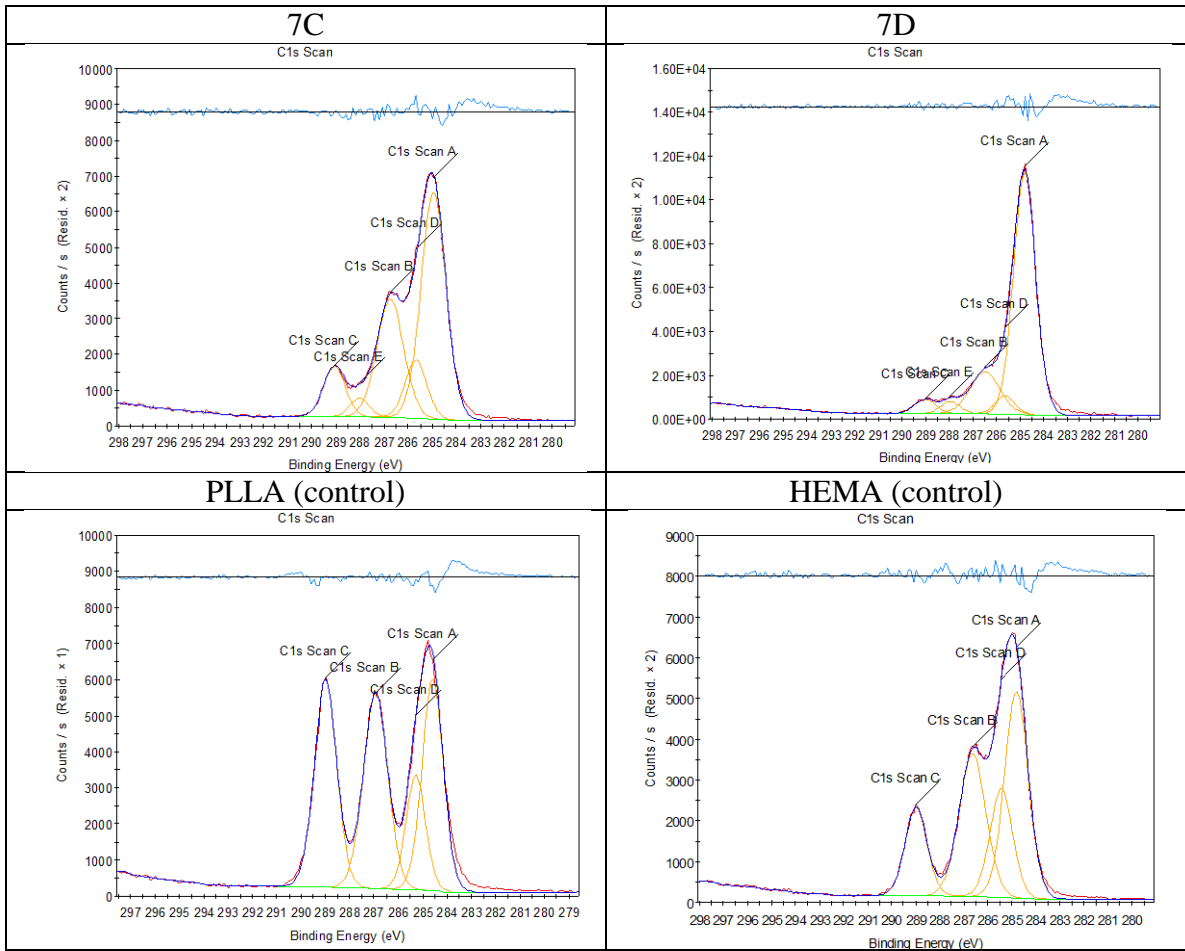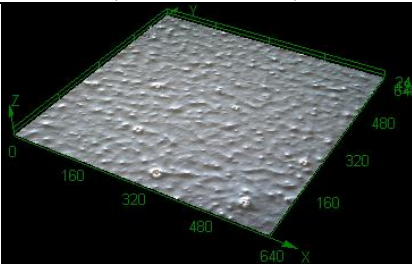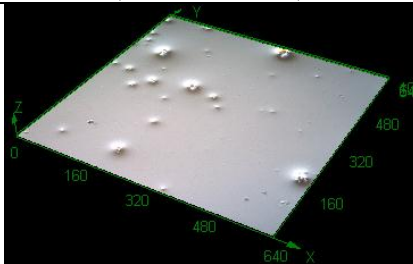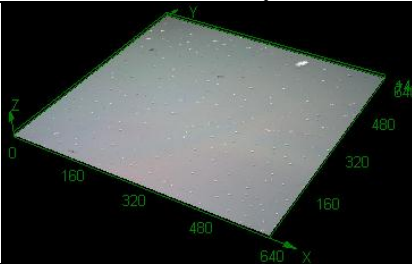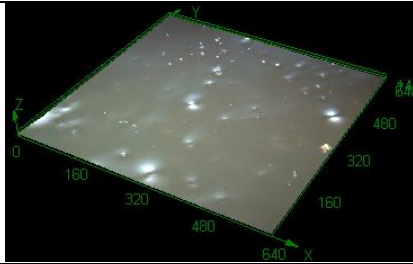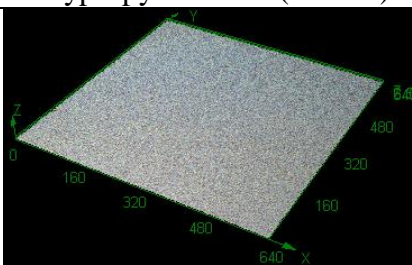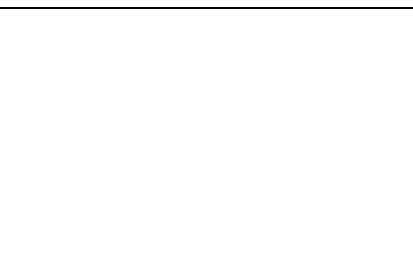
APPENDIX 9

A.9. Representative surface roughness images for polymethacrylate library

(measured by LEXT 3D confocal microscope)
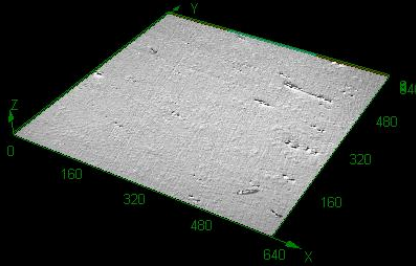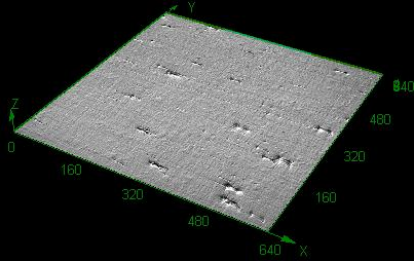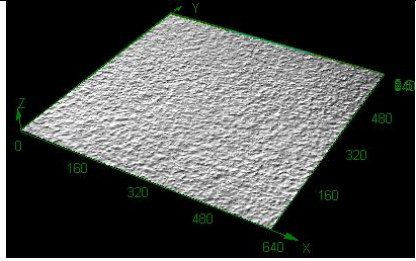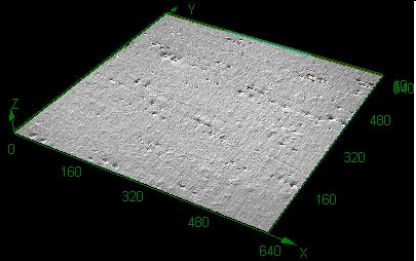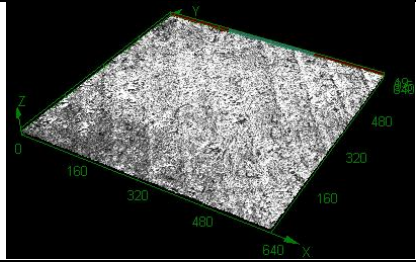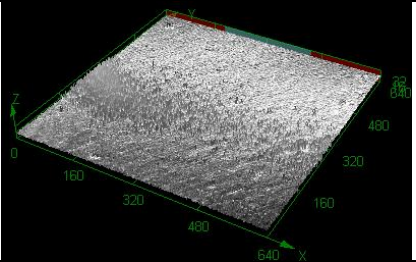
polyEGMA (EGMA)	poly(hydroprypyl)MA (HP)
poly(isobornyl)MA (isobornyl)	poly(methyl-EGMA) (Me-EGMA)
poly(methyl-hydropropyl)MA (Me-HP)	poly(methyl-tetrahydrofurfurl)MA (Me-THFF)
poly(ethyl-benzyl-TEGMA) (E-B-TEGMA)	poly(isobutyl-benzyl-THFF)MA (E-B-TEGMA)

poly(lauryl-isobornyl-hydroxyethyl)MA (E-B-TEGMA)	poly(lauryl-isobornyl-hydroxyethyl)MA (E-B-TEGMA)
poly(octyl-isobornyl-hydroxypropyl)MA (O-I-Undecyl)	polyHEMA (HEMA)
Polypropylene well (control)	

186

APPENDIX 10

A.10. Representative surface roughness images for terpolymer library

(measured by LEXT 3D confocal microscope)

2A	2B
2D	5B
5C	5D
6A	6B

6C	7B
7C	7D
PLLA (control)	HEMA (control)

APPENDIX 11

A.11. Representative ToF-SIMS scans for terpolymer library

Positive ion spectra

Positive spectra (continued)

6A	6B
6C	7B
7C	7D
PLLA (control)	HEMA (control)
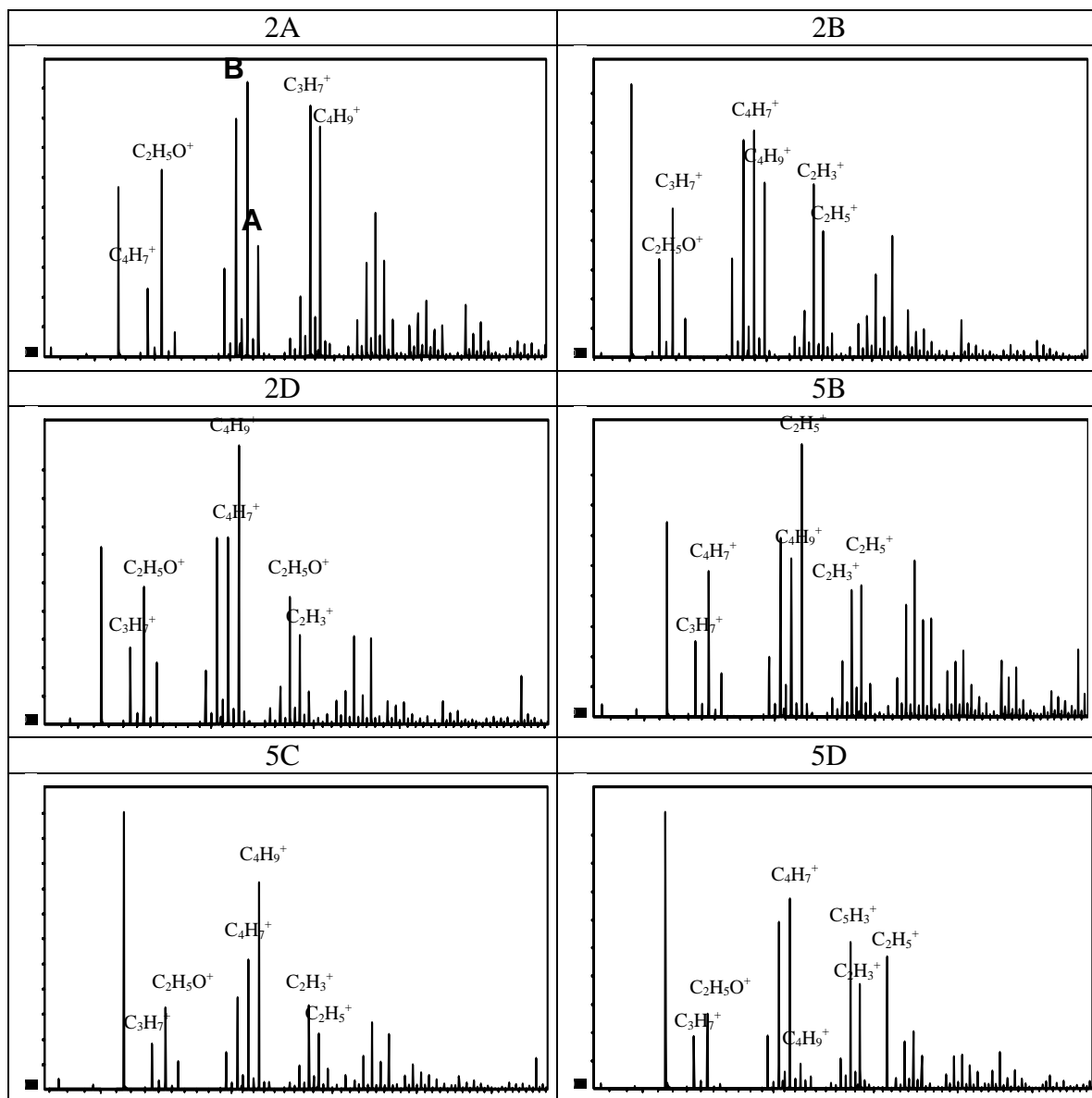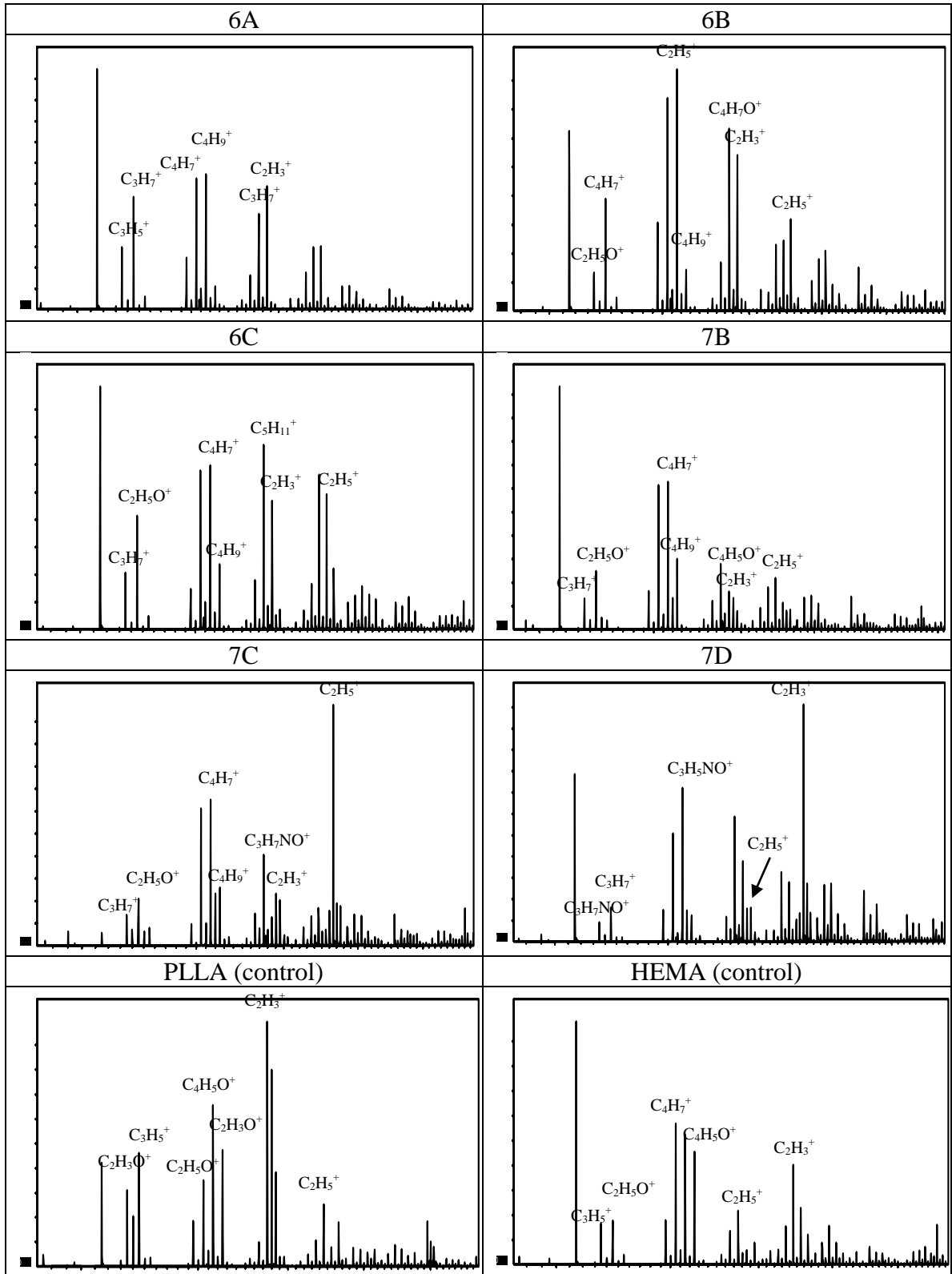
Negative ion spectra

Negative spectra (continued)

6C	7B

Spectrum 6C labeled peaks: C₂H₃O⁻, C₃H₃O₂⁻, C₄H₅O₂⁻, C₂H⁻, C₂HO⁻

Spectrum 7B labeled peaks: C₂H₃O₂⁻, C₃H₃O₂⁻, C₄H₅O₂⁻, C₂H⁻, C₃H₅

7C	7D

Spectrum 7C labeled peaks: C₂H₃O₂⁻, C₃H₇NO⁻, C₄H₅O₂⁻, C₄H₅O₂⁻, C₂H⁻

Spectrum 7D labeled peaks: C₂H₃O₂⁻, C₃H₇NO⁻, C₂H⁻, CNO⁻, C₂HO⁻

PLLA (control)	HEMA (control)

Spectrum PLLA (control) labeled peaks: C₂H₃O⁻, C₃H₃O₂⁻, C₃H₃O₃⁻, C₂H⁻, CNO⁻

Spectrum HEMA (control) labeled peaks: C₂H₃O⁻, C₂H₃O₂⁻, C₂H₇NO⁻, C₄H₅O₂⁻, C₂H⁻, C₂HO⁻

REFERENCES

1. Babensee JE, Anderson JM, McIntire LV, Mikos AG. Host response to tissue engineered devices. Advanced Drug Delivery Reviews 1998;33:111-139.

2. Matzelle MM, Babensee JE. Humoral immune responses to model antigen co-delivered with biomaterials used in tissue engineering. Biomaterials 2004;25:295-304.

3. Bennewitz NL, Babensee JE. The effect of the physical form of poly(lactic-co-glycolic acid) carriers on the humoral immune response to co-delivered antigen. Biomaterials 2005;26:2991-2999.

4. Norton LW, Park J, Babensee JE. Biomaterial adjuvant effect is attenuated by anti-inflammatory drug delivery or material selection. Journal of Controlled Release 2010;146:341-348.

5. Babensee JE, Paranjpe A. Differential levels of dendritic cell maturation on different biomaterials used in combination products. Journal of Biomedical Materials Research Part A 2005;74A:503-510.

6. Yoshida M, Babensee JE. Differential effects of agarose and poly(lactic-co-glycolic acid) on dendritic cell maturation. Journal of Biomedical Materials Research Part A 2006;79A:393-408.

7. Shankar SP, Chen II, Keselowsky BG, García AJ, Babensee JE. Profiles of carbohydrate ligands associated with adsorbed proteins on self-assembled monolayers of defined chemistries. Journal of Biomedical Materials Research Part A 2010;92A:1329-1342.

8. Stock UA, Vacanti JP. Tissue engineering: Current state and prospects. Annual Review of Medicine 2001;52:443-451.

9. Langer R, Vacanti JP. Tissue Engineering. Science 1993;260:920-926.

10. Hubbell JA. Biomaterials in tissue engineering. Bio-Technology 1995;13:565-576.

11. Lee KY, Mooney DJ. Hydrogels for tissue engineering. Chemical Reviews 2001;101:1869-1879.

12. Gupta RK, Siber GR. Adjuvants for human vaccines - current status, problems and future prospects. Vaccine 1995;13:1263-1276.

13. Reid KBM, Porter RR. The proteolytic activation systems of complement. Annual Review of Biochemistry 1981;50:433-464.

14. Burg ND, Pillinger MH. The neutrophil: Function and regulation in innate and humoral immunity. Clinical Immunology 2001;99:7-17.

15. Tosi MF. Innate immune responses to infection. Journal of Allergy and Clinical Immunology 2005;116:241-249.

16. Seong SY, Matzinger P. Hydrophobicity: an ancient damage-associated molecular pattern that initiates innate immune responses. Nature Reviews Immunology 2004;4:469-478.

17. Janeway CA, Travers P, Walport M, Shlomchik M. Immunobiology - The immune systems in health and disease. Garland Science. 2004 p.

18. Roos A, Xu W, Castellano G, Nauta AJ, Garred P, Daha MR, et al. A pivotal role for innate immunity in the clearance of apoptotic cells. European Journal of Immunology 2004;34:921-929.

19. Aderem A, Underhill DM. Mechanisms of phagocytosis in macrophages. Annual Review of Immunology 1999;17:593-623.

20. Mullereberhard HJ. The membrane attack complex of complement. Annual Review of Immunology 1986;4:503-528.

21. Smith JA. Neutrophils, host defense, and inflammation - a double-edged sword. Journal of Leukocyte Biology 1994;56:672-686.

22. Janeway CA, Medzhitov R. Innate immunity: Lipoproteins take their Toll on the host. Current Biology 1999;9:R879-R882.

23. Janeway CA. Approaching the asymptote - evolution and revolution in immunology. Cold Spring Harbor Symposia on Quantitative Biology 1989;54:1-13.

24. Norton LW, Babensee JE. Innate and adaptive immune responses in tissue engineering. In: Fundamentals of tissue engineering and regenerative medicine. Springer, 2009.

25. Akira S, Takeda K, Kaisho T. Toll-like receptors: critical proteins linking innate and acquired immunity. Nature Immunology 2001;2:675-680.

26. Medzhitov R, Janeway CA. Innate immunity: Impact on the adaptive immune response. Current Opinion in Immunology 1997;9:4-9.

27. Janeway CA, Medzhitov R. Innate immune recognition. Annual Review of Immunology 2002;20:197-216.

28. Takeda K, Kaisho T, Akira S. Toll-like receptors. Annual Review of Immunology 2003;21:335-376.

29. Kindt TJ, Goldsby RA, Osborne BA. Kuby Immunology. New York, NY: W.H. Freeman and Company. 2007 p.

30. Beutler B. Innate immunity: an overview. Molecular Immunology 2004;40:845-859.

31. Shi ZC, Cai ZY, Wen S, Chen CY, Gendron C, Sanchez A, et al. Transcriptional Regulation of the Novel Toll-like Receptor Tlr13. Journal of Biological Chemistry 2009;284:20540-20547.

32. Weis WI, Taylor ME, Drickamer K. The C-type lectin superfamily in the immune system. Immunological Reviews 1998;163:19-34.

33. Figdor CG, van Kooyk Y, Adema GJ. C-type lectin receptors on dendritic cells and Langerhans cells. Nature Reviews Immunology 2002;2:77-84.

34. Inohara N, Nunez G. NODs: Intracellular proteins involved in inflammation and apoptosis. Nature Reviews Immunology 2003;3:371-382.

35. Kato H, Takeuchi O, Sato S, Yoneyama M, Yamamoto M, Matsui K, et al. Differential roles of MDA5 and RIG-I helicases in the recognition of RNA viruses. Nature 2006;441:101-105.

36. Takaoka A, Wang Z, Choi MK, Yanai H, Negishi H, Ban T, et al. DAI (DLM-1/ZBP1) is a cytosolic DNA sensor and an activator of innate immune response. Nature 2007;448:501-505.

37. Steinman RM, Cohn ZA. Identification of a novel cell type in peripheral lymphoid organs of mice. Journal of Experimental Medicine 1973;137:1142-1162.

38. Steinman RM, Banchereau J. Taking dendritic cells into medicine. Nature 2007;449:419-426.

39. Banchereau J, Steinman RM. Dendritic cells and the control of immunity. Nature 1998;392:245-252.

40. Shortman K, Naik SH. Steady-state and inflammatory dendritic-cell development. Nature Reviews Immunology 2007;7:19-30.

41. Shortman K, Liu YJ. Mouse and human dendritic cell subtypes. Nature Reviews Immunology 2002;2:151-161.

42. Ouaaz F, Arron J, Zheng Y, Choi YW, Beg AA. Dendritic cell development and survival require distinct NF-kappa B subunits. Immunity 2002;16:257-270.

43. Leon B, Lopez-Bravo M, Ardavin C. Monocyte-derived dendritic cells. Seminars in Immunology 2005;17:313-318.

44. Romani N, Reider D, Heuer M, Ebner S, Kampgen E, Eibl B, et al. Generation of mature dendritic cells from human blood - An improved method with special regard to clinical applicability. Journal of Immunological Methods 1996;196:137-151.

45. Zhou LJ, Tedder TF. CD14+ blood monocytes can differentiate into functionally mature CD83+ dendritic cells. Proceedings of the National Academy of Sciences of the United States of America 1996;93:2588-2592.

46. Chomarat P, Banchereau J, Davoust J, Palucka AK. IL-6 switches the differentiation of monocytes from dendritic cells to macrophages. Nat Immunol 2000;1:510-4.

47. Steinman RM, Hawiger D, Nussenzweig MC. Tolerogenic dendritic cells. Annual Review of Immunology 2003;21:685-711.

48. Pulendran B, Palucka K, Banchereau J. Sensing pathogens and tuning immune responses. Science 2001;293:253-256.

49. Banchereau J, Briere F, Caux C, Davoust J, Lebecque S, Liu Y-J, et al. Immunobiology of dendritic cells. Annual Review of Immunology 2000;18:767-811.

50. Geijtenbeek TBH, van Vliet SJ, Engering A, t Hart BA, van Kooyk Y. Self- and nonself-recognition by C-type lectins on dendritic cells. Annual Review of Immunology 2004;22:33-54.

51. Bajtay Z, Csomor E, Sandor N, Erdei A. Expression and role of Fc- and complement-receptors on human dendritic cells. Immunology Letters 2006;104:46-52.

52. Boruchov AM, Heller G, Veri MC, Bonvini E, Ravetch JV, Young JW. Activating and inhibitory IgG Fc receptors on human DCs mediate opposing functions. Journal of Clinical Investigation 2005;115:2914-2923.

53. Reis ES, Barbuto JAM, Isaac L. Complement components, regulators and receptors are produced by human monocyte-derived dendritic cells. Immunobiology 2007;212:151-157.

54. Castellano G, Woltman AM, Nauta AJ, Roos A, Trouw LA, Seelen MA, et al. Maturation of dendritic cells abrogates C1q production in vivo and in vitro. Blood 2004;103:3813-3820.

55. Reis ES, Barbuto JAM, Köhl J, Isaac L. Impaired dendritic cell differentiation and maturation in the absence of C3. Molecular Immunology 2008;45:1952-1962.

56. Trinchieri G, Sher A. Cooperation of toll-like receptor signals in innate immune defence. Nat Rev Immunol 2007;7:179-190.

57. West MA, Wallin RPA, Matthews SP, Svensson HG, Zaru R, Ljunggren HG, et al. Enhanced dendritic cell antigen capture via toll-like receptor-induced actin remodeling. Science 2004;305:1153-1157.

58. Kalinski P, Hilkens CMU, Wierenga EA, Kapsenberg ML. T-cell priming by type-1and type-2 polarized dendritic cells: the concept of a third signal. Immunology Today 1999;20:561-567.

59. Garrett W. Developmental Control of Endocytosis in Dendritic Cells by Cdc42. Cell 2000;102:325-334.

60. Cravens PD, Lipsky PE. Dendritic cells, chemokine receptors and autoimmune inflammatory diseases. Immunology and Cell Biology 2002;80:497-505.

61. Riol-Blanco L, Sanchez-Sanchez N, Torres A, Tejedor A, Narumiya S, Corbi AL, et al. The chemokine receptor CCR7 activates in dendritic cells two signaling modules that independently regulate chemotaxis and migratory speed. Journal of Immunology 2005;174:4070-4080.

62. Ichiyasu H, McCormack JM, McCarthy KM, Dombkowski D, Preffer FI, Schneeberger EE. Matrix metalloproteinase-9-deficient dendritic cells have impaired migration through tracheal epithelial tight junctions. American Journal of Respiratory Cell and Molecular Biology 2004;30:761-770.

63. Mahnke K, Bhardwaj RS, Luger TA, Schwarz T, Grabbe S. Interaction of murine dendritic cells with collagen up-regulates allostimulatory capacity, surface expression of heat stable antigen, and release of cytokines. Journal of Leukocyte Biology 1996;60:465-472.

64. Brand U, Bellinghausen I, Enk AH, Jonuleit H, Becker D, Knop J, et al. Influence of extracellular matrix proteins on the development of cultured human dendritic cells. European Journal of Immunology 1998;28:1673-1680.

65. Burns S, Hardy SJ, Buddle J, Yong KL, Jones GE, Thrasher AJ. Maturation of DC is associated with changes in motile characteristics and adherence. Cell Motility and the Cytoskeleton 2004;57:118-132.

66. Brown KA, Bedford P, Macey M, McCarthy DA, Leroy F, Vora AJ, et al. Human blood dendritic cells: Binding to vascular endothelium and expression of adhesion molecules. Clinical and Experimental Immunology 1997;107:601-607.

67. Thacker RI, Retzinger GS. Adsorbed fibrinogen regulates the behavior of human dendritic cells in a CD18-dependent manner. Experimental and Molecular Pathology 2008;84:122-130.

68. Jarrossay D, Napolitani G, Colonna M, Sallusto F, Lanzavecchia A. Specialization and complementarity in microbial molecule recognition by human myeloid and

plasmacytoid dendritic cells. European Journal of Immunology 2001;31:3388-3393.

69.   Pulendran B. Modulating vaccine responses with dendritic cells and Toll-like receptors. Immunological Reviews 2004;199:227-250.

70.   Gunzer M, Schafer A, Borgmann S, Grabbe S, Zanker KS, Brocker EB, et al. Antigen presentation in extracellular matrix: Interactions of T cells with dendritic cells are dynamic, short lived, and sequential. Immunity 2000;13:323-332.

71.   Li H, Oliver T, Jia W, He YW. Efficient dendritic cell priming of T lymphocytes depends on the extracellular matrix protein mindin. Embo Journal 2006;25:4097-4107.

72.   Moser M, Murphy KM. Dendritic cell regulation of TH1-TH2 development. Nat Immunol 2000;1:199-205.

73.   Sakaguchi S. Naturally arising CD4(+) regulatory T cells for immunologic self-tolerance and negative control of immune responses. Annual Review of Immunology 2004;22:531-562.

74.   Stockinger B, Veldhoen M. Differentiation and function of Th17 T cells. Current Opinion in Immunology 2007;19:281-286.

75.   Murphy KM, Reiner SL. The lineage decisions of helper T cells. Nature Reviews Immunology 2002;2:933-944.

76.   Kindt TJ, Goldsby RA, Osborne BA. Kuby Immunology. New York, NY: W.H. Freeman and Company. 2007 p.

77.   Steinman RM, Hawiger D, Nussenzweig MC. Tolerogenic dendritic cells. Annual Review Immunology 2003;21:685-711.

78.   Steinman R, Hemmi H. Dendritic Cells: Translating Innate to Adaptive Immunity. In: From Innate Immunity to Immunological Memory.2006. pp. 17-58.

79.   Zal T, Volkmann A, Stockinger B. Mechanisms of tolerance induction in major histocompatibility complex class II-restricted T cells specific for a blood-borne self-antigen. The Journal of Experimental Medicine 1994;180:2089-2099.

80.   Volkmann A, Zal T, Stockinger B. Antigen-presenting cells in the thymus that can negatively select MHC class II-restricted T cells recognizing a circulating self antigen. J Immunol 1997;158:693-706.

81.   Pestka S, Krause CD, Sarkar D, Walter MR, Shi YF, Fisher PB. Interleukin-10 and related cytokines and receptors. Annual Review of Immunology 2004;22:929-979.

82. Shevach EM. CD4(+)CD25(+) suppressor T cells: More questions than answers. Nature Reviews Immunology 2002;2:389-400.

83. Yamazaki S, Bonito AJ, Spisek R, Dhodapkar M, Inaba K, Steinman RM. Dendritic cells are specialized accessory cells along with TGF- for the differentiation of Foxp3+ CD4+ regulatory T cells from peripheral Foxp3 precursors. Blood 2007;110:4293-4302.

84. Yamazaki S, Steinman RM. Dendritic cells as controllers of antigen-specific Foxp3+ regulatory T cells. Journal of Dermatological Science 2009;54:69-75.

85. Green DR, Ferguson T, Zitvogel L, Kroemer G. Immunogenic and tolerogenic cell death. Nat Rev Immunol 2009;9:353-363.

86. Probst HC, McCoy K, Okazaki T, Honjo T, van den Broek M. Resting dendritic cells induce peripheral CD8+ T cell tolerance through PD-1 and CTLA-4. Nat Immunol 2005;6:280-286.

87. Rozkova D, Horvath R, Bartunkova J, Spisek R. Glucocorticoids severely impair differentiation and antigen presenting function of dendritic cells despite upregulation of Toll-like receptors. Clinical Immunology 2006;120:260-271.

88. Muller G, Muller A, Tuting T, Steinbrink K, Saloga J, Szalma C, et al. Interleukin-10-Treated Dendritic Cells Modulate Immune Responses of Naive and Sensitized T Cells In Vivo. 2002;119:836-841.

89. Lan YY, Wang Z, Raimondi G, Wu W, Colvin BL, De Creus A, et al. "Alternatively Activated" Dendritic Cells Preferentially Secrete IL-10, Expand Foxp3+CD4+ T Cells, and Induce Long-Term Organ Allograft Survival in Combination with CTLA4-Ig. J Immunol 2006;177:5868-5877.

90. Riboldi E, Musso T, Moroni E, Urbinati C, Bernasconi S, Rusnati M, et al. Cutting Edge: Proangiogenic Properties of Alternatively Activated Dendritic Cells. J Immunol 2005;175:2788-2792.

91. Qian C, Jiang X, An H, Yu Y, Guo Z, Liu S, et al. TLR agonists promote ERK-mediated preferential IL-10 production of regulatory dendritic cells (diffDCs), leading to NK-cell activation. Blood 2006;108:2307-2315.

92. Zhang M, Tang H, Guo Z, An H, Zhu X, Song W, et al. Splenic stroma drives mature dendritic cells to differentiate into regulatory dendritic cells. Nat Immunol 2004;5:1124-1133.

93. Anderson AE, Sayers BL, Haniffa MA, Swan DJ, Diboll J, Wang X-N, et al. Differential regulation of naive and memory CD4+ T cells by alternatively activated dendritic cells. J Leukoc Biol 2008;84:124-133.

94. Braun D, Galibert L, Nakajima T, Saito H, Quang VV, Rubio M, et al. Semimature Stage: A Checkpoint in a Dendritic Cell Maturation Program That Allows for Functional Reversion after Signal-Regulatory Protein-{alpha} Ligation and Maturation Signals. J Immunol 2006;177:8550-8559.

95. Elzey BD, Tian J, Jensen RJ, Swanson KA, Lees JR, Lentz SR, et al. Platelet-mediated modulation of adaptive immunity: A communication link between innate and adaptive immune compartments. Immunity 2003;19:9-19.

96. Hilf N, Singh-Jasuja H, Schwarzmaier P, Gouttefangeas C, Rammensee HG, Schild H. Human platelets express heat shock protein receptors and regulate dendritic cell maturation. Blood 2002;99:3676-3682.

97. van Gisbergen K, Sanchez-Hernandez M, Geijtenbeek TBH, van Kooyk Y. Neutrophils mediate immune modulation of dendritic cells through glycosylation-dependent interactions between Mac-1 and DC-SIGN. Journal of Experimental Medicine 2005;201:1281-1292.

98. Megiovanni AM, Sanchez F, Robledo-Sarmiento M, Morel C, Gluckman JC, Boudaly S. Polymorphonuclear neutrophils deliver activation signals and antigenic molecules to dendritic cells: a new link between leukocytes upstream of T lymphocytes. Journal of Leukocyte Biology 2006;79:977-988.

99. Griffith LG. Polymeric biomaterials. Acta Materialia 2000;48:263-277.

100. Murthy N, Campbell J, Fausto N, Hoffman AS, Stayton PS. Bioinspired pH-responsive polymers for the intracellular delivery of biomolecular drugs. Bioconjugate Chemistry 2003;14:412-419.

101. Wang X, Uto T, Akagi T, Akashi M, Baba M. Poly(gamma-glutamic acid) nanoparticles as an efficient antigen delivery and adjuvant system: Potential for an AIDS vaccine. Journal of Medical Virology 2008;80:11-19.

102. Zugates GT, Little SR, Anderson DG, Langer R. Poly(beta-amino ester)s for DNA delivery. Israel Journal of Chemistry 2005;45:477-485.

103. Nerem RM. Tissue engineering: The hope, the hype, and the future. Tissue Engineering 2006;12:1143-1150.

104. Ratner BD, Bryant SJ. Biomaterials: Where we have been and where we are going. Annual Review of Biomedical Engineering 2004;6:41-75.

105. Yu XJ, Bellamkonda RV. Tissue-engineered scaffolds are effective alternatives to autografts for bridging peripheral nerve gaps. Tissue Engineering 2003;9:421-430.

106. Zisch AH, Lutolf MP, Ehrbar M, Raeber GP, Rizzi SC, Davies N, et al. Cell-demanded release of VEGF from synthetic, biointeractive cell-ingrowth matrices for vascularized tissue growth. Faseb Journal 2003;17:2260-2262.

107. Lutolf MR, Weber FE, Schmoekel HG, Schense JC, Kohler T, Muller R, et al. Repair of bone defects using synthetic mimetics of collagenous extracellular matrices. Nature Biotechnology 2003;21:513-518.

108. Anderson JM. Biological responses to materials. Annual Review of Materials Research 2001;31:81-110.

109. Harris HE, Raucci A. Alarmin(g) news about danger - Workshop on innate danger signals and HMGB1. Embo Reports 2006;7:774-778.

110. Babensee JE. Interaction of dendritic cells with biomaterials. Tissue Eng. Part A 2008;20:101-108.

111. Yoshida M, Babensee JE. Poly(lactic-co-glycolic acid) enhances maturation of human monocyte-derived dendritic cells. Journal of Biomedical Materials Research Part A 2004;71A:45-54.

112. Yoshida M, Mata J, Babensee JE. Effect of poly(lactic-co-glycolic acid) contact on maturation of murine bone marrow-derived dendritic cells. Journal of Biomedical Materials Research Part A 2007;80A:7-12.

113. Babensee JE, Paranjpe A. Differential levels of dendritic cell maturation on different biomaterials used in combination products. Journal of Biomedical Materials Research Part A 2005;74A:503-510.

114. Park J, Babensee JE. Biomaterial-dependent effects on dendritic cells. Journal of Biomedical Materials Research Part A (submitted for publication).

115. Shankar SP, Petrie TA, García AJ, Babensee JE. Dendritic cell responses to self-assembled monolayers of defined chemistries. Journal of Biomedical Materials Research Part A 2010;92A:1487-1499.

116. Barbosa JN, Madureira P, Barbosa MA, Aguas AP. The influence of functional groups of self-assembled monolayers on fibrous capsule formation and cell recruitment. Journal of Biomedical Materials Research Part A 2006;76A:737-743.

117. Park J, Babensee JE. Control of dendritic cell phenotype by scaffolds for tissue engineering. J Biomed Mater Res A;(In preparation).

118. Stachowiak AN, Irvine DJ. Inverse opal hydrogel-collagen composite scaffolds as a supportive microenvironment for immune cell migration. Journal of Biomedical Materials Research Part A 2008;85A:815-828.

119. Reddy ST, Swartz MA, Hubbell JA. Targeting dendritic cells with biomaterials: developing the next generation of vaccines. Trends in Immunology 2006;27:573-579.

120. Shokouhi B, Coban C, Hasirci V, Aydin E, Dhanasingh A, Shi N, et al. The role of multiple toll-like receptor signalling cascades on interactions between biomedical polymers and dendritic cells. Biomaterials 2010;31:5759-5771.

121. Rogers TH, Babensee JE. The role of integrins in the recognition and response of dendritic cells to biomaterials. Biomaterials 2011;32:1270-1279.

122. Acharya AP, Dolgova NV, Clare-Salzler MJ, Keselowsky BG. Adhesive substrate-modulation of adaptive immune responses. Biomaterials 2008;29:4736-4750.

123. Kwissa M, Kasturi SP, Pulendran B. The science of adjuvants. Expert Review of Vaccines 2007;6:673-684.

124. Singh M, O'Hagan D. Advances in vaccine adjuvants. Nature Biotechnology 1999;17:1075-1081.

125. Alving CR. Design and selection of vaccine adjuvants: animal models and human trials. Vaccine 2002;20:S56-S64.

126. Sharp FA, Ruane D, Claass B, Creagh E, Harris J, Malyala P, et al. Uptake of particulate vaccine adjuvants by dendritic cells activates the NALP3 inflammasome. Proceedings of the National Academy of Sciences 2009;106:870 - 875.

127. Shen H, Ackerman AL, Cody V, Giodini A, Hinson ER, Cresswell P, et al. Enhanced and prolonged cross-presentation following endosomal escape of exogenous antigens encapsulated in biodegradable nanoparticles. Immunology 2006;117:78-88.

128. Tran KK, Shen H. The role of phagosomal pH on the size-dependent efficiency of cross-presentation by dendritic cells. Biomaterials 2009;30:1356-1362.

129. Reddy ST, Rehor A, Schmoekel HG, Hubbell JA, Swartz MA. In vivo targeting of dendritic cells in lymph nodes with poly(propylene sulfide) nanoparticles. Journal of Controlled Release 2006;112:26-34.

130. Singh A, Nie H, Ghosn B, Qin H, Kwak LW, Roy K. Efficient modulation of T-cell response by dual-mode, single-carrier delivery of cytokine-targeted siRNA and DNA vaccine to antigen-presenting cells. Mol Ther 2008;16:2011-21.

131. Singh A, Suri S, Roy K. In-situ crosslinking hydrogels for combinatorial delivery of chemokines and siRNA-DNA carrying microparticles to dendritic cells. Biomaterials 2009.

132. Acharya AP, Clare-Salzler MJ, Keselowsky BG. A high-throughput microparticle microarray platform for dendritic cell-targeting vaccines. Biomaterials 2009;30:4168-4177.

133. Hamdy S, Molavi O, Ma Z, Haddadi A, Alshamsan A, Gobti Z, et al. Co-delivery of cancer-associated antigen and Toll-like receptor 4 ligand in PLGA nanoparticles induces potent CD8+ T cell-mediated anti-tumor immunity. Vaccine 2008;26:5046-57.

134. Little SR, Lynn DM, Ge Q, Anderson DG, Puram SV, Chen J, et al. Poly-beta amino ester-containing microparticles enhance the activity of nonviral genetic vaccines. Proc Natl Acad Sci U S A 2004;101:9534-9.

135. Hori Y, Winans AM, Huang CC, Horrigan EM, Irvine DJ. Injectable dendritic cell-carrying alginate gels for immunization and immunotherapy. Biomaterials 2008;29:3671-3682.

136. Hori Y, Winans AM, Irvine DJ. Modular injectable matrices based on alginate solution/microsphere mixtures that gel in situ and co-deliver immunomodulatory factors. Acta Biomaterialia 2009;5:969-982.

137. Ali OA, Emerich D, Dranoff G, Mooney DJ. In situ regulation of DC subsets and T cells mediates tumor regression in mice. Science translational medicine 2009;1:8ra19-8ra19.

138. Shen H, Goldberg E, Saltzman WM. Gene expression and mucosal immune responses after vaginal DNA immunization in mice using a controlled delivery matrix. Journal of Controlled Release 2003;86:339-348.

139. Hubbell JA, Thomas SN, Swartz MA. Materials engineering for immunomodulation. Nature 2009;462:449-460.

140. Kohn J. New approaches to biomaterials design. Nat Mater 2004;3:745-747.

141. Hubbell JA. Biomaterials science and high-throughput screening. Nature Biotechnology 2004;22:828-829.

142. Anderson DG, Levenberg S, Langer R. Nanoliter-scale synthesis of arrayed biomaterials and application to human embryonic stem cells. Nature Biotechnology 2004;22:863-866.

143. Anderson DG, Putnam D, Lavik EB, Mahmood TA, Langer R. Biomaterial microarrays: rapid, microscale screening of polymer-cell interaction. Biomaterials 2005;26:4892-4897.

144. Faid K, Voicu R, Bani-Yaghoub M, Tremblay R, Mealing G, Py C, et al. Rapid fabrication and chemical patterning of polymer microstructures and their applications as a platform for cell cultures. Biomedical Microdevices 2005;7:179-184.

145. Meredith JC, Sormana JL, Keselowsky BG, Garcia AJ, Tona A, Karim A, et al. Combinatorial characterization of cell interactions with polymer surfaces. Journal of Biomedical Materials Research Part A 2003;66A:483-490.

146. Zapata P, Su J, Garcia AJ, Meredith JC. Quantitative high-throughput screening of osteoblast attachment, spreading, and proliferation on demixed polymer blend micropatterns. Biomacromolecules 2007;8:1907-1917.

147. Washburn NR, Yamada KM, Simon CG, Kennedy SB, Amis EJ. High-throughput investigation of osteoblast response to polymer crystallinity: influence of nanometer-scale roughness on proliferation. Biomaterials 2004;25:1215-1224.

148. Eidelman N, Simon CG. Characterization of combinatorial polymer blend composition gradients by FTIR microspectroscopy. Journal of Research of the National Institute of Standards and Technology 2004;109:219-231.

149. Mei Y, Elliott JT, Smith JR, Langenbach KJ, Wu T, Xu C, et al. Gradient substrate assembly for quantifying cellular response to biomaterials. Journal of Biomedical Materials Research Part A 2006;79A:974-988.

150. Bhat RR, Chaney BN, Rowley J, Liebmann-Vinson A, Genzer J. Tailoring cell adhesion using surface-grafted polymer gradient assemblies. Advanced Materials 2005;17:2802-+.

151. Vogel BM, Cabral JT, Eidelman N, Narasimhan B, Mallapragada SK. Parallel synthesis and high throughput dissolution testing of biodegradable polyanhydride copolymers. Journal of Combinatorial Chemistry 2005;7:921-928.

152. Weber N, Bolikal D, Bourke SL, Kohn J. Small changes in the polymer structure influence the adsorption behavior of fibrinogen on polymer surfaces: Validation of a new rapid screening technique. Journal of Biomedical Materials Research Part A 2004;68A:496-503.

153. Holmes PF, Bohrer M, Kohn J. Exploration of polymethacrylate structure-property correlations: Advances towards combinatorial and high-throughput methods for biomaterials discovery. Progress in polymer science 2008;33:787-796.

154. Kholodovych V, Gubskaya AV, Bohrer M, Harris N, Knight D, Kohn J, et al. Prediction of biological response for large combinatorial libraries of biodegradable polymers: Polymethacrylates as a test case. Polymer 2008;49:2435-2439.

155. Joy A, Cohen DM, Luk A, Anim-Danso E, Chen C, Kohn J. Control of Surface Chemistry, Substrate Stiffness, and Cell Function in a Novel Terpolymer Methacrylate Library. Langmuir 2011;27:1891-1899.

156. James K, Levene H, Parsons JR, Kohn J. Small changes in polymer chemistry have a large effect on the bone-implant interface: evaluation of a series of degradable tyrosine-derived polycarbonates in bone defects. Biomaterials 1999;20:2203-2212.

157. Brocchini S, James K, Tangpasuthadol V, Kohn J. Structure-property correlations in a combinatorial library of degradable biomaterials. Journal of Biomedical Materials Research 1998;42:66-75.

158. Ertel SI, Kohn J. Evaluation of a seires of tyrosine-derived polycarbonates as degradable biomaterials. Journal of Biomedical Materials Research 1994;28:919-930.

159. Unadkat HV, Papenburg BJ, Truckenmueller R, Stamatialis D, Wessling M, van Blitterswijk CA, et al. High-throughput screening of cell-surface topographic interactions. IEEE 35th Annual Northeast Bioengineering Conference 2009:1.

160. Zhao G, Raines AL, Wieland M, Schwartz Z, Boyan BD. Requirement for both micron- and submicron scale structure for synergistic responses of osteoblasts to substrate surface energy and topography. Biomaterials 2007;28:2821-2829.

161. Zhao G, Schwartz Z, Wieland M, Rupp F, Geis-Gerstorfer J, Cochran DL, et al. High surface energy enhances cell response to titanium substrate microstructure. Journal of Biomedical Materials Research Part A 2005;74A:49-58.

162. Boyan BD, Lossdörfer S, Wang L, Zhao G, Lohmann CH, Cochran DL, et al. Osteoblasts generate an osteogenic microenvironment when grown on surfaces with rough microtopographies. European Cells & Materials 2003;6:22-27.

163. Banchereau J, Steinman RM. Dendritic cells and the control of immunity. Nature 1998;392:245-252.

164. Shortman K, Naik SH. Steady-state and inflammatory dendritic-cell development. Nat Rev Immunol 2007;7:19-30.

165. Medzhitov R. Toll-like receptors and innate immunity. Nat Rev Immunol 2001;1:135-145.

166. Gallucci S, Matzinger P. Danger signals: SOS to the immune system. Current Opinion in Immunology 2001;13:114-119.

167. van Kooyk Y, Geijtenbeek TBH. DC-sign: Escape mechanism for pathogens. Nature Reviews Immunology 2003;3:697-709.

168. Selkirk JV, Nottebaum LM, Ford IC, Santos M, Malany S, Foster AC, et al. A novel cell-based assay for G-protein-coupled receptor-mediated cyclic adenosine monophosphate response element binding protein phosphorylation. Journal of Biomolecular Screening 2006;11:351-358.

169. Greenwalt DE, Szabo J, Manchel I. High throughput cell-based assay of hematopoietic progenitor differentiation. Journal of Biomolecular Screening 2001;6:383-392.

170. Romani N, Gruner S, Brang D, Kämpgen E, Lenz A, Trockenbacher B, et al. Proliferating dendritic cell progenitors in human blood. The Journal of Experimental Medicine 1994;180:83-93.

171. Jotwani R, Pulendran B, Agrawal S, Cutler CW. Human dendritic cells respond to Porphyromonas gingivalis LPS by promoting a Th2 effector response in vitro. European Journal of Immunology 2003;33:2980-2986.

172. Lundholt BK, Scudder KM, Pagliaro L. A simple technique for reducing edge effect in cell-based assays. Journal of Biomolecular Screening 2003;8:566-570.

173. Shankar SP, Babensee JE. Comparative characterization of cultures of primary human macrophages or dendritic cells relevant to biomaterial studies. Journal of Biomedical Materials Research Part A 2010;92A:791-800.

174. Kaser A, Dunzendorfer S, Offner FA, Ludwiczek O, Enrich B, Koch RO, et al. B lymphocyte-derived IL-16 attracts dendritic cells and Th cells. Journal of Immunology 2000;165:2474-2480.

175. Bayry J, Lacroix-Desmazes S, Kazatchkine MD, Hermine O, Tough DF, Kaveri SV. Modulation of dendritic cell maturation and function by B lymphocytes. Journal of Immunology 2005;175:15-20.

176. Bayry J, Lacroix-Desmazes S, Donkova-Petrini V, Carbonneil C, Misra N, Lepelletier Y, et al. Natural antibodies sustain differentiation and maturation of human dendritic cells. Proceedings of the National Academy of Sciences of the United States of America 2004;101:14210-14215.

177. Folzenlogen D, Hofer MF, Leung DY, Freed JH, Newell MK. Analysis of CD80 and CD86 expression on peripheral blood B lymphocytes reveals increased expression of CD86 in lupus patients. Clinical Immunology and Immunopathology 1997;83:199-204.

178. Cao XC, Sugita M, van der Wel N, Lai J, Rogers RA, Peters PJ, et al. CD1 molecules efficiently present antigen in immature dendritic cells and traffic independently of MHC class II during dendritic cell maturation. Journal of Immunology 2002;169:4770-4777.

179. Jefford M, Schnurr M, Toy T, Masterman KA, Shin A, Beecroft T, et al. Functional comparison of DCs generated in vivo with Flt3 ligand or in vitro from blood monocytes: differential regulation of function by specific classes of physiologic stimuli. Blood 2003;102:1753-1763.

180. Sozzani S, Longoni D, Bonecchi R, Luini W, Bersani L, D'Amico G, et al. Human monocyte-derived and CD34+ cell-derived dendritic cells express functional receptors for platelet activating factor. FEBS Letters 1997;418:98-100.

181. Jansen JH, Wientjens G, Fibbe WE, Willemze R, Kluinnelemans HC. Inhibition of human macrophage colony formation by interleukin-4. Journal of Experimental Medicine 1989;170:577-582.

182. Santambrogio L, Sato AK, Carven GJ, Belyanskaya SL, Strominger JL, Stern LJ. Extracellular antigen processing and presentation by immature dendritic cells. Proceedings of the National Academy of Sciences of the United States of America 1999;96:15056-15061.

183. Lenschow DJ, Walunas TL, Bluestone JA. CD28/B7 system of T cell costimulation. Annual Reviews Immunology 1996;14:233-58.

184. Jeannin P, Delneste Y, LecoanetHenchoz S, Gauchat JF, Ellis J, Bonnefoy JY. CD86 (B7-2) on human B cells - A functional role in proliferation and selective differentiation into IgE- and IgG4-producing cells. Journal of Biological Chemistry 1997;272:15613-15619.

185. Beckman EM, Melian A, Behar SM, Sieling PA, Chatterjee D, Furlong ST, et al. CD1c restricts responses of mycobacteria-specific T cells - Evidence for antigen presentation by a second member of the human CD1 family. Journal of Immunology 1996;157:2795-2803.

186. Briken V, Jackman RM, Watts GFM, Rogers RA, Porcelli SA. Human CD1b and CD1c isoforms survey different intracellular compartments for the presentation of microbial lipid antigens. Journal of Experimental Medicine 2000;192:281-287.

187. Im JS, Yu KOA, Illarionov PA, LeClair KP, Storey JR, Kennedy MW, et al. Direct measurement of antigen binding properties of CD1 proteins using fluorescent lipid probes. Journal of Biological Chemistry 2004;279:299-310.

188. Brigl M, Brenner MB. CD1: Antigen presentation and T cell function. Annual Review of Immunology 2004;22:817-890.

189. Geijtenbeek TBH, Torensma R, van Vliet SJ, van Duijnhoven GCF, Adema GJ, van Kooyk Y, et al. Identification of DC-SIGN, a novel dendritic cell-specific ICAM-3 receptor that supports primary immune responses. Cell 2000;100:575-585.

190. Woltman AM, Schlagwein N, van der Kooij SW, van Kooten C. The novel cyclophilin-binding drug sanglifehrin A specifically affects antigen uptake receptor expression and endocytic capacity of human dendritic cells. Journal of Immunology 2004;172:6482-6489.

191. Gordon EM, Gallop MA, Patel DV. Strategy and tactics in combinatorial organic synthesis. Applications to drug discovery. Accounts of Chemical Research 1996;29:144-154.

192. Kapsenberg ML. Dendritic-cell control of pathogen-driven T-cell polarization. Nat Rev Immunol 2003;3:984-993.

193. Langenkamp A, Messi M, Lanzavecchia A, Sallusto F. Kinetics of dendritic cell activation: impact on priming of TH1, TH2 and nonpolarized T cells. Nat Immunol 2000;1:311-316.

194. Zvaifler NJ, Steinman RM, Kaplan G, Lau LL, Rivelis M. Identification of immunostimulatory dendritic cells in the synovial effusions of patients with rheumatoid arthritis. Journal of Clinical Investigation 1985;76:789-800.

195. Thomas R, MacDonald K, Pettit A, Cavanagh L, Padmanabha J, Zehntner S. Dendritic cells and the pathogenesis of rheumatoid arthritis. Journal of Leukocyte Biology 1999;66:286-292.

196. Page G, Miossec P. RANK and RANKL expression as markers of dendritic cell-t cell interactions in paired samples of rheumatoid synovium and lymph nodes. Arthritis & Rheumatism 2005;52:2307-2312.

197. Kong Y-Y, Feige U, Sarosi I, Bolon B, Tafuri A, Morony S, et al. Activated T cells regulate bone loss and joint destruction in adjuvant arthritis through osteoprotegerin ligand. Nature 1999;402:304-309.

198. Teng YT, Nguyen H, Gao X, Kong YY, Gorczynski RM, Singh B, et al. Functional human T-cell immunity and osteoprotegerin ligand control alveolar bone destruction in periodontal infection. The Journal of Clinical Investigation 2000;106:R59-67.

199. Gravallese EM. Bone destruction in arthritis. Annals of the Rheumatic Diseases 2002;61 Suppl 2:ii84-86.

200. Teng Y-TA. The role of acquired immunity and periodontal disease progression. Critical Reviews in Oral Biology & Medicine 2003;14:237-252.

201. Taubman MA, Kawai T. Involvement of T-lymphocytes in periodontal disease and in direct and indirect induction of bone resorption. Critical Reviews in Oral Biology & Medicine 2001;12:125-135.

202. Norton LW, Park J, Babensee JE. Biomaterial adjuvant effect is attenuated by anti-inflammatory drug delivery or material selection. Journal of Controlled Release 2010;In Press.

203. Boyan BD, Lossdörfer S, Wang L, Zhao G, Lohmann CH, Cochran DL, et al. Osteoblasts generate an osteogenic microenvironment when grown on surfaces with rough microtopographies. European Cells & Materials 2003;6:22-27.

204. Martin JY, Schwartz Z, Hummert TW, Schraub DM, Simpson J, Lankford J, et al. Effect of titanium surface roughness on proliferation, differentiation, and protein

synthesis of human osteoblast-like cells (MG63). Journal of Biomedical Materials Research 1995;29:389-401.

205. Zhao G, Zinger O, Schwartz Z, Wieland M, Landolt D, Boyan BD. Osteoblast-like cells are sensitive to submicron-scale surface structure. Clinical Oral Implants Research 2006;17:258-264.

206. Buser D, Broggini N, Wieland M, Schenk RK, Denzer AJ, Cochran DL, et al. Enhanced bone apposition to a chemically modified SLA titanium surface. Journal of Dental Research 2004;83:529-533.

207. Bornstein MM, Hart CN, Halbritter SA, Morton D, Buser D. Early loading of nonsubmerged titanium implants with a chemically modified sand-blasted and acid-etched surface: 6-month results of a prospective case series study in the posterior mandible focusing on peri-implant crestal bone changes and implant stability quotient (ISQ) values. Clinical Implant Dentistry and Related Research 2009;11:338-347.

208. Bornstein MM, Wittneben J-G, Brägger U, Buser D. Early loading at 21 Days of non-submerged titanium implants with a chemically modified sandblasted and acid-etched surface: 3-year results of a prospective study in the posterior mandible. Journal of Periodontology 2010;81:809-818.

209. Rupp F, Scheideler L, Olshanska N, Wild M de, Wieland M, Geis-Gerstorfer J. Enhancing surface free energy and hydrophilicity through chemical modification of microstructured titanium implant surfaces. Journal of Biomedical Materials Research Part A 2006;76A:323-334.

210. Schwartz Z, Lohmann CH, Vocke AK, Sylvia VL, Cochran DL, Dean DD, et al. Osteoblast response to titanium surface roughness and 1alpha,25-(OH)2D3 is mediated through the mitogen-activated protein kinase (MAPK) pathway. Journal of Biomedical Materials Research 2001;56:417-426.

211. Kou PM, Babensee JE. Validation of a high-throughput methodology to assess the effects of biomaterials on dendritic cell phenotype. Acta Biomaterialia 2010;6:2621-2630.

212. Babensee JE, De Boni U, Sefton MV. Morphological assessment of hepatoma cells (HepG2) microencapsulated in a HEMA-MMA copolymer with and without Matrigel. Journal of Biomedical Materials Research 1992;26:1401-1418.

213. Janes KA, Yaffe MB. Data-driven modelling of signal-transduction networks. Nat Rev Mol Cell Biol 2006;7:820-828.

214. Albeck JG, MacBeath G, White FM, Sorger PK, Lauffenburger DA, Gaudet S. Collecting and organizing systematic sets of protein data. Nat Rev Mol Cell Biol 2006;7:803-812.

215. Janes KA, Kelly JR, Gaudet S, Albeck JG, Sorger PK, Lauffenburger DA. Cue-signal-response analysis of TNF-induced apoptosis by partial least squares regression of dynamic multivariate data. Journal of Computational Biology: A Journal of Computational Molecular Cell Biology 2004;11:544-561.

216. Rollins BJ. Chemokines. Blood 1997;90:909-928.

217. Rahimi P, Wang CY, Stashenko P, Lee SK, Lorenzo JA, Graves DT. Monocyte chemoattractant protein-1 expression and monocyte recruitment in osseous inflammation in the mouse. Endocrinology 1995;136:2752-2759.

218. Chi H, Barry SP, Roth RJ, Wu JJ, Jones EA, Bennett AM, et al. Dynamic regulation of pro- and anti-inflammatory cytokines by MAPK phosphatase 1 (MKP-1) in innate immune responses. Proceedings of the National Academy of Sciences of the United States of America 2006;103:2274-2279.

219. Cruikshank W, Kornfeld H, Center D. Interleukin-16. J Leukoc Biol 2000;67:757-766.

220. Hessel EM, Cruikshank WW, Van Ark I, De Bie JJ, Van Esch B, Hofman G, et al. Involvement of IL-16 in the induction of airway hyper-responsiveness and up-regulation of IgE in a murine model of allergic asthma. J Immunol 1998;160:2998-3005.

221. Theodore A, Center D, Nicoll J, Fine G, Kornfeld H, Cruikshank W. CD4 ligand IL-16 inhibits the mixed lymphocyte reaction. J Immunol 1996;157:1958-1964.

222. Klimiuk PA, Goronzy JJ, Weyand CM. IL-16 as an Anti-Inflammatory Cytokine in Rheumatoid Synovitis. J Immunol 1999;162:4293-4299.

223. Kim MS, Day CJ, Selinger CI, Magno CL, Stephens SRJ, Morrison NA. MCP-1-induced human osteoclast-like cells are tartrate-resistant acid phosphatase, NFATc1, and calcitonin receptor-positive but require receptor activator of NFκB ligand for bone resorption. Journal of Biological Chemistry 2006;281:1274-1285.

224. Li X, Qin L, Bergenstock M, Bevelock LM, Novack DV, Partridge NC. Parathyroid hormone stimulates osteoblastic expression of MCP-1 to recruit and increase the fusion of pre/osteoclasts. Journal of Biological Chemistry 2007;282:33098-33106.

225. Olivares-Navarrete R, Hyzy SL, Hutton DL, Erdman CP, Wieland M, Boyan BD, et al. Direct and indirect effects of microstructured titanium substrates on the induction of mesenchymal stem cell differentiation towards the osteoblast lineage. Biomaterials 2010;31:2728-2735.

226. Kohn J, Welsh WJ, Knight D. A new approach to the rationale discovery of polymeric biomaterials. Biomaterials 2007;28:4171-4177.

227. Livingstone DJ, Manallack DT. Neural Networks in 3D QSAR. QSAR & Combinatorial Science 2003;22:510-518.

228. Smith JR, Seyda A, Weber N, Knight D, Abramson S, Kohn J. Integration of Combinatorial Synthesis, Rapid Screening, and Computational Modeling in Biomaterials Development. Macromolecular Rapid Communications 2004;25:127-140.

229. Smith JR, Knight D, Kohn J, Rasheed K, Weber N, Kholodovych V, et al. Using Surrogate Modeling in the Prediction of Fibrinogen Adsorption onto Polymer Surfaces. Journal of Chemical Information and Computer Sciences 2004;44:1088-1097.

230. Kholodovych V, Smith JR, Knight D, Abramson S, Kohn J, Welsh WJ. Accurate predictions of cellular response using QSPR: a feasibility test of rational design of polymeric biomaterials. Polymer 2004;45:7367-7379.

231. Smith JR, Kholodovych V, Knight D, Welsh WJ, Kohn J. QSAR Models for the Analysis of Bioresponse Data from Combinatorial Libraries of Biomaterials. QSAR & Combinatorial Science 2005;24:99-113.

232. Chang D, Saidel G, Anderson J. Dynamic Systems Model for Lymphocyte Interactions with Macrophages at Biomaterial Surfaces. Cellular and Molecular Bioengineering 2009;2:573-590.

233. Rojas R, Harris NK, Piotrowska K, Kohn J. Evaluation of automated synthesis for chain and step-growth polymerizations: Can robots replace the chemists? Journal of Polymer Science Part A: Polymer Chemistry 2009;47:49-58.

234. Eriksson L, Johansson E, Kettaneh-Wold N, Trygg J, Wikstrom C, Wold S. Multi- and Megavariate Data Analysis. 2nd ed. Umea, Sweden: Umetrics AB. 2006 p.

235. Wold S, Sjöström M, Eriksson L. PLS-regression: a basic tool of chemometrics. Chemometrics and Intelligent Laboratory Systems 2001;58:109-130.

236. Martens H, Martens M. Multivariate Analysis of Quality An Introduction. John Wiley & Sons. p.

237. Kou PM, Schwartz Z, Boyan BD, Babensee JE. Dendritic cell responses to surface properties of clinical titanium surfaces. Acta Biomaterialia 2011;7:1354-1363.

238. Kwon OH, Kikuchi A, Yamato M, Sakurai Y, Okano T. Rapid cell sheet detachment from Poly(N-isopropylacrylamide)-grafted porous cell culture membranes. Journal of Biomedical Materials Research 2000;50:82-89.

239. Anderson P. Post-transcriptional control of cytokine production. Nat Immunol 2008;9:353-359.

240. Stockinger B, Veldhoen M. Differentiation and function of Th17 T cells. Current Opinion in Immunology 2007;19:281-286.

241. Sakaguchi S. Naturally Arising CD4+ Regulatory T Cells for Immunologic Self-Tolerance and Negative Control of Immune Responses. Annual Review of Immunology 2004;22:531-562.

242. Kalinski P, Hilkens CMU, Wierenga EA, Kapsenberg ML. T-cell priming by type-1 and type-2 polarized dendritic cells: the concept of a third signal. Immunology Today 1999;20:561-567.

243. Manicassamy S, Ravindran R, Deng J, Oluoch H, Denning TL, Kasturi SP, et al. Toll-like receptor 2-dependent induction of vitamin A-metabolizing enzymes in dendritic cells promotes T regulatory responses and inhibits autoimmunity. Nat Med 2009;15:401-409.

244. Takeda K, Akira S. TLR signaling pathways. Seminars in Immunology 2004;16:3-9.

245. Agrawal S, Agrawal A, Doughty B, Gerwitz A, Blenis J, Van Dyke T, et al. Cutting Edge: Different Toll-Like Receptor Agonists Instruct Dendritic Cells to Induce Distinct Th Responses via Differential Modulation of Extracellular Signal-Regulated Kinase-Mitogen-Activated Protein Kinase and c-Fos. J Immunol 2003;171:4984-4989.

246. Mizumoto N, Hui F, Edelbaum D, Weil MR, Wren JD, Shalhevet D, et al. Differential Activation Profiles of Multiple Transcription Factors During Dendritic Cell Maturation. J Investig Dermatol 2005;124:718-724.

247. ScienceDirect Full Text PDF.

248. Kou PM, Babensee JE. Macrophage and dendritic cell phenotypic diversity in the context of biomaterials. Journal of Biomedical Materials Research Part A 2011;96A:239-260.

249. Kou PM, Pallassana N, Cunningham B, Joy A, Kohn J, Babensee JE. Predicing dendritic cell phenotype from polymer material properties through multivariate analysis of a polymethacrylate combinatorial library. Biomaterials;In preparation.

250. van Kooyk Y, Geijtenbeek TBH. DC-sign: Escape mechanism for pathogens. Nat. Rev. Immunol. 2003;3:697-709.

251. Koski GK, Lyakh LA, Cohen PA, Rice NR. CD14+ monocytes as dendritic cell precursors: diverse maturation-inducing pathways lead to common activation of NF-kappab/RelB. Critical Reviews in Immunology 2001;21:179-189.

252. Remoli ME, Ragimbeau J, Giacomini E, Gafa V, Severa M, Lande R, et al. NF-κB is required for STAT-4 expression during dendritic cell maturation. Journal of Leukocyte Biology 2007;81:355 -363.

253. Kriehuber E, Bauer W, Charbonnier A-S, Winter D, Amatschek S, Tamandl D, et al. Balance between NF-κB and JNK/AP-1 activity controls dendritic cell life and death. Blood 2005;106:175 -183.

254. Ardeshna KM, Pizzey AR, Devereux S, Khwaja A. The PI3 kinase, p38 SAP kinase, and NF-κB signal transduction pathways are involved in the survival and maturation of lipopolysaccharide-stimulated human monocyte–derived dendritic cells. Blood 2000;96:1039 -1046.

255. Arimilli S, Johnson JB, Alexander-Miller MA, Parks GD. TLR-4 and -6 agonists reverse apoptosis and promote maturation of simian virus 5-infected human dendritic cells through NFkB-dependent pathways. Virology 2007;365:144-156.

256. Pietilä TE, Veckman V, Lehtonen A, Lin R, Hiscott J, Julkunen I. Multiple NF-κB and IFN Regulatory Factor Family Transcription Factors Regulate CCL19 Gene Expression in Human Monocyte-Derived Dendritic Cells. The Journal of Immunology 2007;178:253 -261.

257. Sallusto F, Palermo B, Lenig D, Miettinen M, Matikainen S, Julkunen I, et al. Distinct patterns and kinetics of chemokine production regulate dendritic cell function. European Journal of Immunology 1999;29:1617-1625.

258. Dieu M-C, Vanbervliet B, Vicari A, Bridon J-M, Oldham E, Aït-Yahia S, et al. Selective Recruitment of Immature and Mature Dendritic Cells by Distinct Chemokines Expressed in Different Anatomic Sites. The Journal of Experimental Medicine 1998;188:373 -386.

259. Casals C, Barrachina M, Serra M, Lloberas J, Celada A. Lipopolysaccharide Up-Regulates MHC Class II Expression on Dendritic Cells through an AP-1 Enhancer without Affecting the Levels of CIITA. The Journal of Immunology 2007;178:6307 -6315.

260. Liu W, Ouyang X, Yang J, Liu J, Li Q, Gu Y, et al. AP-1 Activated by Toll-like Receptors Regulates Expression of IL-23 p19. Journal of Biological Chemistry 2009;284:24006 -24016.

261. Langrish CL, McKenzie BS, Wilson NJ, De Waal Malefyt R, Kastelein RA, Cua DJ. IL-12 and IL-23: master regulators of innate and adaptive immunity. Immunological Reviews 2004;202:96-105.

262. Cua DJ, Sherlock J, Chen Y, Murphy CA, Joyce B, Seymour B, et al. Interleukin-23 rather than interleukin-12 is the critical cytokine for autoimmune inflammation of the brain. Nature 2003;421:744-748.

263. Kikly K, Liu L, Na S, Sedgwick JD. The IL-23/Th17 axis: therapeutic targets for autoimmune inflammation. Current Opinion in Immunology 2006;18:670-675.

264. Stark GR, Kerr IM, Williams BRG, Silverman RH, Schreiber RD. How cells respond to interferons. Annual Review of Biochemistry 1998;67:227-264.

265. Goriely S, Molle C, Nguyen M, Albarani V, Haddou NO, Lin R, et al. Interferon regulatory factor 3 is involved in Toll-like receptor 4 (TLR4)- and TLR3-induced IL-12p35 gene activation. Blood 2006;107:1078 -1084.

266. la Sala A, He J, Laricchia-Robbio L, Gorini S, Iwasaki A, Braun M, et al. Cholera toxin inhibits IL-12 production and CD8α+ dendritic cell differentiation by cAMP-mediated inhibition of IRF8 function. The Journal of Experimental Medicine 2009;206:1227 -1235.

267. Chawla-Sarkar M, Lindner DJ, Liu Y-F, Williams BR, Sen GC, Silverman RH, et al. Apoptosis and interferons: role of interferon-stimulated genes as mediators of apoptosis. Apoptosis: An International Journal on Programmed Cell Death 2003;8:237-249.

268. Cho H-Y, Lee S-W, Seo S-K, Choi I-W, Choi I, Lee S-W. Interferon-sensitive response element (ISRE) is mainly responsible for IFN-[alpha]-induced upregulation of programmed death-1 (PD-1) in macrophages. Biochimica et Biophysica Acta (BBA) - Gene Regulatory Mechanisms 2008;1779:811-819.

269. Wu C. Heat Shock Transcription Factors: Structure and Regulation. Annual Review of Cell and Developmental Biology 1995;11:441-469.

270. Ostberg JR, Repasky EA. Emerging evidence indicates that physiologically relevant thermal stress regulates dendritic cell function. Cancer Immunology, Immunotherapy 2005;55:292-298.

271. Zheng H, Benjamin IJ, Basu S, Li Z. Heat shock factor 1-independent activation of dendritic cells by heat shock: implication for the uncoupling of heat-mediated immunoregulation from the heat shock response. European Journal of Immunology 2003;33:1754-1762.

272. DeFillipo AM, Dai J, Li Z. Heat shock-induced dendritic cell maturation is coupled by transient aggregation of ubiquitinated proteins independently of heat shock factor 1 or inducible heat shock protein 70. Molecular Immunology 2004;41:785-792.

273. Ichiyanagi T, Imai T, Kajiwara C, Mizukami S, Nakai A, Nakayama T, et al. Essential Role of Endogenous Heat Shock Protein 90 of Dendritic Cells in Antigen Cross-Presentation. The Journal of Immunology 2010;185:2693 -2700.

274. Takayama S, Reed JC, Homma S. Heat-shock proteins as regulators of apoptosis. Oncogene;22:9041-9047.

275. Kato S, Akagi T, Sugimura K, Kishida A, Akashi M. Evaluation of biological responses to polymeric biomaterials by RT-PCR analysis III: Study of HSP 70, 90 and 47 mRNA expression. Biomaterials 1998;19:821-827.

276. Helin K. Regulation of cell proliferation by the E2F transcription factors. Current Opinion in Genetics & Development 1998;8:28-35.

277. Tsai S-Y, Opavsky R, Sharma N, Wu L, Naidu S, Nolan E, et al. Mouse development with a single E2F activator. Nature 2008;454:1137-1141.

278. Ginsberg D. E2F1 pathways to apoptosis. FEBS Letters 2002;529:122-125.

279. Field SJ, Tsai F-Y, Kuo F, Zubiaga AM, Kaelin WG, Livingston DM, et al. E2F-1 Functions in Mice to Promote Apoptosis and Suppress Proliferation. Cell 1996;85:549-561.

280. Tanaka H, Matsumura I, Ezoe S, Satoh Y, Sakamaki T, Albanese C, et al. E2F1 and c-Myc Potentiate Apoptosis through Inhibition of NF-[kappa]B Activity that Facilitates MnSOD-Mediated ROS Elimination. Molecular Cell 2002;9:1017-1029.

281. Fang F, Wang Y, Li R, Zhao Y, Guo Y, Jiang M, et al. Transcription Factor E2F1 Suppresses Dendritic Cell Maturation. The Journal of Immunology 2010;184:6084-6091.

282. Joyce DA, Steer JH, Abraham LJ. Glucocorticoid modulation of human monocyte/macrophage function: Control of TNF-alpha secretion. Inflammation Research 1997;46:447-451.

283. Butts CL, Shukair SA, Duncan KM, Bowers E, Horn C, Belyavskaya E, et al. Progesterone inhibits mature rat dendritic cells in a receptor-mediated fashion. International Immunology 2007;19:287-296.

284. Butts CL, Candando KM, Warfel J, Belyavskaya E, D'Agnillo F, Sternberg EM. Progesterone regulation of uterine dendritic cell function in rodents is dependent on the stage of estrous cycle. Mucosal Immunol 2010;3:496-505.

285. Jones LA, Kreem S, Shweash M, Paul A, Alexander J, Roberts CW. Differential Modulation of TLR3- and TLR4-Mediated Dendritic Cell Maturation and Function by Progesterone. The Journal of Immunology 2010;185:4525-4534.

286. Hoetzenecker W, Meindl S, Stuetz A, Stingl G, Elbe-Burger A. Both Pimecrolimus and Corticosteroids Deplete Plasmacytoid Dendritic Cells in Patients with Atopic Dermatitis. J Invest Dermatol 2006;126:2141-2144.

287. Rao A, Luo C, Hogan PG. Transcription factors of the NFAT family: Regulation and Function. Annual Review of Immunology 1997;15:707-747.

288. Goodridge HS, Simmons RM, Underhill DM. Dectin-1 Stimulation by Candida albicans Yeast or Zymosan Triggers NFAT Activation in Macrophages and Dendritic Cells. The Journal of Immunology 2007;178:3107 -3115.

289. Vukcevic M, Zorzato F, Spagnoli G, Treves S. Frequent Calcium Oscillations Lead to NFAT Activation in Human Immature Dendritic Cells. Journal of Biological Chemistry 2010;285:16003 -16011.

290. Zanoni I, Ostuni R, Capuano G, Collini M, Caccia M, Ronchi AE, et al. CD14 regulates the dendritic cell life cycle after LPS exposure through NFAT activation. Nature 2009;460:264-268.

291. Delghandi MP, Johannessen M, Moens U. The cAMP signalling pathway activates CREB through PKA, p38 and MSK1 in NIH 3T3 cells. Cellular Signalling 2005;17:1343-1351.

292. Screaton RA, Conkright MD, Katoh Y, Best JL, Canettieri G, Jeffries S, et al. The CREB Coactivator TORC2 Functions as a Calcium- and cAMP-Sensitive Coincidence Detector. Cell 2004;119:61-74.

293. Illario M, Giardino-Torchia ML, Sankar U, Ribar TJ, Galgani M, Vitiello L, et al. Calmodulin-dependent kinase IV links Toll-like receptor 4 signaling with survival pathway of activated dendritic cells. Blood 2008;111:723 -731.

294. Alvarez Y, Municio C, Alonso S, Sánchez Crespo M, Fernández N. The Induction of IL-10 by Zymosan in Dendritic Cells Depends on CREB Activation by the Coactivators CREB-Binding Protein and TORC2 and Autocrine PGE2. The Journal of Immunology 2009;183:1471 -1479.

295. Kushwah R, Hu J. Dendritic Cell Apoptosis: Regulation of Tolerance versus Immunity. The Journal of Immunology 2010;185:795 -802.

296. Chen M, Wang Y-H, Wang Y, Huang L, Sandoval H, Liu Y-J, et al. Dendritic Cell Apoptosis in the Maintenance of Immune Tolerance. Science 2006;311:1160 - 1164.

297. Kushwah R, Wu J, Oliver JR, Jiang G, Zhang J, Siminovitch KA, et al. Uptake of apoptotic DC converts immature DC into tolerogenic DC that induce differentiation of Foxp3+ Treg. European Journal of Immunology 2010;40:1022-1035.

298. Tang L, Wu Y, Timmons RB. Fibrinogen adsorption and host tissue responses to plasma functionalized surfaces. Journal of Biomedical Materials Research 1998;42:156-163.

299. Shen MC, Martinson L, Wagner MS, Castner DG, Ratner BD, Horbett TA. PEO-like plasma polymerized tetraglyme surface interactions with leukocytes and

proteins: in vitro and in vivo studies. Journal of Biomaterials Science Polymer Edition 2002;13:367-390.

300. Thevenot P, Hu WJ, Tang LP. Surface chemistry influences implant biocompatibility. Current Topics in Medicinal Chemistry 2008;8:270-280.

301. Kamath S, Bhattacharyya D, Padukudru C, Timmons RB, Tang L. Surface chemistry influences implant-mediated host tissue responses. Journal of Biomedical Materials Research Part A 2008;86A:617-626.

302. Bortner CD, Cidlowski JA. A necessary role for cell shrinkage in apoptosis. Biochemical Pharmacology 1998;56:1549-1559.

303. Wagner MS, Castner DG. Characterization of Adsorbed Protein Films by Time-of-Flight Secondary Ion Mass Spectrometry with Principal Component Analysis. Langmuir 2001;17:4649-4660.

304. Takeda K, Akira S. Toll-like receptors in innate immunity. Int. Immunol. 2005;17:1-14.

305. Robinson MJ, Sancho D, Slack EC, LeibundGut-Landmann S, Sousa CRE. Myeloid C-type lectins in innate immunity. Nature Immunology 2006;7:1258-1265.

306. Park YC, Ye H, Hsia C, Segal D, Rich RL, Liou H-C, et al. A Novel Mechanism of TRAF Signaling Revealed by Structural and Functional Analyses of the TRADD-TRAF2 Interaction. Cell 2000;101:777-787.

307. Wu C, Dedhar S. Integrin-linked kinase (ILK) and its interactors. The Journal of Cell Biology 2001;155:505 -510.

308. de Witte L, Bobardt M, Chatterji U, Degeest G, David G, Geijtenbeek TBH, et al. Syndecan-3 is a dendritic cell-specific attachment receptor for HIV-1. Proceedings of the National Academy of Sciences 2007;104:19464 -19469.

309. Hochweller K, Striegler J, Hämmerling GJ, Garbi N. A novel CD11c.DTR transgenic mouse for depletion of dendritic cells reveals their requirement for homeostatic proliferation of natural killer cells. European Journal of Immunology 2008;38:2776-2783.

310. Möller E, Isaksson M, Mandahl N, Mertens F, Panagopoulos I. Comparison of the proximal promoter regions of the PAX3 and PAX7 genes. Cancer Genetics and Cytogenetics 2007;178:114-119.

311. Dhawan L, Liu B, Blaxall BC, Taubman MB. A novel role for the glucocorticoid receptor in the regulation of monocyte chemoattractant protein-1 mRNA stability. The Journal of Biological Chemistry 2007;282:10146-10152.